

## **Distribution Agreement**

In presenting this thesis or dissertation as a partial fulfillment of the requirements for an advanced degree from Emory University, I hereby grant to Emory University and its agents the non-exclusive license to archive, make accessible, and display my thesis or dissertation in whole or in part in all forms of media, now or hereafter known, including display on the world wide web. I understand that I may select some access restrictions as part of the online submission of this thesis or dissertation. I retain all ownership rights to the copyright of the thesis or dissertation. I also retain the right to use in future works (such as articles or books) all or part of this thesis or dissertation.

Signature:

---

Emily Gretchen Kuiper

---

Date

Structure and Function of Methyltransferases that Modify the Bacterial Ribosome  
and Ribosome-Associated Factors

By

Emily Gretchen Kuiper  
Doctor of Philosophy

Division of Biological and Biomedical Sciences  
Biochemistry, Cell and Developmental Biology

\_\_\_\_\_  
[Advisor's Signature]  
Graeme L. Conn, Ph.D.  
Advisor

\_\_\_\_\_  
[Member's Signature]  
Keith D. Wilkinson, Ph.D.  
Committee Member

\_\_\_\_\_  
[Member's Signature]  
Daniel Reines, Ph.D.  
Committee Member

\_\_\_\_\_  
[Member's Signature]  
Haian Fu, Ph.D.  
Committee Member

\_\_\_\_\_  
[Member's Signature]  
Eric A. Ortlund, Ph.D.  
Committee Member

Accepted:

\_\_\_\_\_  
Lisa A. Tedesco, Ph.D.  
Dean of the James T. Laney School of Graduate Studies

\_\_\_\_\_  
Date

Structure and Function of Methyltransferases that Modify the Ribosome and Ribosome-Associated Factors

By

Emily Gretchen Kuiper  
B.S., The Pennsylvania State University, 2010

Advisor: Graeme L. Conn, Ph.D.

An abstract of  
A dissertation submitted to the Faculty of the  
James T. Laney School of Graduate Studies of Emory University  
in partial fulfillment of the requirements for the degree of  
Doctor of Philosophy, in Biological and Biomedical Sciences,  
Biochemistry, Cell and Developmental Biology  
2016

## Abstract

### Structure and Function of Methyltransferases that Modify the Ribosome and Ribosome-Associated Factors

By Emily Gretchen Kuiper

The ribosome is the molecular machine responsible for translating messenger RNA into proteins. Ribosome assembly and function is modulated by posttranscriptional and posttranslational modifications of the ribosomal components and its associated factors. Additionally, other modifications allow the ribosome to adapt to stressors in the environment. While many ribosomal modifications have been identified, less is known about the structural and molecular mechanisms of catalysis of the modification enzymes. In this dissertation I elucidate novel structural and functional characteristics of three methyltransferases that aid bacteria in adapting to environmental stressors such as infection of a host or survival in the presence of antibiotics.

Deletion of EftM, the EF-Tu trimethyltransferase, decreases *Pseudomonas aeruginosa* adherence to and infection of host cells. I show via homology modeling and mutation of the putative S-adenosyl-L-methionine binding motif that EftM belongs to Class I methyltransferases. Further, I show that the observed temperature regulation of the modification is due to a novel regulatory mechanism where the methyltransferase unfolds at the restrictive temperature, resulting in the observed repression of EF-Tu methylation.

Loss of the *Mycobacterium tuberculosis* constitutive ribosomal RNA methyltransferase TlyA renders ribosomes resistant to the antibiotic capreomycin. I identified and characterized a novel auxiliary cosubstrate-binding motif, within an interdomain linker that is essential for cosubstrate binding. This motif is conserved in TlyA orthologs, suggesting that it is functionally important. We speculate that this motif likely coordinates substrate recognition via an amino-terminal domain with cosubstrate binding and catalysis.

The thiostrepton-resistance methyltransferase (Tsr) confers antibiotic resistance in the thiostrepton antibiotic-producing bacterium *Streptomyces azureus*. Here, I elucidate Tsr's cosubstrate binding affinity and catalytic mechanism and show that as a dimer, each protomer acts independently to bind cosubstrate and methylate its 23S rRNA substrate. Furthermore, I present a novel substrate recognition mechanism where Tsr induces conformational changes in the rRNA substrate prior to catalysis. My studies begin to elucidate the coordination involved between the two protomers and between substrate-recognition and catalytic domains for proper enzyme function.

Together, my studies describe the molecular mechanisms of methyltransferases which complements cellular studies that examine the function of a modification in a bacterium or in adaptation to stress.

Structure and Function of Methyltransferases that Modify the Ribosome and Ribosome-Associated Factors

By

Emily Gretchen Kuiper  
B.S., The Pennsylvania State University, 2010

Advisor: Graeme L. Conn, Ph.D.

A dissertation submitted to the Faculty of the  
James T. Laney School of Graduate Studies of Emory University  
in partial fulfillment of the requirements for the degree of  
Doctor of Philosophy, in Biological and Biomedical Sciences,  
Biochemistry, Cell and Developmental Biology  
2016

## Table of Contents

<b>1</b>	<b>CHAPTER 1: INTRODUCTION TO DISSERTATION.....</b>	<b>1</b>
1.1	THE RIBOSOME AND THE TRANSLATIONAL MACHINERY.....	1
1.1.1	<i>Translation Initiation.....</i>	2
1.1.2	<i>Translation Elongation.....</i>	3
1.1.3	<i>Translation Termination.....</i>	4
1.2	ANTIBIOTICS INHIBIT IMPORTANT FUNCTIONAL AREAS OF THE RIBOSOME.....	5
1.2.1	<i>Peptide Exit Tunnel.....</i>	5
1.2.2	<i>Peptidyl-Transferase Center.....</i>	6
1.2.3	<i>30S Subunit and Decoding Center.....</i>	6
1.2.4	<i>GTPase Activation Center and GTPase.....</i>	7
1.3	METHYLATION OF THE RIBOSOMAL MACHINERY: FINE TUNING RIBOSOME FUNCTION, ANTIBIOTIC RESISTANCE AND PATHOGENESIS...8	
1.3.1	<i>Posttranscriptional Modifications of rRNA.....</i>	9
1.3.1.1	Constitutive modifications aid in ribosome function: 30S subunit.....	9
1.3.1.2	Constitutive modifications aid in ribosome function: 50S subunit. ....	10
1.3.1.3	Constitutive modifications aid in antibiotic binding and inhibition.....	11
1.3.1.4	Posttranscriptional modifications can confer antibiotic resistance.	12
1.3.2	<i>Posttranslational Modifications.....</i>	14
1.3.2.1	Ribosomal protein modifications.....	14
1.3.2.2	Modifications of ribosome factors.....	15

1.3.2.3	Control of EF-Tu function by modification during different phases of bacterial growth.....	15
1.4	PREVAILING QUESTIONS IN METHYLTRANSFERASE STRUCTURE AND FUNCTION.....	16
1.5	REFERENCES.....	29
<b>2</b>	<b>CHAPTER 2: <i>PSEUDOMONAS AERUGINOSA</i> EFTM IS A THERMOREGULATED METHYLTRANSFERASE.....</b>	<b>45</b>
2.1	ABSTRACT.....	46
2.2	INTRODUCTION.....	46
2.3	EXPERIMENTAL PROCEDURES.....	49
2.3.1	<i>Bacterial strains, plasmids and primers.....</i>	<i>49</i>
2.3.2	<i>Plasmid construction.....</i>	<i>49</i>
2.3.3	<i>Protein expression and purification.....</i>	<i>50</i>
2.3.4	<i>Preparation of <i>P. aeruginosa</i> whole-cell extracts.....</i>	<i>51</i>
2.3.5	<i>Immunoblot analysis.....</i>	<i>51</i>
2.3.6	<i>EftM homology modeling.....</i>	<i>51</i>
2.3.7	<i>In vitro methyltransferase assay.....</i>	<i>52</i>
2.3.8	<i>MS analysis.....</i>	<i>52</i>
2.3.9	<i>Isothermal titration calorimetry.....</i>	<i>54</i>
2.3.10	<i>Circular dichroism spectroscopy.....</i>	<i>54</i>
2.3.11	<i>Differential scanning fluorimetry.....</i>	<i>55</i>
2.4	RESULTS.....	55
2.4.1	<i>EftM is a SAM-dependent methyltransferase.....</i>	<i>55</i>
2.4.2	<i>EftM is necessary and sufficient to methylate EF-Tu.....</i>	<i>57</i>
2.4.3	<i>EF-Tu methylation by EftM is distributive.....</i>	<i>58</i>

2.4.4	<i>EftM methyltransferase activity is thermosensitive</i> .....	59
2.4.5	<i>Structural thermolability regulates EftM activity</i> .....	59
2.5	DISCUSSION.....	60
2.6	ACKNOWLEDGEMENTS.....	63
2.7	REFERENCES.....	74
<b>3</b>	<b>CHAPTER 3: A NOVEL MOTIF REQUIRED FOR S-ADENOSYL-L-METHIONINE COSUBSTRATE BINDING BY THE 2'-O-METHYLTRANSFERASE TLYA FROM MYCOBACTERIUM TUBERCULOSIS</b> .....	<b>79</b>
3.1	SUMMARY.....	80
3.2	INTRODUCTION.....	80
3.3	RESULTS.....	82
3.3.1	<i>Construct Design, Protein Expression and Purification of TlyA for Structural Studies</i> .....	82
3.3.2	<i>The TlyA CTD Adopts a Class I Methyltransferase Fold</i> .....	84
3.3.3	<i>The Isolated TlyA CTD Protein Does Not Bind SAM</i> .....	85
3.3.4	<i>The RAWV Tetrapeptide Interdomain Linker is Critical for TlyA CTD- SAM Interaction</i> .....	86
3.3.5	<i>Trp62 and Val63 are Critical for SAM Binding</i> .....	88
3.3.6	<i>Structural Plasticity of RAWV Motif</i> .....	89
3.4	DISCUSSION.....	92
3.5	EXPERIMENTAL PROCEDURES.....	94
3.5.1	<i>TlyA Construct Design and Site-directed Mutagenesis</i> .....	94
3.5.2	<i>TlyA Protein Expression and Purification</i> .....	95
3.5.3	<i>CD Spectroscopy</i> .....	96
3.5.4	<i>RT Analysis of 16S and 23S rRNA Methylation</i> .....	96

3.5.5	<i>Protein Crystallization and Structure Determination</i> .....	97
3.5.6	<i>Isothermal Titration Calorimetry Analysis of SAM and SAH Binding</i> ....	98
3.5.7	<i>Analysis of TlyA Domain Association by Gel Filtration Chromatography</i> .....	98
3.5.8	<i>SAM and NTD Modeling</i> .....	99
3.6	ACCESSION NUMBERS.....	99
3.7	ACKNOWLEDGEMENTS.....	99
3.8	SUPPLEMENTAL INFORMATION.....	112
3.9	REFERENCES.....	115

#### **4 CHAPTER 4: BINDING INDUCED RNA CONFORMATIONAL CHANGES**

##### **CONTROL SUBSTRATE RECOGNITION AND CATALYSIS BY THE**

##### **THIOSTREPTON-RESISTANCE METHYLTRANSFERASE (TSR).....120**

4.1	SUMMARY.....	121
4.2	INTRODUCTION.....	121
4.3	EXPERIMENTAL PROCEDURES.....	124
4.3.1	<i>Tsr purification and mutagenesis</i> .....	124
4.3.2	<i>RNA in vitro transcription</i> .....	124
4.3.3	<i>Hydroxyl radical and ribonuclease RNA structure probing</i> .....	125
4.3.4	<i>RNA UV Melting</i> .....	126
4.3.5	<i>Fluorescence polarization</i> .....	126
4.3.6	<i>Methylation Assays</i> .....	126
4.3.7	<i>Electrophoretic mobility shift assay</i> .....	127
4.3.8	<i>Partial Proteolysis</i> .....	127
4.4	RESULTS.....	127
4.4.1	<i>The Tsr NTDs aid in rRNA binding and are necessary for catalysis</i> .....	127

4.4.2	<i>Identification of the RNA binding surface and binding-induced perturbations in the RNA structure by Tsr</i> .....	130
4.4.3	<i>RNA conformational changes induced by Tsr are dependent on its NTD</i> .....	132
4.4.4	<i>Stabilizing the 58 nt RNA tertiary structure does not interfere with RNA conformational changes induced by RNase VI</i> .....	134
4.4.5	<i>Tsr mutants R162A and R26A discriminate between RNA binding and induced conformational changes necessary for catalysis</i> .....	135
4.5	DISCUSSION.....	137
4.6	ACKNOWLEDGEMENTS .....	140
4.7	REFERENCES.....	152

**5 CHAPTER 5: FUNCTIONAL ROLES IN S-ADENOSYL-L-METHIONINE BINDING AND CATALYSIS FOR ACTIVE SITE RESIDUES OF THE THIOSTREPTON RESISTANCE METHYLTRANSFERASE .....157**

5.1	ABSTRACT.....	158
5.2	INTRODUCTION.....	158
5.3	MATERIALS AND METHODS.....	160
5.3.1	<i>Protein expression &amp; purification</i> .....	160
5.3.2	<i>Size exclusion chromatography</i> .....	161
5.3.3	<i>Methylation assays</i> .....	161
5.3.4	<i>Isothermal titration calorimetry</i> .....	162
5.3.5	<i>Circular dichroism spectroscopy</i> .....	163
5.4	RESULTS.....	163
5.4.1	<i>Characterization of SAM binding and turnover by Tsr</i> .....	163
5.4.2	<i>Effect of active site mutations on Tsr activity</i> .....	165

5.4.3	<i>Thermodynamics of SAM binding and kinetics of SAM turnover by select Tsr mutants</i> .....	166
5.4.4	<i>N129 is involved in the structural organization of Tsr</i> .....	167
5.5	DISCUSSION.....	168
5.6	ACKNOWLEDGEMENTS.....	170
5.7	SUPPLEMENTARY MATERIAL.....	177
5.8	REFERENCES .....	183
<b>6</b>	<b>CHAPTER 6: DISCUSSION</b> .....	<b>187</b>
6.1	STRUCTURAL INSIGHTS .....	187
6.1.1	<i>Structural Instability Regulates EftM Activity</i> .....	187
6.1.2	<i>TlyA Linker May Coordinate Interdomain Interactions</i> .....	188
6.1.3	<i>Tsr Protomers Act Independently of Each Other in Catalysis</i> .....	189
6.2	COSUBSTRATE BINDING.....	190
6.2.1	<i>Identification and Characterization of the SAM Binding Motif in EftM</i> .....	190
6.2.2	<i>A Novel Auxiliary SAM Binding Motif in TlyA</i> .....	190
6.2.3	<i>Tsr Cosubstrate Recognition and Catalysis</i> .....	191
6.3	SUBSTRATE RECOGNITION.....	191
6.3.1	<i>A New Model of Tsr Substrate Recognition</i> .....	192
6.3.2	<i>TlyA Recognizes Two Different Substrates</i> .....	193
6.3.3	<i>EF-Tu Lysine Recognition by EftM</i> .....	194
6.4	MODIFICATION ENZYMES AID IN BACTERIAL ADAPTATION.....	195
6.4.1	<i>TlyA is a Methyltransferase and Hemolysin</i> .....	196
6.4.2	<i>EftM Mediated Trimethylation aids in P. aeruginosa Infection</i> .....	197
6.4.3	<i>Thiopeptides and the Antibiotic Resistome</i> .....	197

6.5 FUTURE DIRECTIONS.....	198
6.5.1 <i>EftM</i> .....	198
6.5.2 <i>TlyA</i> .....	199
6.5.3 <i>Tsr</i> .....	199
6.6 CONCLUDING REMARKS.....	200
6.7 REFERENCES.....	202

## List of Figures

### **CHAPTER 1**

FIGURE 1.1. Structure of the bacterial 70S ribosome.....	19
FIGURE 1.2. Translation initiation.....	20
FIGURE 1.3. Translation elongation.....	21
FIGURE 1.4. Translation termination and ribosome recycling.....	22
FIGURE 1.5. Antibiotic binding sites in the ribosome.....	23
FIGURE 1.6. Ribosomal GTPase EF-Tu and EF-G bound to inhibitory antibiotics.....	25
FIGURE 1.7. Posttranscriptional modifications of rRNA.....	26
FIGURE 1.8. Antibiotic resistance conferred by loss of posttranscriptional modifications....	27
FIGURE 1.9. Current knowledge and prevailing questions for Tsr, TlyA and EftM mechanistic studies.....	28

### **CHAPTER 2**

FIGURE 2.1 Wild-type but not G50R substituted EftM is able methylate EF-Tu <i>in vivo</i> .....	65
FIGURE 2.2 EftM shares structural homology with Class I SAM-dependent methyltransferases and binds cosubstrate.....	66
FIGURE 2.3. <i>In vitro</i> lysine 5 trimethylation and quantification on recombinant EF-Tu.....	67
FIGURE 2.4. EftM adds methyl groups to EF-Tu lysine 5 in a distributive manner.....	69
FIGURE 2.5. EftM activity is thermolabile. ....	70
FIGURE 2.6. EftM structure is thermolabile. ....	71

### **CHAPTER 3**

FIGURE 3.1. Recombinant <i>Mtb</i> His-TlyA (Rv1694) is well-folded and active <i>in vitro</i> against both 30S and 50S ribosomal subunits substrates.....	101
FIGURE 3.2. GluC cleavage of TlyA generates two domain fragments that remain associated	102
FIGURE 3.3. The TlyA CTD adopts a Class I methyltransferase fold.....	104

FIGURE 3.4. The isolated TlyA methyltransferase domain (CTD) does not bind SAM.....	105
FIGURE 3.5. The TlyA RAWV tetrapeptide sequence is necessary for SAM binding.....	106
FIGURE 3.6. RxWV motif conservation.....	107
FIGURE 3.7. The TlyA RAWV motif can adopt two distinct conformations.....	108
FIGURE 3.8. Modeling of the TlyA NTD on two RAWV CTD crystal structures.....	109
FIGURE 3.S1. Time course of a partial digest of wild-type (WT) and E59A substituted TlyA with GluC protease.....	112
FIGURE 3.S1 Two approximate orthogonal views of each individual model.....	113
<b>CHAPTER 4</b>	
FIGURE 4.1. Tsr domain organization and 58 nt RNA substrate secondary structure.....	141
FIGURE 4.2. The Tsr NTDs increase RNA binding affinity and are necessary for catalysis..	142
FIGURE 4.3. Hydroxyl radical probing identifies the Tsr footprint and cleavage enhancements upon Tsr binding. ....	143
FIGURE 4.4. UV melting of the wild-type 58 nt RNA with and without full-length Tsr.....	145
FIGURE 4.5. RNase probing identifies RNA structural changes and cleavage protections induced upon binding full-length Tsr or Tsr-CTD. ....	146
FIGURE 4.6. Stabilizing the RNA tertiary structure decreases Tsr binding affinity and catalytic activity independent of RNA structural changes. ....	147
FIGURE 4.7. Tsr-NTD modification of the RNA structure is necessary for catalysis.....	148
FIGURE 4.8. Model of the Tsr substrate recognition mechanism.....	150
<b>CHAPTER 5</b>	
FIGURE 5.1. SAM binding and turnover by Tsr.....	171
FIGURE 5.2. Enzymatic activity of Tsr mutants. ....	172
FIGURE 5.3. R165 functions in SAM binding.....	173
FIGURE 5.4 Structural significance of N129.....	174

FIGURE S5.1. Development of the coupled fluorometric assay for monitoring Tsr catalyzed methylation of 16S/ 23S rRNA in kinetic evaluations of SAM turnover.....	178
FIGURE S5.2. Multiple sequence alignment of SPOUT methyltransferases.....	179
FIGURE S5.3. Tsr mutants with Ala substitutions at N129, R135 or R165 are impaired in the methylation of a 29 nt RNA substrate.....	181

## **CHAPTER 6**

FIGURE 6.1. Current knowledge and prevailing questions for Tsr, TlyA and EftM mechanistic studies. ....	201
---	-----

## List of Tables

### **CHAPTER 2**

TABLE 2.1. Summary of strains and plasmids.....72

TABLE 2.2. Summary of DNA oligonucleotides.....73

### **CHAPTER 3**

TABLE 3.1. Co-substrate binding affinity of full-length TlyA and individual domains.....110

TABLE 3.1. Co-substrate binding affinity of TlyA RAWV variants.....111

TABLE 3.S1. X-ray data collection and refinement statistics for TlyA CTD structures.....114

### **CHAPTER 4**

TABLE 4.1. Dissociation Constants for Tsr and RNA mutants.....151

### **CHAPTER 5**

TABLE 5.1. Parameters for SAM binding by Tsr and N129, R135 or R165 mutants.....175

TABLE 5.2. Parameters for SAH binding by Tsr and mutants with Ala substituted for N129,  
R135 or R165.....176

TABLE S5.1. Primers used to generate Tsr point mutant variants.....177

## Abbreviations

A site,	acceptor transfer RNA binding site
aa-tRNA,	aminoacyl-transfer RNA
AGC,	automatic gain control
CD,	circular dichroism
CTD,	carboxyl-terminal domain
DSF,	differential scanning fluorimetry
DTmK,	di/trimethyl lysine
E site,	ribosome exit transfer RNA binding site
EF-Tu,	elongation factor thermo unstable
EF-G,	elongation factor-G
EMSA,	electrophoretic mobility shift assay
ESI-MS,	electrospray ionization mass spectrometry
FDR,	false discovery rate
FL-Tsr,	full-length Tsr protein
FP,	fluorescence polarization
GTPase center,	GTPase activating center (area of ribosome composed of ribosomal proteins L11 and L12 and rRNA helices 42-44, 95)
HDV,	hepatitis delta virus
IF,	initiation factor
IMAC,	immobilized metal ion affinity chromatography
IPTG,	isopropyl b-D-1-thiogalactopyranoside
ITC,	isothermal titration calorimetry
K <sub>D</sub> ,	dissociation constant
MIC,	minimal inhibitory concentration
mRNA,	messenger RNA

MS,	mass spectrometry
N-His <sub>6</sub> ,	amino-terminal hexahistidine
nt,	nucleotide
NTD,	amino-terminal domain
P site,	peptide transferase center transfer RNA binding site
PAF,	platelet activating factor
PET,	peptidyl exit tunnel
PTC,	peptidyl transferase center
PTM,	posttranslational modification
RF,	release factor
RRF,	ribosome recycling factor
rRNA,	ribosomal RNA
SAM,	<i>S</i> -adenosyl-L-methionine
SAH,	<i>S</i> -adenosyl-L-homocysteine
SDS-PAGE,	sodium dodecyl sulfate polyacrylamide gel electrophoresis
SPOUT,	SpoU/ TrmD (methyltransferase enzyme family)
tRNA,	transfer RNA
Tsr-NTD,	isolated NTD protein
Tsr-CTD,	isolated CTD protein
wt,	wild type
XIC,	extracted ion chromatogram

## CHAPTER 1. INTRODUCTION TO DISSERTATION

Cells from all three kingdoms of life contain three major polymers, DNA, RNA and proteins, that store information and carry out the major functions for cell survival. Bacterial DNA is packaged into chromosomes that are typically circular. The gram-negative bacterium *Escherichia coli* (K-12) for example, contains one chromosome made up of 4.64 million base pairs encoding 4294 proteins (1). To convert a single gene into a protein, the gene is transcribed by a DNA-dependent RNA polymerase creating a messenger RNA (mRNA) molecule, in a process called transcription. In a second process termed translation, a ribosome deciphers the mRNA nucleotide sequence and creates a protein, which goes on to perform a defined function in the cell. This protein can be posttranslationally modified, which typically modulates the protein's activity (2,3). As translation is one of the key processes in a cell, the ribosome and its associated translation factors are highly modified either on the rRNA as posttranscriptional modifications or on the proteins as posttranslational modifications. These modifications aid in the assembly and canonical function of the ribosome, or can alter its activity.

### 1.1 THE RIBOSOME AND THE TRANSLATIONAL MACHINERY

It is estimated that in a rapidly growing bacterium, approximately 50% of available ATP is used for protein synthesis (4). Ribosomes are the molecular machines that, along with ribosomal factors and transfer RNA (tRNA) adaptor molecules, are responsible for decoding the mRNA and translating almost all proteins within the cell. Ribosomes are made up of two subunits, the 30S and 50S, which are composed of both ribosomal RNA (rRNA) and protein. The *E. coli* 30S subunit is composed of 16S rRNA containing 1542 nucleotides and 21 proteins, while the 50S subunit is made up of 23S and 5S rRNA containing 2904 and 120 nucleotides, respectively, and 33 unique

proteins (5). The 30S and 50S subunits associate to form the 70S ribosome of 2.6 MDa (**Figure 1.1**).

Translation of the mRNA message is a sequential process. Each message undergoes three phases of translation: initiation, elongation and termination. During elongation the mRNA nucleotide sequence is read in groups of three nucleotides called codons. For every mRNA codon, there is a tRNA that contains a corresponding anti-codon that is chemically linked to a specific amino acid (amino-acylated tRNA). tRNAs cycle through the ribosome, first binding in the acceptor site (A site) and then translocated to the peptide-transferase site (P site), which houses the tRNA bound to the nascent polypeptide chain and finally to the exit site (E site) where deacylated tRNAs dissociate from the ribosome. The meticulous execution of all translation steps, initiation, elongation and termination, is required for proper protein synthesis.

### *1.1.1 Translation Initiation*

To initiate a new round of translation the 30S subunit must bind mRNA and initiator N-formyl-methionine tRNA<sup>fMet</sup> (**Figure 1.2**). Three initiation factors (IF-1 to 3) aid in this assembly process. Initiation of translation begins with a 30S subunit bound to initiation factor 3 (IF-3), which inhibits non-productive 50S binding (6). Binding of the mRNA is directed by the base pairing of the mRNA Shine-Delgarno sequence with the 3' end of the 16S rRNA to properly position the start codon (AUG or GUG) in the P site (7). IF-2, which has affinity for tRNA<sup>fMet</sup> delivers the tRNA to the P site, while IF-1 binds 30S, blocking the A site and interacting with IF-2 to position tRNA<sup>fMet</sup> (8). In addition to its role in preventing 50S binding, IF-3 also increases the efficiency and fidelity of the codon-anticodon interaction (9, 10). To allow for 50S association, first, IF-1 and IF-3 dissociate from the 30S initiation complex followed by IF-2 orienting the aminoacylated CCA end of the tRNA into the peptidyl-transferase center (PTC) of the 50S subunit (11,12). Once the 70S has formed, IF-2 hydrolyses its bound GTP and dissociates from the ribosome that is now ready to begin elongation of the polypeptide chain.

### 1.1.2 Translation Elongation

tRNAs and two GTPases, elongation factor-Tu (EF-Tu) and elongation factor-G (EF-G), work with the 70S ribosome to translate the mRNA message into a protein. As discussed above, tRNAs are ribonucleic acids that serve as an adaptor between the mRNA codon and an amino acid. There are 86 tRNAs in *E. coli* for the standard 20 amino acids (13). The exact size of each tRNA varies, but each tRNA is roughly 76 nucleotides and all tRNAs have similar secondary and tertiary structures (14). Each tRNA is aminoacylated by its cognate amino acyl tRNA synthetase which covalently links the correct amino acid to the 3' end of the tRNA via an ester linkage. To protect the ester bond and deliver the now aminoacylated (or charged) tRNA to the ribosome, the tRNA is bound to the ribosome-associated GTPase EF-Tu.

The translation elongation cycle begins with a vacant A site and tRNA bound in the P site (either tRNA<sup>fmet</sup> or a tRNA linked to the nascent peptide chain) of the 70S ribosome (**Figure 1.3**). In the latter case, corresponding to a later round of elongation, the growing polypeptide chain snakes through the peptide exit tunnel where it is exposed to the cellular environment. To extend the polypeptide chain, the correct aminoacylated tRNA has to be delivered to the ribosome by GTP-bound EF-Tu. Base-pairing between the first two nucleotides of the mRNA A-site codon and the tRNA anti-codon is inspected by nucleotides of the 16S rRNA: A1492, A1493 and G530 (15). The 30S then undergoes a conformational change and 'closes', creating new contacts between EF-Tu and the shoulder domain of the 30S subunit (16). These structural rearrangements promote changes in EF-Tu allowing for GTP hydrolysis and dissociation of EF-Tu-GDP and accommodation of the tRNA into the A site. GDP is removed from EF-Tu and exchanged for GTP by the guanine exchange factor elongation factor-Ts (EF-Ts) (17).

Once the A-site tRNA has been accommodated, spontaneous peptide bond formation occurs in the peptidyl transferase center (PTC). 23S rRNA nucleotide A2451 has been implicated in peptide bond formation, but its exact role is still highly debated (18,19). After peptide bond

formation, the peptide chain is attached to the A-site tRNA and the ribosome undergoes a spontaneous ratcheting movement that leaves the 3' end of the A-site tRNA in the 50S P site, with its anticodon in the 30S A site. Concurrently the P-site tRNA moves its 3' end to the 50S E site with the anticodon in the 30S P site, resulting in an arrangement called the hybrid state of the ribosome.

In order for a subsequent amino acid to be added to the elongating amino acid chain, the tRNAs and mRNA need to be shifted, or translocated, by one codon on the 30S subunit to fully open the A site. This translocation is performed by the GTPase EF-G. EF-G, bound to GTP, preferentially binds the ribosome in a ratcheted conformation, and in doing so, stabilizes the hybrid tRNA state. EF-G interacts with both 50S and 30S subunits including the GTPase activation center (GTPase center) of the 50S, which includes the sacrin-ricin loop (H95), the L11-binding domain of 23S rRNA (H42-44) and ribosomal proteins L11 and L12 (20, 21). Proper positioning of EF-G domain IV near the anticodon of the A-site tRNA disrupts interactions between A1942, A1943 and G530 and the codon-anticodon base pair (22). Coupled with hydrolysis of GTP by EF-G, movement of the 30S head domain (see **Figure 1.1**) causes the ribosome to unratchet, translocating the mRNA and tRNA, and rearranging the ribosome into the classical conformation and dissociating EF-G (23, 24). This cycle of aminoacylated tRNA delivery, peptide transfer and mRNA translocation continues until a stop codon is encountered in the A site.

### *1.1.3 Translation Termination*

A stop codon in the A site signals the end of the polypeptide chain (**Figure 1.4**). Stop codons are not recognized by tRNA, but instead recognized by the Class 1 release factors, RF-1 and RF-2, which recognize UAA/UAG, and UAA/UGA, respectively (25). Upon binding the ribosome, the RF1/RF2 structure adopts an open conformation that allows the RF to interrogate the stop codon in the 30S A site and promote peptide chain release in the PTC (26, 27, 28). Release factor 3 (RF-3), a GTPase, binds the ribosome to release bound RF-1/RF-2 and causes rotation of, and

conformational changes in the 30S that promote tRNA movement from the P site to E site. Upon hydrolyzing GTP RF-3 dissociates from the ribosome.

After the peptide chain has been released, the 70S ribosome is still assembled and contains bound mRNA and tRNA. Ribosome recycling factor (RRF) and EF-G are responsible for dissociating the 30S and 50S subunits. RRF binding disrupts intersubunit bridges and coupled with EF-G binding and GTP hydrolysis, is sufficient to dissociate the two subunits (29, 30, 31, 32). After dissociation, IF-3 rebinds the 30S and prepares the subunit for another round of translation (6).

## 1.2 ANTIBIOTICS INHIBIT IMPORTANT FUNCTIONAL AREAS OF THE RIBOSOME

Antibiotics revolutionized medicine when they were introduced in the 1940's (33). Antibiotics exploit differences in unique aspects of prokaryote cell biology, such as the bacterial cell wall, or common machinery that is sufficiently structurally and functionally divergent from eukaryotes, like the ribosome. The ribosome is the target for a variety of different classes of antibiotics, each inhibiting a different functional area (34, 35). Studies investigating how antibiotics inhibit the ribosome expand our understanding of the functional intricacies of the machine, which could underpin the development of new or modified antibiotics. The following sections describe mechanisms for select ribosome-targeting antibiotics to illustrate important functional centers of the ribosome and introduce antibiotics that are used as tools to dissect ribosome biology including those relevant to the studies in Chapters 2-5.

### *1.2.1 Peptide Exit Tunnel*

The peptide exit tunnel (PET) is located near the PTC and is gated by 23S rRNA nucleotides A2058 and A2059. Antibiotics of the macrolide, ketolide (a synthetic class of antibiotics derived from macrolides), lincosamide, and streptogramin B classes have different chemical structures, but all bind in the peptide exit tunnel and disrupt the elongation of the peptide chain (**Figure 1.5A**). Biochemical experiments with defined translation systems showed that different macrolide

antibiotics inhibit the growth of the polypeptide chain at defined lengths and can even disrupt peptide bond formation if the molecule extends close to the PTC (36, 37). Crystal structures of antibiotics bound to 50S subunits or 70S ribosomes support these biochemical findings as all of these antibiotics bind near A2058, A2059, and some antibiotics extend chemical moieties near the PTC thereby disrupting peptide bond formation (38, 39).

### *1.2.2 Peptidyl-Transferase Center*

Several classes of antibiotics bind and inhibit the PTC including phenicols (e.g. chloramphenicol), oxazolidinones (e.g. linezolid) and hygromycin A (**Figure 1.5B**) (40). Biochemical studies have shown that chloramphenicol and hygromycin A compete for the same binding site in the PTC (41). Structures of either bound, show that these two antibiotics allow for tRNAs to bind, but the CCA end of the tRNA cannot be accommodated into the acceptor site of the PTC inhibiting peptide bond formation (38, 42). Additionally, the antibiotic puromycin has been used extensively in characterizing the ribosome as it is a mimic of the tRNA amino-acylated CCA end and disrupts the elongation of the nascent peptide chain by binding in the acceptor site of the PTC, and promoting the transfer of the nascent polypeptide chain to the antibiotic (43).

### *1.2.3 30S Subunit and Decoding Center*

The decoding center of the 30S subunit is responsible for interrogating the codon-anticodon base pairing. Conserved nucleotides A1492/A1493 and G530 flip out of h44 and the shoulder domain, respectively, and interact with the minor groove of the first two base pairs of the codon-anticodon pair. A productive interaction, leads to 30S domain closure and the timely activation of GTP-hydrolysis on EF-Tu (15,16,44). Antibiotics of the aminoglycoside class disrupt the fidelity of decoding by binding h44 and pushing A1492 and A1493 into a state resembling that of a proper codon-anticodon pair (Figure 5C) (45,46). This structural change decreases the proofreading ability of the ribosome, increasing the miscoding of the mRNA (47). Furthermore, the constant

interrogation of the codon-anticodon pair by A1492 and A1493 disrupts mRNA translocation as tRNA affinity is increased, which increases the activation energy needed to break this interaction and translocate the mRNA and tRNAs, further disrupting translation (48,49).

The decoding center is also the binding site of two similar tuberactinomycin cyclic peptide antibiotics, viomycin and capreomycin. These antibiotics share a partially overlapping binding site with aminoglycosides on the 30S subunit, but also contact the 50S through the intersubunit bridge made up of h44 and H69 (**Figure 1.5C**) (50). Like aminoglycosides, viomycin and capreomycin flip A1492 and A1493 out of h44 to interrogate the codon-anticodon base pairing, however they exert their inhibitory effect by disrupting translocation (49-52).

#### *1.2.4 GTPase Activation Center and GTPases*

The ribosome associated GTPases, EF-Tu and EF-G, as well as the GTPase activation center (GTPase center) are other antibiotic targets. The GTPase center is made up of ribosomal proteins L11 and L7/L12, and the 23S rRNA L11-binding domain (helices H42, H43 and H44) and sarcin ricin loop (H95). Thiopeptide antibiotics including thiostrepton, nosiheptide and micrococcin bind to the GTPase center, disrupting the interactions between the ribosomal GTPases and the ribosome (53). Biochemical studies and X-ray crystal structures of the ribosome show that thiostrepton binds at the interface between the RNA (the apex of H43 and H44, which fold against each other) and the L11-amino-terminal domain (NTD, **Figure 1.5D**) (53-55).

Thiostrepton was initially shown to inhibit EF-G binding and translocation, until more recent kinetic studies revealed that thiostrepton specifically inhibits EF-G enzymatic turnover by preventing inorganic phosphate release, a step prior to mRNA translocation (56,57). While thiostrepton and micrococcin bind the ribosome in a similar location, micrococcin disrupts EF-G by stimulating its GTPase activity, rather than inhibiting the activity (58,59). Thiostrepton and micrococcin can also inhibit the IF-2-dependent initiation complex as IF-2 and EF-G share an overlapping ribosome footprint (58).

Antibiotics also directly bind to EF-G and EF-Tu, to inhibit their functions. Kirromycin does not bind near the GTP molecule, but its binding causes conformational changes in EF-Tu that mimic a GTP bound state (**Figure 1.6A**) (60). In the presence of kirromycin, GTP bound to EF-Tu can be hydrolyzed and EF-Tu-tRNA, in the absence of GTP, is delivered to the ribosome. This results in translation inhibition as EF-Tu fails to dissociate from the ribosome (61-63).

Fusidic acid binds near the GTP cofactor of EF-G (**Figure 1.6B**). Biochemical and structural studies of EF-G suggest that fusidic acid binds EF-G only after it has bound the ribosome and hydrolyzed GTP, as the antibiotic has low affinity for free EF-G and the antibiotic stabilizes a EF-G conformational state which happens only after GTP hydrolysis (21,64). Additionally, since EF-G functions in ribosome recycling, fusidic acid also interferes with that process (65).

It is clear from the discussions above, that antibiotics have been found to disrupt virtually every important step in protein synthesis from initiation to ribosome recycling. Antibiotics serve as life-saving therapeutics for the promotion of human health and are fundamental to many advances of modern medicine including surgeries and treatments requiring immune suppression such as organ transplants and chemotherapy for the treatment of cancer. Antibiotics have additionally served as tools to dissect the elegant molecular machine that is the ribosome. As many of these antibiotics are natural products originally isolated from bacteria, understanding how drug producers resist their toxic product and when and how such mechanisms can be transferred to human pathogens is critical in an era threatened by the continued emergence of multiple antibiotic-resistant pathogens.

### 1.3 METHYLATION OF THE RIBOSOMAL MACHINERY: FINE TUNING RIBOSOME FUNCTION, ANTIBIOTIC RESISTANCE AND PATHOGENESIS

Ribosome function is predicated on the proper folding and assembly of its constituent rRNA and ribosomal protein components, as well as its interactions with ribosome associated factors.

However, proper function is also dependent on posttranscriptional and posttranslational modification. rRNA and tRNAs are highly decorated with posttranscriptional modifications, many of which are essential for error-free translation. Additionally, posttranslational modifications fine-tune enzymatic functions and can globally affect translation.

### *1.3.1 Posttranscriptional Modifications of rRNA*

There are 35 constitutive modifications on the *E. coli* ribosome including the 2'-O-methylation of the ribose, mono or dimethylation of the nucleotide base, pseudouridylation and saturation of the uridine ring creating dihydrouridine (and combinations of these, for instance 23S rRNA m<sup>3</sup>Ψ1915 or 16S rRNA m<sup>4</sup>Cm1402). Methylations are the most common modifications with 24 identified in the *E. coli* ribosome (**Figure 1.7**). All modifications have recently been identified in ribosome structures revealing a network of modifications and explaining decades of biochemical work describing their locations and functions (63).

#### 1.3.1.1 Constitutive modifications aid in ribosome function: 30S subunit

When rRNA modifications are highlighted within the ribosome structure, they cluster at two functional centers: the decoding center of the 30S subunit (A and P-tRNA binding sites) and the PTC of the 50S subunit. Posttranscriptional modifications of 16S rRNA m<sup>4</sup>Cm1402 and m<sup>3</sup>U1498 are positioned between and interact with the mRNA backbone and m<sup>6</sup><sub>2</sub>A1519 and m<sup>6</sup><sub>2</sub>A1518 in the P site (**Figure 1.7B**). Loss of m<sup>4</sup>Cm1402 methylation increased the use of non-AUG start codons and decreased the rate of stop codon read through, suggesting that this modification fine-tunes the decoding center (66). Additionally, deletion of RsmA (KsgA), the A1518/A1519 di-methyltransferase, increased non-AUG start codon usage and exhibited a cold-sensitive growth phenotype with ribosome assembly defects (67,68). RmsA is also proposed to remain bound to the assembling 30S subunit, incorporating its modifications as a signal for

completed 30S assembly confirming a role for these modifications in ribosome function and assembly (69).

When initiator tRNA binds the P site, m<sup>2</sup>G966 and m<sup>5</sup>C967 secure the positioning of the tRNA anticodon–codon base pair. Deletion of both RsmB (G967) and RsmD (C967) decreased bacterial fitness and a translation initiation defect was observed, suggesting that these methylations are important for translation initiation, but have some redundancy in the action (70). Furthermore, this translation initiation defect causes differential expression of translation-regulated genes such as the tryptophan operon, confirming a role for these modifications in fine-tuning translation (71).

#### 1.3.1.2 Constitutive modifications aid in ribosome function: 50S subunit

The 2'-O-methylation of U2552 is important for the function and assembly of the PTC. This nucleotide is 5' to G2553, which stabilizes the CCA end of the A-site tRNA. Deletion of the methyltransferase, RlmE (formerly RrmJ, or FtsJ) confers a bacterial growth defect and decreases the rate of programmed frame-shifting and stop codon read through, suggesting a role in translational accuracy (72). Additionally, this modification serves as an important late step in ribosome biogenesis as its loss results in 50S subunit assembly defects (73). Furthermore, addition of the methyltransferase during *in vitro* reconstitution of 50S subunits, aids in ribosome assembly, promoting rRNA domain interactions and ribosomal protein L36 binding and resulting in the organization of the PTC (74). These studies demonstrate the importance of this modification in 50S assembly and function.

Methylations within the PET are important for ribosome function, ribosome assembly and antibiotic resistance (discussed below). Loss of methylation at m<sup>1</sup>G745 by RlmA resulted in drastic changes in cellular growth and defects in ribosome function including decreased peptide elongation and a decrease in the number of 70S particles and polysomes (75). Additionally, loss of m<sup>6</sup>A1618 modification by RlmF also decreased cellular growth and fitness and, since

methylation only occurred on partially assembled 50S subunits, this methylation is likely to be important for ribosome assembly (76). These findings illustrate the importance of rRNA methylations in ribosome assembly in the PET.

Not all methylations are important for the function or ribosome assembly under laboratory conditions. Defects in cellular fitness were observed during competition growth experiments between individual methyltransferase deleted *E. coli* strains (RlmI (m<sup>5</sup>C1962), RlmH (m<sup>3</sup>Ψ1915), RlmM (Cm24980)) and control strains that otherwise have no cellular growth or ribosome assembly phenotype (77,78). Further, loss methylation of m<sup>6</sup>A2030 by RlmJ, Gm2251 by RlmB, m<sup>5</sup>U1939 by RlmD (formerly RumA) displayed no phenotype when grown under laboratory conditions (79-81). However, these modifications could be required to fine-tune the ribosome function under other conditions like cellular stress.

### 1.3.1.3 Constitutive modifications aid in antibiotic binding and inhibition

As both antibiotic binding sites and rRNA modifications cluster at functional areas of the ribosome, has been be hypothesized that they influence each other. Indeed, some modifications are not only important for ribosome function, but make up the binding site of antibiotics and removing such modifications can lead to antibiotic resistance. For example, in a *Staphylococcus aureus* isolate, loss of RlmN, the 23S m<sup>2</sup>A2503 methyltransferase, conferred resistance to the antibiotic linezolid (82).

Modifications in the decoding center are also important for binding antibiotics. Binding of the aminoglycoside antibiotic kasugamycin to the 30S subunit is dependent on two 16S rRNA dimethylations, m<sup>6</sup><sub>2</sub>A1518 and m<sup>6</sup><sub>2</sub>1519. Loss of these modifications by mutation or deletion of the methyltransferase RsmA (KsgA) renders the ribosomes drug resistant (83). Additionally, m<sup>5</sup>G1407 in the A site interacts with aminoglycoside antibiotics that bind near h44 and loss of this methylation decreases aminoglycoside binding and has a modest effect in antibiotic

susceptibility (84). In *Mycobacteria tuberculosis* loss of the housekeeping methyltransferase TlyA, which incorporates 16S rRNA Cm1409 and 23S rRNA Cm1920 modifications, causes resistance to the cyclic peptide antibiotics capreomycin and viomycin used to treat multi-drug resistant TB (**Figure 1.8A**) (85). Documenting and understanding the role of constitutive methylations and how they differ between *E. coli* and pathogenic bacteria is important for understanding resistance and developing new therapies.

#### 1.3.1.4 Posttranscriptional modifications can confer antibiotic resistance

Just as loss of constitutive methylations can disrupt antibiotic binding, antibiotic-producing bacteria commonly encode rRNA methyltransferases that block their own antibiotic products from binding their target rRNA sites. Methylation typically causes a direct steric clash with the antibiotic, disrupting binding and causing a high-level of resistance (86). While these antibiotic-resistance methyltransferases are most commonly found in antibiotic-producing bacteria to protect themselves from their own toxic product, these enzymes can be spread by lateral gene transfer to pathogenic bacteria contributing to the antibiotic resistance epidemic (87).

As described above, the PET is a major binding site for the clinically relevant macrolide and ketolide antibiotics. Members of the Erm family of methyltransferases either N<sup>6</sup>-mono- or dimethylate A2058 causing resistance to these drugs (see **Figure 1.5A**) (88,89). Erm enzymes are endogenous to *Streptomyces fradiae* (tylosin producer) and *Streptomyces erythreus* (erythromycin producer) and have been found in *E. coli*, *B. subtilis*, *Clostridium perfringens*, *Streptococcus pneumoniae*, *M. tuberculosis* (90,91). With this wide assortment of bacteria that possess Erm it is not surprising that these resistance determinants have been spread by lateral gene transfer (92).

Resistance to antibiotics that bind the PTC, including phenicols (chloramphenicol), lincosamides (clindamycin), and streptogramin A, can be caused by methylation of m<sup>8</sup>A2503 by the Cfr methyltransferase (see **Figure 1.5B**) (93,94). This methyltransferase has been identified on

plasmids isolated from *Staphylococcus sciuri* and *Staphylococcus aureus* from animal sources as well as humans (95,96). As Cfr confers resistance to a number of clinically relevant antibiotics, the spread of this enzyme to pathogens diminishes treatment options for drug-resistant infections.

Resistance to aminoglycosides antibiotics occurs through methylation of the 16S rRNA at m<sup>7</sup>G1405 and m<sup>1</sup>A1408 (see **Figure 1.8B**). The m<sup>7</sup>G1405 modification confers resistance to all 4,6-disubstituted deoxystreptamine aminoglycosides while m<sup>1</sup>A1408 confers resistance to some 4,5 and 4,6-disubstituted members of aminoglycoside family including kanamycin and apramycin (97). G1405 modifiers have been found in antibiotic-producing bacteria (eg. Sgm from the sisomicin producer *Micromonospora zionensis*) and on mobile genetic elements including transposons and plasmids (ArmA, RmtA-G) (98-100). Members of the A1408 methyltransferase family are typically from antibiotic-producing bacteria (eg. KamB from *Streptomyces tenebrarius*) but one member, NpmA, was found on a plasmid from an *E. coli* (ARS3) clinical isolate (101-103). The presence of these genes on mobile genetic elements threatens the clinical effectiveness of these antibiotics if these genes continue to spread among pathogens.

Modification of the antibiotic binding site conferring resistance has also been documented for GTPase center targeting antibiotics thiostrepton and nosiheptide (**Figure 1.5D**). Resistance to these antibiotics is conferred by 2'-O-methylation of A1067 by *tsr* and *nhr* (104). However, since their usage has been limited in the clinic, resistance to thiostrepton and nosiheptide has only been documented in the antibiotic-producing bacteria *Streptomyces azureus* and *Streptomyces actuosus*, respectively (105,106). While not a threat in the clinic today, Tsr and Nhr, are part of the 'antibiotic resistome' that describes all potential mechanisms of resistance that could spread given the correct selection pressures.

Methylation of the antibiotic target site is one mechanism of antibiotic resistance that threatens treatment options in the clinic. As the spread of mobile genetic elements containing antibiotic resistance genes increase, the effectiveness and use of the safest antibiotics declines. This forces

clinicians to turn to second-line drugs and combinations of drugs, which increases the toxicity of the treatment and decreases the effectiveness of the treatment. In order to combat resistance, a complete understanding antibiotic resistance conferring enzymes should be described.

### *1.3.2 Posttranslational Modifications*

#### *1.3.2.1 Ribosomal protein modifications*

Like rRNA, ribosomal proteins and associated factors are also chemically modified. Six ribosomal proteins are methylated (S11, L3, L11, L7/L12, L16, L33), three are acetylated (S5, S18, L7) and one is methylthiolated (S12). While all three acetyltransferases have been identified, the methyltransferases for S11, L7/L12, L16 and L33 have yet to be identified. PrmA, the L11 methyltransferase, methylates three amino acids of *E. coli* L11: Lys3, Lys39 and the amino group of the N-terminal alanine (107,108). All three methylations occur on the flexible NTD of the protein that interacts with ribosomal GTPases as part of the GTPase center, however the modifications appear dispensable for ribosome function under normal growth conditions (109).

PrmB methylates L3 on the amide of Gln150 (110). Loss of PrmB confers a cold growth sensitivity. As L3 is one of the first proteins assembled onto the 23S rRNA, it is likely that this modification is important for ribosome assembly (111).

The identity of L7/L12 is linked to its posttranslational modifications. These proteins have the same primary sequence, but L7 is monomethylated at Lys81 and L12 is acetylated at Ser1 by RimL (112). Methylation is temperature dependent with almost no methylation at 37°C, but increasing to ~60% as the temperature is decreased (113). Acetylation of L12 is dependent on the growth conditions, with 85% not acetylated during log phase and the extent of modification increasing as cells approach stationary phase (114). The function of these modifications is not fully understood.

RimJ and RimI acetylate S5 and S18, respectively (115). Deletion of RimI showed no deleterious effect on cell growth, while a cold growth phenotype was observed for RimJ due to the disruption of ribosome assembly and reduction of translational accuracy (116).

#### 1.3.2.2 Modifications of ribosome factors

As ribosomal factors control translation, it should not be surprising that their activity is modulated by posttranslational modifications. PrmC methylates Class I release factors (RF1/2), which detect the presence of a stop codon in the ribosomal A site and stimulate peptide bond release (117). The Gln252 of the GGQ motif of RF1/2, which probes the tRNA in the PTC stimulating peptide release, is methylated. Loss of this modification decreases termination efficiency of the ribosome (118,119).

The elongation factor EF-P aids the ribosome in translating poly-proline stretches (120,121). EF-P is posttranslationally modified with  $\beta$ -lysine at Lys34 (122,123). Modified EF-P increased peptide-bond formation (in a N-formyl-methiyl-puromycin reaction) by four-fold over unmodified EF-P and the mutation K34A inactivated EF-P, demonstrating the importance of this modified lysine (123).

#### 1.3.2.3 Control of EF-Tu function by modification during different phases of bacterial growth

The GTPase EF-Tu is the target for multiple modifications including methylation and phosphorylation. Three sites of phosphorylation have been described. In the *B. subtilis* forespore, a metabolically dormant entity, YabT phosphorylates the conserved Thr63 near the GTP binding site. This phosphorylation allows GTP to bind, but decreases GTP hydrolysis and modulates EF-Tu function in translation, likely keeping the forespore in a metabolically inactive state (124). In *M. tuberculosis* phosphorylation at as many as three unidentified sites resulted in decreased GTP binding, but also rendered the enzyme insensitive to the antibiotic kirromycin, suggesting a protective role in translation for the modification (125). Lastly, the toxin Doc, which is found in

*E. coli* and other species of Entrobacteria including pathogens, phosphorylates Thr382 inactivating EF-Tu down-regulating translation during the bacterial stress response (126).

Methylation has also been documented to regulate the function of EF-Tu. EF-Tu Lys56 methylation depends on *E. coli* growth phase with mono-methylation identified during logarithmic growth and di-methylation during stationary phase. This modification decreases GTP hydrolysis, but its biological function is not well understood (127). Also in *E. coli*, methylation of a membrane bound fraction of EF-Tu increases in response to nutrient deprivation, however the biological role for this methylation has not been elucidated (128,129). In *Pseudomonas aeruginosa* EF-Tu is trimethylated at Lys5 (130). However, this modification is only present when the bacterium is grown near environmental temperatures (25°C), rather than host temperatures (37°C). A role for this modification in translation has not been studied, but loss of the methyltransferase decreases the adherence to and infection of host cells by *P. aeruginosa* (131). These studies suggest a link between the bacterium's environment and a role for EF-Tu trimethylation either in translation or in adherence.

#### 1.4 PREVAILING QUESTIONS IN METHYLTRANSFERASE STRUCTURE AND FUNCTION

It is evident that posttranscriptional and posttranslational modifications of the translation machinery are necessary for ribosome function in translating proteins and for bacterial survival when adapting to changing environments (such as environmental stressors or the presence of antibiotics). While the functions of many methylations have been described, less is known about the methyltransferases and the molecular mechanisms needed to catalyze the reactions including: enzyme structure and *S*-adenosyl-L-methionine (SAM) binding, substrate recognition and catalytic mechanisms (**Figure 1.9**). In the following chapters, I describe studies that examine the molecular characteristics of three methyltransferases, defined by their methyltransferase class, to understand their enzyme structure and features that regulate their activity.

Two of the methyltransferases TlyA and EftM, are belong to the most common family, Class I, containing a Rossmann-like methyltransferase fold. Within this fold, specific conserved motifs have been identified (I-V) including the SAM-binding motif (motif I) with a consensus sequence GxGxG (132-134). Additional structural elements or domains can accessorize the methyltransferase domain, for example to confer specific substrate recognition. Our studies of the rRNA methyltransferase TlyA from *M. tuberculosis* and EF-Tu trimethyltransferase EftM from *P. aeruginosa* will address the following questions:

- What is the structure of these methyltransferases and what auxiliary domains decorate the methyltransferase domain?
- What structural elements govern SAM binding and with what affinity do these enzymes bind SAM?
- What controls the temperature regulation of the EftM modification?

Studies of a third methyltransferase, Tsr, will extend initial characterizations of the structure, which defined the enzyme as a Class IV SpoU/TrmD (SPOUT) methyltransferase (135). The majority of identified SPOUT methyltransferases are obligate homodimers with amino acids of each protomer functioning in each round of catalysis. Like Class I methyltransferases, SPOUT methyltransferase contain additional features or domains important for substrate recognition. Our studies of the 23S rRNA methyltransferase Tsr from *S. azureus* will address the following questions:

- What role does the dimerization of the enzyme play in substrate recognition and catalysis?
- How does Tsr recognize its rRNA substrate?

Through these studies I gained novel insights into methyltransferase structure, SAM binding and substrate recognition. Together these studies will describe mechanisms that control enzyme

activity that influences important biological processes, and could underpin the development of future antibiotics.

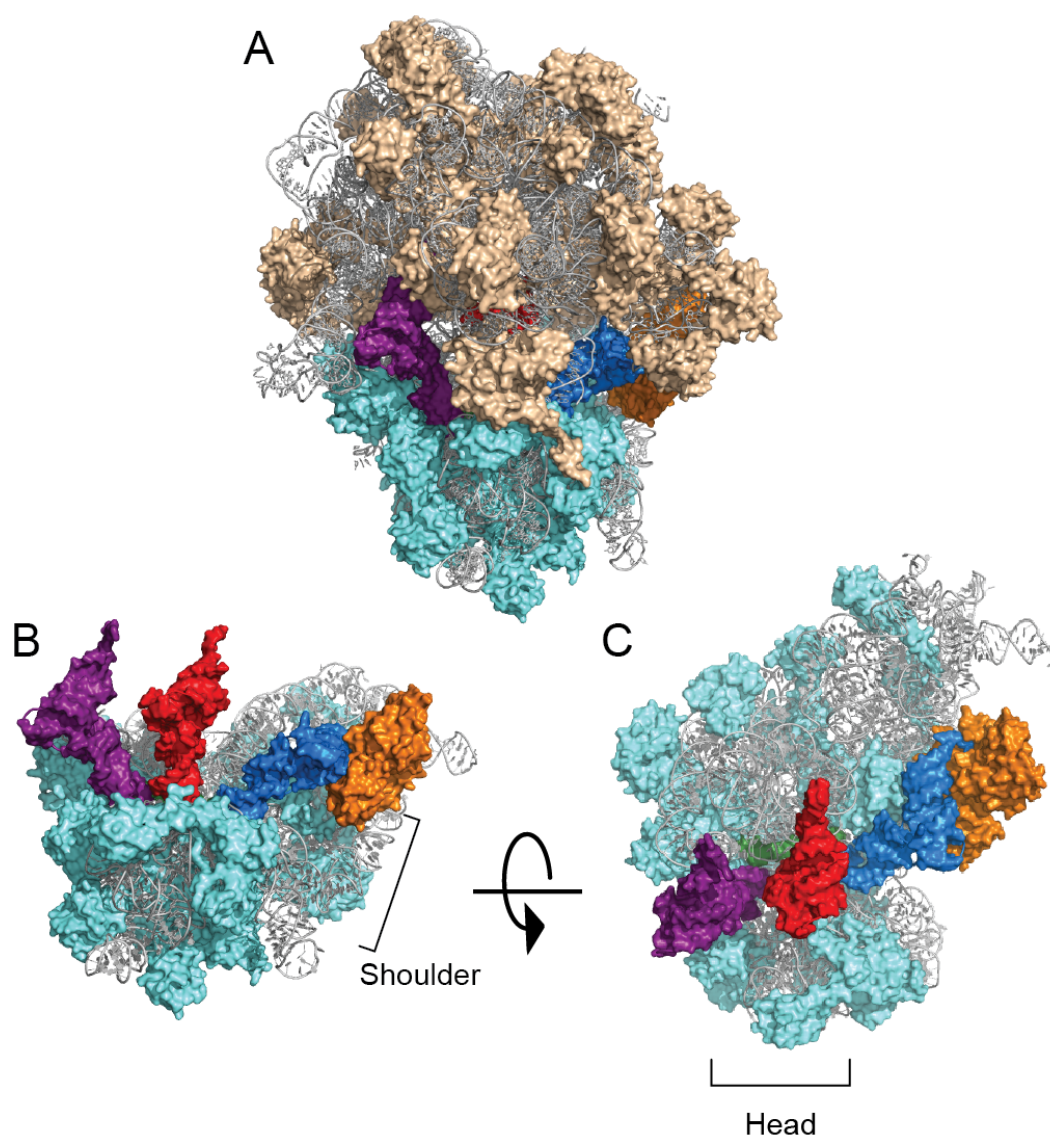


**FIGURE 1.1 Structure of the bacterial 70S ribosome.** *A*, Crystal structure of the 70S ribosome bound to E, P and A-site tRNAs and EF-Tu (PDB ID: 5AFI). Components are colored as follows: rRNA (grey), 50S proteins (tan), 30S proteins (cyan), E-site tRNA (purple), P-site tRNA (magenta), A-site tRNA (blue), and EF-Tu (orange). *B*, Front view of 30S with components colored as (A). The general location of the shoulder domain is shown. *C*, Top view of 30S as colored in (A) and also showing the mRNA (green) and general location of 30S head domain.

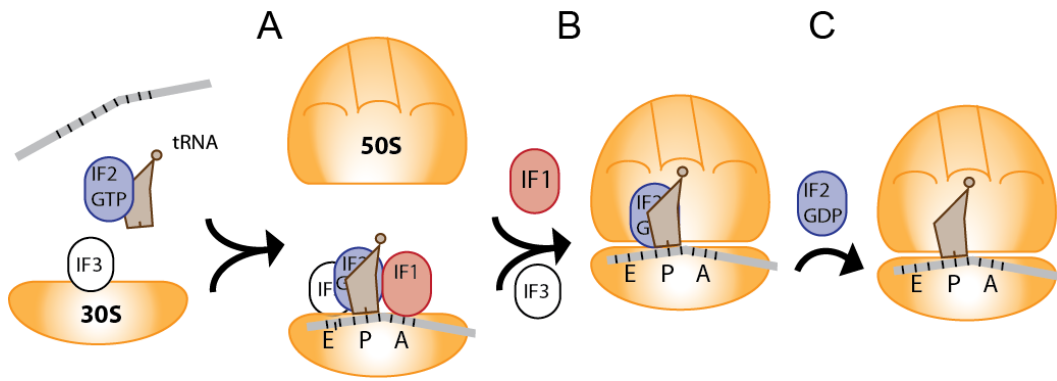


**FIGURE 1.2 Translation initiation.** *A*, Initiator fmet-tRNA<sup>fmet</sup> (brown) is positioned in the tRNA P site in the 30S by initiation factors (IF1- IF3). *B*, IF-1 and IF-3 dissociate before the GTPase IF-2, which helps position the 50S subunit onto the 30S. *C*, Upon GTP hydrolysis IF-2 dissociates and the ribosome is poised for elongation.

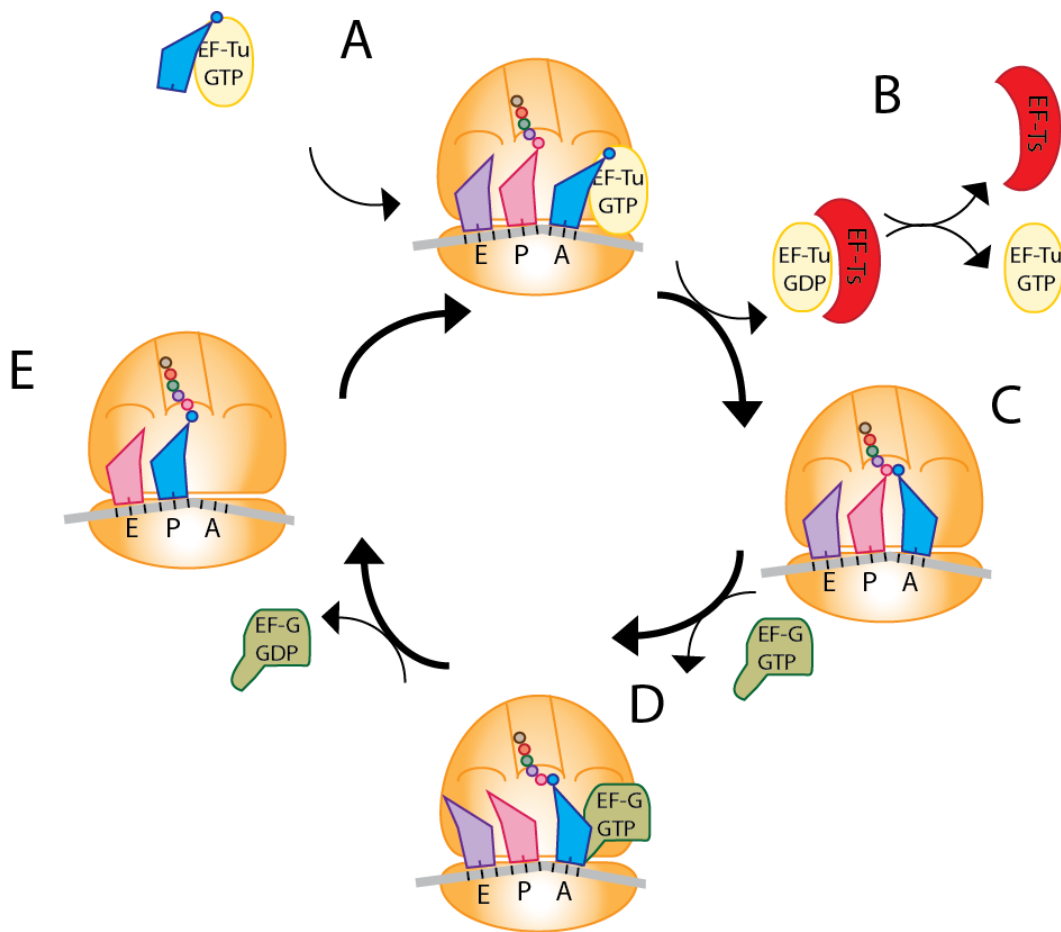


**FIGURE 1.3 Translation elongation.** *A*, EF-Tu delivers tRNA to the A site and hydrolyses GTP. *B*, EF-Ts acts as a guanine exchange factor dissociating GDP from EF-Tu. *C*, the tRNA is accommodated into the peptidyl-transferase center (PTC) and the nascent peptide chain is transferred to the A site amino acid through peptide bond formation. *D*, EF-G binds near the A site and translocates the tRNA and mRNA one codon. After EF-G hydrolyses GTP, it dissociates leaving an empty A site, (*E*).

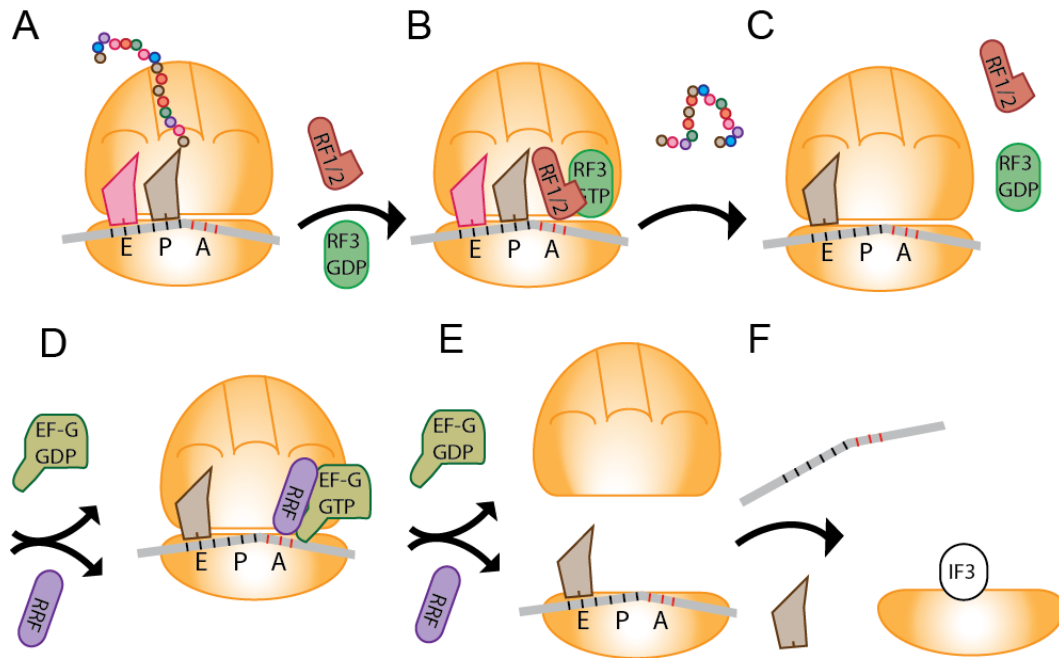


**FIGURE 1.4 Translation termination and ribosome recycling.** *A*, A stop codon (red ticks) appears in the A site. *B*, Release Factor 1 or 2 (RF1/2, depending on the codon) recognizes the stop codon and binds in the A site with GTP-bound RF-3 and stimulates hydrolysis of the peptide chain from the P-site tRNA. *C*, RF-3 hydrolyzes GTP and RF1/2 and RF-3 dissociate. *D*, Ribosome recycling factor (RRF) and EF-G bind in the A site and with GTP hydrolysis, dissociate the 50S and 30S subunits shown in *E*. *F*, IF-3 binds 30S preparing it for another round of protein synthesis (see Figure 1.2).

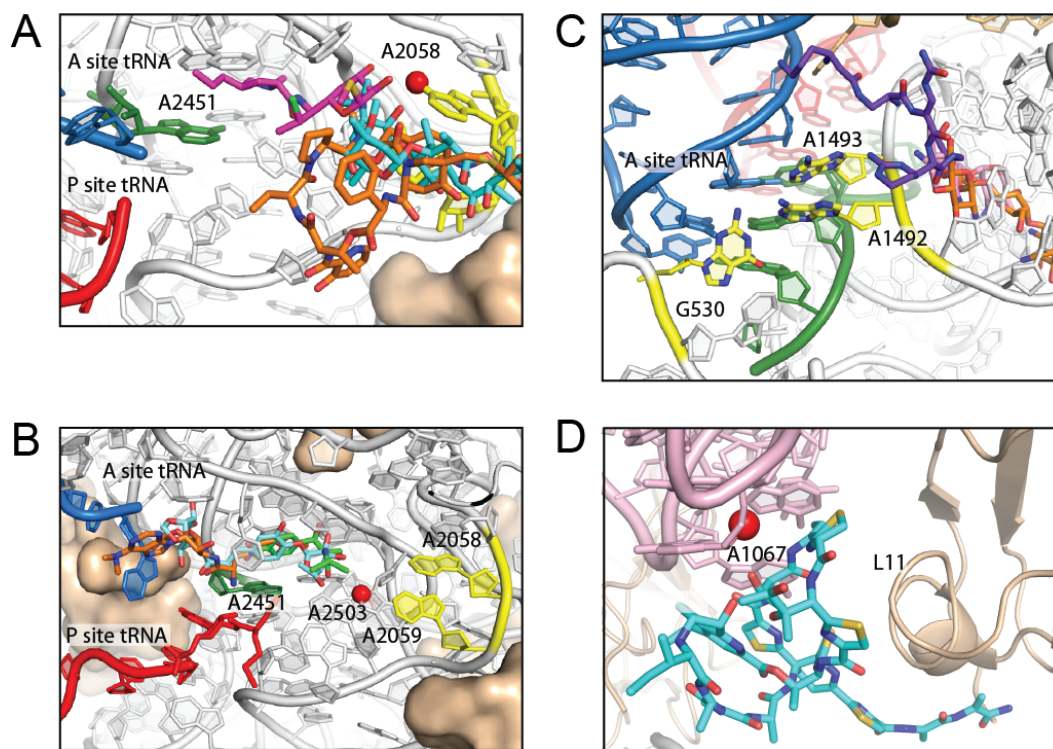


**FIGURE 1.5 Antibiotic binding sites in the ribosome.** *A.* Antibiotics bind in the peptide exit tunnel (PET). Overlay of 70S structures bound to examples of macrolide (PDB: 4V7U, erythromycin, cyan), lincosamide (PDB: 4V7V, clindamycin, pink), streptogramin B (PDB: 4V56, quinuprist, orange). m<sup>6</sup>A2058 confers resistance to macrolides, lincosamides and streptogramin B (red sphere). Ribosome features are colored as follows: 23S nucleotides A2058 and A2059 designate the entrance to the PET (yellow), A2451 designates the PTC (green), rRNA (gray), r-proteins (tan surface), P-site tRNA (red) and A-site tRNA (blue). *B.* Antibiotics bound to the peptidyl-transferase center. Overlay of 70S structures of chloramphenicol (PDB: 4V7W, green), hygromycin A (PDB: 5D0Y, cyan), CC-puromycin (PDB:1VY6, orange). m<sup>8</sup>A2503 methylation confers resistance to these antibiotics (red sphere). Coloring same as (A). *C.* Antibiotics binding the decoding center. Overlay of 30S structures bound to capreomycin (PDB: 4V7M, purple), paramomycin (PDB: 4V5D, pink), neomycin (PDB: 4V52, orange). mRNA (green), A-site tRNA (pink), ‘decoding’ 16S nucleotides (G530, A1492, A1493, yellow). *D.* Thiostrepton bound to 50S subunit GTPase activation center (PDB: 3CF5, blue). 2’-O-methylation of A1067 confers thiostrepton resistance (red sphere). Coloring scheme is as follows: L11 (tan), L11-binding domain of 23S rRNA (pink),

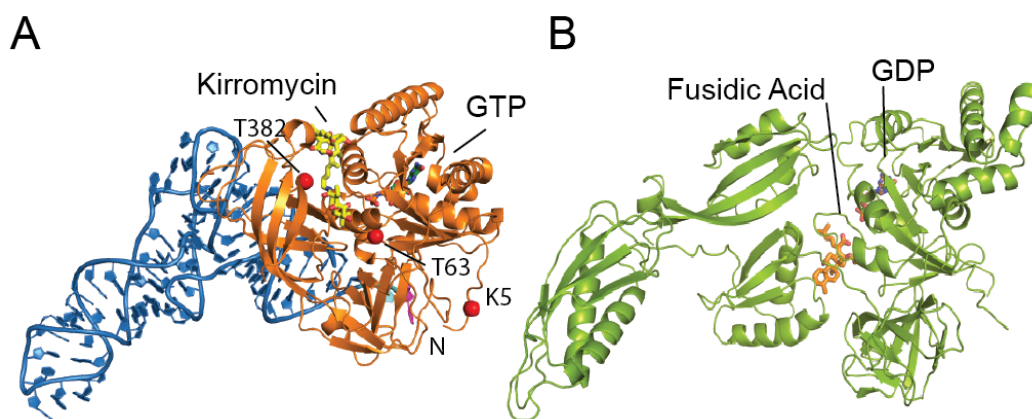


**FIGURE 1.6 Ribosomal GTPases EF-Tu and EF-G bound to inhibitory antibiotics.** *A*, EF-Tu: tRNA complex bound to kirromycin and GTP (PDB 1OB2). Components colored as follows: tRNA (blue), EF-Tu (orange), kirromycin (yellow), GTP (green), and sites of posttranslational modification (red spheres). *B*, EF-G (green) bound to fusidic acid (orange) and GDP (brown; 4V5F).

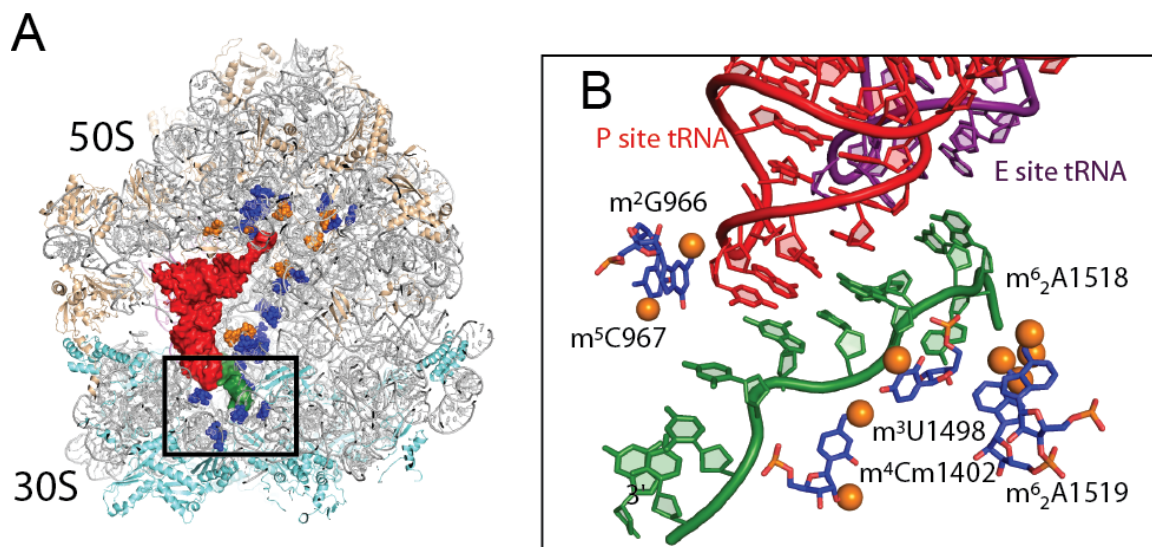


**FIGURE 1.7 Posttranscriptional modifications of rRNA.** *A*, View of ribosome from the tRNA A site highlighting sites of modification (PDB: 5AFI). Components colored as follows: rRNA (grey), 50S r-proteins (tan), 30S r-proteins (cyan), mRNA (green), P-site tRNA (red), methylated nucleotides (blue), pseudouridine (orange). *B*, Methylated nucleotides of the decoding center as colored in (A) and methylation sites (orange spheres).

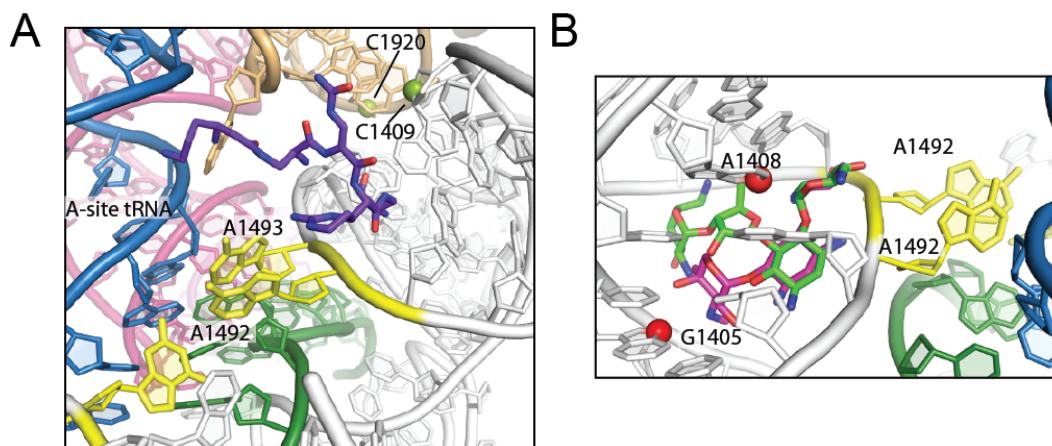


**FIGURE 1.8 Antibiotic resistance conferred by loss of posttranscriptional modifications.** *A*, Loss of methylation of 16S rRNA Cm1409 and 23S rRNA Cm1920 (green spheres) by TlyA confers resistance to capreomycin (4V7M, purple). Other highlighted ribosome features are the mRNA (green), A-site tRNA (blue), and the ‘decoding’ nucleotides A1492, A1493, G530 (yellow). *B*, Acquired methylations  $m^7G1505$  and  $m^1A1408$  (red spheres) confer resistance to aminoglycosides such as gentamicin (PDB: 4V53, light green) and neomycin (PDB: 4V52, pink).

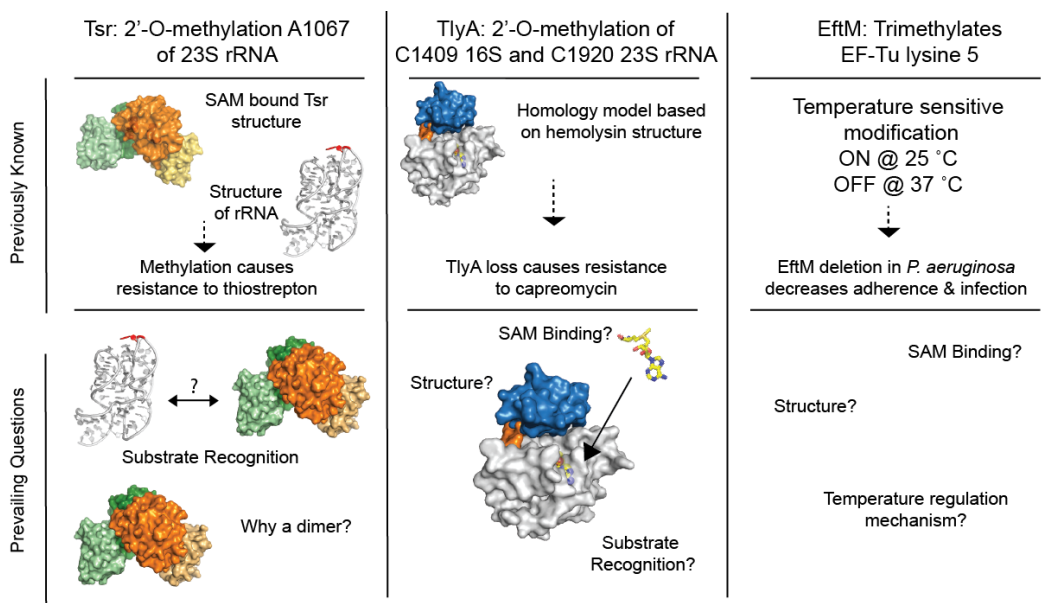


**FIGURE 1.9 Current knowledge and prevailing questions for Tsr, TlyA and EftM mechanistic studies.** Studies will elucidate the structure and biochemical properties of these enzymes and describe mechanisms of activity regulation by substrate recognition, cofactor binding or enzyme structural stability.

## 1.5 REFERENCES

1. Riley, M., Abe, T., Arnaud, M. B., Berlyn, M. K., Blattner, F. R., Chaudhuri, R. R., Glasner, J. D., Horiuchi, T., Keseler, I. M., Kosuge, T., Mori, H., Perna, N. T., Plunkett, G., 3rd, Rudd, K. E., Serres, M. H., Thomas, G. H., Thomson, N. R., Wishart, D., and Wanner, B. L. (2006) Escherichia coli K-12: a cooperatively developed annotation snapshot--2005. *Nucleic Acids Res* **34**, 1-9
2. Cozzone, A. J. (1998) Post-translational modification of proteins by reversible phosphorylation in prokaryotes. *Biochimie* **80**, 43-48
3. Walsh, C. T., Garneau-Tsodikova, S., and Gatto, G. J., Jr. (2005) Protein posttranslational modifications: the chemistry of proteome diversifications. *Angew Chem Int Ed Engl* **44**, 7342-7372
4. Stouthamer, A. H. (1973) A theoretical study on the amount of ATP required for synthesis of microbial cell material. *Antonie van Leeuwenhoek* **39**, 545-565
5. Ban, N., Beckmann, R., Cate, J. H., Dinman, J. D., Dragon, F., Ellis, S. R., Lafontaine, D. L., Lindahl, L., Liljas, A., Lipton, J. M., McAlear, M. A., Moore, P. B., Noller, H. F., Ortega, J., Panse, V. G., Ramakrishnan, V., Spahn, C. M., Steitz, T. A., Tchorzewski, M., Tollervey, D., Warren, A. J., Williamson, J. R., Wilson, D., Yonath, A., and Yusupov, M. (2014) A new system for naming ribosomal proteins. *Current opinion in structural biology* **24**, 165-169
6. Hirokawa, G., Nijman, R. M., Raj, V. S., Kaji, H., Igarashi, K., and Kaji, A. (2005) The role of ribosome recycling factor in dissociation of 70S ribosomes into subunits. *Rna* **11**, 1317-1328
7. Shine, J., and Dalgarno, L. (1975) Determinant of cistron specificity in bacterial ribosomes. *Nature* **254**, 34-38

8. Carter, A. P., Clemons, W. M., Jr., Brodersen, D. E., Morgan-Warren, R. J., Hartsch, T., Wimberly, B. T., and Ramakrishnan, V. (2001) Crystal structure of an initiation factor bound to the 30S ribosomal subunit. *Science* **291**, 498-501
9. Hartz, D., McPheeters, D. S., and Gold, L. (1989) Selection of the initiator tRNA by *Escherichia coli* initiation factors. *Genes & development* **3**, 1899-1912
10. Gualerzi, C., Risuleo, G., and Pon, C. L. (1977) Initial rate kinetic analysis of the mechanism of initiation complex formation and the role of initiation factor IF-3. *Biochemistry* **16**, 1684-1689
11. Eiler, D., Lin, J., Simonetti, A., Klaholz, B. P., and Steitz, T. A. (2013) Initiation factor 2 crystal structure reveals a different domain organization from eukaryotic initiation factor 5B and mechanism among translational GTPases. *Proc Natl Acad Sci U S A* **110**, 15662-15667
12. Simonetti, A., Marzi, S., Billas, I. M., Tsai, A., Fabbretti, A., Myasnikov, A. G., Roblin, P., Vaiana, A. C., Hazemann, I., Eiler, D., Steitz, T. A., Puglisi, J. D., Gualerzi, C. O., and Klaholz, B. P. (2013) Involvement of protein IF2 N domain in ribosomal subunit joining revealed from architecture and function of the full-length initiation factor. *Proc Natl Acad Sci U S A* **110**, 15656-15661
13. Lowe, T. M., and Eddy, S. R. (1997) tRNAscan-SE: a program for improved detection of transfer RNA genes in genomic sequence. *Nucleic Acids Res* **25**, 955-964
14. Juhling, F., Morl, M., Hartmann, R. K., Sprinzl, M., Stadler, P. F., and Putz, J. (2009) tRNAdb 2009: compilation of tRNA sequences and tRNA genes. *Nucleic Acids Res* **37**, D159-162
15. Ogle, J. M., Brodersen, D. E., Clemons, W. M., Jr., Tarry, M. J., Carter, A. P., and Ramakrishnan, V. (2001) Recognition of cognate transfer RNA by the 30S ribosomal subunit. *Science* **292**, 897-902
16. Ogle, J. M., Murphy, F. V., Tarry, M. J., and Ramakrishnan, V. (2002) Selection of tRNA by the ribosome requires a transition from an open to a closed form. *Cell* **111**, 721-732

17. Wieden, H. J., Gromadski, K., Rodnin, D., and Rodnina, M. V. (2002) Mechanism of elongation factor (EF)-Ts-catalyzed nucleotide exchange in EF-Tu. Contribution of contacts at the guanine base. *J Biol Chem* **277**, 6032-6036
18. Nissen, P., Hansen, J., Ban, N., Moore, P. B., and Steitz, T. A. (2000) The structural basis of ribosome activity in peptide bond synthesis. *Science* **289**, 920-930
19. Schmeing, T. M., and Ramakrishnan, V. (2009) What recent ribosome structures have revealed about the mechanism of translation. *Nature* **461**, 1234-1242
20. Brilot, A. F., Korostelev, A. A., Ermolenko, D. N., and Grigorieff, N. (2013) Structure of the ribosome with elongation factor G trapped in the pretranslocation state. *Proc Natl Acad Sci U S A* **110**, 20994-20999
21. Gao, Y. G., Selmer, M., Dunham, C. M., Weixlbaumer, A., Kelley, A. C., and Ramakrishnan, V. (2009) The structure of the ribosome with elongation factor G trapped in the posttranslocational state. *Science* **326**, 694-699
22. Liu, G., Song, G., Zhang, D., Zhang, D., Li, Z., Lyu, Z., Dong, J., Achenbach, J., Gong, W., Zhao, X. S., Nierhaus, K. H., and Qin, Y. (2014) EF-G catalyzes tRNA translocation by disrupting interactions between decoding center and codon-anticodon duplex. *Nature structural & molecular biology* **21**, 817-824
23. Holtkamp, W., Cunha, C. E., Peske, F., Konevega, A. L., Wintermeyer, W., and Rodnina, M. V. (2014) GTP hydrolysis by EF-G synchronizes tRNA movement on small and large ribosomal subunits. *Embo J* **33**, 1073-1085
24. Frank, J., Gao, H., Sengupta, J., Gao, N., and Taylor, D. J. (2007) The process of mRNA-tRNA translocation. *Proc Natl Acad Sci U S A* **104**, 19671-19678
25. Scolnick, E., Tompkins, R., Caskey, T., and Nirenberg, M. (1968) Release factors differing in specificity for terminator codons. *Proc Natl Acad Sci U S A* **61**, 768-774

26. Klaholz, B. P., Pape, T., Zavialov, A. V., Myasnikov, A. G., Orlova, E. V., Vestergaard, B., Ehrenberg, M., and van Heel, M. (2003) Structure of the Escherichia coli ribosomal termination complex with release factor 2. *Nature* **421**, 90-94
27. Rawat, U., Gao, H., Zavialov, A., Gursky, R., Ehrenberg, M., and Frank, J. (2006) Interactions of the release factor RF1 with the ribosome as revealed by cryo-EM. *J Mol Biol* **357**, 1144-1153
28. Petry, S., Brodersen, D. E., Murphy, F. V. t., Dunham, C. M., Selmer, M., Tarry, M. J., Kelley, A. C., and Ramakrishnan, V. (2005) Crystal structures of the ribosome in complex with release factors RF1 and RF2 bound to a cognate stop codon. *Cell* **123**, 1255-1266
29. Pai, R. D., Zhang, W., Schuwirth, B. S., Hirokawa, G., Kaji, H., Kaji, A., and Cate, J. H. (2008) Structural Insights into ribosome recycling factor interactions with the 70S ribosome. *J Mol Biol* **376**, 1334-1347
30. Gao, N., Zavialov, A. V., Li, W., Sengupta, J., Valle, M., Gursky, R. P., Ehrenberg, M., and Frank, J. (2005) Mechanism for the disassembly of the posttermination complex inferred from cryo-EM studies. *Mol Cell* **18**, 663-674
31. Zavialov, A. V., Haurlyliuk, V. V., and Ehrenberg, M. (2005) Splitting of the posttermination ribosome into subunits by the concerted action of RRF and EF-G. *Mol Cell* **18**, 675-686
32. Borg, A., Pavlov, M., and Ehrenberg, M. (2016) Complete kinetic mechanism for recycling of the bacterial ribosome. *Rna* **22**, 10-21
33. Zaffiri, L., Gardner, J., and Toledo-Pereyra, L. H. (2012) History of antibiotics. From salvarsan to cephalosporins. *Journal of investigative surgery : the official journal of the Academy of Surgical Research* **25**, 67-77
34. Blanchard, S. C., Cooperman, B. S., and Wilson, D. N. (2010) Probing translation with small-molecule inhibitors. *Chem Biol* **17**, 633-645
35. Tenson, T., and Mankin, A. (2006) Antibiotics and the ribosome. *Molecular microbiology* **59**, 1664-1677

36. Tenson, T., Lovmar, M., and Ehrenberg, M. (2003) The mechanism of action of macrolides, lincosamides and streptogramin B reveals the nascent peptide exit path in the ribosome. *J Mol Biol* **330**, 1005-1014
37. Poulsen, S. M., Kofoed, C., and Vester, B. (2000) Inhibition of the ribosomal peptidyl transferase reaction by the mycarose moiety of the antibiotics carbomycin, spiramycin and tylosin. *J Mol Biol* **304**, 471-481
38. Dunkle, J. A., Xiong, L., Mankin, A. S., and Cate, J. H. (2010) Structures of the Escherichia coli ribosome with antibiotics bound near the peptidyl transferase center explain spectra of drug action. *Proc Natl Acad Sci U S A* **107**, 17152-17157
39. Hansen, J. L., Ippolito, J. A., Ban, N., Nissen, P., Moore, P. B., and Steitz, T. A. (2002) The structures of four macrolide antibiotics bound to the large ribosomal subunit. *Mol Cell* **10**, 117-128
40. Wilson, D. N., Schluenzen, F., Harms, J. M., Starosta, A. L., Connell, S. R., and Fucini, P. (2008) The oxazolidinone antibiotics perturb the ribosomal peptidyl-transferase center and effect tRNA positioning. *Proc Natl Acad Sci U S A* **105**, 13339-13344
41. Guerrero, M. D., and Modolell, J. (1980) Hygromycin A, a novel inhibitor of ribosomal peptidyltransferase. *Eur J Biochem* **107**, 409-414
42. Polikanov, Y. S., Starosta, A. L., Juette, M. F., Altman, R. B., Terry, D. S., Lu, W., Burnett, B. J., Dinos, G., Reynolds, K. A., Blanchard, S. C., Steitz, T. A., and Wilson, D. N. (2015) Distinct tRNA Accommodation Intermediates Observed on the Ribosome with the Antibiotics Hygromycin A and A201A. *Mol Cell* **58**, 832-844
43. Yarmolinsky, M. B., and Haba, G. L. (1959) Inhibition by Puromycin of Amino Acid Incorporation into Protein. *Proc Natl Acad Sci U S A* **45**, 1721-1729
44. Gromadski, K. B., and Rodnina, M. V. (2004) Kinetic determinants of high-fidelity tRNA discrimination on the ribosome. *Mol Cell* **13**, 191-200

45. Voorhees, R. M., Weixlbaumer, A., Loakes, D., Kelley, A. C., and Ramakrishnan, V. (2009) Insights into substrate stabilization from snapshots of the peptidyl transferase center of the intact 70S ribosome. *Nature structural & molecular biology* **16**, 528-533
46. Borovinskaya, M. A., Pai, R. D., Zhang, W., Schuwirth, B. S., Holton, J. M., Hirokawa, G., Kaji, H., Kaji, A., and Cate, J. H. (2007) Structural basis for aminoglycoside inhibition of bacterial ribosome recycling. *Nature structural & molecular biology* **14**, 727-732
47. Davies, J., Gorini, L., and Davis, B. D. (1965) Misreading of RNA codewords induced by aminoglycoside antibiotics. *Mol Pharmacol* **1**, 93-106
48. Tsai, A., Uemura, S., Johansson, M., Puglisi, E. V., Marshall, R. A., Aitken, C. E., Korlach, J., Ehrenberg, M., and Puglisi, J. D. (2013) The impact of aminoglycosides on the dynamics of translation elongation. *Cell reports* **3**, 497-508
49. Peske, F., Savelsbergh, A., Katunin, V. I., Rodnina, M. V., and Wintermeyer, W. (2004) Conformational changes of the small ribosomal subunit during elongation factor G-dependent tRNA-mRNA translocation. *J Mol Biol* **343**, 1183-1194
50. Stanley, R. E., Blaha, G., Grodzicki, R. L., Strickler, M. D., and Steitz, T. A. (2010) The structures of the anti-tuberculosis antibiotics viomycin and capreomycin bound to the 70S ribosome. *Nature structural & molecular biology* **17**, 289-U248
51. Modolell, J., and Vazquez. (1977) The inhibition of ribosomal translocation by viomycin. *Eur J Biochem* **81**, 491-497
52. Holm, M., Borg, A., Ehrenberg, M., and Sanyal, S. (2016) Molecular mechanism of viomycin inhibition of peptide elongation in bacteria. *Proc Natl Acad Sci U S A* **113**, 978-983
53. Lentzen, G., Klinck, R., Matassova, N., Aboul-ela, F., and Murchie, A. I. (2003) Structural basis for contrasting activities of ribosome binding thiazole antibiotics. *Chem Biol* **10**, 769-778

54. Harms, J. M., Wilson, D. N., Schluenzen, F., Connell, S. R., Stachelhaus, T., Zaborowska, Z., Spahn, C. M., and Fucini, P. (2008) Translational regulation via L11: molecular switches on the ribosome turned on and off by thiostrepton and micrococcin. *Mol Cell* **30**, 26-38
55. Jonker, H. R., Ilin, S., Grimm, S. K., Wohnert, J., and Schwalbe, H. (2007) L11 domain rearrangement upon binding to RNA and thiostrepton studied by NMR spectroscopy. *Nucleic Acids Res* **35**, 441-454
56. Pestka, S. (1970) Thiostrepton: a ribosomal inhibitor of translocation. *Biochemical and biophysical research communications* **40**, 667-674
57. Rodnina, M. V., Savelsbergh, A., Matassova, N. B., Katunin, V. I., Semenov, Y. P., and Wintermeyer, W. (1999) Thiostrepton inhibits the turnover but not the GTPase of elongation factor G on the ribosome. *Proc Natl Acad Sci U S A* **96**, 9586-9590
58. Cameron, D. M., Thompson, J., March, P. E., and Dahlberg, A. E. (2002) Initiation factor IF2, thiostrepton and micrococcin prevent the binding of elongation factor G to the Escherichia coli ribosome. *J Mol Biol* **319**, 27-35
59. Cundliffe, E., and Thompson, J. (1981) Concerning the mode of action of micrococcin upon bacterial protein synthesis. *Eur J Biochem* **118**, 47-52
60. Voegelé, L., Palm, G. J., Mesters, J. R., and Hilgenfeld, R. (2001) Conformational change of elongation factor Tu (EF-Tu) induced by antibiotic binding. Crystal structure of the complex between EF-Tu.GDP and aurodox. *J Biol Chem* **276**, 17149-17155
61. Wolf, H., Chinali, G., and Parmeggiani, A. (1974) Kirromycin, an inhibitor of protein biosynthesis that acts on elongation factor Tu. *Proc Natl Acad Sci U S A* **71**, 4910-4914
62. Schmeing, T. M., Voorhees, R. M., Kelley, A. C., Gao, Y. G., Murphy, F. V. t., Weir, J. R., and Ramakrishnan, V. (2009) The crystal structure of the ribosome bound to EF-Tu and aminoacyl-tRNA. *Science* **326**, 688-694

63. Fischer, N., Neumann, P., Konevega, A. L., Bock, L. V., Ficner, R., Rodnina, M. V., and Stark, H. (2015) Structure of the E. coli ribosome-EF-Tu complex at <3 Å resolution by Cs-corrected cryo-EM. *Nature* **520**, 567-570
64. Borg, A., Holm, M., Shiroyama, I., Hauryliuk, V., Pavlov, M., Sanyal, S., and Ehrenberg, M. (2015) Fusidic acid targets elongation factor G in several stages of translocation on the bacterial ribosome. *J Biol Chem* **290**, 3440-3454
65. Borg, A., Pavlov, M., and Ehrenberg, M. (2016) Mechanism of fusidic acid inhibition of RRF- and EF-G-dependent splitting of the bacterial post-termination ribosome. *Nucleic Acids Res* **44**, 3264-3275
66. Kimura, S., and Suzuki, T. (2010) Fine-tuning of the ribosomal decoding center by conserved methyl-modifications in the Escherichia coli 16S rRNA. *Nucleic Acids Res* **38**, 1341-1352
67. O'Connor, M., Thomas, C. L., Zimmermann, R. A., and Dahlberg, A. E. (1997) Decoding fidelity at the ribosomal A and P sites: influence of mutations in three different regions of the decoding domain in 16S rRNA. *Nucleic Acids Res* **25**, 1185-1193
68. Connolly, K., Rife, J. P., and Culver, G. (2008) Mechanistic insight into the ribosome biogenesis functions of the ancient protein KsgA. *Molecular microbiology* **70**, 1062-1075
69. Boehringer, D., O'Farrell, H. C., Rife, J. P., and Ban, N. (2012) Structural insights into methyltransferase KsgA function in 30S ribosomal subunit biogenesis. *J Biol Chem* **287**, 10453-10459
70. Burakovsky, D. E., Prokhorova, I. V., Sergiev, P. V., Milon, P., Sergeeva, O. V., Bogdanov, A. A., Rodnina, M. V., and Dontsova, O. A. (2012) Impact of methylations of m2G966/m5C967 in 16S rRNA on bacterial fitness and translation initiation. *Nucleic Acids Res* **40**, 7885-7895
71. Prokhorova, I. V., Osterman, I. A., Burakovsky, D. E., Serebryakova, M. V., Galyamina, M. A., Pobeguts, O. V., Altukhov, I., Kovalchuk, S., Alexeev, D. G., Govorun, V. M.,

- Bogdanov, A. A., Sergiev, P. V., and Dontsova, O. A. (2013) Modified nucleotides m(2)G966/m(5)C967 of Escherichia coli 16S rRNA are required for attenuation of tryptophan operon. *Scientific reports* **3**, 3236
72. Caldas, T., Binet, E., Bouloc, P., Costa, A., Desgres, J., and Richarme, G. (2000) The FtsJ/RrmJ heat shock protein of Escherichia coli is a 23 S ribosomal RNA methyltransferase. *J Biol Chem* **275**, 16414-16419
73. Bugl, H., Fauman, E. B., Staker, B. L., Zheng, F., Kushner, S. R., Saper, M. A., Bardwell, J. C., and Jakob, U. (2000) RNA methylation under heat shock control. *Mol Cell* **6**, 349-360
74. Arai, T., Ishiguro, K., Kimura, S., Sakaguchi, Y., Suzuki, T., and Suzuki, T. (2015) Single methylation of 23S rRNA triggers late steps of 50S ribosomal subunit assembly. *Proc Natl Acad Sci U S A* **112**, E4707-4716
75. Gustafsson, C., and Persson, B. C. (1998) Identification of the rrmA gene encoding the 23S rRNA m1G745 methyltransferase in Escherichia coli and characterization of an m1G745-deficient mutant. *J Bacteriol* **180**, 359-365
76. Sergiev, P. V., Serebryakova, M. V., Bogdanov, A. A., and Dontsova, O. A. (2008) The ybiN gene of Escherichia coli encodes adenine-N6 methyltransferase specific for modification of A1618 of 23 S ribosomal RNA, a methylated residue located close to the ribosomal exit tunnel. *J Mol Biol* **375**, 291-300
77. Purta, E., Kaminska, K. H., Kasprzak, J. M., Bujnicki, J. M., and Douthwaite, S. (2008) YbeA is the m3Psi methyltransferase RlmH that targets nucleotide 1915 in 23S rRNA. *Rna* **14**, 2234-2244
78. Purta, E., O'Connor, M., Bujnicki, J. M., and Douthwaite, S. (2008) YccW is the m5C methyltransferase specific for 23S rRNA nucleotide 1962. *J Mol Biol* **383**, 641-651
79. Golovina, A. Y., Dzama, M. M., Osterman, I. A., Sergiev, P. V., Serebryakova, M. V., Bogdanov, A. A., and Dontsova, O. A. (2012) The last rRNA methyltransferase of E. coli

- revealed: the yhiR gene encodes adenine-N6 methyltransferase specific for modification of A2030 of 23S ribosomal RNA. *Rna* **18**, 1725-1734
80. Lovgren, J. M., and Wikstrom, P. M. (2001) The rlmB gene is essential for formation of Gm2251 in 23S rRNA but not for ribosome maturation in Escherichia coli. *J Bacteriol* **183**, 6957-6960
  81. Agarwalla, S., Kealey, J. T., Santi, D. V., and Stroud, R. M. (2002) Characterization of the 23 S ribosomal RNA m5U1939 methyltransferase from Escherichia coli. *J Biol Chem* **277**, 8835-8840
  82. LaMarre, J. M., Howden, B. P., and Mankin, A. S. (2011) Inactivation of the indigenous methyltransferase RlmN in Staphylococcus aureus increases linezolid resistance. *Antimicrob Agents Chemother* **55**, 2989-2991
  83. Helser, T. L., Davies, J. E., and Dahlberg, J. E. (1972) Mechanism of kasugamycin resistance in Escherichia coli. *Nature: New biology* **235**, 6-9
  84. Gutierrez, B., Escudero, J. A., San Millan, A., Hidalgo, L., Carrilero, L., Ovejero, C. M., Santos-Lopez, A., Thomas-Lopez, D., and Gonzalez-Zorn, B. (2012) Fitness cost and interference of Arm/Rmt aminoglycoside resistance with the RsmF housekeeping methyltransferases. *Antimicrob Agents Chemother* **56**, 2335-2341
  85. Maus, C. E., Plikaytis, B. B., and Shinnick, T. M. (2005) Mutation of tlyA confers capreomycin resistance in Mycobacterium tuberculosis. *Antimicrob Agents Chemother* **49**, 571-577
  86. Cundliffe, E. (1989) How antibiotic-producing organisms avoid suicide. *Annu Rev Microbiol* **43**, 207-233
  87. van Hoek, A. H., Mevius, D., Guerra, B., Mullany, P., Roberts, A. P., and Aarts, H. J. (2011) Acquired antibiotic resistance genes: an overview. *Frontiers in microbiology* **2**, 203
  88. Gandecha, A. R., and Cundliffe, E. (1996) Molecular analysis of tlrD, an MLS resistance determinant from the tylosin producer, Streptomyces fradiae. *Gene* **180**, 173-176

89. Pernodet, J. L., Fish, S., Blondelet-Rouault, M. H., and Cundliffe, E. (1996) The macrolide-lincosamide-streptogramin B resistance phenotypes characterized by using a specifically deleted, antibiotic-sensitive strain of *Streptomyces lividans*. *Antimicrob Agents Chemother* **40**, 581-585
90. Cundliffe, E. (1992) Resistance to macrolides and lincosamides in *Streptomyces lividans* and to aminoglycosides in *Micromonospora purpurea*. *Gene* **115**, 75-84
91. Roberts, M. C., Sutcliffe, J., Courvalin, P., Jensen, L. B., Rood, J., and Seppala, H. (1999) Nomenclature for macrolide and macrolide-lincosamide-streptogramin B resistance determinants. *Antimicrob Agents Chemother* **43**, 2823-2830
92. Brisson-Noel, A., Arthur, M., and Courvalin, P. (1988) Evidence for natural gene transfer from gram-positive cocci to *Escherichia coli*. *J Bacteriol* **170**, 1739-1745
93. Kehrenberg, C., Schwarz, S., Jacobsen, L., Hansen, L. H., and Vester, B. (2005) A new mechanism for chloramphenicol, florfenicol and clindamycin resistance: methylation of 23S ribosomal RNA at A2503. *Molecular microbiology* **57**, 1064-1073
94. Long, K. S., Poehlsgaard, J., Kehrenberg, C., Schwarz, S., and Vester, B. (2006) The Cfr rRNA methyltransferase confers resistance to Phenicol, Lincosamides, Oxazolidinones, Pleuromutilins, and Streptogramin A antibiotics. *Antimicrob Agents Chemother* **50**, 2500-2505
95. Kehrenberg, C., and Schwarz, S. (2004) *fexA*, a novel *Staphylococcus lentus* gene encoding resistance to florfenicol and chloramphenicol. *Antimicrob Agents Chemother* **48**, 615-618
96. Cai, J. C., Hu, Y. Y., Zhang, R., Zhou, H. W., and Chen, G. X. (2012) Linezolid-resistant clinical isolates of methicillin-resistant coagulase-negative staphylococci and *Enterococcus faecium* from China. *Journal of medical microbiology* **61**, 1568-1573
97. Doi, Y., and Arakawa, Y. (2007) 16S ribosomal RNA methylation: emerging resistance mechanism against aminoglycosides. *Clin Infect Dis* **45**, 88-94

98. Liou, G. F., Yoshizawa, S., Courvalin, P., and Galimand, M. (2006) Aminoglycoside resistance by ArmA-mediated ribosomal 16S methylation in human bacterial pathogens. *J Mol Biol* **359**, 358-364
99. Lioy, V. S., Goussard, S., Guerineau, V., Yoon, E. J., Courvalin, P., Galimand, M., and Grillot-Courvalin, C. (2014) Aminoglycoside resistance 16S rRNA methyltransferases block endogenous methylation, affect translation efficiency and fitness of the host. *Rna* **20**, 382-391
100. Zacharczuk, K., Piekarska, K., Szych, J., Jagielski, M., Hidalgo, L., San Millan, A., Gutierrez, B., Rastawicki, W., Gonzalez-Zorn, B., and Gierczynski, R. (2011) Plasmid-borne 16S rRNA methylase ArmA in aminoglycoside-resistant *Klebsiella pneumoniae* in Poland. *Journal of medical microbiology* **60**, 1306-1311
101. Holmes, D. J., and Cundliffe, E. (1991) Analysis of a ribosomal RNA methylase gene from *Streptomyces tenebrarius* which confers resistance to gentamicin. *Molecular & general genetics : MGG* **229**, 229-237
102. Kelemen, G. H., Cundliffe, E., and Financsek, I. (1991) Cloning and characterization of gentamicin-resistance genes from *Micromonospora purpurea* and *Micromonospora rosea*. *Gene* **98**, 53-60
103. Wachino, J., Shibayama, K., Kurokawa, H., Kimura, K., Yamane, K., Suzuki, S., Shibata, N., Ike, Y., and Arakawa, Y. (2007) Novel plasmid-mediated 16S rRNA m1A1408 methyltransferase, NpmA, found in a clinically isolated *Escherichia coli* strain resistant to structurally diverse aminoglycosides. *Antimicrob Agents Chemother* **51**, 4401-4409
104. Cundliffe, E., and Thompson, J. (1979) Ribose methylation and resistance to thiostrepton. *Nature* **278**, 859-861
105. Cundliffe, E. (1978) Mechanism of resistance to thiostrepton in the producing-organism *Streptomyces azureus*. *Nature* **272**, 792-795

106. Dosch, D. C., Strohl, W. R., and Floss, H. G. (1988) Molecular cloning of the nosiheptide resistance gene from *Streptomyces actuosus* ATCC 25421. *Biochemical and biophysical research communications* **156**, 517-523
107. Demirci, H., Gregory, S. T., Dahlberg, A. E., and Jogl, G. (2007) Recognition of ribosomal protein L11 by the protein trimethyltransferase PrmA. *Embo J* **26**, 567-577
108. Demirci, H., Gregory, S. T., Dahlberg, A. E., and Jogl, G. (2008) Multiple-site trimethylation of ribosomal protein L11 by the PrmA methyltransferase. *Structure* **16**, 1059-1066
109. Vanet, A., Plumbridge, J. A., Guerin, M. F., and Alix, J. H. (1994) Ribosomal protein methylation in *Escherichia coli*: the gene *prmA*, encoding the ribosomal protein L11 methyltransferase, is dispensable. *Molecular microbiology* **14**, 947-958
110. Lhoest, J., and Colson, C. (1977) Genetics of ribosomal protein methylation in *Escherichia coli*. II. A mutant lacking a new type of methylated amino acid, N5-methylglutamine, in protein L3. *Molecular & general genetics : MGG* **154**, 175-180
111. Lhoest, J., and Colson, C. (1981) Cold-sensitive ribosome assembly in an *Escherichia coli* mutant lacking a single methyl group in ribosomal protein L3. *Eur J Biochem* **121**, 33-37
112. Chang, F. N., Chang, C. N., and Paik, W. K. (1974) Methylation of ribosomal proteins in *Escherichia coli*. *J Bacteriol* **120**, 651-656
113. Chang, F. N. (1978) Temperature-dependent variation in the extent of methylation of ribosomal proteins L7 and L12 in *Escherichia coli*. *J Bacteriol* **135**, 1165-1166
114. Ramagopal, S., and Subramanian, A. R. (1974) Alteration in the acetylation level of ribosomal protein L12 during growth cycle of *Escherichia coli*. *Proc Natl Acad Sci U S A* **71**, 2136-2140
115. Yoshikawa, A., Isono, S., Sheback, A., and Isono, K. (1987) Cloning and nucleotide sequencing of the genes *rimI* and *rimJ* which encode enzymes acetylating ribosomal proteins S18 and S5 of *Escherichia coli* K12. *Molecular & general genetics : MGG* **209**, 481-488

116. Roy-Chaudhuri, B., Kirthi, N., Kelley, T., and Culver, G. M. (2008) Suppression of a cold-sensitive mutation in ribosomal protein S5 reveals a role for RimJ in ribosome biogenesis. *Molecular microbiology* **68**, 1547-1559
117. Nakahigashi, K., Kubo, N., Narita, S., Shimaoka, T., Goto, S., Oshima, T., Mori, H., Maeda, M., Wada, C., and Inokuchi, H. (2002) HemK, a class of protein methyl transferase with similarity to DNA methyl transferases, methylates polypeptide chain release factors, and hemK knockout induces defects in translational termination. *Proc Natl Acad Sci U S A* **99**, 1473-1478
118. Mora, L., Heurgue-Hamard, V., de Zamaroczy, M., Kervestin, S., and Buckingham, R. H. (2007) Methylation of bacterial release factors RF1 and RF2 is required for normal translation termination in vivo. *J Biol Chem* **282**, 35638-35645
119. Dincbas-Renqvist, V., Engstrom, A., Mora, L., Heurgue-Hamard, V., Buckingham, R., and Ehrenberg, M. (2000) A post-translational modification in the GGQ motif of RF2 from *Escherichia coli* stimulates termination of translation. *Embo J* **19**, 6900-6907
120. Doerfel, L. K., Wohlgemuth, I., Kothe, C., Peske, F., Urlaub, H., and Rodnina, M. V. (2013) EF-P is essential for rapid synthesis of proteins containing consecutive proline residues. *Science* **339**, 85-88
121. Ude, S., Lassak, J., Starosta, A. L., Kraxenberger, T., Wilson, D. N., and Jung, K. (2013) Translation elongation factor EF-P alleviates ribosome stalling at polyproline stretches. *Science* **339**, 82-85
122. Roy, H., Zou, S. B., Bullwinkle, T. J., Wolfe, B. S., Gilreath, M. S., Forsyth, C. J., Navarre, W. W., and Ibba, M. (2011) The tRNA synthetase paralog PoxA modifies elongation factor-P with (R)-beta-lysine. *Nature chemical biology* **7**, 667-669
123. Park, J. H., Johansson, H. E., Aoki, H., Huang, B. X., Kim, H. Y., Ganoza, M. C., and Park, M. H. (2012) Post-translational modification by beta-lysylation is required for activity of *Escherichia coli* elongation factor P (EF-P). *J Biol Chem* **287**, 2579-2590

124. Pereira, S. F., Gonzalez, R. L., Jr., and Dworkin, J. (2015) Protein synthesis during cellular quiescence is inhibited by phosphorylation of a translational elongation factor. *Proc Natl Acad Sci U S A* **112**, E3274-3281
125. Sajid, A., Arora, G., Gupta, M., Singhal, A., Chakraborty, K., Nandicoori, V. K., and Singh, Y. (2011) Interaction of Mycobacterium tuberculosis elongation factor Tu with GTP is regulated by phosphorylation. *J Bacteriol* **193**, 5347-5358
126. Cruz, J. W., Rothenbacher, F. P., Maehigashi, T., Lane, W. S., Dunham, C. M., and Woychik, N. A. (2014) Doc toxin is a kinase that inactivates elongation factor Tu. *J Biol Chem* **289**, 7788-7798
127. Van Noort, J. M., Kraal, B., Sinjorgo, K. M., Persoon, N. L., Johanns, E. S., and Bosch, L. (1986) Methylation in vivo of elongation factor EF-Tu at lysine-56 decreases the rate of tRNA-dependent GTP hydrolysis. *Eur J Biochem* **160**, 557-561
128. Young, C. C., Alvarez, J. D., and Bernlohr, R. W. (1990) Nutrient-dependent methylation of a membrane-associated protein of Escherichia coli. *J Bacteriol* **172**, 5147-5153
129. Young, C. C., and Bernlohr, R. W. (1991) Elongation factor Tu is methylated in response to nutrient deprivation in Escherichia coli. *J Bacteriol* **173**, 3096-3100
130. Barbier, M., Oliver, A., Rao, J., Hanna, S. L., Goldberg, J. B., and Alberti, S. (2008) Novel phosphorylcholine-containing protein of Pseudomonas aeruginosa chronic infection isolates interacts with airway epithelial cells. *J Infect Dis* **197**, 465-473
131. Barbier, M., Owings, J. P., Martinez-Ramos, I., Damron, F. H., Gomila, R., Blazquez, J., Goldberg, J. B., and Alberti, S. (2013) Lysine trimethylation of EF-Tu mimics platelet-activating factor to initiate Pseudomonas aeruginosa pneumonia. *mBio* **4**, e00207-00213
132. Kozbial, P. Z., and Mushegian, A. R. (2005) Natural history of S-adenosylmethionine-binding proteins. *BMC structural biology* **5**, 19
133. Schubert, H. L., Blumenthal, R. M., and Cheng, X. (2003) Many paths to methyltransfer: a chronicle of convergence. *Trends Biochem Sci* **28**, 329-335

134. Kagan, R. M., and Clarke, S. (1994) Widespread occurrence of three sequence motifs in diverse S-adenosylmethionine-dependent methyltransferases suggests a common structure for these enzymes. *Archives of biochemistry and biophysics* **310**, 417-427
135. Dunstan, M. S., Hang, P. C., Zelinskaya, N. V., Honek, J. F., and Conn, G. L. (2009) Structure of the thiostrepton resistance methyltransferase.S-adenosyl-L-methionine complex and its interaction with ribosomal RNA. *J Biol Chem* **284**, 17013-17020

**CHAPTER 2:*****PSEUDOMONAS AERUGINOSA* EFTM IS A THERMOREGULATED  
METHYLTRANSFERASE**

Joshua P. Owings<sup>1</sup>, Emily G. Kuiper<sup>1</sup>, Samantha M. Prezioso, Jeffrey Meisner, John J. Varga, Natalia Zelinskaya, Eric B. Dammer, Duc M. Duong, Nicholas T. Seyfried, Sebastián Albertí, Graeme L. Conn, and Joanna B. Goldberg.

<sup>1</sup>These authors contributed equally and should be considered joint first authors.

This work was originally published in the Journal of Biological Chemistry. Owings, J.P., Kuiper, E.G., Prezioso, S.M., Meisner, J., Varga, J.J., Zelinskaya, N., Dammer, E.B., Duong, D.M., Seyfried, N.T., Alberti, S. Conn, G.L., and Goldberg, J.B. *Pseudomonas aeruginosa* EftM Is a Thermoregulated Methyltransferase. *J Biol Chem*, 2016; 291, 3280-3290. © the American Society for Biochemistry and Molecular Biology.

E.G.K. Contributed directly to figures: 2.2, 2.5 and 2.6. JBG, GLC, SA, and NTS conceived and coordinated the study. JPO, EGK, SMP, JM, JJV, NZ, EBD, and DMD performed the experiments and analyzed the data. JPO, EGK, JM, NTS, SA, GLC, and JBG wrote the paper.

## 2.1 ABSTRACT

*Pseudomonas aeruginosa* is a Gram-negative opportunistic pathogen that trimethylates elongation factor-Tu (EF-Tu) on lysine 5. Lysine 5 methylation occurs in a temperature-dependent manner and is generally only seen when *P. aeruginosa* is grown at temperatures close to ambient (25°C), but not at higher temperatures (37°C). We have previously identified the gene, *eftM* (for EF-Tu modifying enzyme), responsible for this modification and shown its activity to be associated with increase adhesion to and invasion of respiratory epithelial cells. Bioinformatic analyses predicted EftM to be a Class I S-adenosyl-L-methionine (SAM)-dependent methyltransferase. An *in vitro* methyltransferase assay was employed to show that, in the presence of SAM, EftM directly trimethylates EF-Tu. A natural variant of EftM, with a glycine to arginine substitution at position 50, in the predicted SAM-binding domain lacks both SAM binding and enzyme activity. Mass spectrometry analysis of the *in vitro* methyltransferase reaction products revealed that EftM exclusively methylates at lysine 5 of EF-Tu in a distributive manner. Consistent with the *in vivo* temperature dependence of methylation of EF-Tu, pre-incubation of EftM at 37°C abolished methyltransferase activity, while this activity was retained when EftM was pre-incubated at 25°C. Irreversible protein unfolding at 37°C was observed and we propose is the molecular basis for the temperature dependence of EftM activity. Collectively, our results show that EftM is a thermolabile, SAM-dependent methyltransferase that directly trimethylates lysine 5 of EF-Tu in *P. aeruginosa*.

## 2.2 INTRODUCTION

Protein post-translational modification (PTM) adds an additional level of complexity that can influence protein function, as well as change the protein charge and tertiary structure. The protein PTM landscape is vast; more than half of the natural amino acids are substrates for chemical modification and lysine, for example, can be modified with at least 10 different PTMs, including methylation (1).

Though first discovered on the bacterial flagellum (2), the study of lysine methylation in prokaryotes has lagged behind that of eukaryotes. In eukaryotes, the most well-studied effect of lysine methylation is within the field of epigenetics, where patterns of methylation form the ‘histone code,’ and serve as another level of DNA transcriptional control (3). In bacteria, methylated lysines have been found on flagella, specific outer membrane proteins, and the ribosome translational machinery; however, for the most part, the functional consequences of these modifications are not known (2,4-8).

PTM of proteins involved in protein synthesis has the potential to exert a significant effect on bacterial gene expression. Lysine methylation of components of the translational machinery, including essential translation factors such as elongation factor-Tu (EF-Tu), which binds to and delivers aminoacylated tRNA (aa-tRNA) to the ribosome has been identified (9). In *Escherichia coli* for example, EF-Tu lysine 57 is mono-methylated during logarithmic growth phase (10) but as cells transition to stationary phase there is a gradual conversion of mono-methyllysine to dimethyllysine (11). While methylation of EF-Tu at lysine 57 does not significantly alter its interaction with GTP, GDP, EF-Ts, or aa-tRNA, there is a two-fold decrease in GTP hydrolysis when EF-Tu is 20% mono- and 80% di-methylated compared to unmethylated (11). These findings suggest that *in vivo*, any methylation of lysine 57 of EF-Tu would prolong the interaction of EF-Tu-GTP-aa-tRNA complex with the ribosome leading to an increase in translational accuracy (11,12). To date, the enzyme responsible for this modification in *E. coli* is not known.

We recently recognized that *Pseudomonas aeruginosa* EF-Tu is trimethylated at lysine 5 in a temperature dependent manner (13). Through screening of a *P. aeruginosa* transposon mutant library at 22°C, a strain lacking methylated EF-Tu was identified and subsequent analysis revealed a transposon insertion in *eftM*. A mutant constructed with a deletion in *eftM* does not

trimethylate EF-Tu, and plasmid complementation with *eftM* restored trimethylation of EF-Tu on lysine 5, indicating that *eftM* is necessary for this process (13). EftM activity is associated with increased adhesion to and invasion of respiratory epithelial cells and is more prominent at 22-25°C than at 37°C (14). These observations and the fact that modified EF-Tu can be recognized by antibodies to phosphorylcholine (ChoP) lead to the speculation that trimethylation of EF-Tu functions like ChoP-modified surface-associated molecules of other respiratory pathogens. Similar to ChoP-modified molecules, trimethylated EF-Tu interacts with platelet-activating factor receptor (PAFR) on host cells. In many ChoP-containing microbes, the expression of this modification is controlled in a variable manner; for example, phase variation controls ChoP expression in commensal *Neisseria* spp. and *Haemophilus influenzae* (15). Trimethylation of EF-Tu is also variable being more prominent at lower, but not higher temperatures (13). This temperature-dependent activity appears independent of transcriptional regulation of *eftM*, as both RNA-seq (16) and DNA microarray (17) studies of *P. aeruginosa* grown at 37°C show no differences in *eftM* transcription when compared to *P. aeruginosa* grown at lower temperatures. Therefore, how EftM activity and the modification of EF-Tu are controlled by temperature is not known.

In the current study, we show that EftM is structurally homologous to Class I S-adenosyl-L-methionine (SAM)-dependent methyltransferases and that purified recombinant EftM is necessary and sufficient for the trimethylation of *P. aeruginosa* EF-Tu in the presence of SAM cosubstrate. Analyses of EftM stability reveal that the protein undergoes an irreversible structural reorganization at 37°C resulting in loss of methyltransferase activity. Together, these data suggest that the *in vivo* temperature-dependent methylation and associated effect on adhesion may be explained by direct thermoregulation of EftM resulting in structural instability at human body temperature (37°C).

## 2.3 EXPERIMENTAL PROCEDURES

*2.3.1 Bacterial strains, plasmids and primers* – The strains and plasmids used in this study are listed in Table 1. All DNA oligonucleotide primers used for cloning and sequence analysis in this study are listed in Table 2.

*2.3.2 Plasmid construction* – For complementation experiments, the PAHM23 *eftM* gene (with G148C mutation encoding a G50R amino acid substitution) was cloned into the broad-host-range expression vector pUCP18ApGw, as previously described for the wild-type gene from PAO1 (13). Briefly, the coding sequence was amplified using purified PAHM23 genomic DNA as template with primers oJPO18 and oJPO19 (Table 2). The amplicon was cloned into the Gateway entry vector pENTR/SD/D-TOPO (Life Technologies) following manufacturer's instructions. Gateway LR Clonase II enzyme mix (Life Technologies) was then used to clone from the entry vector into the destination vector pUCP18ApGw (13) to generate plasmid pJPO7. The nucleotide sequence of the plasmid insert was verified using automated DNA sequencing.

To create plasmids for overexpression of wild-type and K5A substituted EF-Tu, the coding sequence of PAO1 *tufB* (PA4277) was amplified from PAO1 genomic DNA with an engineered amino-terminal hexahistidine (N-His<sub>6</sub>) affinity tag using primer pairs *tufBF* and *tufBR* or *tufBFK5A* and *tufBR*, respectively (13). Amplicons were Gateway cloned as described above into the destination vector pDEST14 (Life Technologies) to generate expression plasmids pJPO4 and pJPO5 containing N-His<sub>6</sub> *tufB* and N-His<sub>6</sub> *tufB* K5A, respectively. Similarly, for EftM, the coding sequences of PAO1 *eftM* (PA4178) and PAHM23 *eftM* (G50R) were amplified from PAO1 and PAHM23 genomic DNA, respectively, using primers oJPO20 and oJPO21 (Table 2). PCR products were digested with NdeI and HindIII (New England Biolabs) and cloned into pCOLD II (Takara Bio) in-frame with a N-His<sub>6</sub> affinity tag to generate expression plasmids pJPO1 and pJPO2, respectively.

*2.3.3 Protein expression and purification* – Expression of N-His<sub>6</sub>-tagged EF-Tu or EF-Tu K5A was accomplished in *E. coli* BL21-AI cells transformed with pJPO4 or pJPO5, respectively, in 1 L cultures of ZYM-5052 media (18) supplemented with 0.2% arabinose [wt/vol] and carbenicillin (100 µg/mL). Cultures were incubated with shaking at 25°C for 14 hours. Cells were pelleted at 12,000 x g for 10 minutes at 4°C and resuspended in 25 mL of lysis buffer (GoldBio Bacterial Cell Lysis Buffer and 10 mM imidazole) with 100 µl of DNase I (10 mg/mL, GoldBio), 300 µl ProBlock Gold Protease Inhibitor (GoldBio), and 0.2 mg/mL lysozyme (Roche). Cell suspensions were lysed using a French Pressure Cell (American Instrument Company) at 16-18k PSI. Lysates were then subjected to centrifugation at 12,000 x g for 10 minutes at 4°C to remove cellular debris before applying the supernatants to columns containing HisPur Ni-NTA resin (Thermo Scientific). The columns were washed three times with 1 mL wash buffer (50 mM sodium phosphate, 150 mM sodium chloride, 20% glycerol [vol/vol], 6 mM β-mercaptoethanol, and 50 mM imidazole, pH 7.4) and eluted in four sequential 1 mL fractions of elution buffer (wash buffer with 250 mM imidazole).

For over expression of N-His<sub>6</sub>-tagged EftM (PAO1) and N-His<sub>6</sub>-tagged EftM G50R (PAHM23), chemically competent BL21(DE3) cells were transformed with pJPO1 or pJPO2, respectively, along with pG-Tf2 helper plasmid encoding *groES-groEL-tig* (Takara Bio) and cultured overnight, at 37°C in lysogeny broth (LB) containing chloramphenicol (20 µg/mL) and carbenicillin (100 µg/mL). LB (1 L) supplemented with carbenicillin, chloramphenicol, and tetracycline (5 ng/mL) was inoculated with 14 mL of overnight culture and then incubated at 37°C until the OD<sub>600</sub> reached 0.8-1.0. Cultures were then cooled in a 15°C water bath for 30 minutes before the addition of 0.5 mM IPTG for induction of protein expression. Induced cultures were incubated with shaking at 15°C for a further 20 hours. Purification was accomplished as described for EF-Tu but with altered compositions of the lysis buffer (50 mM Tris-HCl, 10 mM

magnesium acetate, 250 mM ammonium chloride, 20% glycerol [vol/vol], 6 mM  $\beta$ -mercaptoethanol, and 10 mM imidazole, pH 7.5) and wash buffer (50 mM Tris-HCl, 150 mM sodium chloride, 50 mM imidazole, 5 mM magnesium chloride, 20% glycerol [vol/vol], 6 mM  $\beta$ -mercaptoethanol, pH 7.5). EftM was further purified by gel filtration chromatography on a Superdex200 10/300 column (GE Healthcare) equilibrated in gel filtration buffer (Tris-HCl pH 7.5, 75 mM potassium chloride, 150 mM sodium chloride, 5 mM magnesium chloride, 20% glycerol, and 2 mM  $\beta$ -mercaptoethanol).

*2.3.4 Preparation of P. aeruginosa whole-cell extracts* – Cells were grown overnight with shaking in LB at either 25°C or 37°C. Whole cell extracts were prepared by taking a volume equivalent to 0.5 mL of an OD<sub>600</sub> = 1.0 culture, pelleting the cells, and resuspending in 60  $\mu$ l of 1x Laemmli buffer (BioRad). Samples were boiled for 10 minutes before being analyzed by immunoblot analysis.

*2.3.5 Immunoblot analysis* – Immunoblots were performed by running samples on 10% Mini-PROTEAN TGX gels (BioRad), transferring proteins to PVDF membranes (BioRad), and blocking for 1 hour in 5% non-fat dry milk [wt/vol]. After blocking, blots were incubated in primary antibody specific for di/trimethyl lysine (DTmK) (Millipore) or RpoA (Neoclone) overnight at 4°C, and then an appropriate secondary antibody (anti-rabbit IgG or anti-mouse IgG, respectively) conjugated to horseradish peroxidase (Sigma) at room temperature for 1 hour. Antibody binding was detected using BioRad Clarity Western ECL reagent and the BioRad ChemiDoc MP imager. All images were analyzed using Image Lab version 5.1 (BioRad).

*2.3.6 EftM homology modeling* – The amino acid sequence of EftM was analyzed using the homology detection program HHpred ([19](#)). The hit with the highest probability (DesVI, PDB ID 3BXO) was used as a template for comparative modeling using MODELLER software ([20](#)).

DaliLite (EMBL-EBI) was used to align (superimpose) the DesVI-SAM structure and the EftM structural model. SAM was modeled on EftM by overlaying the EftM homology model and the DesVI-SAM complex structure in PyMOL (Schrödinger, LLC).

*2.3.7 In vitro methyltransferase assay* – Methyltransferase assays comparing modification of wild-type EF-Tu or Ef-Tu K5A by EftM or EftM G50R contained 1x HMT reaction buffer (New England Biolabs; 50 mM Tris-HCl, 5 mM magnesium chloride, 4 mM dithiothreitol, pH 9), 10  $\mu$ M EF-Tu, 1 mM SAM (Sigma-Aldrich), and 6  $\mu$ M EftM. Reactions were incubated at 25°C for 20 minutes and heat inactivated by boiling in 2x Laemmli sample buffer (BioRad) for 5 minutes. All samples were analyzed using immunoblotting with antibodies to detect DTmK (Millipore). These assays were repeated at least three times with similar results.

Methyltransferase assays with heat pre-treatment were performed in gel filtration buffer and contained 10  $\mu$ M EftM, 16  $\mu$ M EF-Tu and 1 mM SAM. EftM was preincubated at either 25°C or 37°C for 0, 5, 10 and 20 minutes prior to addition to the methyltransferase assay. Reactions were incubated at 25°C for 20 minutes and inactivated as described above. Samples were run on 14% SDS-PAGE gels and stained with Coomassie or immunoblotted using a DTmK antibody (Upstate Biotech). These assays were repeated two times with similar results.

*2.3.8 MS analysis* – MS analysis was used to assess EF-Tu methylation *in vivo* and from *in vitro* assays performed under conditions designed to produce partial or complete methylation. For *in vivo* methylation, recombinant N-His<sub>6</sub>-tagged EF-Tu was purified from *P. aeruginosa* strain PAO1 grown at 25°C as described in Barbier *et al.* (13) and digested directly with chymotrypsin for MS analysis. Partial methylation of EF-Tu was accomplished using products of *in vitro* methyltransferase assays performed with excess SAM and EF-Tu but limiting EftM (0.6  $\mu$ M) and short incubation times (5 and 10 minutes). Products of *in vitro* assays were run on a 10% SDS-

PAGE gel (BioRad) and stained with GelCode Blue (Thermo Scientific) for protein visualization. Bands were excised and protein digested in-gel with chymotrypsin. The resulting peptides were extracted with a solution of 5% formic acid and 50% acetonitrile and speed vacuumed to dryness.

An equal volume of each peptide sample was resuspended in loading buffer (0.1% formic acid, 0.03% trifluoroacetic acid, 1% acetonitrile) and peptide eluents were separated using a 15 cm 1.9  $\mu\text{m}$  C18 (Dr. Maisch, High Performance LC GmbH, Germany) self-packed column (New Objective) on a NanoAcquity UHPLC (Waters) and monitored on an Q-Exactive Plus mass spectrometer (ThermoFisher Scientific). Elution was performed over a 120-minute gradient at a rate of 325 nl/minute with buffer B ranging from 3% to 80% (buffer A: 0.1% formic acid and 5% DMSO in water, buffer B: 0.1 % formic and 5% DMSO in acetonitrile). The mass spectrometer cycle was programmed to collect one full MS scan followed by 10 data dependent MS/MS scans. The MS scans were collected at a resolution of 35,000 (300-1800  $m/z$  range, 1,000,000 automatic gain control (AGC), 100 millisecond (ms) maximum ion time) and the MS/MS spectra were acquired at a resolution of 17,500 (2  $m/z$  isolation width, 30% collision energy, 10,000 AGC target, and 50 ms maximum ion time). Dynamic exclusion was set to exclude previous sequenced peaks within a 10 ppm window for 30 seconds.

The SageN Sorcerer SEQUEST 4.3 algorithm was used to search and match MS/MS spectra to a complete semi-chymotryptic *E. coli* database harboring the recombinant EF-Tu sequence from *P. aeruginosa* PAO1 strain (total with 11,541 entries), including pseudo-reversed *E. coli* decoy sequences ([21,22](#)). Searching parameters included mass tolerance of precursor ions ( $\pm 20$  ppm) semi-chymotryptic restriction, dynamic modifications for oxidized Met (+15.9949 Da), trimethyl lysine (+42.0470 Da), four maximal modification sites and a maximum of two missed cleavages. Only b and y ions were considered for scoring (Xcorr) and Xcorr along with  $\Delta\text{Cn}$  were dynamically increased for groups of peptides organized by a combination of chymotrypticity

(fully or partial) and precursor ion charge state to remove false positive hits along with decoys until achieving a false discovery rate (FDR) of  $< 5\%$  ( $< 0.25\%$  for proteins identified by more than one peptide) (23).

Following discovery-based identification of the trimethylated EF-Tu lysine 5 peptide ( $m/z = 398.231$ ) and corresponding unmodified peptide ( $m/z = 377.208$ ), both were quantified on an LTQ Orbitrap XL hybrid mass spectrometer (ThermoFisher Scientific) using a targeted MS approach essentially as described (24). A user defined precursor mass tolerance of  $\pm 20$  ppm was employed for extracted ion chromatogram (XIC) based quantification. For time course assays, fully chymotryptic peptides representing unmodified (AKEKF,  $m/z = 311.68$ ), mono-methylated (AKEKmeF,  $m/z = 318.69$ ), di-methylated (AKEKme<sub>2</sub>F,  $m/z = 325.70$ ) and tri-methylated (AKEKme<sub>3</sub>F,  $m/z = 332.71$ ) EF-Tu lysine 5 were directly monitored and quantified by XIC on an Orbitrap Fusion mass spectrometer (ThermoFisher Scientific).

*2.3.9 Isothermal titration calorimetry* – SAM and S-adenosyl-L-homocysteine (SAH) (Sigma-Aldrich) were each dissolved in gel filtration buffer to 1 mM final concentration and titrated into EftM (30-50  $\mu$ M) in  $16 \times 2.4$   $\mu$ l injections using an Auto-iTC<sub>200</sub> microcalorimeter (Malvern/MicroCal) at 25°C. After accounting for the heat of dilution by subtraction of the residual heat measured at the end of the titration, the data were fit using a model for one set of sites to determine the binding affinity ( $K_d$ ). Values reported are the average of at least two independent titrations and the associated standard deviation between these measurements.

*2.3.10 Circular dichroism spectroscopy* – Analysis of EftM (10  $\mu$ M, in gel filtration buffer) unfolding by circular dichroism (CD) was recorded using a Jasco J-810 spectropolarimeter with a Peltier temperature controller. Data were collected using a 1 mm path-length cuvette at 218 nm collecting data every 0.5°C and a heating rate of 1°C/minute from 20-45°C.

*2.3.11 Differential scanning fluorimetry* – The ability of SAM to stabilize the EftM structure was assessed using differential scanning fluorimetry (DSF) essentially as described by Neisen *et al.* (25). Briefly, the change in fluorescence arising from binding of SYPRO Orange dye (5000-fold dilution) to hydrophobic residues upon unfolding of EftM (24  $\mu$ M) was measured over a linear temperature gradient (0.5°C/minute from 25-75°C) in the presence of SAM (150  $\mu$ M) in a StepOne Plus Real-Time PCR instrument (Applied Biosystems), and compared to control experiments containing SAM and dye alone. The first derivative of the melting curve was calculated using GraphPad Prism software to determine melting temperature ( $T_m$ ) corresponding to 50% unfolded protein.

## 2.4 RESULTS

*2.4.1 EftM is a SAM-dependent methyltransferase* – We have previously demonstrated that the laboratory *P. aeruginosa* strain PAO1 shows EF-Tu methylation at 25°C, but not at 37°C (**Figure 2.1**). Deletion of *eftM* (PAO1 $\Delta$ *eftM*) results in no methylation of EF-Tu at either temperature. When PAO1 $\Delta$ *eftM* was complemented with *eftM* under the control of a constitutive promoter, EF-Tu methylation is present at both temperatures, likely due to the overexpression of EftM (**Figure 2.1**) (13). Through the screening of clinical isolates, we identified the strain PAHM23, which failed to methylate EF-Tu at either temperature. Sequencing of *eftM* from PAHM23 revealed a single nucleotide change (G148C) resulting in a single amino acid substitution, G50R. To determine whether this amino acid substitution impacted EftM function, we attempted to complement the EF-Tu methylation-deficient phenotype of PAO1 $\Delta$ *eftM* with the PAHM23 *eftM* gene. In contrast to previous experiments with wild-type PAO1 *eftM* gene (13), the *eftM* gene from PAHM23 was unable to complement PAO1 $\Delta$ *eftM* (**Figure 2.1**). This result thus identifies an amino acid residue critical for EftM activity.

To define the function of EftM, we analyzed the amino acid sequence of EftM using the remote homology detection program HHPred (19). This search revealed that EftM shares predicted structural similarity with Class I SAM-dependent methyltransferases and identified the best homology modeling template as DesVI (PDB ID 3BXO), a *N,N*-dimethyltransferase found in *Streptomyces venezuelae* (26). The EftM homology model has a core domain consisting of seven  $\beta$ -strands with three  $\alpha$ -helices on either side of the  $\beta$ -sheet (Figure 2.2A), characteristic of the Class I methyltransferase fold. This fold loosely divides the protein into two lobes, one of which is responsible for binding to SAM, and the other for target substrate specificity (27).

Augmentations of the conserved Class I methyltransferase core fold vary both in size and architecture. Based on the DesVI template, EftM is predicted to possess an auxiliary domain comprised of an  $\alpha$ -helix derived from the EftM N-terminus and a C-terminal four-stranded anti-parallel  $\beta$ -sheet. This domain forms a structure that covers the SAM-binding cleft of the methyltransferase core fold and could thus define substrate specificity and/or access to the bound SAM cosubstrate.

To experimentally test the structural prediction that EftM is a SAM-dependent methyltransferase and whether SAM and SAH have similar binding affinities ( $K_d$ ) for EftM, we used isothermal titration calorimetry (ITC). These analyses revealed that EftM binds SAM and SAH with  $K_d$  values of  $20 \pm 10 \mu\text{M}$  and  $26 \pm 19 \mu\text{M}$  (Figure 2.2B,C), respectively. Although relatively weak, these binding affinities are comparable to other bacterial methyltransferases (28,29).

EftM residue G50 is located in a SAM-binding motif (motif I, E/DXGXG) conserved among Class I methyltransferases (30), corresponding to residues 46-52 of EftM. To test whether a defect in SAM binding results in the inactivity of the EftM-G50R variant from PAHM23, we again used ITC to assess the EftM-G50R-SAM interaction. EftM-G50R affinity for SAM was dramatically reduced, falling below the limit of detection by ITC (~millimolar) (Figure 2.2D).

This result confirms the importance of G50 for interaction with SAM and explains the observation that PAHM23 EftM-G50R fails to modify EF-Tu (**Figure 2.1**).

*2.4.2 EftM is necessary and sufficient to methylate EF-Tu* – To determine if EftM is sufficient to directly methylate EF-Tu in the presence of SAM, an *in vitro* methyltransferase assay was employed. Purified EftM was incubated with and without SAM and purified EF-Tu at 25°C. Modified EF-Tu was detected by immunoblot analysis using an anti-di/trimethyl lysine antibody only when EftM, SAM, and EF-Tu were all present in the reaction (**Figure 2.3A**). The EftM G50R substitution in EftM ablated methylation of EF-Tu in the assay (**Figure 2.3A**), consistent with *in vivo* observations (**Figure 2.1**) and the effect of the substitution on SAM binding affinity *in vitro* (**Figure 2.2D**). Additionally, no modification was detected using a K5A variant of EF-Tu, consistent with exclusive *in vitro* methylation at this residue (**Figure 2.3A**).

Liquid chromatography-tandem mass spectrometry (LC-MS/MS) analysis was used to further confirm the amino acid methylated by EftM in the *in vitro* assay was lysine 5, as observed for *in vivo* methylated EF-Tu ([13](#)). EF-Tu from *in vitro* reactions with and without EftM was subjected to LC-MS/MS and the peptide corresponding to EF-Tu amino acids 1-6 was identified in both reactions. However, in the reaction containing EftM, a mass shift of 42 Da was observed on the  $y_2$  and  $y_3$  ions in the MS/MS spectrum (**Figure 2.3B**, lower panel) compared to the unmodified peptide spectrum (**Figure 2.3B**, upper panel). Comparison of the complete MS data showed no other differential methylation of EF-Tu. Taken together, these results confirm our previous observations that the site of lysine trimethylation as EF-Tu specifically on residue 5 ([13](#)) and further that both purified EftM and its co-substrate SAM are necessary to specifically and exclusively methylate K5.

*2.4.3 EF-Tu methylation by EftM is distributive* – Examination of the precursor (MS1 scans) extracted ion chromatograms showed that trimethylated lysine 5 peptide ( $m/z = 398.231$ ) was observed only when EftM was present in the *in vitro* reaction (**Figure 2.3C**, right). However, while exclusively unmodified EF-Tu peptide ( $m/z = 377.208$ ) was detected in the untreated sample, some unmodified peptide was also found in the EftM-treated sample (**Figure 2.3C**, left). In these samples from an end-point methylation reaction, no mono- or dimethylated lysine 5 was detected. This result could indicate that EftM acts in a processive manner such that trimethyl lysine 5 is the only product of the enzyme. Alternatively, the observation could reflect a complete reaction with a remaining fraction of recombinant EF-Tu that is not an active substrate of EftM, e.g. due to misfolding. In this scenario, whether EftM could act in a processive or distributive manner would be ambiguous. To address this question, we performed similar MS analyses on *in vivo* methylated EF-Tu and with an *in vitro* methylation time course designed to capture intermediate species should they exist.

To determine if species other than trimethylated lysine 5 exist *in vivo*, recombinant EF-Tu was purified from *P. aeruginosa* grown at 25°C and analyzed by MS. This analysis revealed that while the majority of purified EF-Tu (79%) was indeed trimethylated at lysine 5, each of the un-, mono-, and dimethylated species could also be detected, albeit at much smaller percentages of the purified EF-Tu: 6%, 5%, and 10%, respectively. To determine whether such intermediates, indicative of a distributive enzyme action, are also observed in a controlled *in vitro* methylation reaction, additional EftM methyltransferase assays were performed using 10-fold lower enzyme concentration compared to our standard assay. Under these conditions, Western blot analysis of reaction time course showed a modest level of modification 5 minutes, which increased after 10 minutes (**Figure 2.4**). MS analysis of EF-Tu modification at each of these time points revealed that the majority of EF-Tu was not trimethylated. Concomitant with a decrease in unmethylated lysine 5, the amount of mono-, di-, and trimethylated lysine 5 was greater after 10 minutes

compared to 5 minutes (**Figure 2.4**). This distribution of methyl species indicates that EftM functions in a non-processive (distributive) manner.

*2.4.4 EftM methyltransferase activity is thermosensitive* – In the wild-type strain PAO1, methylation of EF-Tu was observed exclusively at 25°C and not at 37°C (**Figure 2.1**). To assess whether EftM was not only sufficient for the methylation of EF-Tu, but in addition whether the temperature-dependent phenotype is recapitulated using purified proteins in our defined *in vitro* methylation assay, EftM was pre-incubated at either 25°C or 37°C for between 0-20 minutes and then used in the *in vitro* methyltransferase assay at 25°C. Pre-incubation of EftM at 25°C at all times tested had no effect on its activity. In contrast, pre-treatment of EftM at 37°C for 5 minutes resulted in a sharp decrease in EF-Tu modification; by 10 minutes no *in vitro* modified product was detected (**Figure 2.5**). Amounts of both EftM and EF-Tu present in the reaction were verified, and the levels of each remained constant in each of these reactions (**Figure 2.5**, lower panel) indicating that protein degradation was not responsible for the decreased activity. When EftM was subjected to pre-incubation at 37°C in the presence of 2 mM SAM, methyltransferase activity was still lost (data not shown) suggesting that SAM does not stabilize the activity.

*2.4.5 Structural thermolability regulates EftM activity* – As EftM methyltransferase activity is abolished at 37°C both *in vivo* and *in vitro*, we investigated using circular dichroism (CD) spectroscopy whether temperature is affecting the enzyme secondary structure, which might account for this temperature sensitivity. At 25°C, the CD spectrum of recombinant EftM is consistent with a well-folded protein of mixed  $\alpha/\beta$  secondary structure. To determine the unfolding temperature ( $T_m$ ) of EftM, we monitored the CD signal at 218 nm ( $CD_{218}$ ) over a linear temperature gradient. The EftM structure remains stably folded over the range 20-30°C but subsequently begins unfolding as the temperature is increased further. The decrease in strongly negative  $CD_{218}$  signal is indicative of the secondary structure unfolding with an estimated melting

temperature (50% unfolded,  $T_m$ ) of 37°C (**Figure 2.6A**). The observed unfolding was irreversible: the alteration in CD spectrum was retained upon cooling and induced visible precipitation of the protein. We conclude from these results that the temperature sensitivity of EftM activity is due to irreversible protein unfolding at elevated temperature.

We next asked whether EftM is stabilized by its obligatory co-substrate SAM. As the addition of SAM complicates CD analysis, we used differential scanning fluorimetry (DSF) to measure the thermal stability of EftM in the presence of the co-substrate (**Figure 2.6B**). DSF experiments monitor the binding of SYPRO Orange dye to hydrophobic amino acids as they become progressively exposed during protein unfolding at higher temperatures (25). The  $T_m$  for EftM unfolding in the absence of ligand is comparable to that derived from the CD melt, with a value of 30.5°C. The difference in measured  $T_m$  is likely due to the dye binding and stabilizing an unfolded form of EftM resulting in a lower  $T_m$  compared to CD analysis. Adding SAM (150  $\mu$ M) stabilized EftM, raising the  $T_m$  to ~36°C (**Figure 2.6B**). Though EftM may be modestly stabilized by its co-substrate SAM, this effect would not be sufficient to preserve the enzymatic activity at the elevated temperature. These protein-unfolding experiments thus show that EftM is thermosensitive and becomes nonfunctional at higher temperatures, revealing the molecular basis for the temperature dependence of EftM activity observed *in vitro* and *in vivo*.

## 2.5 DISCUSSION

Bacteria possess multiple strategies to adapt to changes in temperature: the heat shock, cold shock, and the low and the high temperature responses (31). These distinct pathways each employ DNA, RNA, or protein molecules as the effectors of the response. In contrast to the heat shock response, which is induced incrementally and is transient, the high temperature response requires a specific elevated temperature and remains active above that point. As such, the high temperature response is an important mechanism by which pathogenic bacteria can detect entry

into a mammalian host, leading to induction and continued expression of virulence genes.

Temperature related changes in gene expression are typically regulated at the level of transcription, via changes in DNA structure that expose RNA polymerase, activator or repressor binding sites, activation of alternative sigma factors, or through changes in promoter or repressor protein structure or oligomeric state that influence DNA binding. Alternatively, regulation can occur at the level of translation initiation through “RNA thermometer” structures that allow the ribosome access only at the elevated temperature (31). In this study, we have provided evidence for another mechanism of thermoregulation through direct protein structural changes in the *P. aeruginosa* methyltransferase EftM.

Collectively, our results demonstrate that EftM is a SAM-dependent methyltransferase that rapidly loses activity via irreversible unfolding of its protein structure at ~37°C. The temperature optimum for growth of *P. aeruginosa* is ~37°C (32), but this opportunistic pathogen can grow at temperatures from 22°C-45°C (33). Our finding that EftM unfolds at 37°C suggests that the activity of this enzyme is not essential for maximum *P. aeruginosa* growth but, rather, may play an important role in the transition from environment to host. “Moonlighting roles” for EF-Tu have been described in various bacteria, and include chaperone-like properties involved in the bacterial stress response (34) and, through its localization to the bacterial surface, involvement in adherence to numerous proteins and host factors (13,14,35-40). A *P. aeruginosa* EftM mutant that cannot methylate EF-Tu adheres and invades epithelial cells less well compared to a wild-type strain and that this strain is also less virulent in a murine acute pneumonia model (13). While we have not excluded that EftM may methylate other targets, we have shown that trimethylated EF-Tu binds to epithelial cells better than non-modified EF-Tu (13) indicating a direct role of this modification in adherence and presumably virulence. Collectively, these observations and our new findings suggest that the temperature dependence of EftM activity may be one mechanism by

which this opportunistic pathogen promotes adherence via lysine 5 trimethylated EF-Tu as it transitions from the environment to the host.

EftM thermoinstability can rapidly halt methyltransferase activity but does not influence the fate of previously methylated EF-Tu. In *P. aeruginosa*, modified EF-Tu persists for at least 4 hours in cells switched from growth at 20°C to 37°C (41), providing good evidence that there is no demethylase capable of specifically reversing EF-Tu lysine 5 trimethylation. Thus, the ultimate loss of trimethylated EF-Tu over a timeframe of several hours is likely dependent on the rate of EF-Tu, and not EftM, turnover, implying that the effects of trimethylated EF-Tu will continue to be manifested as *P. aeruginosa* transitions from the environment to the human host during the disease process.

In contrast to the potential influence of lysine 57 modification on *E. coli* growth, we observed no alteration in growth rate in an *eftM* deletion mutant under standard laboratory conditions (13). Although our MS analysis of *in vivo* modified recombinant EF-Tu suggests the majority of protein is trimethylated at lysine 5, the fraction of native EF-Tu that is trimethylated in *P. aeruginosa* is not known. If a large proportion of lysine 5-modified is observed, as was seen with the recombinant EF-Tu protein, this could point to an influence upon EF-Tu function in protein chain elongation (e.g. altering the speed of translation and/or increasing fidelity). The potential that EF-Tu lysine 5 methylation could impact protein chain elongation is supported by the finding that residues 1-4 of *E. coli* EF-Tu are responsible for properly aligning residues 5-9 to complex with guanine nucleotides and aa-tRNA for efficient protein chain elongation (42). Perhaps the distribution of mono-, di-, and trimethylated EF-Tu impact these interactions differently, which may provide a previously unappreciated means to control gene expression. If, on the other hand, if a relatively small fraction of EF-Tu is methylated, it could suggest that methylation specifically targets EF-Tu to perform functions outside its established role in protein

synthesis. And, while the effect of EF-Tu as an adhesin has been described ([14,39](#)), whether and/or how methylation influences the export of EF-Tu to the bacterial cell surface is currently unknown.

In summary, we have expressed and characterized the thermoregulated SAM-dependent methyltransferase EftM, responsible for methylating lysine 5 of the essential translation factor EF-Tu. EftM binds SAM and SAH with similar affinity and appears to modify EF-Tu in a distributive manner. Most importantly, we have shown that the EftM structure is thermosensitive, a feature which we propose is responsible for driving the observed temperature-dependent methylation phenotype in *P. aeruginosa*. The ability to express and purify functional EftM is a major step necessary for detailed structural and functional analyses of EftM cosubstrate and substrate recognition, and enzymatic turnover. Additionally, this work provides a platform to study the potential impacts of EftM methylation of EF-Tu on its canonical role in protein synthesis and other moonlighting functions in *P. aeruginosa*. Methylation of translation factors may be a conserved means of regulating protein chain elongation in bacteria and, as such, has the potential to provide us with deeper understanding of the mechanisms that bacterial protein synthesis.

## 2.6 ACKNOWLEDGEMENTS

JPO was supported in part from a training grant from the National Institute of Allergy And Infectious Diseases (NIAID) of the National Institutes of Health (NIH) to the University of Virginia (T32AI007046). SMP was supported in part by a training grant from the NIAID of the NIH to Emory University (T32AI106699). EGK was supported by the Agriculture and Food Research Initiative Competitive Grant No. 2013-67011-21133 from the USDA National Institute of Food and Agriculture. This work was supported in part through grants (GOLDBE10G0; GOLDBE14P0) from the Cystic Fibrosis Foundation to JBG, from the NIH (R21AI103651) to

JBG and from the Ministerio de Economía y Competitividad of Spain, through the grant SAF2012-38426 and the Spanish Network for the Research in Infectious Diseases (REIPI RD12/0015) from Instituto de Salud Carlos III (both co-financed by European Development Regional Fund (ERDF)) to SA. Mass spectrometry was supported by the Emory Neuroscience NINDS Core Facilities (P30NS055077). The Auto-iTC<sub>200</sub> instrument was purchased with support from the NSF MRI program (grant 104177), the Winship Cancer Institute's shared resource program and the Biochemistry Department of Emory University. The content is solely the responsibility of the authors and does not necessarily represent the official views of the NIH.

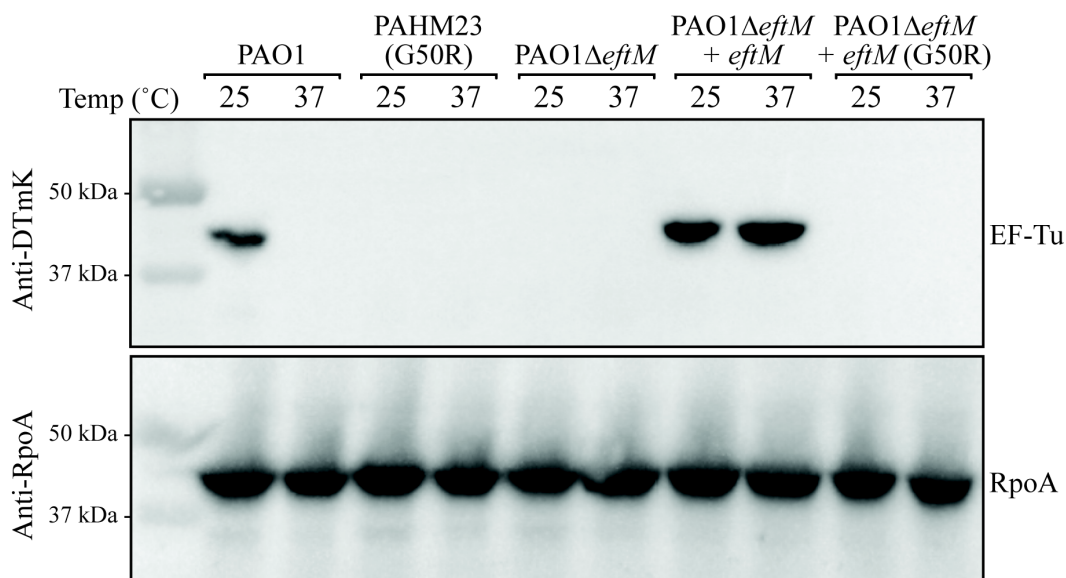


**FIGURE 2.1 Wild-type but not G50R substituted EftM is able methylate EF-Tu *in vivo*.**

Western blot analysis of whole cell lysates from the indicated *P. aeruginosa* strains, as well as a previously described *eftM* deletion mutant, PAO1 $\Delta$ *eftM*, complemented with a plasmid (pUCP18ApGw (*eftM*)) containing the wild-type PAO1 EftM (+*eftM*) or a plasmid (pJO7) containing the G50R EftM (+*eftM* G50R) blotted with both anti-DTmK (upper) and anti-RpoA (lower) antibodies.

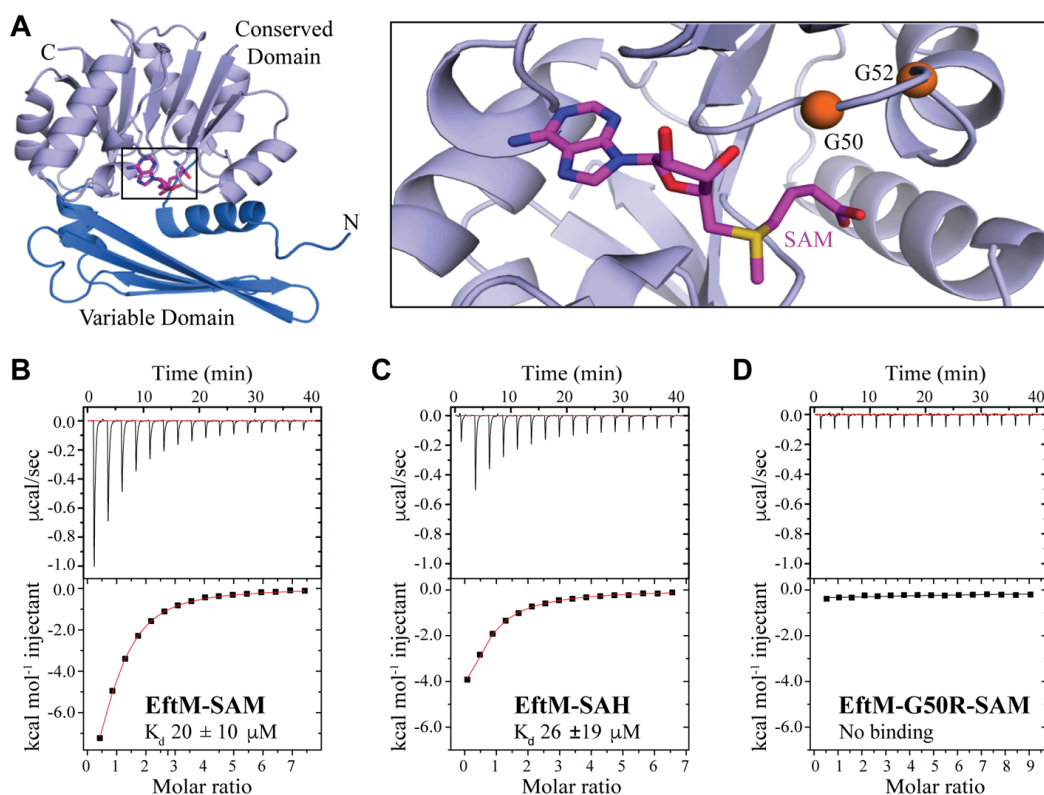


**FIGURE 2.2 EftM shares structural homology with Class I SAM-dependent methyltransferases and binds cosubstrate.** (A) Homology model of the EftM-SAM complex produced using the structure of DesVI as template. The conserved Class I methyltransferase domain (light blue), variable domain (blue) and SAM (pink sticks) are indicated. The *box* indicates the SAM binding pocket of EftM shown in a magnified view on the *right*. The  $\alpha$ -carbons of residues G50 and G52 (orange spheres) of the conserved E/DXGXG SAM binding motif are highlighted. Isothermal titration calorimetry (ITC) analysis of wild-type EftM interaction with (B) SAM and (C) SAH. (D) ITC analysis of EftM-G50R interaction with SAM.

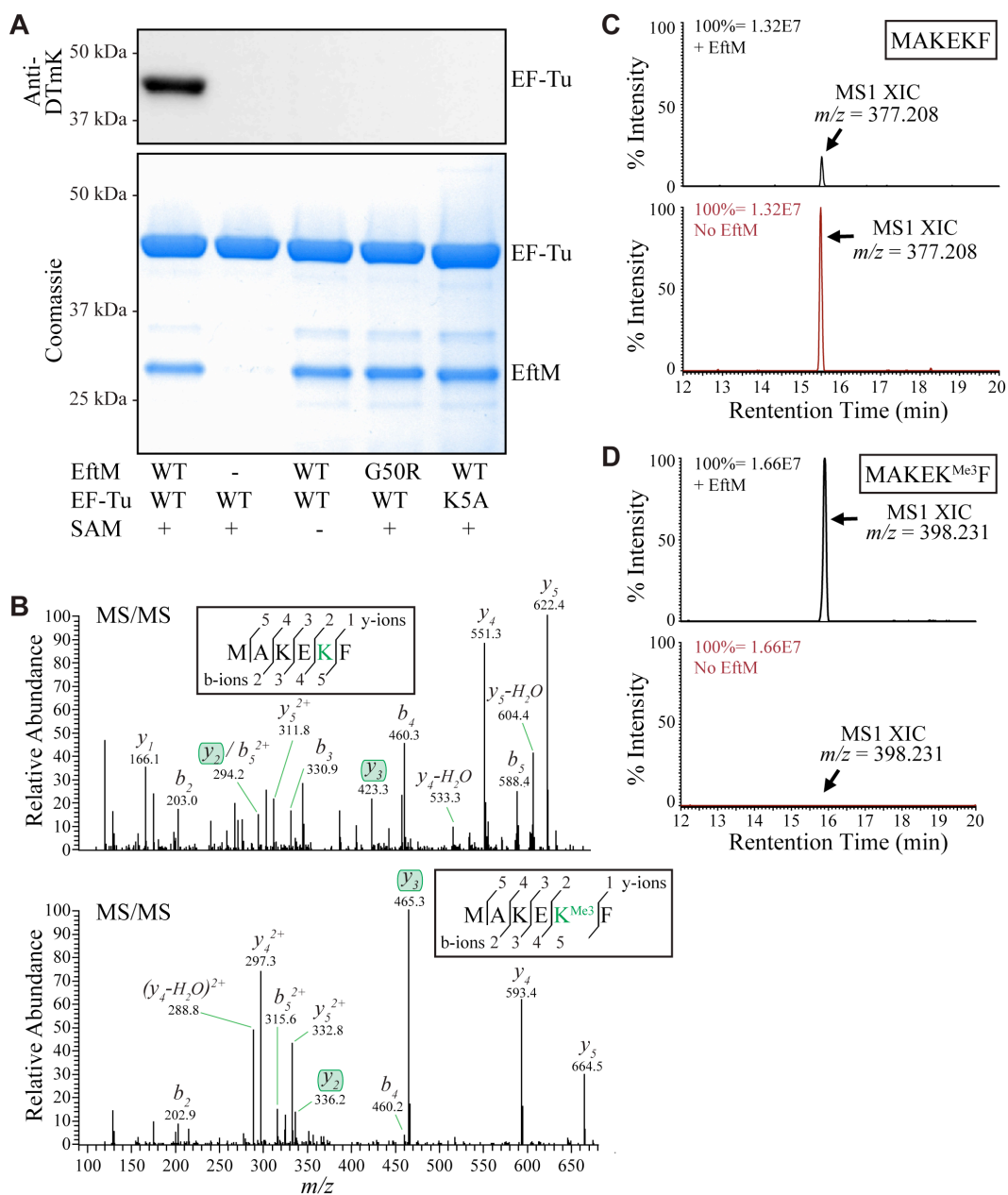


**FIGURE 2.3 *In vitro* lysine 5 trimethylation and quantification on recombinant EF-Tu.** (A)

A representative *in vitro* methylation assay ( $n = 3$ ) with wild-type (WT) PAO1 EftM or EftM G50R and wild-type PAO1 EF-Tu or EF-Tu K5A shows that EftM requires SAM and methylates EF-Tu exclusively at lysine 5. Upper panel: Western blot of methyltransferase assay products detected with DTmK antibodies. Lower panel: Coomassie stained gel of the same reaction products. (B) Chymotrypsin-digested EF-Tu from *in vitro* reactions examined by LC-MS/MS. Representative MS/MS spectra are shown of the EF-Tu doubly charged  $(M+2H)^{2+}$  unmodified (top) and EftM modified (bottom) peptide sequence corresponding to residues 1-6. Fragment ions  $y_2$  and  $y_3$  (green) are shifted by 42 kDa in mass, confirming lysine 5 trimethylation. Precursor (MS1 scans) extracted ion chromatograms (measured as the percentage intensity using  $\pm 20$  ppm mass tolerance) for (C) the unmodified EF-Tu peptide ( $m/z = 377.208$ ;  $m/z = 377.2018$  theoretical) and (D) the trimethylated EF-Tu lysine 5 peptide ( $m/z = 398.231$ ;  $m/z = 398.2253$  theoretical) are shown for EftM treated and untreated samples (top and bottom in each panel, respectively). The X-axis indicates the retention time when the peptide eluted from the LC column. Peptide intensities were normalized to 100% for sample with the most intense signal in each panel.

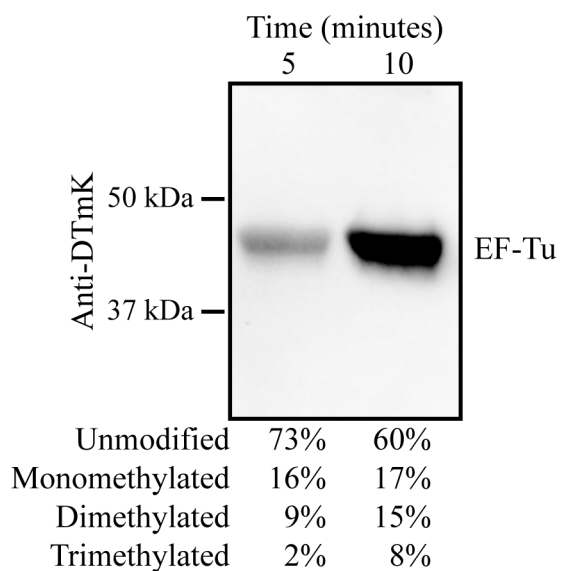


**FIGURE 2.4 EftM adds methyl groups to EF-Tu lysine 5 in a distributive manner.** Western blot of methyltransferase assay products using antibodies to detect DTmK. Reactions were performed using excess SAM and EF-Tu at 25°C and analyzed at 5 and 10 minute time points. The proportion of each lysine 5 methyl species (un-, mono-, di- and trimethylated) as determined by mass spectrometry are shown. Percentages indicate the proportion of total signal intensity of all lysine 5 peptides detected represented by each methyl lysine 5 species.

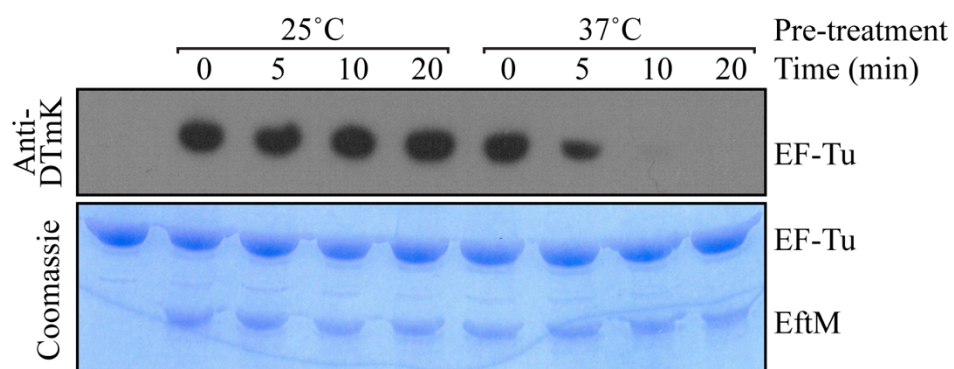


**FIGURE 2.5 EftM activity is thermolabile.** Representative Western blot (upper) using antibodies to detect DTmK of products from methyltransferase assays using wild-type PAO1 EftM and EF-Tu, and 1 mM SAM incubated at 25°C after incubation (0 minutes-20 minutes) at 25°C or 37°C. Loss of activity is not due to protein degradation as seen by Coomassie staining of reaction products (lower) (n = 2).

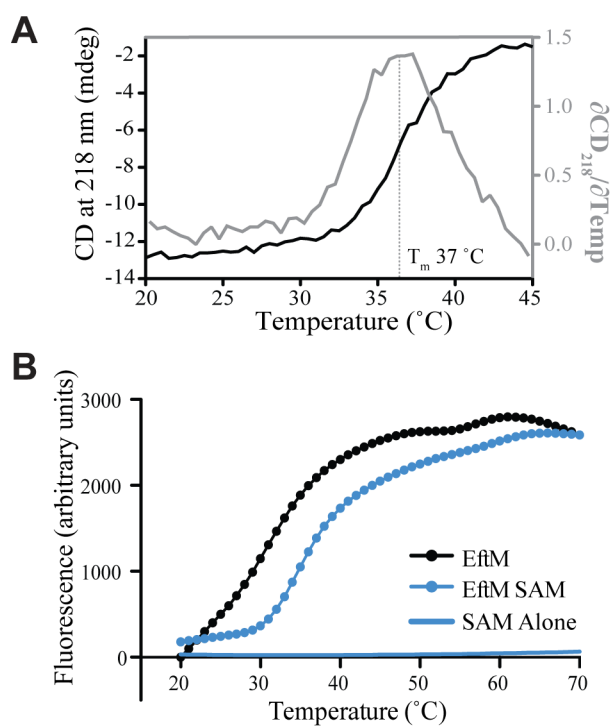


**FIGURE 2.6 EftM structure is thermolabile.** (A) EftM secondary structure unfolding over a linear temperature gradient as shown by CD signal at 218 nm (black; left axis) with the first-derivative of the unfolding curve (gray; right axis). (B) DSF analysis of the thermal stability of EftM alone (black circles), in the presence of EftM and 150  $\mu\text{M}$  SAM (blue circles), or with 150  $\mu\text{M}$  SAM alone (blue line).

**TABLE 2.1. Summary of strains and plasmids**

Strain	Relevant Characteristics or Genotype	Source/Reference
<i>P. aeruginosa</i> PAO1	Wild-type	(14)
<i>P. aeruginosa</i> PAO1 $\Delta$ <i>eftM</i>	Deletion of <i>eftM</i> derived from PAO1	(14)
<i>P. aeruginosa</i> PAHM23	Chronic infection isolate with G50R mutation in <i>eftM</i>	(15)
<i>E. coli</i> BL21	<i>fhuA2 [lon] ompT gal [dcm] <math>\Delta</math>hsdS</i>	New England Biolabs
<i>E. coli</i> BL21-AI	F <sup>-</sup> <i>ompT hsdS<sub>B</sub>(r<sub>B</sub><sup>-</sup>m<sub>B</sub><sup>-</sup>) gal dcm araB::T7RNAP-tetA</i>	Invitrogen
<i>E. coli</i> Top10	F <sup>-</sup> <i>mcrA <math>\Delta</math>(mrr-hsdRMS-mcrBC) <math>\Phi</math>80lacZ<math>\Delta</math>M15 <math>\Delta</math>lacX74 recA1 araD139 <math>\Delta</math>(ara-leu)7697 galU galK rpsL (Str<sup>R</sup>) endA1 nupG</i>	Invitrogen
<i>E. coli</i> DH5 $\alpha$ Library Efficiency	F <sup>-</sup> $\phi$ 80lacZ $\Delta$ M15 $\Delta$ (lacZYA-argF)U169 <i>recA1 endA1 hsdR17(r<sub>k</sub><sup>-</sup>,m<sub>k</sub><sup>+</sup>)phoA supE55 thi-1 gyrA96 relA1 <math>\lambda</math><sup>-</sup></i>	Invitrogen
Plasmid	Description	Source/Reference
pUCP18ApGw	Gateway compatible broad-host-range vector	(14)
pENTR/SD/D-TOPO	Gateway <sup>®</sup> compatible directional cloning entry vector with Shine-Dalgarno sequence; Km <sup>r</sup>	Life Technologies
pUCP18ApGw ( <i>eftM</i> )	pUCP18ApGw + PAO1 <i>eftM</i> C-terminal FLAG fusion	(14)
pUCP18ApGw ( <i>tufB</i> )	pUCP18ApGw + PAO1 <i>tufB</i> N-His <sub>6</sub> tag	(14)
pJPO7	pUCP18ApGw + PAHM23 (G50R) <i>eftM</i> C-terminal FLAG fusion	This study
pCOLDII	Cold shock expression vector; Ap <sup>r</sup>	Takara
pDEST14	Gateway <sup>®</sup> compatible arabinose inducible expression vector; Ap <sup>r</sup>	Life Technologies
pG-Tf2	Tetracycline inducible chaperone plasmid containing <i>groES-groEL-tig</i> ; Cm <sup>r</sup>	Takara
pJPO1	pCOLDII + <i>eftM</i> N-His <sub>6</sub> fusion	This study
pJPO2	pCOLDII + <i>eftM</i> G50R N-His <sub>6</sub> fusion	This study
pJPO4	pDEST14 + <i>tufB</i> N-His <sub>6</sub> fusion	This study
pJPO5	pDEST14 + <i>tufB</i> K5A N-His <sub>6</sub> fusion	This study

Ap<sup>r</sup> - Ampicillin resistance, Km<sup>r</sup> - Kanamycin resistance, Cm<sup>r</sup> - Chloramphenicol resistance

**TABLE 2.2. Summary of DNA oligonucleotides**

<b>Primer</b>	<b>Sequence</b>	<b>Description</b>
<i>tuf</i> BF	CACCATGCATCATCATCATCATATGGCTAA AGAAAAATTTGA	See (14)
<i>tuf</i> BR	TTATTCGATGATCTTGGCAACC	See (14)
<i>tuf</i> BF K5A	CACCATGCATCATCATCATCATATGGCTAA AGAAGCATTGA	See (14)
oJPO18	CACCATGTCCGCCACCGCGCTG	<i>eftM</i> Forward Gateway
oJPO19	CTACTTGTCATCGTCATCCTTGTAGTCGCGCTTC ACGCAGAC	<i>eftM</i> Reverse C-FLAG
oJPO20	CATCATATGTCCGCCACCGCGCTG	<i>eftM</i> Forward NdeI
oJPO21	CTAAAGCTTCTAGCGCTTCACGCAGACGAACAG	<i>eftM</i> Reverse HindIII
oJPO120	CATCCATGGCATCCGCCACCGCGCTGTACA	<i>eftM</i> Forward NcoI
oJPO121	ATGAAGCTTCTACTTGTGCATCGTCATCCTTGTAG TCGCGCTTCACGCAGAC	<i>eftM</i> Reverse FLAG HindIII

## 2.7 REFERENCES

1. Azevedo, C., and Saiardi, A. (2015) Why always lysine? The ongoing tale of one of the most modified amino acids. *Adv Biol Regul*
2. Ambler, R. P., and Rees, M. W. (1959) Epsilon-N-methyl-lysine in bacterial flagellar protein. *Nature* **184**, 56-57
3. Greer, E. L., and Shi, Y. (2012) Histone methylation: a dynamic mark in health, disease and inheritance. *Nat Rev Genet* **13**, 343-357
4. Garcia-Fontana, C., Corral Lugo, A., and Krell, T. (2014) Specificity of the CheR2 methyltransferase in *Pseudomonas aeruginosa* is directed by a C-terminal pentapeptide in the McpB chemoreceptor. *Sci Signal* **7**, ra34
5. Schmidt, J., Musken, M., Becker, T., Magnowska, Z., Bertinetti, D., Moller, S., Zimmermann, B. Herberg, F. W., Jansch, L., and Haussler, S. (2011) The *Pseudomonas aeruginosa* chemotaxis methyltransferase CheR1 impacts on bacterial surface sampling. *PLoS One* **6**, e18184
6. Wuichet, K., and Zhulin, I. B. (2010) Origins and diversification of a complex signal transduction system in prokaryotes. *Sci Signal* **3**, ra50
7. Chang, F. N., Chang, C. N., and Paik, W. K. (1974) Methylation of ribosomal proteins in *Escherichia coli*. *J Bacteriol* **120**, 651-656
8. Abeykoon, A., Wang, G., Chao, C. C., Chock, P. B., Gucek, M., Ching, W. M., and Yang, D. C. (2014) Multimethylation of *Rickettsia* OmpB catalyzed by lysine methyltransferases. *J Biol Chem* **289**, 7691-7701
9. Lanouette, S., Mongeon, V., Figeys, D., and Couture, J. F. (2014) The functional diversity of protein lysine methylation. *Mol Syst Biol* **10**, 724
10. L'Italien, J. J., and Laursen, R. A. (1979) Location of the site of methylation in elongation factor Tu. *FEBS Lett* **107**, 359-362

11. Van Noort, J. M., Kraal, B., Sinjorgo, K. M., Persoon, N. L., Johanns, E. S., and Bosch, L. (1986) Methylation *in vivo* of elongation factor EF-Tu at lysine-56 decreases the rate of tRNA-dependent GTP hydrolysis. *Eur J Biochem* **160**, 557-561
12. Kraal, B., Lippmann, C., and Kleanthous, C. (1999) Translational regulation by modifications of the elongation factor Tu. *Folia Microbiol (Praha)* **44**, 131-141
13. Barbier, M., Owings, J. P., Martinez-Ramos, I., Damron, F. H., Gomila, R., Blazquez, J., Goldberg, J. B., and Alberti, S. (2013) Lysine trimethylation of EF-Tu mimics platelet-activating factor to initiate *Pseudomonas aeruginosa* pneumonia. *MBio* **4**, e00207-00213
14. Barbier, M., Oliver, A., Rao, J., Hanna, S. L., Goldberg, J. B., and Alberti, S. (2008) Novel phosphorylcholine-containing protein of *Pseudomonas aeruginosa* chronic infection isolates interacts with airway epithelial cells. *J Infect Dis* **197**, 465-473
15. Clark, S. E., and Weiser, J. N. (2013) Microbial modulation of host immunity with the small molecule phosphorylcholine. *Infect Immun* **81**, 392-401
16. Wurtzel, O., Yoder-Himes, D. R., Han, K., Dandekar, A. A., Edelheit, S., Greenberg, E. P., Sorek, R., and Lory, S. (2012) The single-nucleotide resolution transcriptome of *Pseudomonas aeruginosa* grown in body temperature. *PLoS Pathog* **8**, e1002945
17. Barbier, M., Damron, F. H., Bielecki, P., Suarez-Diez, M., Puchalka, J., Alberti, S., Dos Santos, V. M., and Goldberg, J. B. (2014) From the Environment to the Host: Re-Wiring of the Transcriptome of *Pseudomonas aeruginosa* from 22 degrees C to 37 degrees C. *PLoS One* **9**, e89941
18. Studier, F. W. (2005) Protein production by auto-induction in high density shaking cultures. *Protein Expr Purif* **41**, 207-234
19. Soding, J., Biegert, A., and Lupas, A. N. (2005) The HHpred interactive server for protein homology detection and structure prediction. *Nucleic Acids Res* **33**, W244-248
20. Sali, A., and Blundell, T. L. (1993) Comparative protein modelling by satisfaction of spatial restraints. *J Mol Biol* **234**, 779-815

21. Elias, J. E., and Gygi, S. P. (2007) Target-decoy search strategy for increased confidence in large-scale protein identifications by mass spectrometry. *Nat Methods* **4**, 207-214
22. Xu, P., Duong, D. M., and Peng, J. (2009) Systematical optimization of reverse-phase chromatography for shotgun proteomics. *J Proteome Res* **8**, 3944-3950
23. Seyfried, N. T., Gozal, Y. M., Donovan, L. E., Herskowitz, J. H., Dammer, E. B., Xia, Q., Ku, L., Chang, J., Duong, D. M., Rees, H. D., Cooper, D. S., Glass, J. D., Gearing, M., Tansey, M. G., Lah, J. J., Feng, Y., Levey, A. I., and Peng, J. (2012) Quantitative analysis of the detergent-insoluble brain proteome in frontotemporal lobar degeneration using SILAC internal standards. *J Proteome Res* **11**, 2721-2738
24. Gozal, Y. M., Seyfried, N. T., Gearing, M., Glass, J. D., Heilman, C. J., Wu, J., Duong, D. M., Cheng, D., Xia, Q., Rees, H. D., Fritz, J. J., Cooper, D. S., Peng, J., Levey, A. I., and Lah, J. J. (2011) Aberrant septin 11 is associated with sporadic frontotemporal lobar degeneration. *Mol Neurodegener* **6**, 82
25. Niesen, F. H., Berglund, H., and Vedadi, M. (2007) The use of differential scanning fluorimetry to detect ligand interactions that promote protein stability. *Nat Protoc* **2**, 2212-2221
26. Burgie, E. S., and Holden, H. M. (2008) Three-dimensional structure of DesVI from *Streptomyces venezuelae*: a sugar *N,N*-dimethyltransferase required for dTDP-desosamine biosynthesis. *Biochemistry* **47**, 3982-3988
27. Schubert, H. L., Blumenthal, R. M., and Cheng, X. (2003) Many paths to methyltransfer: a chronicle of convergence. *Trends Biochem Sci* **28**, 329-335
28. Garcia-Fontana, C., Reyes-Darias, J. A., Munoz-Martinez, F., Alfonso, C., Morel, B., Ramos, J. L., and Krell, T. (2013) High specificity in CheR methyltransferase function: CheR2 of *Pseudomonas putida* is essential for chemotaxis, whereas CheR1 is involved in biofilm formation. *J Biol Chem* **288**, 18987-18999

29. Witek, M. A., and Conn, G. L. (2014) Expansion of the aminoglycoside-resistance 16S rRNA (m(1)A1408) methyltransferase family: expression and functional characterization of four hypothetical enzymes of diverse bacterial origin. *Biochim Biophys Acta* **1844**, 1648-1655
30. Martin, J. L., and McMillan, F. M. (2002) SAM (dependent) I AM: the S-adenosylmethionine-dependent methyltransferase fold. *Curr Opin Struct Biol* **12**, 783-793
31. Lam, O., Wheeler, J., and Tang, C. M. (2014) Thermal control of virulence factors in bacteria: a hot topic. *Virulence* **5**, 852-862
32. Tsuji, A., Kaneko, Y., Takahashi, K., Ogawa, M., and Goto, S. (1982) The effects of temperature and pH on the growth of eight enteric and nine glucose non-fermenting species of gram-negative rods. *Microbiol Immunol* **26**, 15-24
33. Kropinski, A. M., Lewis, V., and Berry, D. (1987) Effect of growth temperature on the lipids, outer membrane proteins, and lipopolysaccharides of *Pseudomonas aeruginosa* PAO. *J Bacteriol* **169**, 1960-1966
34. Caldas, T. D., El Yaagoubi, A., and Richarme, G. (1998) Chaperone properties of bacterial elongation factor EF-Tu. *J Biol Chem* **273**, 11478-11482
35. Marques, M. A., Chitale, S., Brennan, P. J., and Pessolani, M. C. (1998) Mapping and identification of the major cell wall-associated components of *Mycobacterium leprae*. *Infect Immun* **66**, 2625-2631
36. Porcella, S. F., Belland, R. J., and Judd, R. C. (1996) Identification of an EF-Tu protein that is periplasm-associated and processed in *Neisseria gonorrhoeae*. *Microbiology* **142 ( Pt 9)**, 2481-2489
37. Granato, D., Bergonzelli, G. E., Pridmore, R. D., Marvin, L., Rouvet, M., and Corthesy-Theulaz, I. E. (2004) Cell surface-associated elongation factor Tu mediates the attachment of *Lactobacillus johnsonii* NCC533 (La1) to human intestinal cells and mucins. *Infect Immun* **72**, 2160-2169

38. Schaumburg, J., Diekmann, O., Hagendorff, P., Bergmann, S., Rohde, M., Hammerschmidt, S., Jansch, L., Wehland, J., and Karst, U. (2004) The cell wall subproteome of *Listeria monocytogenes*. *Proteomics* **4**, 2991-3006
39. Kunert, A., Losse, J., Gruszyn, C., Huhn, M., Kaendler, K., Mikkat, S., Volke, D., Hoffmann, R., Jokiranta, T. S., Seeberger, H., Moellmann, U., Hellwage, J., and Zipfel, P. F. (2007) Immune evasion of the human pathogen *Pseudomonas aeruginosa*: elongation factor Tuf is a factor H and plasminogen binding protein. *J Immunol* **179**, 2979-2988
40. Balasubramanian, S., Kannan, T. R., and Baseman, J. B. (2008) The surface-exposed carboxyl region of *Mycoplasma pneumoniae* elongation factor Tu interacts with fibronectin. in *Infect Immun*, 2008/04/16 Ed.
41. Weiser, J. N., Goldberg, J. B., Pan, N., Wilson, L., and Virji, M. (1998) The phosphorylcholine epitope undergoes phase variation on a 43-kilodalton protein in *Pseudomonas aeruginosa* and on pili of *Neisseria meningitidis* and *Neisseria gonorrhoeae*. *Infect Immun* **66**, 4263-4267
42. Laurberg, M., Mansilla, F., Clark, B. F., and Knudsen, C. R. (1998) Investigation of functional aspects of the N-terminal region of elongation factor Tu from *Escherichia coli* using a protein engineering approach. *J Biol Chem* **273**, 4387-4391

**CHAPTER 3:****A NOVEL MOTIF REQUIRED FOR S-ADENOSYL-L-METHIONINE COSUBSTRATE  
BINDING BY THE 2'-O-METHYLTRANSFERASE TLYA FROM *MYCOBACTERIUM  
TUBERCULOSIS***

Marta A. Witek\*, Emily G. Kuiper\*, Elizabeth Minten, Emily K. Crispell and Graeme L. Conn

\*Co-first authors.

This manuscript is in preparation for submission to Structure. E.G.K. directly contributed to Figures: 3.2B; 3.5B, 3.5F; 3.6, 3.7, 3.8, 3.S1, Table 3.2 and Table 3.S1 and made all figures.

Author Contributions: Conceptualization, G.L.C.; Methodology, M.A.W., E.G.K. and G.L.C.; Investigation, M.A.W., E.G.K., E.K.C. and E.M.; Writing – Original Draft, E.G.K and M.A.W.; Writing – Review & Editing, E.G.K., M.A.W., E.K.C. and E.M. and G.L.C.; Funding Acquisition, G.L.C.; Supervision, G.L.C..

### 3.1 SUMMARY

Capreomycin is a potent ribosome-targeting antibiotic that is an essential component of current antituberculosis treatments, particularly in the case of multi-drug resistant (MDR) *Mycobacterium tuberculosis* (*Mtb*). Optimal capreomycin binding and *Mtb* ribosome inhibition requires ribosomal RNA (rRNA) methylation in both ribosome subunits by TlyA (Rv1694), an enzyme with dual 2'-O-methyltransferase and putative hemolytic activities. Here, we present structural and functional analyses of *Mtb* TlyA interaction with its obligatory cosubstrate for methyltransferase activity, S-adenosyl-L-methionine (SAM). Despite adopting a complete Class I methyltransferase fold containing conserved SAM-binding and catalytic motifs, the isolated TlyA carboxyterminal domain (CTD) exhibits no detectable affinity for SAM. Further analyses identify a novel tetrapeptide motif (RxWV) in the TlyA interdomain linker as indispensable for cosubstrate binding. Our results also suggest that structural plasticity of the RxWV motif could contribute to TlyA domain interactions as well as specific recognition of its two structurally distinct rRNA targets.

### 3.2 INTRODUCTION

*Mycobacterium tuberculosis* (*Mtb*), the etiological agent of tuberculosis (TB), infects approximately one-third of the world's population and resulted in an estimated 9.6 million new cases of active TB disease and 1.5 million deaths in 2014 ((WHO), 2015). Of further significant concern is the rising number of TB cases involving *Mtb* strains that are either multidrug-resistant, defined as being resistant to the first-line antibiotics isoniazid and rifampicin, or extensively drug-resistant, defined as being additionally resistant to any fluoroquinolone and at least one of the three injectable second-line drugs, amikacin, kanamycin, or capreomycin (Dorman and Chaisson, 2007; Mukherjee et al., 2004).

Capreomycin is a cyclic aminoglycoside-like peptide antibiotic belonging to the tuberactinomycin family of antibiotics, which are among the most effective drugs against multidrug-resistant *Mtb*. Capreomycin targets the mycobacterial ribosome at the interface of the small and large subunits (Stanley et al., 2010) and requires ribosomal RNA (rRNA) methylation for optimal binding and thus inhibition of ribosome function. Resistance to capreomycin in *Mtb* can arise via mutation of *tlyA*, the gene encoding the protein TlyA (Rv1694), a proposed virulence factor for *Mtb* with dual hemolytic and rRNA methyltransferase activities (Johansen et al., 2006; Maus et al., 2005a, b; Rahman et al., 2010). Resistance to ribosome-targeting drugs is generally associated with the addition of methyl groups rather than their loss (Conn et al., 2009; Cundliffe, 1989; Long and Vester, 2009). Thus, TlyA belongs to a unique group of methyltransferases for which loss of function confers bacterial antibiotic resistance. Additionally, as many bacterial genera lack *tlyA*, the potent antibiotic activity of capreomycin is specific against *Mtb* (Johansen et al., 2006; Wren et al., 1998). However, treatment of TB has become problematic due not only to the side effects of aminoglycosides but also to the increased incidence of virulent, capreomycin-resistant *Mtb* strains generated by inactivation of *tlyA* (Avent et al., 2011; Johansen et al., 2006).

The *S*-adenosyl-L-methionine (SAM)-dependent methyltransferase activity of TlyA results in ribose 2'-OH methylation of two cytidine residues: 16S rRNA C1409, which is located within the 30S (small) ribosomal subunit "decoding center", and 23 rRNA C1920, present in a highly conserved region of the 50S (large) ribosomal subunit near the subunit interface (Johansen et al., 2006; Stanley et al., 2010; Wimberly et al., 2000). Despite the importance of TlyA methyltransferase activity in capreomycin action and resistance, many molecular details of TlyA's mechanism of action remain largely unknown, including interaction with cosubstrate SAM and how TlyA recognizes and methylates its two structurally distinct substrates (23S and

16S rRNA). Therefore, detailed molecular studies of TlyA are urgently required to better understand this resistance determinant and its contribution to capreomycin susceptibility.

Here, we demonstrate experimentally that TlyA folds into two stable structural domains connected by a protease-sensitive linker, with rRNA binding and SAM binding/methyltransferase activities expected to reside in the amino- and carboxy-terminal domains (NTD and CTD), respectively. A high-resolution X-ray crystal structure of the TlyA CTD reveals a Class I methyltransferase fold containing all expected conserved SAM binding and catalytic motifs. Remarkably, however, this isolated protein domain has no detectable affinity for SAM and further structural and functional studies reveal a novel tetrapeptide motif (RxWV) in the region linking the two structural domains as indispensable for cosubstrate binding. Finally, our results also suggest that structural plasticity within this interdomain linker could play a role in TlyA recognition of its two structurally distinct rRNA targets.

### 3.3 RESULTS

#### 3.3.1 Construct Design, Protein Expression and Purification of TlyA for Structural Studies.

A plasmid encoding N-terminally hexahistidine-tagged *Mtb* TlyA (His-TlyA) was generated for heterologous expression in *E. coli* and the resulting protein purified to near homogeneity using Ni<sup>2+</sup>-affinity and gel filtration chromatographies. The circular dichroism (CD) spectrum of His-TlyA is consistent with that of a well-folded protein with a mixed  $\alpha/\beta$  structure (**Figure 3.1A**). We additionally showed our purified recombinant His-TlyA to be active in methylation of both target nucleotides, C1920 (23S rRNA) and C1409 (16S rRNA), by primer extension analysis of *in vitro* methylated *E. coli* 50S and 30S subunits (**Figure 3.1B**).

We next attempted to crystallize full-length His-TlyA to solve its high-resolution X-ray crystal structure but efforts to obtain suitable crystals were unsuccessful. Therefore, His-TlyA

was treated with various proteases with the goal of identifying stable fragment(s) of TlyA better suited to structural studies. The endopeptidase GluC, a serine proteinase that selectively cleaves peptide bonds C-terminal to glutamic acid residues (Drapeau et al., 1972), produced two stable fragments of ~10 kDa and ~20 kDa (**Figure 3.2A**). Based on the observed digestion pattern and inspection of the TlyA sequence and homology model (Arenas et al., 2011), we identified glutamic acid 59 (Glu59) as the most likely site of GluC cleavage. The TlyA homology model predicts Glu59 to be surface exposed in an unstructured region that links the predicted NTD and CTD (**Figure 3.2B**), and GluC cleavage this residue would result in products of 7.9 or 6.2 kDa (NTD; with or without the hexhistidine tag) and 21.8 kDa (CTD), correlating well with the observed products. Cleavage products of similar sizes were also previously observed for TlyA treated with Proteinase K which was hypothesized to target a site within the interdomain linker (Rahman et al., 2010). To test whether Glu59 was indeed the GluC cleavage site, a TlyA-E59A variant was generated and the purified protein similarly subjected to GluC cleavage. Although GluC cleavage was not abolished, the pattern of fragments produced from the variant protein was altered, suggesting that Glu59 is the major, but not the only, cleavage site recognized by the protease (**Figure 3.S1**). We next asked whether these two GluC-derived TlyA fragments remain stably folded and associated by applying partially cleaved protein to a gel filtration column. Two major peaks were observed (**Figure 3.2C**), with the earlier eluting protein corresponding to the remaining uncleaved full-length His-TlyA protein. Although eluting at a volume corresponding to a significantly lower molecular weight entity, the later peak was found to contain both stable fragments (**Figure 3.2C,D**) suggesting that the TlyA NTD and CTD remain stably folded and associated following GluC cleavage.

We conclude from these results that treatment of His-TlyA with GluC produces two stable protein fragments that likely correspond to the predicted TlyA NTD and CTD, and that these domains have sufficient affinity that they remain associated following cleavage under the

solution conditions used. Based on these observations, we generated a new expression construct for crystallographic studies of the TlyA methyltransferase domain (CTD) beginning at residue Ser64, which immediately follows the predicted interdomain linker and corresponds to the first amino acid of  $\alpha$ -helix 1 ( $\alpha$ 1) in the TlyA homology model (**Figure 3.2E**). Crystals of TlyA CTD suitable for structural determination formed within five days and diffracted to 1.7 Å resolution.

### 3.3.2 *The TlyA CTD Adopts a Class I Methyltransferase Fold*

The structure of TlyA CTD was solved using a TlyA homology model and unambiguous electron density allowed modeling of amino acids Ser64-Pro268, producing a final refined model with  $R_{\text{work}}/R_{\text{free}}$  of 0.188/0.218 (also see **Table 3.S1**). The TlyA CTD structure contains a RrmJ/FtsJ Rossmann-like methyltransferase fold comprising seven  $\beta$ -strands (with topology  $\uparrow 3 \uparrow 2 \uparrow 1 \bullet \uparrow 4 \uparrow 5 \downarrow 7 \uparrow 6$ ) sandwiched between six  $\alpha$ -helices (**Figure 3.3A**). The TlyA CTD structure contains the glycine-rich SAM binding motif I GxGxG (Kagan and Clarke, 1994) albeit with the atypical sequence G<sup>90</sup>ASTG<sup>94</sup>, containing a central Gly to Ser variation. The TlyA CTD structure additionally confirms the location of the proposed TlyA catalytic tetrad K<sup>69</sup>/D<sup>154</sup>/K<sup>182</sup>/E<sup>238</sup> (Arenas et al., 2011; Feder et al., 2003).

The TlyA CTD domain overlays well with other Class I methyltransferases including the archetypical member of the TlyA family the 2'-O-methyltransferase RrmJ, and the DNA C5-methyltransferase HhaI (Bugl et al., 2000; O'Gara et al., 1999). Structural superimposition of TlyA-CTD with other Class I methyltransferases was used to model the likely location of SAM in the TlyA binding pocket. While most features of protein secondary structure overlay well between TlyA and RrmJ (PDB ID: 1EIZ), severe clashes were observed when the RrmJ bound SAM was placed within the TlyA CTD via protein superimposition due to differences in the loops that link the core  $\beta$ -strands. In contrast, modeling using the SAM-bound structure of either

the HhaI DNA methyltransferase (PDB ID: 2HMY) or RlmM 2'-O-methyltransferase (PDB ID: 4B17) (Punekar et al., 2012), places SAM nicely into the TlyA binding pocket with no significant clashes (shown for HhaI in **Figure 3.3B**). The modeled SAM is positioned on top of the loop connecting TlyA core strand  $\beta 1$  and  $\alpha 2$  which contains the SAM-binding motif I G<sup>90</sup>ASTG<sup>94</sup>. The central Ser residue of TlyA's atypical SAM-binding motif is oriented toward the modeled SAM and positioned to directly hydrogen bond with the ribose 3'-OH. Additionally, by adopting a different rotameric state, the hydroxyl of residue Thr93 within this motif would be positioned for interaction with the carboxyl end of the modeled SAM. Finally, the SAM adenine moiety is modeled within a largely hydrophobic pocket on the surface of TlyA comprising the side chains of residues Val113, Ala136 and Ile158, the backbone of Gly114, and Asn135 (**Figure 3.3C**). Thus, the TlyA CTD structure possesses the expected features necessary for interaction with the obligatory methyltransferase cosubstrate SAM.

We additionally note that the proposed TlyA catalytic residue Asp154 is positioned adjacent the transferable methyl group of the modeled SAM (**Figure 3.3B, C**). Interestingly, two aromatic amino acids Tyr115 and Phe157 also line the SAM binding pocket, but are oriented into the solvent. These residues could play an important functional role in recognizing the rRNA substrate and coordinating the target nucleotide for catalysis as seen with NpmA-30S complex (Dunkle et al., 2014).

### *3.3.3 The Isolated TlyA CTD Protein Does Not Bind SAM*

To begin examining TlyA-cosubstrate interactions, we used isothermal titration calorimetry (ITC) to compare binding of SAM and the methylation reaction by-product S-adenosylhomocysteine (SAH) to the full-length enzyme. His-TlyA bound both SAM and SAH with similar affinities in the low micromolar range (**Figure 3.4A, Table 3.1**), comparable to other rRNA

methyltransferases (Savic et al., 2008; Witek and Conn, 2016). Surprisingly, however, despite retaining a complete Class I methyltransferase SAM-binding fold with the expected conserved motifs, the isolated TlyA CTD protein did not exhibit detectable binding of SAM (**Figure 3.4B**, **Table 3.1**). In contrast, GluC-cleaved full-length His-TlyA (His-TlyA<sup>GluC</sup>), *i.e.* the co-purified NTD and CTD fragments (**Figure 3.2D**), bound SAM with similar affinity to the intact protein (**Figure 3.4C**, **Table 3.1**). Together, these data indicate that the methyltransferase fold of our TlyA CTD construct is not sufficient for SAM binding and, thus, one or more elements of the N-terminal 1-63 residues of TlyA must also play a critical role in SAM cosubstrate binding.

#### 3.3.4 The RAWV Tetrapeptide Interdomain Linker is Critical for TlyA CTD-SAM Interaction

To assess the potential contribution of the TlyA NTD to SAM binding, an N-terminal domain expression construct was created corresponding to residues 1-63 ending with the RAWV tetrapeptide domain linker sequence (NTD<sup>RAWV</sup>; **Figure 3.2E**). Expression and purification of the NTD<sup>RAWV</sup> required an N-terminal SUMO-fusion tag which was removed using the ubiquitin-like protease (Ulp) prior to use in experiments. Using this new construct, we first tested whether the NTD<sup>RAWV</sup> and CTD proteins interact, recapitulating the retained association of the GluC-derived NTD and CTD fragments of His-TlyA (**Figure 3.2C**). The NTD<sup>RAWV</sup> and CTD proteins were mixed with 1:1 stoichiometry and applied to a gel filtration column under identical conditions as used previously for the full-length and GluC-cleaved His-TlyA. In contrast to GluC-cleaved His-TlyA, each individual protein domain eluted as a separate peak with no evidence for their direct association (**Figure 3.5A**). Additionally, no SAM binding was detected by ITC when SAM was titrated into the sample cell containing NTD<sup>RAWV</sup>/CTD mixture (data not shown). Thus, separate expression of the NTD<sup>RAWV</sup> and CTD proteins and *in vitro* reconstitution failed to recapitulate the observed domain association and SAM binding affinity of the GluC-cleaved full-length His-TlyA protein.

We reasoned that the inability of the separately expressed TlyA domains to interact and bind SAM (either the CTD alone or as an NTD<sup>RAWV</sup>/CTD mixture) might arise from an inappropriate choice of domain boundary in our expression constructs. Although the NTD and CTD derived from full-length TlyA by GluC cleavage appear to remain strongly associated (**Figure 3.2C**), we determined that dialysis against high salt (1 M NaCl) containing buffer and subsequent application to the gel filtration column was sufficient to isolate a sample highly enriched for TlyA CTD<sup>GluC</sup> (**Figure 3.5B**). This CTD<sup>GluC</sup> bound SAM with an affinity essentially identical to full-length His-TlyA despite depletion of the NTD fragment (**Figure 3.5C**, **Table 3.1**), indicating that the majority of the NTD is dispensable for TlyA interaction with cosubstrate. We therefore prepared a new TlyA CTD expression construct corresponding to the precise fragment produced by GluC at the predicted Glu59 cleavage site, thus placing the RAWV tetrapeptide interdomain linker sequence on the N-terminus of the CTD (residues 60-268, RAWV<sup>CTD</sup>; **Figure 3.2E**). Remarkably, addition of the RAWV sequence in RAWV<sup>CTD</sup> restored wild-type SAM binding affinity to the isolated domain protein (**Figure 3.5D**, **Table 3.1**). Thus, the RAWV tetrapeptide sequence appears essential for SAM binding in TlyA.

Given the predicted location of the RAWV sequence in the region linking the two domains of TlyA, we next evaluated the possibility that this tetrapeptide motif might also contribute to TlyA domain interaction only when present on the CTD. An additional construct was therefore generated corresponding to the N-terminal 1-59 amino acids of TlyA (NTD; **Figure 3.2E**) and the purified, tag-free NTD/RAWV<sup>CTD</sup> domain proteins mixed and applied to the gel-filtration column as before. Although SDS-PAGE analysis revealed less than stoichiometric association, some NTD protein was found to co-elute with RAWV<sup>CTD</sup>, in contrast to the alternate fragment combination NTD<sup>RAWV</sup>/CTD (compare **Figure 3.5E** and **3.5A**, respectively). We speculate that the weaker association observed for the separately expressed NTD/RAWV<sup>CTD</sup> domain mixture compared to the GluC-cleaved protein likely arises due to the need to

accommodate, within the protein-protein interface, an additional Gly-Ser dipeptide on <sup>RAWV</sup>CTD arising from the thrombin cleavage site used to remove its N-terminal His tag (**Figure 3.2E**). Additionally, given that the isolated NTD protein required an N-terminal SUMO fusion for soluble expression, the Ulp-cleaved TlyA NTD may also be heterogeneously folded compared to the native domain derived from full-length TlyA. Nonetheless, while not fully recapitulating the domain complex stability following cleavage with GluC, this result suggests that the RAWV tetrapeptide linker may play a role in association and coordination of the TlyA domains, in addition to being essential for SAM binding.

### 3.3.5 Trp62 and Val63 are the Most Critical Residues for SAM Binding

BLAST search and multiple sequence alignment of the <sup>RAWV</sup>CTD sequence in UniProt revealed that the tetrapeptide sequence is strongly conserved in the top 250 TlyA homologs. In particular, position 62 is most highly conserved as a tryptophan and position 63 is invariant as either a valine or alanine (**Figure 3.6A**). Proteins identified as TlyA homologs include TlyA 2'-O-methyltransferases, RrmJ methyltransferases, cytotoxins/hemolysins, cytochrome C oxidase subunit II, and TlyA family members. Similar analysis of all SAM-binding proteins within this set of homologs (*i.e.* either TlyA or RrmJ methyltransferases) revealed an almost identical pattern of sequence conservation as for all 250 proteins (**Figure 3.6B**). In contrast, among Mycobacterial methyltransferases and hemolysins, Arg60 was more conserved and Trp62/Val63 were invariant. TlyA homologs from all other species were more variable with valine and proline conserved at position 60 and alanine conserved at position 63 (**Figure 3.6C,D**). Finally, among six functionally characterized TlyA methyltransferases with overall identities of 38-100% to *Mtb* TlyA (Monshupanee et al., 2012), Val63 was found to be invariant, with either a tryptophan or tyrosine present at position 62 (**Figure 3.6E**). Based on this conservation, we predicted Arg60 and, in particular, Trp62 and Val63 may play important roles in TlyA function.

To begin experimentally testing the impact of the RAWV tetrapeptide sequence on the TlyA-SAM interaction, individual single amino acid substitutions were made of each of the four residues within full-length TlyA. Each variant was expressed and purified similarly to the wild-type protein, and CD spectroscopy was used to confirm that none of the substitutions resulted in gross changes to the protein fold (data not shown). The SAM binding affinity of each variant was then measured by ITC as before (**Table 3.2**). Arg60 substitution with either Ala or Glu modestly impacted SAM binding affinity (~3-fold decrease), while an A61V variant had wild-type affinity for the cosubstrate. In contrast, substitution of Trp62 with Phe or Ala resulted in ~4- and 10-fold reduction in SAM binding affinity, confirming a significant role for Trp62 in SAM binding and suggesting that the aromatic nature of the side chain is important given the lesser impact of the Trp to Phe substitution. Finally, the most pronounced decrease in SAM binding affinity was observed for the V63A variant (20-fold) pointing to a critical role for this hydrophobic residue in SAM binding.

### *3.3.6 Structural Plasticity of the RAWV Motif*

As Trp62 and Val63 are not predicted by our TlyA CTD structure or the TlyA homology model to interact with SAM, we next wanted to determine their local structural environments to assess how they might stabilize amino acids that directly contact SAM. Two different crystallization conditions were identified for TlyA<sup>RAWV</sup>CTD that produced distinct crystal forms with the same space group and similar cell dimensions, but which differed slightly in their packing within the crystal lattice. In both crystal forms of<sup>RAWV</sup>CTD, the presence of a symmetry related molecule near the SAM binding site precluded obtaining a structure of SAM-bound<sup>RAWV</sup>CTD via soaking of preformed crystals with SAM and efforts to complex crystals by direct co-crystallization were unsuccessful. Nevertheless, the two structures of<sup>RAWV</sup>CTD offer significant insight into the potential molecular mechanism by which the RAWV motif influences SAM binding. While the

core methyltransferase fold in the two structures is essentially identical (aligning with 0.27 Å r.m.s.d. for 160 residues), the structure and position of the RAWV motif varies significantly, adopting an unstructured loop in one crystal (“Form 1-Loop”) and an extension of  $\alpha 1$  of the methyltransferase domain in the second (“Form 2-Helix”; **Figure 3.7A,C**).

In Form 1-Loop, electron density allowed modeling of Trp62 and Val63 peptide backbone and also the Trp62 side chain (**Figure 3.7B**). In Form 2-Helix, clear density was also observed for the peptide backbone of RAWV motif as well as side chains of residues Ala61-Val63 (**Figure 3.7D**). In the Form 2-Helix structure, extension of  $\alpha 1$  by the RAWV tetrapeptide sequence positions Trp62 to interact with the backbone of Lys254 and Gly255 of a symmetry-related molecule. This arrangement is similar to that of the CTD structure (which lacks Trp62) in which an extended  $\alpha 1$  would be accommodated, if the RAWV sequence were present, without clashing with a symmetry related molecule. In contrast, the altered crystal packing of Form 1-Loop restricts the ability of the RAWV sequence to extend  $\alpha 1$ . Strikingly, the RAWV sequence instead adopts the same structure as observed for the equivalent sequence in hemolysin proteins from *Streptococcus thermophilus* (PDB ID: 3HP7) and *Lactococcus lactis* (PDB ID: 3OPN) with Trp62 overlaying with Tyr62 and Tyr36, respectively, and stabilized by a hydrophobic interaction with Val99/99/73 (TlyA/ 3HP7/ 3OPN; **Figure 3.7E**). Although detailed interpretations are potentially complicated by the influence of crystal packing contacts on the position of the RAWV CTD N-terminus residues, the two structures nonetheless reveal that the *Mtb* TlyA RAWV motif is capable of adopting two strikingly different conformations. We speculate that these two conformations might reflect an important functional transition in TlyA, for example if the relative orientation of the NTD and CTD is altered by interaction with ribosomal subunit substrate. An important final question, however, is whether one or both of the observed conformations of the RAWV motif can provide a suitable mechanistic explanation as to its contribution to SAM affinity.

Comparison of the two<sup>RAWV</sup>CTD structures and the CTD structure reveals changes in regions surrounding the SAM binding pocket in addition to those in the RAWV sequence structure itself (**Figure 3.7F**). In the  $\alpha$ -helical conformation Trp62 is rotated by 180° from its position in the Form 1-Loop structure. On the opposite side of the SAM binding pocket, a shift in the peptide backbone is also observed for the loops containing Thr134 and Tyr115, with movements of 3.1 Å and 3.9 Å for their C $\alpha$  atoms, respectively, upon comparison of the Form 1-Loop to Form 2-Helix structure. As Tyr115 interacts with symmetry related molecules in each structure, we cannot eliminate the possibility that this structural change is influenced in part by crystal packing. However, it is noteworthy that while the Tyr115 backbone moves away from the SAM molecule, its side chain is reoriented closer to the SAM pocket such that it could contribute to positioning of SAM or the target nucleotide in the TlyA active site.

The most striking differences between the two<sup>RAWV</sup>CTD structures surround Val63, the residue most critical for SAM affinity. In the extended  $\alpha$ 1 of the Form2-Helix structure, Val63, shifted 4.4 Å towards Thr93 of the SAM binding motif I (**Figure 3.7G**). Additional small differences are seen in the positions of both Thr93 and Ser92 C $\alpha$ , shifted 1.4 Å and 1.9 Å, respectively, towards the expected position of the bound SAM. Additionally, we note that in both the Form 1-Loop and, to a lesser extent, CTD structures that the Thr93 side chain is oriented with its hydroxyl group oriented away from the SAM pocket. In contrast, in the Form 2-Helix structure the Thr93 side chain is reoriented with its hydroxyl group pointing into the SAM pocket and positioned to interact directly with the cosubstrate carboxylate group. The position and influence of Val63 in its  $\alpha$ -helical conformation thus appears to drive formation of an optimally formed SAM-binding pocket, underpinning the unexpected contribution of the RxWV motif and this residue in particular to TlyA-SAM binding affinity.

### 3.4 DISCUSSION

In the present study we have shown that the TlyA methyltransferase contains a Class I Rossmann-like methyltransferase fold with a complete SAM-binding motif. However, the methyltransferase domain (amino acids 64-268) is not competent for SAM binding, and we identified an additional tetrapeptide motif RxWV as essential for SAM interaction with the methyltransferase domain. In particular, the final two amino acids, Trp62 and Val63, have the most pronounced impacts on SAM affinity. Our structural studies illustrated a role for these amino acids in organizing the conserved GxGxG SAM-binding motif I when they are part of an extended  $\alpha$  helix 1 of the TlyA methyltransferase domain.

Whether the RxWV motif is an important determinant of SAM binding when present in methyltransferases other than TlyA is an open question. TlyA and its homologs RrmJ and RrmM contain a SAM binding motif I divergent from the typical 'GxGxG' (TlyA G<sup>90</sup>ASTG<sup>94</sup>, RrmJ G<sup>59</sup>AAPG<sup>63</sup>, and RrmM G<sup>219</sup>ACPG<sup>223</sup> (Punekar et al., 2012) that introduces a bulkier amino acid side chain that could point into the SAM binding pocket, either creating or disrupting interactions important for SAM binding. In the case of Ala61 and Cys221 of RrmJ and RrmM, respectively, the bulkier side chain is accommodated through its orientation away from the bound SAM molecule, and instead positioning the common backbone carboxyl group within hydrogen bonding distance of the SAM 3'-OH. In contrast, in TlyA, residue Ser92 points towards the SAM binding pocket suggesting that the side chain could potentially make a direct hydrogen bond with the SAM 3'-OH. Our structures show that reorientation Thr93, towards the carboxylate of the SAM molecule is associated with the formation of an extended helical structure within  $\alpha$ 1 by the RxWV motif. As both an atypical SAM binding motif G<sup>90</sup>ASTG<sup>94</sup> and Trp62-Val63 are conserved in characterized TlyA homologs, Trp62-Val63 could represent a mechanism to compensate for deleterious effects on SAM affinity arising from the need to correctly organize the atypical motif I of TlyA for optimal SAM binding.

The RxWV motif connects the methyltransferase domain to the TlyA N-terminal domain which is predicted to adopt an S4 ribosomal protein binding fold (Arenas et al., 2011) and likely plays a critical role in rRNA recognition (Monshupanee et al., 2012). However, precisely how TlyA recognizes its two different nucleotide targets, 16S rRNA C1409 and 23S rRNA C1920, remains to be elucidated. While both C1409 and C1920 reside within RNA helical structures with similar sequences, their overall structural context differs significantly. C1409 is located in a region of h44 which packs near multiple 16S rRNA helices to form a complex RNA tertiary surface in the assembled 30S subunit, while C1920 is within a stem-loop (23S rRNA H69) that protrudes from the surface of the free 50S subunit (Noeske et al., 2015). Could the structural plasticity we observe in the TlyA interdomain linker (RxWV tetrapeptide) also play a role in TlyA's recognition of its two substrates? A mechanism of this type has been described for the tRNA G37 methyltransferase TrmD, in which an interdomain linker transitions from being structurally disordered to helical upon substrate binding (Ito et al., 2015). To begin exploring this question, we manually appended the TlyA NTD homology model onto each of our two TlyA<sup>RAWV</sup>CTD structures followed by geometry minimization to reveal the potential for the NTD to be oriented in two very different ways (**Figures 3.8** and **3.S2**). On the Form 1-Loop structure, the NTD is more loosely associated with the CTD, and in a similar orientation to hemolysin structures and the full-length TlyA homology model which is based on a hemolysin template (Arenas et al., 2011). In contrast, modeled on the Form 2-Helix structure, the NTD is significantly repositioned and packs more closely against the TlyA CTD surface surrounding the SAM binding pocket, more consistent with our observation that the domain fragments from GluC-cleaved His-TlyA remain tightly associated. From this preliminary modeling we speculate that TlyA may employ a mechanism in which specific recognition via the NTD of its two different substrates may be mediated via a common conformational change in the RxWV interdomain linker. Substitutions of some positively charged residues in the TlyA NTD are known to have differential impacts on the activity of TlyA against the 30S and 50S substrates (Monshupanee et al., 2012).

Thus an appealing feature of a TlyA substrate recognition mechanism exploiting the structural plasticity of the RxWV motif is that interactions made by different regions of the N-terminal S4 domain, with either 30S or 50S, could lead to a common signal via the interdomain linker for correct substrate recognition and activation of methyltransferase activity.

In summary, the present study has revealed the unexpected but critical importance of the RxWV tetrapeptide motif in the TlyA interdomain linker for SAM binding. Our structures of the RAWV<sup>CTD</sup> and modeling further suggest a potential role for the RxWV motif's structural plasticity in regulating communication between the TlyA domains and in specific substrate recognition. Further structural studies of TlyA and its complexes with both 30S and 50S subunits are next needed to fully understand the molecular details of specific substrate recognition and the role of the RxWV motif in the activity of this important antibiotic-resistance associated enzyme.

### 3.5 EXPERIMENTAL PROCEDURES

#### 3.5.1 *TlyA* Construct Design and Site-directed Mutagenesis

An *E. coli* codon optimized gene encoding TlyA (Rv1694; UniProt P9WJ63) from *Mtb* (strain ATCC 25618/ H37Rv) was obtained by chemical synthesis (GeneArt) and subcloned into a modified pET44 plasmid (Zelinskaya et al., 2011) for expression of protein with a thrombin-cleavable aminoterminal hexahistidine tag (His-TlyA). Screening for proteolytic fragments of His-TlyA suitable for structural studies with the Proti-Ace kit (Hampton Research) identified the endopeptidase GluC (*Staphylococcus aureus* Protease V8) as producing two stable domain fragments and this observation was used as a guide to produce additional domain constructs (see Results for details). Plasmids encoding His-CTD (amino acids 64-268), His-RAWV<sup>CTD</sup> (amino acids 60-268), and full-length His-TlyA with single amino acid substitutions were generated using a whole plasmid PCR protocol (Miyazaki, 2011). Constructs for expression of amino-

terminal domain proteins SUMO-NTD (amino acids 1-59) and SUMO-NTD<sup>RAWV</sup> (amino acids 1-63) were generated by PCR amplification of the corresponding coding region in pET44-His-TlyA using primers containing BsaI and XbaI sites for ligation of the amplicon into the pE-SUMOpro vector (LifeSensors).

### 3.5.2 *TlyA* Protein Expression and Purification

*E. coli* BL21 (DE3) cells transformed with protein-encoding plasmid were grown at 37 °C in terrific broth supplemented with ampicillin (100 µg/ml) to mid-log phase ( $OD_{600} \sim 0.4-0.6$ ), induced with 0.5 mM isopropyl  $\beta$ -D-1-thiogalactopyranoside (IPTG) and grown for an additional 3-4 hours. Following harvesting by centrifugation, cells were resuspended in 50 mM sodium phosphate buffer (pH 8.0) containing 300 mM NaCl and 10 mM imidazole, and lysed by sonication. The resulting soluble fraction was applied to a HisTrap HP column (GE Healthcare) equilibrated in the same buffer. The column was washed with 10 column volumes of 50 mM sodium phosphate (pH 8.0) buffer containing 300 mM NaCl and 20 mM imidazole, and subsequently eluted with the same buffer, but containing 250 mM imidazole. Further purification was accomplished using a Superdex 75 16/60 gel filtration column (GE Healthcare) equilibrated in gel filtration buffer (20 mM Tris pH 8.0, 10 mM magnesium acetate, 250 mM ammonium chloride, 6 mM  $\beta$ -mercaptoethanol and 10% glycerol). All domain proteins and sequence variants were expressed and purified in the same way as full-length His-TlyA.

For removal of the N-terminal hexahistidine tag, protein was mixed overnight with thrombin (Sigma-Aldrich; 5 U per 1 mg of fusion protein) and passed over tandem HiTrap Benzamidine FF and HisTrap HP columns (GE Healthcare). To remove the His-SUMO tag, His-SUMO-NTD and His-SUMO-NTD<sup>RAWV</sup> were incubated with Ulp and passed over a HisTrap HP

column. After tag cleavage and initial purification step, cleaved TlyA or TlyA domains were concentrated and purified in a second gel filtration chromatography step (as described above).

### 3.5.3 CD Spectroscopy

CD spectroscopy was performed for full-length wild-type His-TlyA and variants with single amino acid substitutions in the RAWV tetrapeptide sequence on a Jasco J810 spectropolarimeter using solution conditions and instrument settings as described previously (Witek and Conn, 2014). Spectra (260-190 nm) were collected at 20 °C. Averaging and background correction were performed using the Spectra Manager software provided with the instrument and analysis of TlyA secondary structure was accomplished using the CDSSTR deconvolution algorithm via Dichroweb (Whitmore and Wallace, 2008).

### 3.5.4 RT Analysis of 16S and 23S rRNA Methylation

Methylation of 30S and 50S was determined using RT assays with *E.coli* MRE600 30S and 50S subunits purified as described previously (Moazed and Noller, 1989; Monshupanee et al., 2012). In brief, *E.coli* cells were lysed using a French press, and the 50S and 30S ribosomal subunits fractionated by sucrose gradient centrifugation and individually isolated by pelleting of the respective fractions. For the methylation assay, 200 pmol purified His-TlyA was incubated for 1 hour at 37 °C with 100 pmol of ribosome subunit (30S or 50S) in the presence of 1 mM SAM in 10 mM HEPES-KOH buffer (pH 7.5) containing 10 mM MgCl<sub>2</sub>, 50 mM NH<sub>4</sub>Cl, and 5 mM β-mercaptoethanol. The reaction was terminated by phenol/chloroform extraction followed by ethanol precipitation to recover 16S or 23S rRNA from the 30S or 50S ribosomal subunits, respectively. The reaction products were analyzed by RT using <sup>32</sup>P-labeled DNA primers complementary to *E.coli* 16S rRNA nucleotides 1457-1473 (5'-CAAAGTGGTAAGCGCCC-3')

and 23S rRNA nucleotides 1964-1980 (5'-CATTACGCCATTCGTGC-3'). The 2'-O-ribose methylation on C1409 and C1920 was observed with low dGTP concentration (0.5  $\mu$ M) in the presence of 75  $\mu$ M each of dATP, dTTP and dCTP. Extension products were run on 10% PAGE-urea gels and visualized using Typhoon Trio phosphorimaging system (GE Healthcare).

### *3.5.5 Protein Crystallization and Structure Determination*

His-CTD (6 mg/ml) was crystallized at 20 °C in 0.2 M Hepes pH 7.5 and 2.5 M NaCl using the vapor diffusion method. His-<sup>RAWV</sup>CTD (8 mg/ml) was crystallized in the same way but using 8% tascimate pH 8.0 and 20% PEG 3350 (Form 1-Loop) or 0.3 M Hepes pH 7.5 and 2.8 M NaCl (Form 2-Helix). Crystals were cryo-protected with reservoir solution supplemented with 20% glycerol and flash frozen by plunging in liquid nitrogen. Data was collected at the Southeast Regional Collaborative Access Team (SER-CAT) ID-22 beamline at the Advanced Photon Source (APS) at the Argonne National Laboratory. The initial structure of His-CTD was solved by molecular replacement using a homology model of TlyA amino acids 59-265 based on the hemolysin from *Lactococcus lactis* (PDB ID: 3OPN) generated by SWISS-MODEL (Arnold et al., 2006). Data was indexed and scaled using HKL2000 (Otwinowski and Minor, 1997). Data analysis, structure refinement and validation for all structures were performed using the programs of the Phenix crystallography software suite (Adams et al., 2010). The quality of each model was assessed with PDB\_Redo (Joosten et al., 2014). Details of data processing, refinement and accession codes for the final coordinates deposited in the Protein Data Bank are provided in **Table 3.S1**.

### 3.5.6 Isothermal Titration Calorimetry Analysis of SAM and SAH Binding

TlyA was dialyzed at 4 °C against 50 mM Tris buffer (pH 7.5) containing 120 mM NaCl and 10% glycerol, and concentrated to 60-100 μM. The same dialysis buffer was used to resuspend SAM and SAH (Sigma-Aldrich) at 1.5 mM final concentration. Experiments were performed at 25 °C and comprised 16 injections of 2.4 μl SAM or SAH into the cell containing protein. Data were fit to a model for one-binding site after subtraction of residual heats yielding equilibrium dissociation constants ( $K_D$ ) which are reported as an average of at least three experiments with the associated standard deviation, unless otherwise noted.

For analysis of the isolated CTD<sup>GluC</sup> fragment, gel filtration chromatography on a Superdex 75 16/60 column was used to separate the major protein fragments generated by GluC cleavage of full-length His-TlyA. Following overnight dialysis against gel filtration buffer supplemented with 1 M NaCl, the GluC cleaved His-TlyA was applied to the column and fractions containing the GluC-derived carboxyterminal domain fragment (CTD<sup>GluC</sup>) were pooled and concentrated prior to use as above.

### 3.5.7 Analysis of TlyA Domain Association by Gel Filtration Chromatography

Gel filtration analysis of the GluC cleavage products of full-length His-TlyA was accomplished using a Superdex 75 16/60 column equilibrated in gel filtration buffer. Collected fractions were analyzed by SDS-PAGE. For analysis of interaction of separately expressed domain proteins, tag-free CTD or <sup>RAWV</sup>CTD protein (500 μg) was mixed with an equimolar ratio of the corresponding tag-free amino terminal domain protein, NTD<sup>RAWV</sup> or NTD, respectively. After incubation for 30 minutes at 4 °C, protein mixtures were analyzed on a Superdex 75 16/60 column and fractions corresponding to each observed peak pooled, concentrated and an equal mass of protein resolved on a 15% SDS-PAGE gel.

### 3.5.8 SAM and NTD Modeling

SAM from the HhaI DNA methyltransferase (PDB ID: 2HMY) (O'Gara et al., 1999) was modeled onto the TlyA CTD structures by superimposition of the protein structures in PyMOL. The TlyA NTD from the homology model was modeled onto the CTD structures by aligning the CTD structure with the CTD of the homology model, and deleting the homology model CTD. The NTD was manually translocated and rotated to reduce steric clashes with the CTD and orient the last amino acid of the NTD with the first amino acid of the CTD (Ala61 with Trp62 of Form1-Loop, Glu59 with Arg60 of Form2-Helix CTD). Each model of the TlyA (NTD homology model-CTD structure):SAM complex was then regularized using geometry minimization in Phenix (Adams et al., 2010).

## 3.6 ACCESSION NUMBERS

Structures were deposited in the Protein Data Bank under accession numbers: TlyA CTD (5EOV), RAWV-CTD, Form 1-Loop, (XXXX) and RAWV-CTD, Form 2-Helix (5KS2)

## 3.7 ACKNOWLEDGMENTS

We are grateful to Dr. Christine M. Dunham and her group, as well as other members of the Conn lab for useful discussions during this work and the preparation of the manuscript. We also thank Drs. Haiyan Fu, Eric A. Ortlund, Daniel Reines, and Keith D. Wilkinson for comments on the final manuscript. This work was supported by the National Institutes of Health-National Institute of Allergy and Infectious Diseases [R01-AI088025]. The Auto-iTC<sub>200</sub> instrument was purchased with support from the NSF MRI program [104177], the Winship Cancer Institute's shared resource program and the Biochemistry Department of Emory University. Use of the Advanced

Photon Source, an Office of Science User Facility operated for the US Department of Energy (DOE) Office of Science by Argonne National Laboratory, was supported by the USA DOE under Contract DE-AC02-06CH11357. The authors declare there are no conflicts of interest.

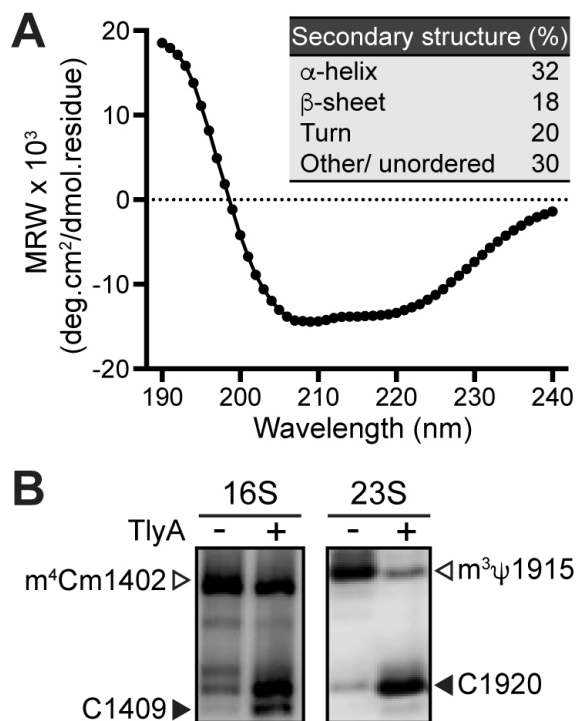
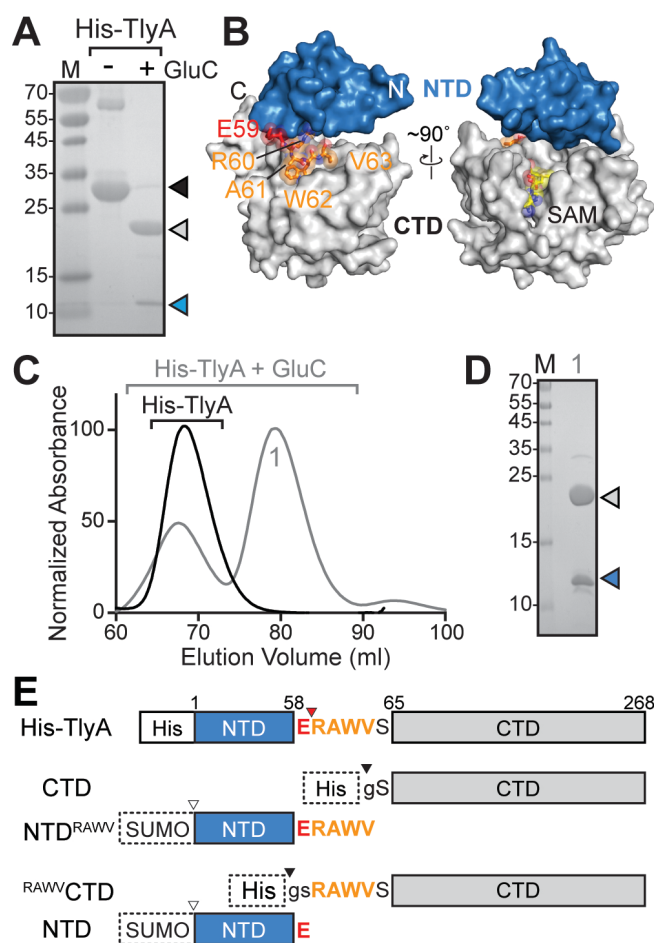
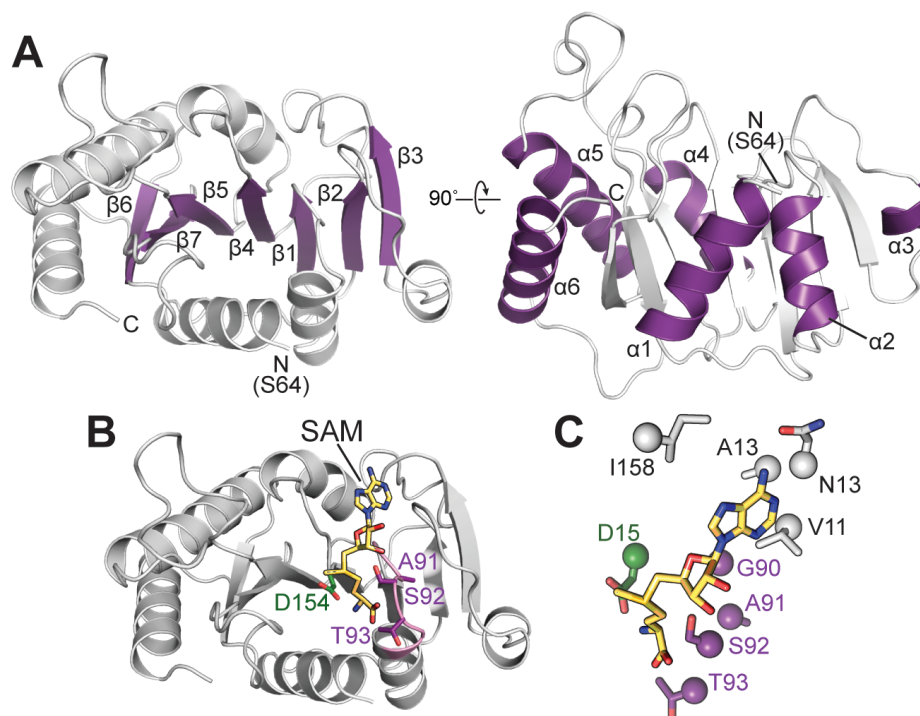


FIGURE 3.1. Recombinant *Mtb* His-TlyA (Rv1694) is well-folded and active *in vitro* against both 30S and 50S ribosomal subunit substrates. *A*, CD spectrum of His-TlyA and results of secondary structural deconvolution (*inset*). *B*, RT analysis of *in vitro* 2'-O-methylation by TlyA (solid arrowheads) of residues C1409 (16S rRNA, *left*) and C1920 (23S rRNA, *right*). The positions of nearby modifications normally present in *E. coli* are also indicated (open arrowheads).



**FIGURE 3.2. GluC cleavage of TlyA generates two domain fragments that remain associated.** *A*, SDS-PAGE of His-TlyA (black arrow) and stable fragments generated by GluC cleavage: CTD<sup>GluC</sup> (grey arrow) and NTD<sup>GluC</sup> (blue arrow); M is protein gel standards (masses in kDa are shown to the left). *See also Figure S1.* *B*, Homology model (PM0076044) of TlyA highlighting the locations of the proposed GluC cleavage site (Glu59; red), the tetrapeptide interdomain linker (RAWV motif; orange), and the predicted SAM (yellow) binding site modeled using the structure of HhaI methyltransferase (PDB ID: 2HMY). *C*, Gel filtration chromatogram of His-TlyA (black) and TlyA partially digested with GluC (grey). *D*, SDS-PAGE of pooled fractions from peak 1 indicating the CTD<sup>GluC</sup> and NTD<sup>GluC</sup> as in *panel A*. *E*, Schematic diagrams of full-length TlyA and individual domain expression constructs highlighting the proposed GluC cleavage (red arrowhead), thrombin cleavable hexahistidine tag (black arrowhead) and amino

acids retained after thrombin cleavage (lowercase text), and the Ulp cleavable SUMO domain (white arrowhead). Solid and dashed lines for the N-terminal tags (His and SUMO) denote those retained and cleaved in the expressed proteins used in the present studies, respectively.



**FIGURE 3.3. The TlyA CTD adopts a Class I methyltransferase fold.** *A*, Two orthogonal views of the TlyA CTD crystal structure with the conserved seven-stranded  $\beta$ -sheet core (*left*) and six surrounding  $\alpha$ -helices (*right*) highlighted in purple. *B*, Model of the TlyA CTD interaction with SAM (yellow; from PDB 2HMY) shown in the same orientation as *panel A*. Residues highlighted are from the SAM binding motif I G<sup>90</sup>ASTG<sup>94</sup> (pink backbone, purple side chains) and D154 of the proposed TlyA catalytic tetrad (green). *C*, Amino acids proposed to make up the SAM binding pocket in TlyA, colored as in *panel B*.

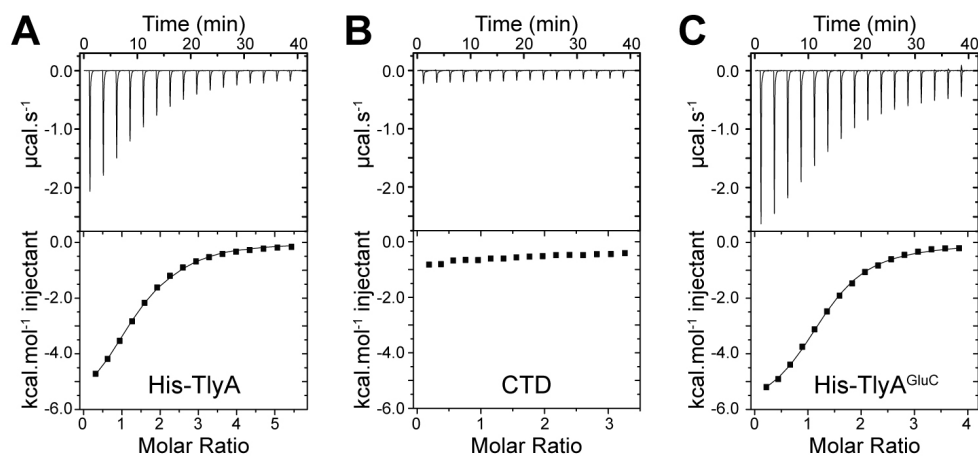
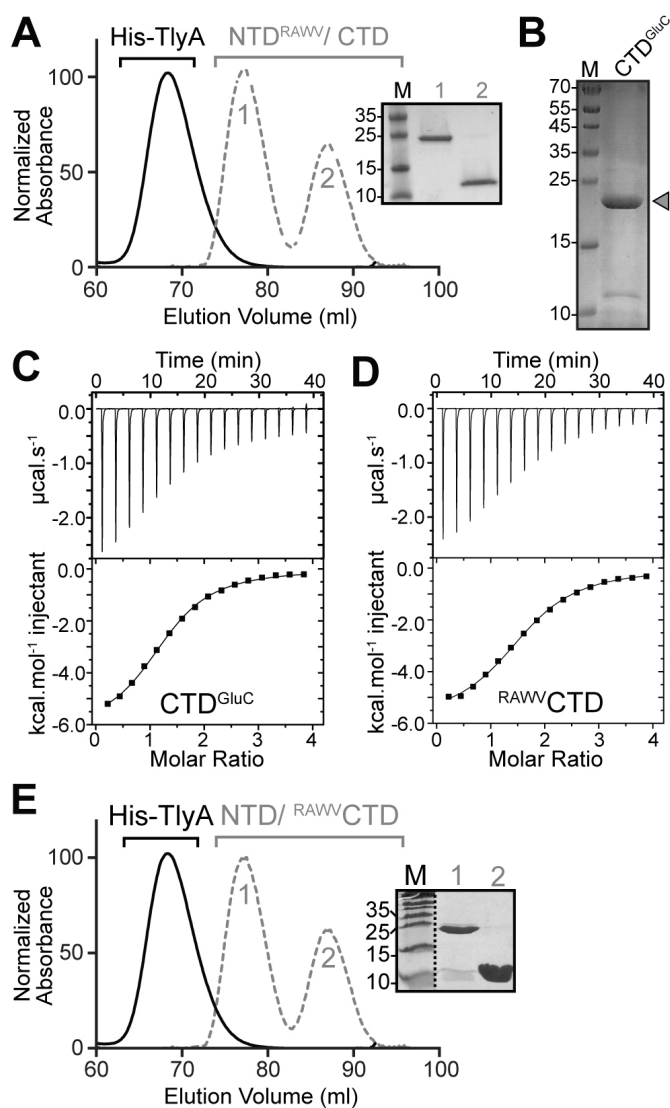


FIGURE 3.4. **The isolated TlyA methyltransferase domain (CTD) does not bind SAM.** ITC analysis of TlyA-SAM interaction for titration by SAM into the cell containing *A*, His-TlyA, *B*, tag-free CTD and *C*, His-TlyA after cleavage with GluC (His-TlyA<sup>GluC</sup>).



**FIGURE 3.5. The TlyA RAWV tetrapeptide sequence is necessary for SAM binding.** *A*, Gel filtration analysis of His-TlyA (black) and individually expressed and purified, tag-free NTD<sup>RAWV</sup> and CTD (grey dashed line). *Inset*, SDS-PAGE of pooled fractions from peaks 1 and 2. *B*, SDS-PAGE of sample enriched for TlyA CTD derived from GluC cleavage of full-length His-TlyA (CTD<sup>GluC</sup>). *C*, ITC analysis of SAM binding to the CTD<sup>Glu</sup> fragment. *D*, ITC analysis of SAM binding to the RAWVCTD protein construct. *E*, Gel filtration chromatogram of His-TlyA (black) and individually expressed and purified, tag-free NTD and RAWVCTD (grey dashed line). *Inset*, SDS-PAGE of pooled fractions from peaks 1 and 2.

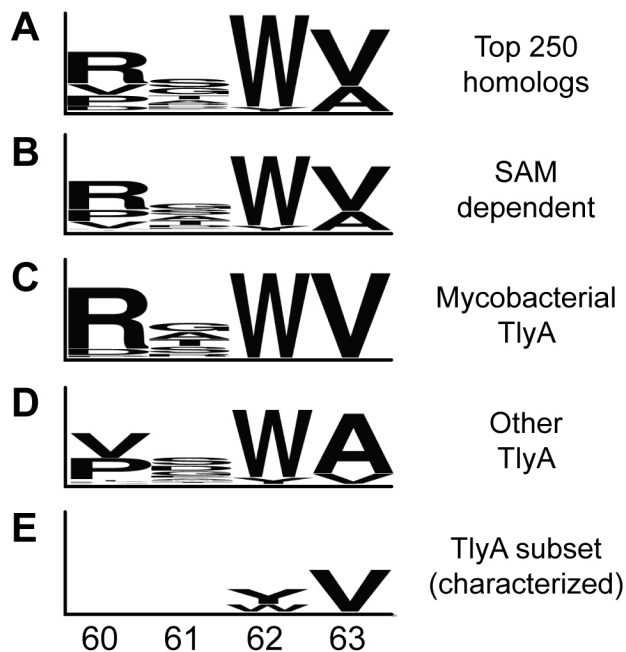
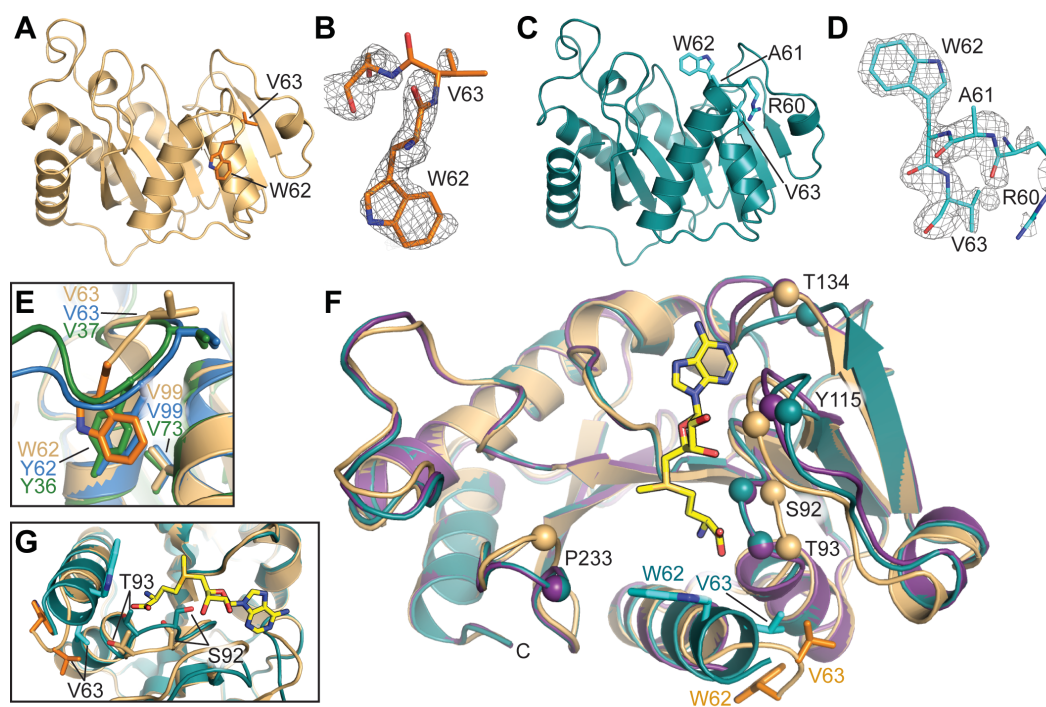


FIGURE 3.6. **RxWV motif conservation.** *A*, Weblogo representation of RAWV conservation of the top 250 homolog sequences retrieved using a BLAST search with the TlyA<sup>RAWV</sup>CTD sequence in UniProt. Additional Weblogo representations for subsets of these 250 homologs: *B*, all SAM-dependent (methyltransferase) proteins; *C*, TlyA family members from *Mycobacteria* (sequence identity 68-100%); and *D*, TlyA family members from species other than *Mycobacteria* (sequence identity 66-68%). *E*, Conservation of the RAWV sequences among TlyA homologs functionally characterized by Monshupanee and colleagues (identity 38-100%) (Crooks et al., 2004; Monshupanee et al., 2012).



**FIGURE 3.7, The TlyA RAWV motif can adopt two distinct conformations.** *A*, Cartoon of Form 1-Loop<sup>RAWV</sup> CTD structure. The amino acids side chains of Trp62 and Val63 are shown as orange sticks. *B*, Zoomed view of Trp62 and Val63 in Form 1-loop shown in 2mFo-DFc omit electron density contoured at 1 $\sigma$ . *C*, Form 2-Helix structure shown as a cartoon with all side chains of the RAWV sequence shown as sticks (cyan). *D*, Zoomed view of the helical RAWV sequence shown in 2mFo-DFc omit electron density contoured at 1 $\sigma$ . *E*, Overlay of Form 1-Loop with two hemolysin structures (PDB ID: 3HP7 and 3OPN, blue and green, respectively). *F*, Superimposition of TlyA CTD (purple), Form 1-Loop (tan) and Form 2-Helix (teal) structures modeled with SAM (PDB ID: 2HMY; yellow). Val63 and Trp62 are as colored as in panels *A* and *C*. Additional residues which differ in their C $\alpha$  positions between the two structures are shown as spheres. *G*, Zoomed view of Val63 and Thr92 reorientation towards the modeled SAM.

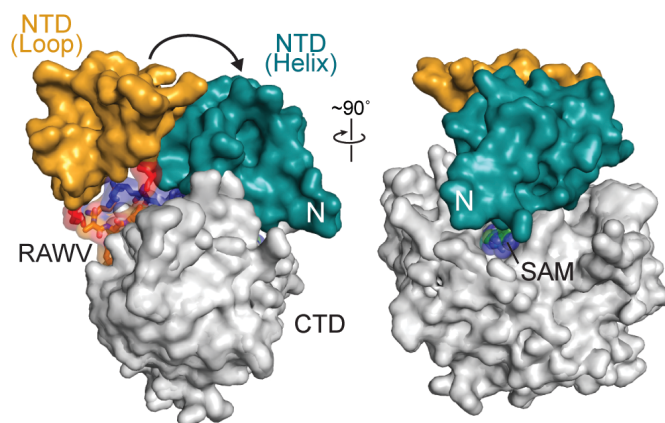


FIGURE 3.8. **Modeling of the TlyA NTD on the two<sup>RAWV</sup>CTD crystal structures.** Two approximately orthogonal views of the overlaid TlyA NTD modeled onto Form 1-Loop (orange NTD) and Form 2-Helix (teal NTD). *See also Figure S2*

**TABLE 3.1.** Co-substrate binding affinity of full-length TlyA and individual domains.

Protein	Ligand	Binding affinity, $K_D$ ( $\mu\text{M}$ ) <sup>a</sup>
His-TlyA	SAM	23.4 $\pm$ 2.9
His-TlyA	SAH	39.2 $\pm$ 7.3
His-TlyA <sup>GluC</sup>	SAM	17.3
CTD	SAM	No binding
CTD <sup>GluC</sup>	SAM	17.9
RAWV <sup>CTD</sup>	SAM	20.0 $\pm$ 1.1
NTD <sup>RAWV</sup>	SAM	No binding

<sup>a</sup>Values are the average  $K_D$  from three independent experiments  $\pm$  standard deviation, except for GluC-cleaved proteins which were performed once.

**TABLE 3.2.** Cosubstrate binding affinity of TlyA RAWV variants.

TlyA variant	Binding affinity, $K_D$ ( $\mu\text{M}$ ) <sup>a</sup>	Decrease compared to wild-type (fold)
R60A	$87.2 \pm 8.5$	3.6
R60E	$62.8 \pm 23$	2.7
A61V	$21.1 \pm 4.3$	0
W62A	$234 \pm 56$	10
W62F	$98.5 \pm 27$	4.3
V63A	$470 \pm 19$	20

<sup>a</sup>Values are the average  $K_D$  from three independent experiments  $\pm$  standard deviation.

## 3.8 SUPPLEMENTAL INFORMATION

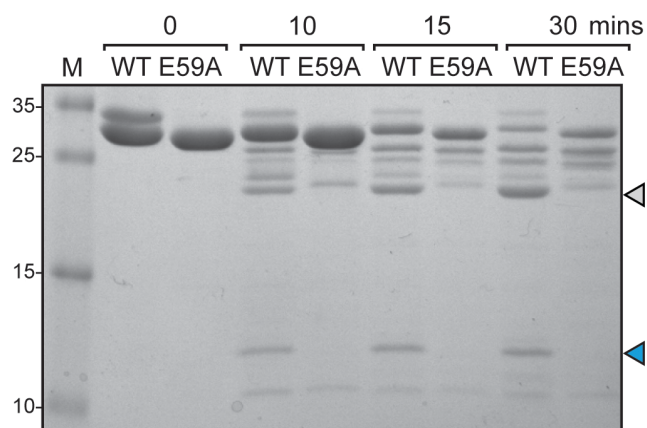


FIGURE 3.S1. *Related to Figure 3.2. Time course of a partial digest of wild-type (WT) and E59A substituted TlyA with GluC protease* demonstrating that the E59A substitution decreases GluC cleavage and alters the cleavage pattern. TlyA (black arrow) and stable fragments generated from GluC cleavage highlighted: CTD<sup>GluC</sup> (grey arrow) and NTD<sup>GluC</sup> (blue arrow); SDS-PAGE standards (M, in kDa) are shown to the left.

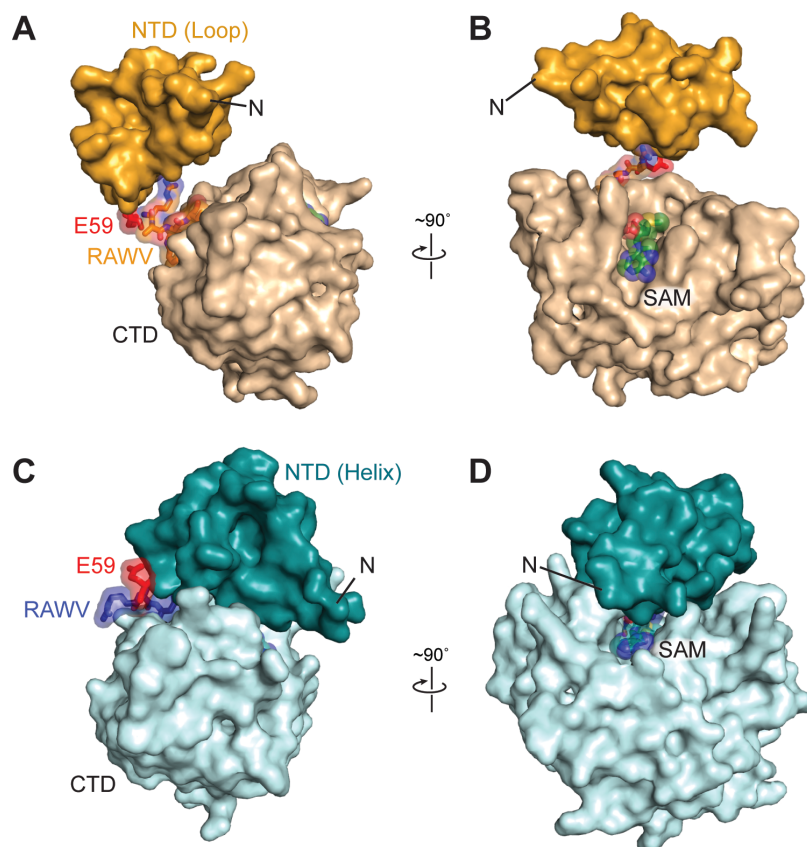


FIGURE 3.S2. Related to Figure 3.8. **Two approximately orthogonal views of each individual model** with the NTD appended to *A, B*, the Form1-Loop structure and *C, D*, the Form2-Helix structure. The same structures are shown overlaid in Figure 8 in the main text.

TABLE 3.S1. Related to Experimental Procedures: X-ray data collection and refinement statistics for TlyA CTD structures.

	CTD	<sup>RAWV</sup> CTD (Form 1-Loop)	<sup>RAWV</sup> CTD (Form 2-Helix)
PDB code	5EOV	####	5KS2
Space group	P4 <sub>3</sub> 2 <sub>1</sub> 2	P4 <sub>3</sub> 2 <sub>1</sub> 2	P4 <sub>3</sub> 2 <sub>1</sub> 2
Resolution (Å) <sup>a</sup>	47.93-1.70 (1.73-1.70)	34.8-1.90 (1.97-1.90)	47.98-2.18 (2.24-2.18)
Cell dimensions			
<i>a, b, c</i> (Å)	67.78, 67.78, 80.29	70.92, 70.92, 79.88	67.85, 67.85, 79.46
$\alpha, \beta, \gamma$ (°)	90, 90, 90	90, 90, 90	90, 90, 90
Wavelength (Å)	1.000	1.000	1.000
$R_{\text{merge}}^b$	0.109 (0.871)	0.121 (0.763)	0.319 (0.984)
$R_{\text{pim}}$	0.025 (0.234)	0.035 (0.762)	0.079 (0.431)
$CC_{1/2}$	(0.891)	(0.928)	(0.558)
$I / \sigma I$	65.2 (3.2)	45.8 (3.6)	19.2 (4.7)
Completeness (%)	100.0 (100.0)	99.9 (99.9)	99.9 (99.9)
Redundancy	19.2 (13.7)	12.8 (9.1)	13.2 (5.6)
Total. reflections (used)	407,555 (21,238)	213,448 (16,726)	187,428 (10,175)
$R_{\text{work}} / R_{\text{free}}^c$	0.188/0.218	0.194/0.244	0.195/0.246
Number of atoms	1,587	1,588	1,622
Protein	1,507	1,528	1,550
Water	80	59	71
Ligand	0	0	1
B-factors			
Protein	38.70	36.71	34.61
Water	44.90	37.33	37.84
Ligand	-	-	30.21
Ramachandran Plot			
Favorable (%)	98.00	100.0	98.00
Outliers (%)	0.49	0.00	0.00
R.m.s. deviations			
Bond lengths (Å)	0.007	0.0108	0.0125
Bond angles (°)	1.09	1.263	1.384

<sup>a</sup>Values in parenthesis are for the highest resolution shell.

<sup>b</sup> $R_{\text{merge}} = \sum hkl \sum i |I_i(hkl) - \langle I(hkl) \rangle| / \sum hkl \sum i I_i(hkl)$ .

<sup>c</sup> $R_{\text{work}} = \sum hkl |F_o(hkl) - F_c(hkl)| / \sum hkl |F_o(hkl)|$ , where  $F_o$  and  $F_c$  are observed and calculated structure factors, respectively.  $R_{\text{free}}$ , applies to the 10% of reflections chosen at random to constitute the test set.

## 3.9 REFERENCES

(WHO), W.H.O. (2015). Global Tuberculosis Report 2015. (Geneva, Switzerland).

Adams, P.D., Afonine, P.V., Bunkoczi, G., Chen, V.B., Davis, I.W., Echols, N., Headd, J.J., Hung, L.W., Kapral, G.J., Grosse-Kunstleve, R.W., *et al.* (2010). PHENIX: a comprehensive Python-based system for macromolecular structure solution. *Acta Crystallogr D Biol Crystallogr* *66*, 213-221.

Arenas, N.E., Salazar, L.M., Soto, C.Y., Vizcaino, C., Patarroyo, M.E., Patarroyo, M.A., and Gomez, A. (2011). Molecular modeling and in silico characterization of Mycobacterium tuberculosis TlyA: possible misannotation of this tubercle bacilli-hemolysin. *BMC Struct. Biol.* *11*, 16.

Arnold, K., Bordoli, L., Kopp, J., and Schwede, T. (2006). The SWISS-MODEL workspace: a web-based environment for protein structure homology modelling. *Bioinformatics* *22*, 195-201.

Avent, M.L., Rogers, B.A., Cheng, A.C., and Paterson, D.L. (2011). Current use of aminoglycosides: indications, pharmacokinetics and monitoring for toxicity. *Intern. Med. J.* *41*, 441-449.

Bugl, H., Fauman, E.B., Staker, B.L., Zheng, F., Kushner, S.R., Saper, M.A., Bardwell, J.C., and Jakob, U. (2000). RNA methylation under heat shock control. *Mol. Cell* *6*, 349-360.

Conn, G.L., Savic, M., and Macmaster, R. (2009). Resistance to antibiotics in bacteria through modification of nucleosides in 16S ribosomal RNA. In *DNA and RNA Modification Enzymes: Comparative Structure, Mechanism, Functions, Cellular Interactions and Evolution*, H. Grosjean, ed. (Austin, TX: Landes Bioscience).

- Crooks, G.E., Hon, G., Chandonia, J.M., and Brenner, S.E. (2004). WebLogo: a sequence logo generator. *Genome Res.* *14*, 1188-1190.
- Cundliffe, E. (1989). How antibiotic-producing organisms avoid suicide. *Annu. Rev. Microbiol.* *43*, 207-233.
- Dorman, S.E., and Chaisson, R.E. (2007). From magic bullets back to the Magic Mountain: the rise of extensively drug-resistant tuberculosis. *Nat. Med.* *13*, 295-298.
- Drapeau, G.R., Boily, Y., and Houmard, J. (1972). Purification and properties of an extracellular protease of *Staphylococcus aureus*. *J. Biol. Chem.* *247*, 6720-6726.
- Dunkle, J.A., Vinal, K., Desai, P.M., Zelinskaya, N., Savic, M., West, D.M., Conn, G.L., and Dunham, C.M. (2014). Molecular recognition and modification of the 30S ribosome by the aminoglycoside-resistance methyltransferase NpmA. *Proc Natl Acad Sci U S A* *111*, 6275-6280.
- Feder, M., Pas, J., Wyrwicz, L.S., and Bujnicki, J.M. (2003). Molecular phylogenetics of the RrmJ/fibrillarlin superfamily of ribose 2'-O-methyltransferases. *Gene* *302*, 129-138.
- Ito, T., Masuda, I., Yoshida, K., Goto-Ito, S., Sekine, S., Suh, S.W., Hou, Y.M., and Yokoyama, S. (2015). Structural basis for methyl-donor-dependent and sequence-specific binding to tRNA substrates by knotted methyltransferase TrmD. *Proc Natl Acad Sci U S A* *112*, E4197-4205.
- Johansen, S.K., Maus, C.E., Plikaytis, B.B., and Douthwaite, S. (2006). Capreomycin binds across the ribosomal subunit interface using tlyA-encoded 2'-O-methylations in 16S and 23S rRNAs. *Mol. Cell* *23*, 173-182.
- Joosten, R.P., Long, F., Murshudov, G.N., and Perrakis, A. (2014). The PDB\_REDO server for macromolecular structure model optimization. *IUCrJ* *1*, 213-220.

- Kagan, R.M., and Clarke, S. (1994). Widespread occurrence of three sequence motifs in diverse S-adenosylmethionine-dependent methyltransferases suggests a common structure for these enzymes. *Arch Biochem Biophys* 310, 417-427.
- Long, K.S., and Vester, B. (2009). Resistance to antibiotics in bacteria through modification of nucleosides in 23S ribosomal RNA. In *DNA and RNA Modification Enzymes: Comparative Structure, Mechanism, Functions, Cellular Interactions and Evolution*, H. Grosjean, ed. (Austin, TX: Landes Bioscience).
- Maus, C.E., Plikaytis, B.B., and Shinnick, T.M. (2005a). Molecular analysis of cross-resistance to capreomycin, kanamycin, amikacin, and viomycin in *Mycobacterium tuberculosis*. *Antimicrob. Agents Chemother.* 49, 3192-3197.
- Maus, C.E., Plikaytis, B.B., and Shinnick, T.M. (2005b). Mutation of *tlyA* confers capreomycin resistance in *Mycobacterium tuberculosis*. *Antimicrob. Agents Chemother.* 49, 571-577.
- Miyazaki, K. (2011). MEGAWHOP cloning: a method of creating random mutagenesis libraries via megaprimer PCR of whole plasmids. *Methods Enzymol.* 498, 399-406.
- Moazed, D., and Noller, H.F. (1989). Interaction of tRNA with 23S rRNA in the ribosomal A, P, and E sites. *Cell* 57, 585-597.
- Monshupanee, T., Johansen, S.K., Dahlberg, A.E., and Douthwaite, S. (2012). Capreomycin susceptibility is increased by TlyA-directed 2'-O-methylation on both ribosomal subunits. *Mol. Microbiol.* 85, 1194-1203.
- Mukherjee, J.S., Rich, M.L., Socci, A.R., Joseph, J.K., Viru, F.A., Shin, S.S., Furin, J.J., Becerra, M.C., Barry, D.J., Kim, J.Y., *et al.* (2004). Programmes and principles in treatment of multidrug-resistant tuberculosis. *Lancet* 363, 474-481.

- Noeske, J., Wasserman, M.R., Terry, D.S., Altman, R.B., Blanchard, S.C., and Cate, J.H. (2015). High-resolution structure of the Escherichia coli ribosome. *Nat. Struct. Mol. Biol.* *22*, 336-341.
- O'Gara, M., Zhang, X., Roberts, R.J., and Cheng, X. (1999). Structure of a binary complex of HhaI methyltransferase with S-adenosyl-L-methionine formed in the presence of a short non-specific DNA oligonucleotide. *J. Mol. Biol.* *287*, 201-209.
- Otwinowski, Z., and Minor, W. (1997). Processing of X-ray diffraction data collected in oscillation mode. *Macromolecular Crystallography, Pt A* *276*, 307-326.
- Punekar, A.S., Shepherd, T.R., Liljeruhm, J., Forster, A.C., and Selmer, M. (2012). Crystal structure of RlmM, the 2'O-ribose methyltransferase for C2498 of Escherichia coli 23S rRNA. *Nucleic Acids Res.* *40*, 10507-10520.
- Rahman, A., Srivastava, S.S., Sneh, A., Ahmed, N., and Krishnasastry, M.V. (2010). Molecular characterization of tlyA gene product, Rv1694 of Mycobacterium tuberculosis: a non-conventional hemolysin and a ribosomal RNA methyl transferase. *BMC Biochem.* *11*, 35.
- Savic, M., Ilic-Tomic, T., Macmaster, R., Vasiljevic, B., and Conn, G.L. (2008). Critical residues for cofactor binding and catalytic activity in the aminoglycoside resistance methyltransferase Sgm. *J. Bacteriol.* *190*, 5855-5861.
- Stanley, R.E., Blaha, G., Grodzicki, R.L., Strickler, M.D., and Steitz, T.A. (2010). The structures of the anti-tuberculosis antibiotics viomycin and capreomycin bound to the 70S ribosome. *Nat. Struct. Mol. Biol.* *17*, 289-U248.
- Whitmore, L., and Wallace, B.A. (2008). Protein secondary structure analyses from circular dichroism spectroscopy: methods and reference databases. *Biopolymers* *89*, 392-400.

Wimberly, B.T., Brodersen, D.E., Clemons, W.M., Jr., Morgan-Warren, R.J., Carter, A.P., Vonrhein, C., Hartsch, T., and Ramakrishnan, V. (2000). Structure of the 30S ribosomal subunit. *Nature* *407*, 327-339.

Witek, M.A., and Conn, G.L. (2014). Expansion of the aminoglycoside-resistance 16S rRNA (m(1)A1408) methyltransferase family: expression and functional characterization of four hypothetical enzymes of diverse bacterial origin. *Biochim. Biophys. Acta* *1844*, 1648-1655.

Witek, M.A., and Conn, G.L. (2016). Functional dichotomy in the 16S rRNA (m1A1408) methyltransferase family and control of catalytic activity via a novel tryptophan mediated loop reorganization. *Nucleic Acids Res.* *44*, 342-353.

Wren, B.W., Stabler, R.A., Das, S.S., Butcher, P.D., Mangan, J.A., Clarke, J.D., Casali, N., Parish, T., and Stoker, N.G. (1998). Characterization of a haemolysin from *Mycobacterium tuberculosis* with homology to a virulence factor of *Serpulina hydysenteriae*. *Microbiology* *144* (Pt 5), 1205-1211.

Zelinskaya, N., Rankin, C.R., Macmaster, R., Savic, M., and Conn, G.L. (2011). Expression, purification and crystallization of adenosine 1408 aminoglycoside-resistance rRNA methyltransferases for structural studies. *Protein Expr Purif* *75*, 89-94.

**CHAPTER 4:****BINDING INDUCED RNA CONFORMATIONAL CHANGES CONTROL SUBSTRATE  
RECOGNITION AND CATALYSIS BY THE THIOSTREPTON-RESISTANCE  
METHYLTRANSFERASE (TSR)**

Emily G. Kuiper and Graeme L. Conn

This work was originally published in the Journal of Biological Chemistry. Kuiper, E.G. and Conn, G.L. Binding induced RNA conformational changes control substrate recognition and catalysis by the thiostrepton resistance methyltransferase (tsr). *J Biol Chem*, 2014; 289:26189-26200. © the American Society for Biochemistry and Molecular Biology.

E.G.K performed experiments; E.G. K and G. L. C. conceived the studies, analyzed data, wrote the manuscript and acquired funding.

## 4.1 SUMMARY

Ribosomal RNA (rRNA) posttranscriptional modifications are essential for ribosome maturation, translational fidelity and are one mechanism used by both antibiotic-producing and pathogenic bacteria to resist the effects of antibiotics that target the ribosome. The thiostrepton producer *Streptomyces azureus* prevents self-intoxication by expressing the thiostrepton-resistance methyltransferase (Tsr), which methylates the 2'-hydroxyl of 23S rRNA nucleotide adenosine 1067 within the thiostrepton binding site. Tsr is a homodimer with each protomer containing an L30e-like amino-terminal domain (NTD) and a SPOUT methyltransferase family catalytic carboxyl-terminal domain (CTD). We show that both domains of the enzyme are required for high affinity RNA substrate binding. The Tsr-CTD has intrinsic, weak RNA affinity that is necessary to direct the specific high-affinity Tsr-RNA interaction via the NTDs, which have no detectable RNA affinity in isolation. RNA structure probing experiments identify the Tsr footprint on the RNA and structural changes in the substrate, induced specifically upon NTD binding, that are necessary for catalysis by the CTD. Additionally, we identify a key amino acid in each domain responsible for CTD-RNA binding and the observed NTD-dependent RNA structural changes. These studies allow us to develop a model for Tsr-RNA interaction in which the coordinated substrate recognition of each Tsr structural domain is an obligatory pre-catalytic recognition event. Our findings underscore the complexity of substrate recognition by RNA modification enzymes and the potential for direct involvement of the RNA substrate in controlling the process of its modification.

## 4.2 INTRODUCTION

Posttranscriptional modification of RNA is a conserved and essential process in all kingdoms of life. While many details remain to be uncovered, important roles played by such modifications

have steadily emerged for tRNAs and rRNAs, which are the best studied and among the most highly modified RNAs. Many tRNA modifications are essential in bacteria, for example, methylation of tRNA anticodon stem loop at G37 by TrmD prevents frameshifting during translation (1). rRNA modifications are not essential for growth under laboratory conditions, but frequently exhibit cold sensitive growth phenotypes and a variety of translational defects (2). Deletion of RsmA (formally KsgA; 16S rRNA m<sup>6</sup><sub>2</sub>A1518/ m<sup>6</sup><sub>2</sub>A1519) disrupts 30S biogenesis, while deletion of RsmB and RsmD (16S rRNA m<sup>5</sup>C967 and m<sup>2</sup>G966, respectively) disrupts translation initiation (2,3). Additionally, in antibiotic-producing and resistant pathogenic bacteria, methylation of rRNA at antibiotic binding sites disrupts drug binding and thus their toxic effects (4,5). The *Escherichia coli* 16S and 23S rRNAs contain 24 constitutively methylated nucleotides and the enzyme responsible for catalyzing each has been identified (6). Structural and biochemical studies of these enzymes and their homologs have provided significant insight into their interactions with the essential co-substrate S-adenosyl-L-methionine (SAM) and their catalytic mechanisms (7,8). However, due to the relative paucity of structural studies methyltransferase-RNA substrate complexes, much less is understood about rRNA substrate recognition.

Thiostrepton is the prototypical member of the thiazole-containing class of antibiotics and is produced by a number of *Streptomyces* strains including *Streptomyces azureus* (9). Thiostrepton has been used in veterinary medicine to treat mastitis and as a topical agent for dogs but, due to its poor solubility and toxicity, has found only limited applications to date. However, there is renewed interest in the clinical use of thiostrepton as an antibiotic, and also as a therapy for cancer and malaria (10-12). Thiostrepton binds to a compact 58 nucleotide (nt) rRNA domain within 23S rRNA, which is also the binding site for ribosomal protein L11 (13,14). This rRNA-protein complex forms part of the ribosomal functional center known as the GTPase center which interacts with the translational factors EF-G, EF-Tu and RF3. Resistance to thiostrepton can arise

from L11 loss or mutation, rRNA mutation or the specific methylation of the rRNA that makes up the drug-RNA binding interface (15-17).

In *S. azureus*, resistance is specifically conferred by methylation of 23S rRNA on the ribose 2' hydroxyl of adenosine 1067 (A1067, *E. coli* numbering) by the thiostrepton-resistance methyltransferase (Tsr) (15,18). Tsr uses the co-substrate SAM to methylate the 23S rRNA, presumably prior to the assembly of the 50S subunit as the L11 and proposed Tsr binding surfaces are overlapping. The crystal structure of the Tsr-SAM complex definitively classified the enzyme as a member of the SPOUT family of methyltransferases (19,20). As such, it is an obligate homodimer through interactions mediated by its carboxyl-terminal domain (CTD; **Fig. 4.1A**). The CTD also contains a characteristic trefoil knot structure that makes up the SAM binding site. Furthermore, the Tsr structure illustrated the organization of each CTD and its associated amino-terminal domain (NTD). The NTD is structurally similar to the yeast ribosomal protein L30e and is presumed to be involved in RNA substrate recognition. However, its specific contribution(s) to recognition and which structural elements of the 58 nt RNA domain (**Fig. 4.1B**) are essential for interaction with Tsr are unknown.

Two lines of evidence from previous studies have suggested that unfolding the 58 nt RNA domain tertiary structure may be required in substrate recognition by Tsr. First, stabilization of the RNA tertiary structure decreased *in vitro* methylation of the 58 nt RNA by Tsr (21). Second, a model 29 nt RNA hairpin containing the target loop and its associated stem, but lacking the full tertiary structure, was more readily methylated than the full 58 nt domain. These observations suggest that there maybe an energetic penalty paid by the enzyme to unfold the RNA tertiary structure prior to catalysis (20). We therefore sought to determine whether Tsr must alter the RNA structure as part of its substrate recognition mechanism. Here, we demonstrate that specific RNA recognition by Tsr involves docking of its CTD on the A1067 target loop, followed by the engagement of one or both NTDs in a process that drives specific RNA conformational changes

at a site distant from the target loop. Further, this RNA structural change is an essential step for catalysis and may form part of a pre-catalytic recognition signal from the N-terminal RNA recognition domain. Collectively, these studies reveal new mechanistic details of the intricate process of specific substrate recognition by Tsr and suggest a direct role for the RNA substrate in control of catalysis.

### 4.3 EXPERIMENTAL PROCEDURES

*4.3.1 Tsr purification and mutagenesis*—Tsr was expressed from plasmid pET28a-Tsr in *E. coli* BL21(DE3)-pLysS as described previously (20), and purified using Ni<sup>2+</sup>-affinity, heparin-affinity, and gel filtration chromatographies. Elution volume from the Superdex 200 10/300 gel filtration column (GE Healthcare) was calibrated using Gel Filtration Standards (BioRad). Purified enzyme was flash frozen and stored at -80 °C.

Tsr mutagenesis was performed using the MEGAWHOP protocol (22) to modify pET28a-Tsr. The Tsr amino terminal domain (Tsr-NTD) construct was created by inserting two stop codons after that coding for residue R101. The Tsr carboxy terminal domain (Tsr-CTD) construct was made by deletion of codons corresponding to amino acids 1-105. Individual domain proteins were expressed and purified as described for full-length (FL) Tsr. Each protein was expressed with a 6×His tag and thrombin cleavage site, giving calculated molecular weights of 31 kDa (61 kDa dimer), 19.5 kDa (39 kDa dimer) and 13 kDa for the FL-Tsr, Tsr-CTD, and Tsr-NTD proteins, respectively.

*4.3.2 RNA in vitro transcription*—Wild-type and U1061A 58 nt RNAs (**Fig. 4.1B**) were *in vitro* transcribed from linearized plasmid DNA as previously described (23). Prior to use, RNA was annealed by incubation at 65 °C for 10 minutes and slowly cooled to 25 °C.

*4.3.3 Hydroxyl radical and ribonuclease RNA structure probing*—RNA was dephosphorylated by alkaline phosphatase treatment and then [ $^{32}\text{P}$ ]-5'-end labeled using [ $\gamma$ - $^{32}\text{P}$ ]-ATP and T4 polynucleotide kinase. The products of the kinase reaction were resolved on a 12% (w/v) polyacrylamide, 50% urea denaturing sequencing gel, and full-length  $^{32}\text{P}$ -labeled RNA excised and recovered from gel slices by soaking in 0.3 M sodium acetate and subsequent ethanol precipitation.

Hydroxyl radical probing experiments contained FL-Tsr dialyzed overnight against assay buffer, 50 mM Tris pH 7.5, 75 mM KCl, 5 mM  $\text{MgCl}_2$ , at a final concentration of 20, 10, 5, 1 or 0.2  $\mu\text{M}$  with annealed  $^{32}\text{P}$ -labeled RNA (50,000 cpm) in a 20  $\mu\text{l}$  reaction. One microliter each of 50 mM  $\text{Fe}(\text{SO}_4)_2$ , 100 mM EDTA, 250 mM ascorbic acid and 3%  $\text{H}_2\text{O}_2$  were added to the side of the tube and pulsed in a microcentrifuge to mix rapidly. After 5 minutes on ice, the reaction was quenched by ethanol precipitation and the recovered RNA resuspended in 8  $\mu\text{l}$  of denaturing loading dye. Radioactivity was quantified by liquid scintillation counting and equal counts were loaded for each reaction and resolved on a 12% (w/v) polyacrylamide, 50% urea denaturing sequencing gel. Gels were run at a constant 55 W for 1.5 hours, dried, exposed to a phosphor screen overnight and scanned using a Typhoon FLA 7000 laser scanner (GE Healthcare). Band intensities were quantified using ImageQuant TL software (GE Healthcare) applying the rubber band background subtraction method. Band intensities were normalized to the most intense band in 0  $\mu\text{M}$  lane and normalized intensities were compared between 0 and 20  $\mu\text{M}$  Tsr. A nucleotide was considered protected or enhanced if the difference in relative intensity was  $\pm 15\%$ . An alkaline hydrolysis ladder (AH) and denaturing RNase T1 pattern (guanosine sequence) were used to identify the specific nucleotides cleaved.

For RNase enzymatic probing experiments, annealed  $^{32}\text{P}$ -labeled RNA (50,000 cpm) was mixed with assay buffer alone (supplemented with 10% glycerol) or a final concentration of 20  $\mu\text{M}$  Tsr. The optimal concentration of each RNase (V1, T1 or A) was empirically identified by performing

reactions with 10-fold serial dilutions of the RNase. Additional control reactions with RNA ( $\pm$  protein), but without RNase were also performed to ensure no contaminating RNases were present. Reactions were incubated for 10 minutes at 25 °C. The RNA was recovered by ethanol precipitation and resuspended in denaturing gel loading dye. Samples were analyzed by PAGE and recorded as described for the hydroxyl radical probing experiments.

*4.3.4 RNA UV Melting*—FL-Tsr and RNA were dialyzed overnight against 10 mM Hepes buffer pH 7.5, 100 mM NH<sub>4</sub>Cl, 5 mM Mg<sub>2</sub>SO<sub>4</sub>, and 10% glycerol. After annealing, RNA (25  $\mu$ g per sample) was melted alone or with an equal or half molar ratio of Tsr. The UV absorbance at 260 nm and 280 nm was measured over a linear temperature gradient (18-65 °C) with a heating rate of 1 °/min. The first derivative of each melting curve, referred to as its ‘melting profile’, was calculated as described previously (24,25).

*4.3.5 Fluorescence polarization*—RNA was 5'-end labeled with a fluorescein analog as described previously (26). Binding experiments were performed in the same assay buffer as used for structure probing experiments with a final concentration of 10 nM annealed RNA and protein concentrations ranging from 1 nM to 50  $\mu$ M. Polarization was measured in black, non-binding surface, 96 well plates (Corning) using a Synergy4 plate reader running Gen5 software (BioTek). Data was background subtracted and non-linear curve fitting performed in GraphPad Prism. Fits for all binding isotherms were compared between one-site and two-site specific binding, and the latter accepted only when the p-value was <0.05.

*4.3.6 Methylation Assays*—Methylation assays using illustra MicroSpin G-25 columns (GE Healthcare) to separate [<sup>3</sup>H]-labeled RNA and remaining [<sup>3</sup>H]-SAM were performed as described previously (20) with the following modifications. Assays were performed in 200  $\mu$ l reactions in assay buffer supplemented with 10% glycerol. After 30 minutes at 37 °C, 3  $\times$  50  $\mu$ l samples (technical triplicates) were applied to the spin column and 40  $\mu$ l of filtrate was counted in 2 ml of Ecoscint Ultra scintillation fluid (National Diagnostics). Assays were performed with three

independent preparations of Tsr. Tritium incorporation values in counts per minute (cpm) were averaged and plotted with the associated standard error of the mean (SEM).

*4.3.7 Electrophoretic mobility shift assay*—58 nt RNA (100 nM) was incubated with a range of concentrations of FL-Tsr or Tsr-CTD (two-fold dilutions from 10  $\mu$ M to 78 nM) at room temperature for 15 minutes and then separated on a 10% acrylamide, tris-borate-EDTA (TBE) native gel. The gel was stained with SYBR Gold and imaged using a Typhoon Trio imager (GE Healthcare). For binding specificity experiments, 100 nM *in vitro* transcribed 58 nt RNA, HDV ribozyme or tRNA<sup>Asn</sup> were incubated with FL-Tsr (1 or 10  $\mu$ M) or Tsr-CTD (10  $\mu$ M) and analyzed as above.

*4.3.8 Partial Proteolysis*—Purified wild-type and mutant Tsr proteins were treated with chymotrypsin at 1:100 (w/w) chymotrypsin:Tsr ratio using the same assay buffer as for probing experiments but supplemented with 10% glycerol. Samples were incubated for 30 minutes at room temperature. Reactions were stopped by adding SDS-loading dye and heating to 90 °C, and the products resolved on a 10% SDS-PAGE gel and visualized by staining with Coomassie Brilliant Blue dye. Otherwise identical samples were run without chymotrypsin as control for each protein.

## 4.4 RESULTS

*4.4.1 The Tsr NTDs aid in rRNA binding and are necessary for catalysis*—We predicted that the Tsr NTD and CTD domains might form stable and correctly folded proteins in isolation as homologous proteins are known, e.g. L30e and TrmL (a minimal SPOUT methyltransferase), and inspection of the Tsr NTD-CTD interface revealed it to be comprised primarily of polar and charged amino acids with almost no hydrophobic residues that would be exposed to solvent. Thus, to define the contribution of each Tsr domain to rRNA substrate recognition and catalysis,

proteins corresponding to FL-Tsr (**Fig. 4.1A**), the NTD (Tsr-NTD; amino acids 1-101) and CTD (Tsr-CTD; amino acids 106-269) were expressed, purified and their binding and catalytic activities quantified. Each isolated domain was indeed soluble and could be purified identically to FL-Tsr. In support of their correct, stable folding, FL-Tsr and Tsr-CTD eluted from the gel filtration column at a volume corresponding to the dimeric proteins (62 and 39 kDa, respectively), whereas Tsr-NTD was monomeric (13 kDa) (**Fig. 4.2A**). Further, in each case the target protein eluted a highly symmetrical peak indicative of well folded proteins suitable for subsequent biochemical analysis.

The binding dissociation constant ( $K_D$ ) of FL-Tsr for the 58 nt RNA was determined using fluorescence polarization (FP; **Fig. 4.2B**). Interaction of FL-Tsr and the 58 nt RNA was best fit using a two-site binding model yielding  $K_D$  values of 160 nM and  $\sim 10 \mu\text{M}$  (**Table 4.1**). Two binding events were previously observed for Tsr and other SPOUT-family members using electrophoretic mobility shift assays (EMSAs) and the shifted bands attributed to dimeric and tetrameric complexes of enzyme with RNA (7,20,27). We performed EMSAs using a similar range of Tsr concentrations as the FP experiments and confirmed the presence of these same complexes and their formation consistent with the  $K_D$  values determined by FP (**Fig. 4.2C**).

We next performed FP binding assays for each Tsr domain protein. In isolation, the monomeric Tsr-NTD had no measurable affinity for the RNA (**Fig. 4.2B**) suggesting that the CTD dimer is necessary to properly position both NTDs to achieve high affinity substrate binding. In contrast, the isolated Tsr-CTD dimer retained the ability to bind the 58 nt RNA but with  $>30$ -fold weaker affinity than FL-Tsr (**Table 4.1**), and the data was best fit with a one-site binding model.

However, an EMSA performed with the Tsr-CTD protein (**Fig. 4.2D**) clearly indicated that the isolated domain forms equivalent complexes to FL-Tsr, in a protein concentration dependent manner, albeit with reduced affinities. Fit of the Tsr-CTD FP data using the same two-site binding model as for FL-Tsr yielded  $K_D$  values of  $\sim 3$  and  $\sim 13 \mu\text{M}$ . We note that these values are

entirely consistent with the appearance of protein-RNA complexes in the Tsr-CTD EMSA (**Fig. 4.2D**), but the errors associated with the fit values are unacceptably large (presumably due to the transient nature of the faster migrating band with respect to protein concentration and the closeness of the  $K_D$  values compared to FL-Tsr). Most importantly, however, the FP and EMSA experiments together demonstrate that the catalytic CTD of Tsr interacts with the 58 nt RNA substrate similarly whether part of FL-Tsr or as the isolated Tsr-CTD but with substantially reduced affinity in the latter case. This observation is also reinforced by the ribonuclease probing experiments described below which clearly demonstrate that Tsr-CTD binds the RNA substrate in an identical manner as when it is part of full-length Tsr. Specifically, Tsr-CTD is able to confer protection of a subset of the same residues in the RNA as the full-length enzyme.

The proposed RNA-binding cleft of Tsr (20) contains positively charged amino acids on the CTD surface that could potentially promote non-specific interactions with any nucleic acid. We therefore sought to explore the specificity of RNA binding by Tsr and Tsr-CTD using EMSAs with the 58 nt RNA and two other structured RNAs with stem-loops: hepatitis delta virus (HDV) ribozyme and tRNA<sup>Asn</sup>. With both concentrations of FL-Tsr and 10  $\mu$ M Tsr-CTD, all of the 58 nt RNA was bound and its mobility retarded, resulting in the absence of a band with mobility corresponding to the free RNA (**Fig. 4.2E**). Conversely, neither FL-Tsr nor Tsr-CTD shifted all HDV RNA, suggesting that both proteins have significantly weaker affinity for HDV than the 58 nt RNA. A similar result was obtained with tRNA<sup>Asn</sup>, except that the highest FL-Tsr concentration, but not Tsr-CTD, resulted in a significant fraction of shifted RNA. These results indicate that while Tsr does have a propensity to bind other nucleic acids, binding of both Tsr and Tsr-CTD to the 58 nt RNA substrate is of higher affinity and specificity compared to other structured RNAs.

Collectively, these RNA binding data for FL-Tsr and the domain constructs indicate that the CTD plays a direct role in binding the RNA substrate and is critical for optimally positioning the NTDs

to fulfill their essential role in forming a specific, high-affinity complex. As Tsr-CTD preserves its dimeric state, binds the 58 nt RNA and, most importantly, maintains both intact SAM binding pockets and active sites, we next asked whether Tsr-CTD additionally retains any ability to methylate the 58 nt RNA. We compared the ability of full-length Tsr and Tsr-CTD to methylate the 58 nt RNA substrate and found that deletion of the NTDs, reduces Tsr activity to background (**Fig. 4.2D**). Collectively, from these binding and activity assays we conclude that the CTD has weak RNA binding affinity, but proper recognition of the substrate by the NTDs is necessary for substrate specificity and stimulation of catalysis of methyl transfer by its CTD.

*3.4.2 Identification of the RNA binding surface and binding-induced perturbations in the RNA structure by Tsr*—To identify the RNA surface contacted by Tsr we performed solution hydroxyl radical probing of [<sup>32</sup>P]-5'-end labeled wild-type 58 nt RNA in the absence and presence of various concentrations of full-length Tsr. Comparison of probing experiments performed without Tsr or in the presence of 20 μM Tsr revealed the protection of nucleotides 1058, 1059, and 1061-1068 in Helix 43 (H43) from hydroxyl radical-mediated strand scission, defining at least part of the Tsr-RNA 'footprint' (**Fig. 4.3**). This region is smaller than expected and most likely does not reflect the entirety of the interaction surface between Tsr and the 58 nt RNA. One complication in this analysis is that the compact tertiary structure of the 58 nt RNA protects many nucleotides from strand scission (28) and as a result such residues might concomitantly be relieved of protection by RNA-RNA contacts but protected by newly formed RNA-protein interactions. In support of this are observations of multiple regions of enhancement of hydroxyl radical cleavage and Tsr-mediated protection from RNase cleavage outside of this observed footprint region (described below and in the next section respectively).

Enhancement of hydroxyl radical cleavage upon protein binding could arise through Tsr-mediated distortion(s) of the RNA backbone that make it more susceptible to radical cleavage at specific nucleotides. In the presence of Tsr, enhancements are observed at three disparate

locations: U1083/ A1084 of the helical junction; A1087, located opposite the Tsr footprint surface at the base of H44; and U1094/ A1095 at the apex of H44 (**Fig. 4.3**). The enhancements in H44 are likely due to structural rearrangement of the target loop or H43, which are necessary to orient the target nucleotide A1067 into the catalytic site of Tsr. However, the induced changes to hydroxyl radical sensitivity more distant from the target nucleotide offer a first experimental indication of a more global RNA structural alteration, potentially unfolding of the RNA tertiary structure, induced by Tsr binding.

Given that the 58 nt RNA has a unique, compact tertiary structure with H44 juxtaposed to H43, and the identified role of the NTDs in activation of catalysis, we sought further evidence that Tsr could be unfolding the RNA structure. The 58 nt RNA has been extensively characterized by UV melting analysis and its melting profile includes a low temperature unfolding transition ( $T_m \sim 45$  °C), observed at 260 nm but invisible at 280 nm (**Fig. 4.4A**), that has been definitively demonstrated to correspond to the RNA tertiary structure (29,30). The remaining RNA secondary structures unfold in a single apparent transition (with apparent  $T_m \sim 63$  °C), corresponding to multiple two-state unfolding transitions. We tested whether Tsr is capable of altering the RNA structure upon binding, with the anticipation that stabilization or destabilization of the RNA tertiary structure would manifest as a higher or lower unfolding  $T_m$ , corresponding to a rightward or leftward shift in the unfolding transition, respectively (**Fig. 4.4B**). At 0.5 or 1 molar ratio of Tsr to 58 nt RNA, the tertiary structure unfolding transition in the melting profile was partially or fully eliminated, respectively, over the temperature range 20-40 °C. The relatively low unfolding  $T_m$  ( $\sim 40$  °C) and subsequent precipitation of Tsr does not allow for this experiment to definitively distinguish whether the RNA tertiary structure is stabilized or destabilized. However, it can nonetheless be concluded that the stability of the 58 nt RNA tertiary structure is indeed altered in a Tsr concentration-dependent manner. Together, the hydroxyl radical cleavage enhancements

and UV melting experiments in the presence of Tsr provide strong evidence that Tsr directly perturbs the RNA tertiary structure upon binding.

*3.4.3 RNA conformational changes induced by Tsr are dependent on its NTD*—To examine the Tsr-induced RNA conformational changes in more detail, we assessed the relative sensitivities to RNases V1, T1 and A of the wild-type 58 nt RNA in isolation and when complexed with either full-length Tsr or Tsr-CTD (**Fig. 4.5**). These enzymes preferentially cleave the RNA sugar-phosphate backbone at double-stranded/ stacked nucleotides, single-stranded G or single-stranded C/U nucleotides, respectively.

With the exception of G1062, the wild-type 58 nt RNA is almost entirely resistant to RNase V1 cleavage (**Fig. 4.5A, lane 3**). While much of the RNA is base paired, this result is not entirely unexpected given the highly complex nature of the RNA tertiary structure and distortion of helices from regular A-form RNA (31). In complex with Tsr, new strong cleavages are observed at nucleotides 1078-1080 while G1062 is protected (**Fig. 4.5A, compare lanes 3 and 4**).

Protections from RNase cleavage could be due to physical occlusion of the RNase from its target site (analogous to protections from hydroxyl radicals) or, alternatively, Tsr-induced alteration of the RNA structure so that it no longer meets the RNase substrate specification. In the case of G1062, which was also protected from hydroxyl radical cleavage (**Fig. 4.3**), the observed protection further confirms the surrounding region as part of the direct Tsr binding surface. The strongly enhanced RNase V1 cleavage of nucleotides 1078-1080 is unexpected and particularly noteworthy as it indicates that these nucleotides are substantially remodeled, presumably becoming more base-stacked, upon Tsr binding. Mapping the changes induced by full-length Tsr in RNase V1 sensitivities onto the 58 nt RNA structure (PDB ID: 1HC8) reveals that they cluster around an unusual RNA backbone conformation (**Fig. 4.5C**). Given their colocalization around this structurally unique region, protection of G1062 and enhancement of RNase V1 cleavage at 1078-1080 likely arise in concert through their interaction with a specific region of Tsr.

In contrast to the observed changes upon full-length Tsr binding, Tsr-CTD fails to induce the same pattern of changes in sensitivity to RNase V1 despite maintaining interaction with the RNA. Tsr-CTD neither protects G1062 nor induces the strong new cleavage sites at 1078-1080 (**Fig. 4.5A, lanes 3 and 5**). This result indicates that the Tsr NTD is in proximity of G1062 and directly implicates this domain as the primary driver of the conformational changes induced in the RNA.

RNase A treatment of the 58 nt RNA revealed six sites of sensitivity at nucleotides U1066, U1072, U1079, U1083, U1094 and U1097 (**Fig. 4.5A, lane 6**). Binding of full-length Tsr protects U1066 within the target loop, enhances cleavage of U1083 at the central helical junction, but has no effect on the sensitivities of U1072, U1079, U1094 and U1097 to RNase A cleavage (**Fig. 4.5A, lanes 6 and 7**). In contrast, binding of Tsr-CTD conferred only partial protection of U1066 and failed to induce enhancement of cleavage at U1083 (**Fig. 4.5A, lanes 6 and 8**). These results indicate, as might be expected given the location of the Tsr catalytic centers, that the CTD binds at the A1067 target loop directly occluding U1066 from cleavage in both the full-length and Tsr-CTD complexes. Additionally, the specificity of enhanced RNase A cleavage at U1083 within the helical junction to full-length Tsr provides further evidence, correlating with the hydroxyl radical probing results, that the structure of this region of the RNA is modified upon Tsr binding in a process dependent on the Tsr NTDs.

Subjecting the same samples to RNase T1 treatment revealed a similar pattern. The 58 nt RNA in isolation was cleaved three times, at residues G1068, G1071 and G1087 (**Fig. 4.5A, lane 9**).

Sensitivity at all three sites was reduced by binding of full-length Tsr, whereas only G1087 was protected by the Tsr-CTD (**Fig. 4.5A, lanes 9-11**). In the tertiary structure of the RNA, G1087 is adjacent to 1078-1080 where cleavage was enhanced when probed with RNase V1 (**Fig. 4.5C**).

This protection could be due to the CTD blocking RNase A from accessing this nucleotide.

Interestingly, while G1068 is immediately adjacent to the target nucleotide A1067, it is only strongly protected by full-length Tsr, suggesting that its environment and/ or conformation is only

significantly changed in a catalytically-competent complex and this change in the target loop is dependent on the distal interactions made by the Tsr-NTDs.

In summary, RNase probing of the isolated 58 nt RNA and its complexes with full-length Tsr or Tsr-CTD have identified unique RNA structural changes that occur upon Tsr binding and clearly identify the Tsr NTDs as the primary drivers of the RNA structural rearrangements necessary for specific recognition and methylation of A1067 by Tsr.

*4.4.4 Stabilizing the 58 nt RNA tertiary structure does not interfere with RNA conformational changes induced by RNase VI*—UV melting analysis and both hydroxyl radical and RNase structure probing indicate that binding of full-length Tsr induces RNA conformational changes, most likely partial unfolding of the tertiary structure. We next asked, whether a point mutation (U1061A) known to specifically stabilize the 58 nt RNA tertiary structure ( $>10\text{ }^{\circ}\text{C}$  to  $T_m \sim 58\text{ }^{\circ}\text{C}$ ) (32) and to reduce Tsr activity (20,21) effects methylation by blocking this unfolding event. We confirmed that Tsr activity was substantially reduced against the U1061A RNA correlating with a reduced binding affinity of  $1.56 \pm 0.33\text{ }\mu\text{M}$ ,  $\sim 10$ -fold weaker than for the wild-type 58 nt RNA (**Table 4.1, Fig. 4.6A,B**).

To investigate whether Tsr is still able to induce structural changes in the U1061A RNA, we probed the isolated RNA and its complex with full-length Tsr with RNases as before. U1061A RNA is generally more sensitive RNase VI with weak cleavages throughout both strands of H43, presumably because this helix is more ordered in this RNA tertiary structure stabilized mutant. Two pronounced cuts were observed with U1061A alone, G1062 and U1082, the latter unique to U1061A (**Fig. 4.6C, lane 3**). When bound by Tsr, both G1062 and U1082 were protected from cleavage, while strong enhancements were also observed at U1078-A1080 (**Fig. 4.6C, lane 4**), as seen with the wild-type 58 nt RNA. These strong cleavage enhancements at nucleotides 1078-1080 demonstrate that Tsr is still able to change the tertiary structure of this stabilized RNA. The pattern of U1061A RNA sensitivity to RNase T1 was also very similar to the wild-type 58 nt

RNA with three strong cleavages at G1067, G1071 and G1087. As for wild-type 58 nt RNA, these cleavages were protected in the presence of full-length Tsr (**Fig. 4.6C, lanes 7 and 8**).

When U1061A RNA was probed with RNase A, eight sites of strong strand scission were observed at U1060, U1066, C1072, C1075, C1079, U1083 U1094 and U1097. The cleavages at U1060, C1072, C1075, C1079 are much stronger in U1061A RNA (**Fig. 4.6C, lane 5**) compared to the wild-type 58 nt RNA, probably because these nucleotides are stabilized within this deformed A-helix and better recognized by RNase A. In the presence of full-length Tsr, U1066 and U1094 are protected from cleavage (**Fig. 4.6C, lanes 5 and 6**), the latter unique to U1061A RNA. These protections of U1066 and U1094 are most likely due to direct occlusion of the RNase by Tsr as they are near the target nucleotide (**Fig. 4.6D,E**). In contrast, the cleavages at C1072, C1075, U1083 and C1079 were enhanced, most likely due to the unfolding of the RNA structure in the presence of Tsr.

These data identify nucleotides with differing environments between the wild-type and U1061A mutant 58 nt RNAs that result in partially different RNase cleavage sensitivities. In addition, these data also clearly demonstrate that full-length Tsr can induce similar RNA tertiary conformational changes. However, the energetic penalty associated with unfolding this stabilized structure, reflected in the ~10-fold weaker binding affinity, most likely results in the dramatically reduced methylation efficiency compared to the wild-type 58 nt RNA.

#### *4.4.5 Tsr mutants R162A and R26A discriminate between RNA binding and induced*

*conformational changes necessary for catalysis*—We sought to identify key Tsr amino acids responsible for driving the RNA tertiary structure unfolding through mutagenesis and subsequent analysis of the ability of the mutant protein to induce the RNase V1-dependent cleavage of nucleotides 1078-1080. Potential targets for mutation in Tsr were selected based on their conservation among SPOUT family members with an L30e-like NTD and by inspection of their location in the modeled Tsr-58 nt RNA complex (20). Seven single alanine point mutations were

created, each resulting in a mutant enzyme containing two alanine mutations, one on each protomer of the Tsr homodimer. Each mutant protein was expressed, found to be soluble and purified as for Tsr. Two arginine to alanine Tsr mutants, R26A and R162A (**Fig. 4.7A,B**), were found to be deficient in their ability to promote strongly enhanced RNase V1 cleavage of nucleotides 1078-1080 in the wild-type 58 nt RNA despite retaining the native Tsr fold as assessed by partial proteolysis (**Fig. 4.7C,D**). These two Tsr mutants were therefore selected for further analysis.

We tested whether these mutations disrupted binding to and/ or methylation of the wild-type 58 nt RNA (**Fig. 4.7F and G**). Using the FP binding assay as before, the Tsr-R162A CTD mutant was found to bind with ~100-fold weaker affinity than wild-type Tsr, with a  $K_D$  of  $18 \pm 9.4 \mu\text{M}$  (close to the limit of measurement in this assay; **Table 4.1**). Thus, the R162A mutation dramatically reduces RNA binding, resulting in an ~3-fold weaker binding affinity than for Tsr-CTD which lacks the entire NTD. Methylation by Tsr-R162A was effectively ablated and comparable to background levels, correlating with the weakened affinity for the substrate. Since the RNA binding ability of Tsr-R162A is disrupted, this mutant cannot unfold the RNA structure. These data further implicate the CTD in an initial RNA docking event prior to the engagement of the NTDs, and demonstrate the critical role of R162 in this process.

Binding of the Tsr-R26A NTD mutant to wild-type 58 nt RNA was also reduced but more modestly with a ~30-fold weaker  $K_D$  ( $4.6 \pm 1.1 \mu\text{M}$ ), comparable to the affinity for Tsr-CTD (**Table 4.1, Fig. 4.7G**). While Tsr-R26A is unable to promote the RNase V1 sensitive RNA structural changes (**Fig 4.7D**), this mutant maintains its interaction with the RNA under the conditions used as demonstrated by the protection of nucleotides G1068 and G1071 from cleavage by RNase T1 (**Fig. 4.7E**). Correlating with the lack of structural rearrangement, methylation of the wild-type 58 nt RNA by Tsr-R26A was reduced to near background levels. These data demonstrate the critical importance of residue R26 for interaction of the Tsr NTDs

with the 58 nt RNA and specifically in promoting the RNA structural conformational changes necessary for activation of catalysis. Furthermore, these two mutants establish a decoupling between the CTD docking on the RNA target loop and distal RNA structural changes induced by the NTD necessary for catalysis.

#### 4.5 DISCUSSION

Modifications of rRNA are important for translational fitness and resistance against ribosome-targeting antibiotics. However, there is limited knowledge about how the enzymes responsible for their incorporation recognize their modification targets. We therefore sought to biochemically elucidate how the resistance-conferring enzyme Tsr recognizes its substrate rRNA domain. Our data show that the Tsr NTD in isolation does not bind the RNA, but must be delivered to the RNA via the Tsr-CTD-RNA interaction in order to achieve a specific, high-affinity complex. An essential part of the substrate recognition mechanism for Tsr involves the precise reorganization of the RNA tertiary and secondary structures coordinated by the accessory NTD in a process that is indispensable for catalysis in the distant CTD active site. Collectively, our results suggest a two-step model for substrate recognition (**Fig. 4.8**) and a direct role for the rRNA in control of Tsr activity on its substrate.

Tsr is a member of the SPOUT family of methyltransferases. These enzymes contain a common SPOUT domain catalytic core which may be decorated by several different RNA binding structural elements, ranging from a few helices as in TrmH (tRNA Gm18) (33,34) or larger structural domains like the L30e domain of Tsr or PUA domain of RsmE (16S rRNA m<sup>3</sup>U1498) (35,36). Our results showed that without its N-terminal RNA binding domain, Tsr is catalytically inactive despite retaining an ability to bind the RNA substrate with ~30-fold weaker affinity than the full-length enzyme. Such intrinsic RNA binding ability is also exhibited by the SPOUT

family tRNA methyltransferase TrmL (formerly YibK; tRNA Um34/Cm34) which does not contain an accessory RNA-binding domain but instead interacts with its tRNA substrate via a flexible, positively charged patch of amino acids located on the non-catalytic protomer near the active site (27). The initial step of Tsr-CTD docking on its RNA substrate proposed in our model for Tsr action is thus reminiscent of the ability of this minimal SPOUT methyltransferase to bind its tRNA substrate, despite Tsr containing a defined RNA binding domain.

While the Tsr CTD binds RNA, it is remarkable that a single point mutation in the CTD, R162A, weakens the RNA binding affinity 500-fold compared to full-length Tsr. This residue is absolutely conserved in the closely related nosiheptide-resistance methyltransferase (Nhr; 23S rRNA Am1067) and the avilamycin-resistance conferring methyltransferase AviRb (23S rRNA Um2479), and functionally conserved in other SPOUT family members (8,37). The dramatic decrease in binding affinity is readily rationalized by examining the position of each R162 residue in the dimeric Tsr structure. Each R162 is solvent exposed and positioned  $\sim 20$  Å apart on opposite sides of a cleft made by the anti-parallel orientation of each Tsr CTD where the RNA must bind to access the SAM co-substrate. Therefore, the alanine mutation disrupts two essential interactions with the RNA that may be essential for recognizing the target loop backbone geometry.

Our studies have revealed that the NTD of Tsr is an essential component of the RNA substrate recognition mechanism by both promoting high-affinity RNA binding and activation of catalysis by the CTD. In the absence of the NTD, the Tsr is catalytically inactive despite possessing the intact SAM binding sites and catalytic center. The Tsr-CTD dimer binds the RNA  $\sim 30$ -fold more weakly than the wild-type enzyme and, most critically, is unable to promote the NTD-dependent RNA conformational change. The Tsr NTD is structurally similar to the yeast ribosomal protein L30e, which binds both yeast 26S rRNA (nucleotides 1711-1733) and its own mRNA for transcriptional autoregulation. Both RNA domains contain a unique RNA structural motif known

as a kink-turn (38). While not geometrically identical, the 58 nt RNA also contains an unusual backbone secondary structure that reverses the RNA backbone in a similar way. Despite these structural similarities in both protein and RNA target, the Tsr-NTD in isolation showed no detectable affinity for the 58 nt RNA domain. We conclude, therefore that the weak intrinsic affinity of the CTD is essential for it to deliver and correctly position the Tsr NTDs in order for them to productively contribute to high-affinity, specific recognition of the RNA substrate. This coordinated binding of the CTD and NTD positioning may allow for the potential crosstalk between the two domains to relay a signal to perform catalysis.

Tsr recognition and subsequent methylation of its substrate requires significant perturbations in the 58 nt RNA structure. Hydroxyl radical and RNase structure probing of the Tsr-RNA complex revealed unique cleavage enhancements throughout H43 distant from the target loop, suggesting that the RNA is being unfolded, presumably to allow for proper orientation of A1067 into the catalytic center. The most significant specific structural change occurs at nucleotides 1078-1080 and is driven by the Tsr NTD. We have identified arginine 26 as a critical residue for NTD-mediated RNA recognition and the RNase V1-sensitive RNA structural change. This amino acid is conserved in the L30e-SPOUT methyltransferases AviRb, Nhr, RrmA (23S rRNA m<sup>1</sup>G745) and RlmB (23S rRNA Gm2251). In a previously published model of the Tsr-58 nt RNA complex, R26 is positioned near U1058 (20). Given its sequence conservation, potential role recognizing the rRNA and demonstrated importance in promoting the RNase V1-sensitive structural change, we propose that R26 directly recognizes the RNA nucleotides near 1058-1060. In doing so, this residue enhances base stacking of nucleotides on the opposite strand (1078-1080), increasing their sensitivity to RNase V1. As the catalytic activity of the Tsr-R26A mutant is drastically decreased compared to wild-type, we hypothesize that this RNA structural reorganization at the base of H43 may be relayed to induce changes in the target loop necessary for proper orientation of A1067 into the active site of Tsr. In further support of this concept is the observation that the

RNase T1 protection of the adjacent nucleotide, G1068, is also dependent on the presence of the Tsr NTD.

There is precedent for the direct involvement of RNA structure and structural reorganization in the process of substrate recognition by rRNA modification enzymes. The crystal structure of RlmD (formerly RumA; 23S rRNA m<sup>5</sup>U1939) in complex with a 29 nt model RNA (nucleotides 1932-1961) revealed that flipping of U1939 into the RlmD catalytic site was facilitated and stabilized by a major reorganization of the RNA (39). Additionally, two nucleotides fill the space the flipped target nucleotide 1939 would otherwise occupy, stabilizing the target nucleotide in the catalytic pocket. In contrast, the crystal structure of the aminoglycoside-resistance conferring enzyme NpmA (16S rRNA m<sup>1</sup>A1408)-30S ribosomal subunit complex showed minimal RNA structural changes were induced upon recognition, with the striking exception of the flipping of the target nucleotide out of its RNA helix (40). Perhaps, as RlmD and Tsr recognize rRNA prior to subunit maturation, their RNA substrates are structurally more plastic and thus reorganization of the RNA is an effective mechanism to accomplish the necessary level of discrimination during substrate recognition.

4.6 ACKNOWLEDGEMENTS—We are grateful to Dr. Christine Dunham for critical reading of this manuscript and to members of the Conn and Dunham laboratories for many useful discussions during the course of this work. \*EGK was supported by the Agriculture and Food Research Initiative Competitive Grant No. 2013-67011-21133 from the USDA National Institute of Food and Agriculture. This work was supported in part by NIH grants R01-AI088025 and T32-GM008367.

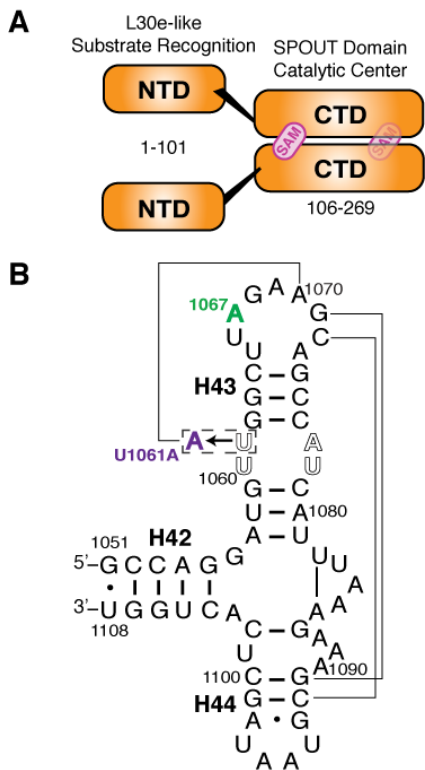


**FIGURE 4.1. Tsr domain organization and 58 nt RNA substrate secondary structure.** *A*, Tsr is a homodimer consisting of protomers each containing an amino-terminal domain (NTD) proposed to direct substrate recognition and a carboxy-terminal domain (CTD) containing the catalytic centers and SAM binding sites. *B*, Secondary structure of the 58 nt RNA substrate comprising *E. coli* 23S rRNA Helices 42 through 44 (H42, H43 and H44). The Tsr target nucleotide (A1067, green) and tertiary structure stabilizing point mutation (U1061A, purple) are highlighted. Lines indicate key long-range interactions within the 58 nt domain tertiary fold.

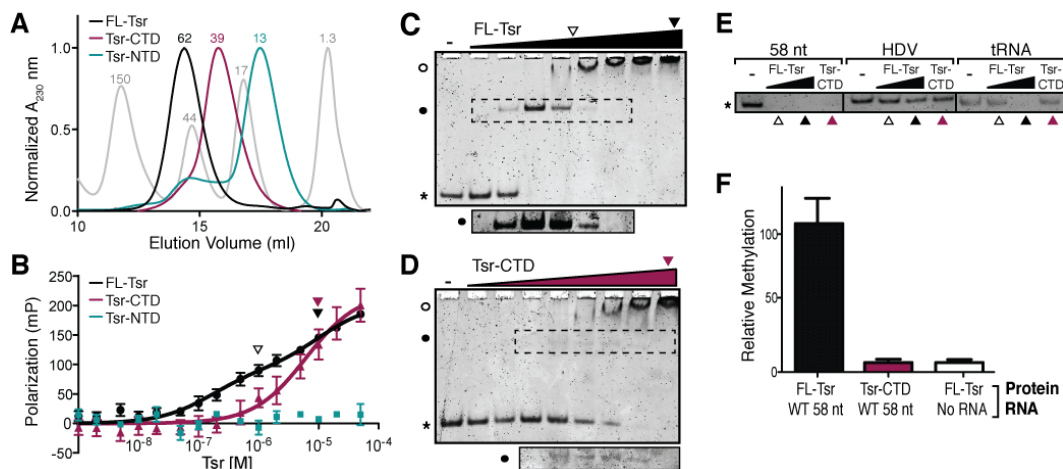


**FIGURE 4.2. The Tsr NTDs increase RNA binding affinity and are necessary for catalysis**

*A*, Chromatograms of the final gel-filtration purification for full-length Tsr (FL-Tsr, black), Tsr-CTD (purple) and Tsr-NTD (teal). Gel-filtration standards are shown (grey) and the approximate molecular weight (kDa) indicated above each peak. *B*, FP analysis of FL-Tsr (black), Tsr-CTD (purple), and Tsr-NTD (teal) binding to the wild-type (WT) 58 nt RNA. Arrowheads (open and solid) shown in *panels B-D* indicate Tsr concentrations (1 and 10  $\mu$ M, respectively) used in the control EMSAs of *panel E*. *C*, EMSA of FL-Tsr (0.078 to 10  $\mu$ M, *left to right lanes*) interaction with 58 nt RNA. Free 58 nt (\*), Tsr: 58 nt RNA complex (solid circle) and higher molecular weight complexes (open circle) are indicated. The dashed box indicates the region of the gel shown (*bottom*) at greater exposure. *D*, As *panel C* but for Tsr-CTD. *E*, Control EMSAs comparing FL-Tsr (1 or 10  $\mu$ M) and Tsr-CTD (10  $\mu$ M) affinity for the 58 nt substrate and two unrelated *in vitro* transcribed RNAs: the HDV ribozyme and tRNA<sup>Asn</sup>. *F*, Relative methylation of 58 nt RNA by FL-Tsr and Tsr-CTD, relative to background in the absence of RNA substrate.

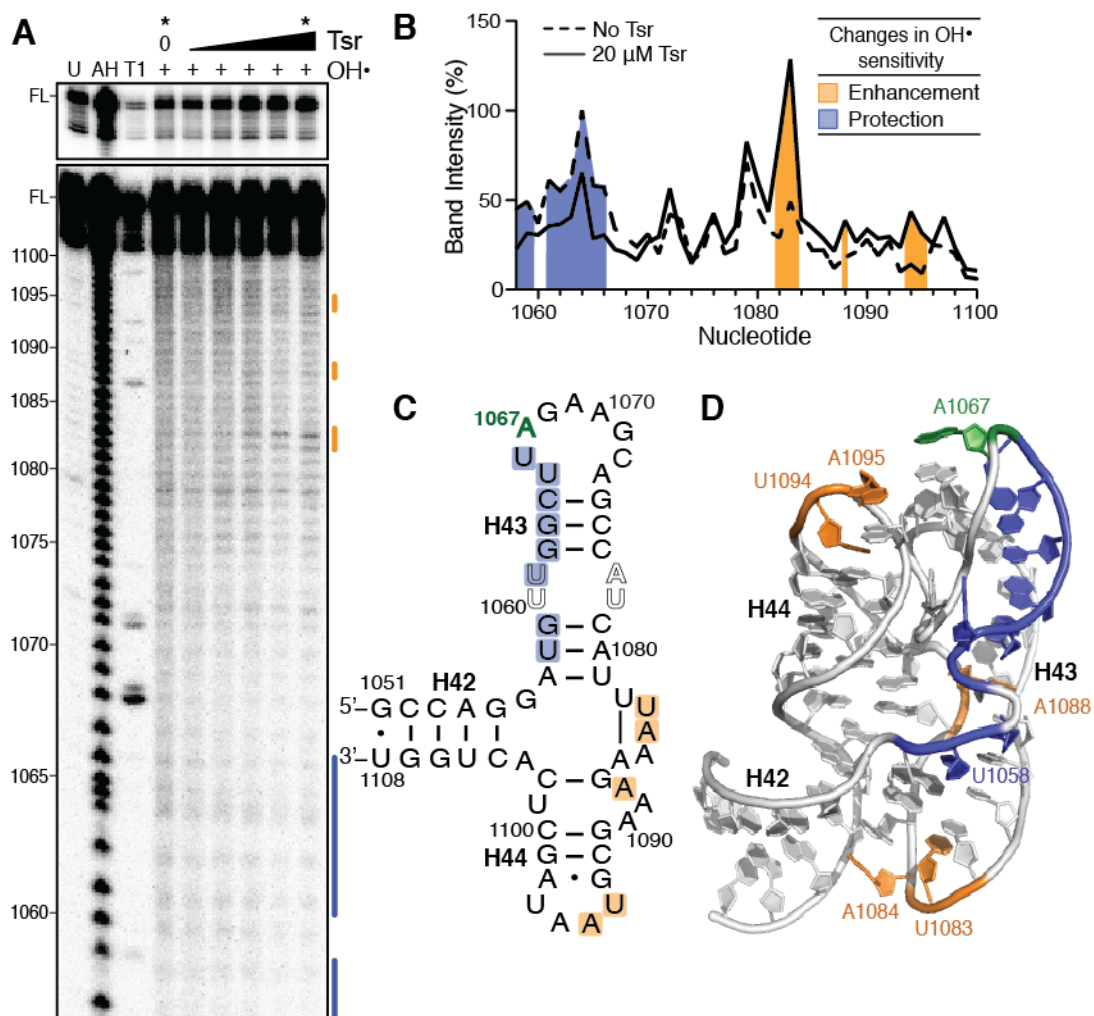


**FIGURE 4.3. Hydroxyl radical probing identifies the Tsr footprint and cleavage**

**enhancements upon Tsr binding.** *A*, Representative hydroxyl radical probing gel of wild-type 58 nt RNA complexed with an increasing concentration of Tsr (*left to right*: 0.2, 1, 5 10 and 20  $\mu\text{M}$ ). Untreated RNA (U), partial alkaline hydrolysis nucleotide ladder (AH), and RNase T1 digestion under denaturing conditions (T1) allow nucleotide identification (marked on *left*); FL is the full-length 58 nt RNA band, also shown with lighter exposure in the top panel. *B*, Quantification of each band in the lanes without Tsr and with Tsr at 20  $\mu\text{M}$  (noted \* at *top*). Cleavage protections and enhancements are shown as blue and orange shading, respectively. Changes in sensitivity to hydroxyl radicals are mapped as protections (blue) and enhancements (orange) onto *C*, the 58 nt RNA secondary structure, and *D*, the X-ray crystal structure (PDB ID: 1HC8).

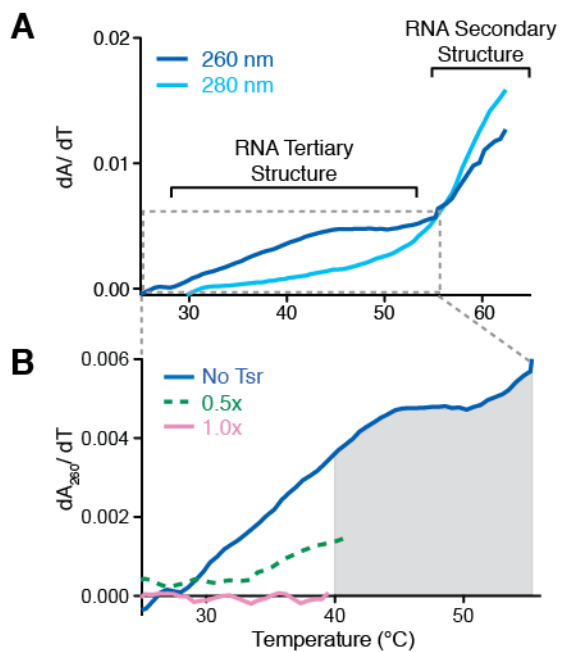


**FIGURE 4.4. UV melting of the wild-type 58 nt RNA with and without full-length Tsr.** *A*, Melting profile of the 58 nt RNA at 260 (solid line) and 280 nm (dashed line). *B*, RNA melting profiles at 260 nm in the presence of 0 (solid blue line), 0.5 (dashed green line) and 1:1 (solid pink line) molar equivalents of Tsr. Tsr precipitation is denoted by the grey shaded region of the plot.

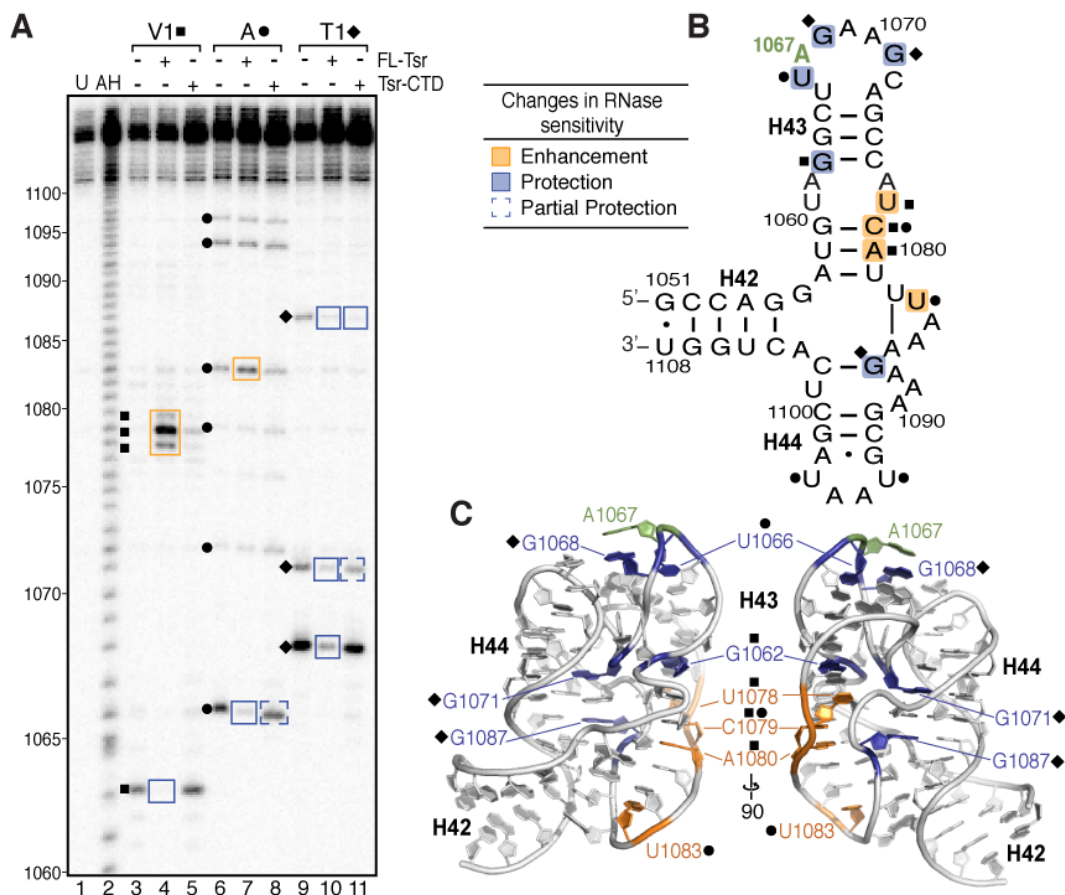


**FIGURE 4.5. RNase probing identifies RNA structural changes and cleavage protections induced upon binding full-length Tsr or Tsr-CTD.** *A*, Representative RNase structure probing gel of 58 nt RNA only, and complexes of 58 nt RNA with full-length Tsr or Tsr-CTD. Untreated RNA (U) and partial alkaline hydrolysis nucleotide ladder (AH) are also shown for nucleotide identification (numbering noted on *left*). Sites of cleavage are noted for RNase V1 (squares), RNase A (circles), RNase T1 (diamonds). Changes in sensitivity to RNases (boxed on the gel) are mapped as protections (blue) and enhancements (orange) onto *B*, the 58 nt RNA secondary structure, and *C*, two views of X-ray crystal structure (PDB ID: 1HC8) related by a 90° rotation around the vertical axis.

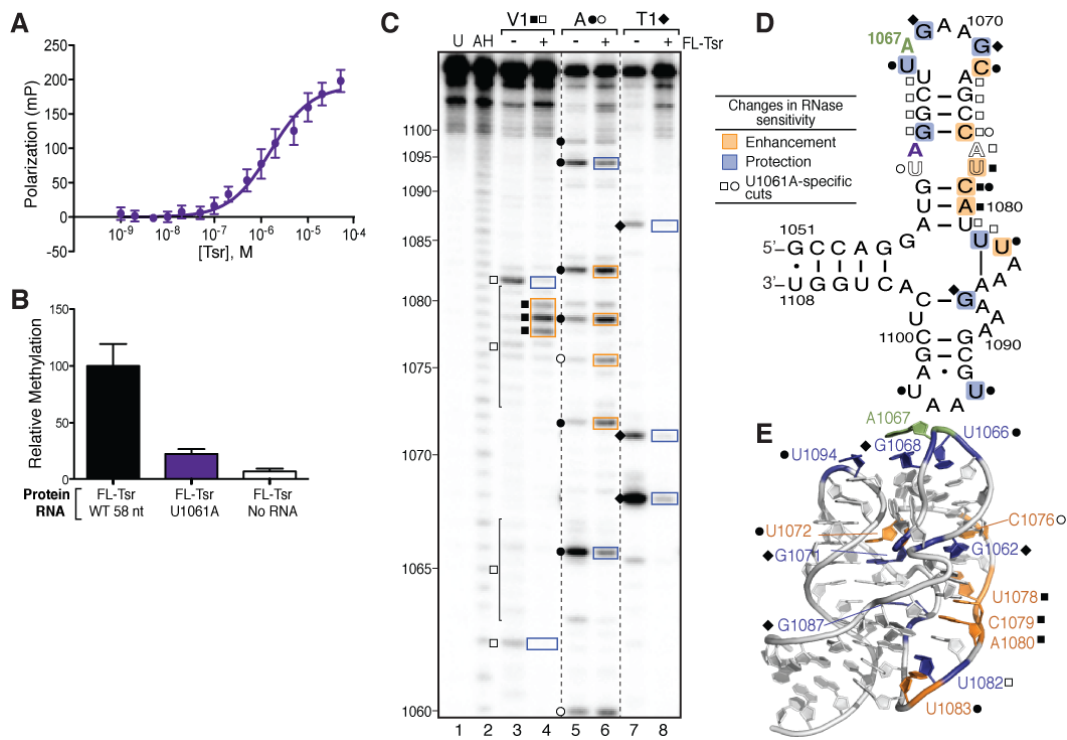


**FIGURE 4.6. Stabilizing the RNA tertiary structure decreases Tsr binding affinity and catalytic activity independent of RNA structural changes.** *A*, FP binding analysis of U1061A RNA and full-length (FL) Tsr interaction. *B*, Relative methylation activity of full-length Tsr on the wild-type (WT) and U1061A mutant 58 nt RNAs. *C*, Representative RNase structure probing gel of U1061A RNA in the absence and presence of full-length Tsr. Untreated RNA (U) and partial alkaline hydrolysis nucleotide ladder (AH) are also shown for nucleotide identification (numbering noted on *left*). Sites of cleavage are noted for RNase V1 (squares), RNase A (circles), and RNase T1 (diamonds); cleavage sites unique to the U1061A mutant are shown as outline symbols. Changes in sensitivity to RNase are mapped as protections (blue) and enhancements (orange) onto the 58 nt RNA *D*, secondary structure, and *E*, X-ray crystal structure (PDB ID: 1HC8).

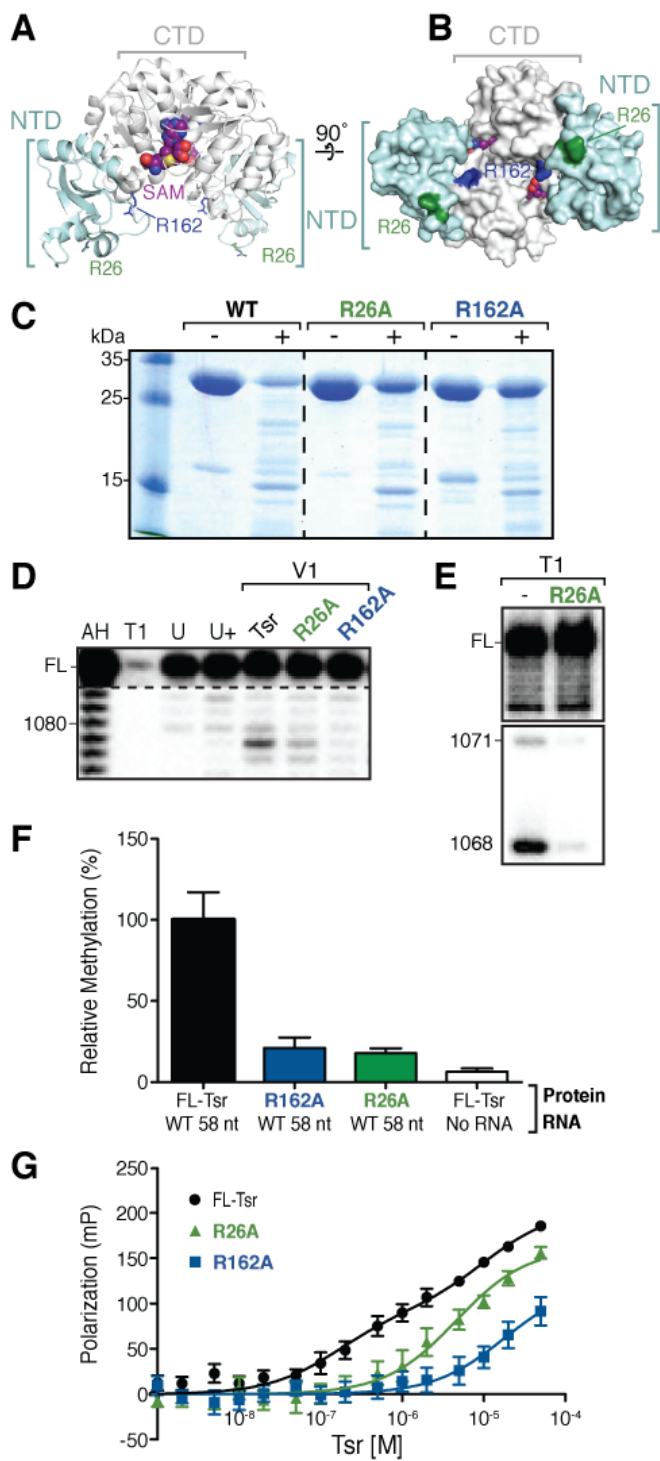


**FIGURE 4.7. Tsr-NTD modification of the RNA structure is necessary for catalysis.**

*A*, Cartoon representation of Tsr-SAM complex (PDB ID: 3GYQ) with sites of mutation indicated as sticks: R26 (green) and R162 (blue). SAM co-substrate (magenta) is also shown. *B*, Surface representation of the same complex rotated 90° around the horizontal axis. The color scheme is the same as in *panel A*. *C*, SDS-PAGE analysis of protein samples following incubation without (-) and with (+) chymotrypsin. Partial proteolytic cleavage of wild-type and mutant full-length Tsr proteins demonstrates that each adopts the same, native fold. *D*, RNase V1 probing of the wild-type 58 nt RNA in complex with wild-type and each mutant Tsr. Additional lanes are: partial alkaline hydrolysis nucleotide ladder (AH), denaturing RNase T1 digest (T1), untreated RNA (U), and Tsr-RNA complex with no added RNase V1 (U+). *E*, RNase T1 sensitivity of two cleavage sites within the 58 nt RNA in the absence (-) or presence of Tsr-R26A mutant. *F*, Relative enzymatic activity and *G*, FP binding analysis of the indicated Tsr mutants with wild-type 58 nt RNA.

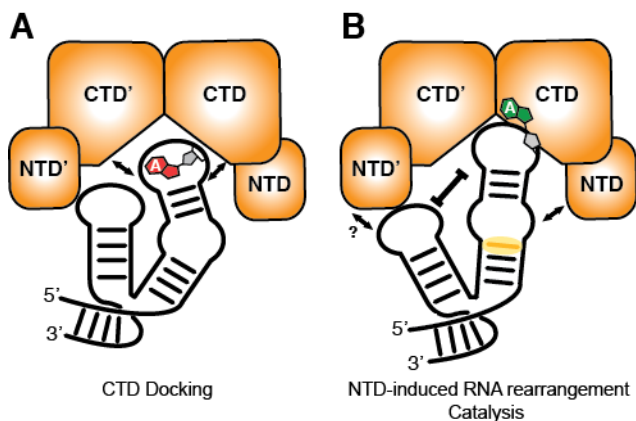


**FIGURE 4.8. Model of the Tsr substrate recognition mechanism.** *A*, The Tsr CTD mediates initial docking on the RNA substrate, with binding driven largely by the critical residue R162. *B*, Once bound, the Tsr NTDs are engaged and induce a rearrangement of the RNA structure (yellow shaded region is the most pronounced RNase V1 enhancement) that is signaled to the CTD to stimulate catalysis.

**TABLE 4.1: Dissociation Constants for Tsr and RNA mutants**

<b>Protein</b>	<b>58 nt RNA</b>	<b><math>K_D</math> (<math>\mu\text{M}</math>)</b>	<b>Fig.</b>
<b>FL-Tsr</b>	Wild-type	1) $0.16 \pm 0.06$	2A
		2) $10 \pm 6.7$	
<b>Tsr-CTD</b>	Wild-type	$6.1 \pm 1.6$	2A
<b>Tsr-NTD</b>	Wild-type	NB	2A
<b>FL-Tsr</b>	U1061A	$1.6 \pm 0.3$	6A
<b>Tsr-R26A</b>	Wild-type	$4.6 \pm 1.1$	7G
<b>Tsr-R162A</b>	Wild-type	$18 \pm 9.4$	7G

*NB, No binding detected*

## 4.7 REFERENCES

1. O'Dwyer, K., Watts, J. M., Biswas, S., Ambrad, J., Barber, M., Brule, H., Petit, C., Holmes, D. J., Zalacain, M., and Holmes, W. M. (2004) Characterization of *Streptococcus pneumoniae* TrmD, a tRNA methyltransferase essential for growth. *J Bacteriol* **186**, 2346-2354
2. Burakovsky, D. E., Prokhorova, I. V., Sergiev, P. V., Milon, P., Sergeeva, O. V., Bogdanov, A. A., Rodnina, M. V., and Dontsova, O. A. (2012) Impact of methylations of m2G966/m5C967 in 16S rRNA on bacterial fitness and translation initiation. *Nucleic Acids Res* **40**, 7885-7895
3. Connolly, K., Rife, J. P., and Culver, G. (2008) Mechanistic insight into the ribosome biogenesis functions of the ancient protein KsgA. *Molecular microbiology* **70**, 1062-1075
4. Wilson, D. N. (2014) Ribosome-targeting antibiotics and mechanisms of bacterial resistance. *Nature reviews. Microbiology* **12**, 35-48
5. Cundliffe, E. (1989) How antibiotic-producing organisms avoid suicide. *Annu Rev Microbiol* **43**, 207-233
6. Machnicka, M. A., Milanowska, K., Osman Oglou, O., Purta, E., Kurkowska, M., Olchowik, A., Januszewski, W., Kalinowski, S., Dunin-Horkawicz, S., Rother, K. M., Helm, M., Bujnicki, J. M., and Grosjean, H. (2013) MODOMICS: a database of RNA modification pathways--2013 update. *Nucleic Acids Res* **41**, D262-267
7. Watanabe, K., Nureki, O., Fukai, S., Ishii, R., Okamoto, H., Yokoyama, S., Endo, Y., and Hori, H. (2005) Roles of conserved amino acid sequence motifs in the SpoU (TrmH) RNA methyltransferase family. *J Biol Chem* **280**, 10368-10377
8. Yang, H., Wang, Z., Shen, Y., Wang, P., Jia, X., Zhao, L., Zhou, P., Gong, R., Li, Z., Yang, Y., Chen, D., Murchie, A. I., and Xu, Y. (2010) Crystal structure of the nosiheptide-resistance methyltransferase of *Streptomyces actuosus*. *Biochemistry* **49**, 6440-6450

9. Cundliffe, E. (1978) Mechanism of resistance to thiostrepton in the producing-organism *Streptomyces azureus*. *Nature* **272**, 792-795
10. Bhat, U. G., Halasi, M., and Gartel, A. L. (2009) Thiazole antibiotics target FoxM1 and induce apoptosis in human cancer cells. *PLoS One* **4**, e5592
11. Hegde, N. S., Sanders, D. A., Rodriguez, R., and Balasubramanian, S. (2011) The transcription factor FOXM1 is a cellular target of the natural product thiostrepton. *Nature chemistry* **3**, 725-731
12. Aminake, M. N., Schoof, S., Sologub, L., Leubner, M., Kirschner, M., Arndt, H. D., and Pradel, G. (2011) Thiostrepton and derivatives exhibit antimalarial and gametocytocidal activity by dually targeting parasite proteasome and apicoplast. *Antimicrob Agents Chemother* **55**, 1338-1348
13. Thompson, J., Cundliffe, E., and Stark, M. (1979) Binding of thiostrepton to a complex of 23-S rRNA with ribosomal protein L11. *Eur J Biochem* **98**, 261-265
14. Ryan, P. C., Lu, M., and Draper, D. E. (1991) Recognition of the highly conserved GTPase center of 23 S ribosomal RNA by ribosomal protein L11 and the antibiotic thiostrepton. *J Mol Biol* **221**, 1257-1268
15. Cundliffe, E., and Thompson, J. (1979) Ribose methylation and resistance to thiostrepton. *Nature* **278**, 859-861
16. Cameron, D. M., Thompson, J., Gregory, S. T., March, P. E., and Dahlberg, A. E. (2004) Thiostrepton-resistant mutants of *Thermus thermophilus*. *Nucleic Acids Res* **32**, 3220-3227
17. Wienen, B., Ehrlich, R., Stoffler-Meilicke, M., Stoffler, G., Smith, I., Weiss, D., Vince, R., and Pestka, S. (1979) Ribosomal protein alterations in thiostrepton- and Micrococin-resistant mutants of *Bacillus subtilis*. *J Biol Chem* **254**, 8031-8041

18. Thompson, J., Schmidt, F., and Cundliffe, E. (1982) Site of action of a ribosomal RNA methylase conferring resistance to thiostrepton. *J Biol Chem* **257**, 7915-7917
19. Anantharaman, V., Koonin, E. V., and Aravind, L. (2002) SPOUT: a class of methyltransferases that includes spoU and trmD RNA methylase superfamilies, and novel superfamilies of predicted prokaryotic RNA methylases. *J Mol Microbiol Biotechnol* **4**, 71-75
20. Dunstan, M. S., Hang, P. C., Zelinskaya, N. V., Honek, J. F., and Conn, G. L. (2009) Structure of the thiostrepton resistance methyltransferase.S-adenosyl-L-methionine complex and its interaction with ribosomal RNA. *J Biol Chem* **284**, 17013-17020
21. Bechthold, A., and Floss, H. G. (1994) Overexpression of the thiostrepton-resistance gene from *Streptomyces azureus* in *Escherichia coli* and characterization of recognition sites of the 23S rRNA A1067 2'-methyltransferase in the guanosine triphosphatase center of 23S ribosomal RNA. *Eur J Biochem* **224**, 431-437
22. Chen, G. J., Qiu, N., Karrer, C., Caspers, P., and Page, M. G. (2000) Restriction site-free insertion of PCR products directionally into vectors. *BioTechniques* **28**, 498-500, 504-495
23. Linpinsel, J. L., and Conn, G. L. (2012) General protocols for preparation of plasmid DNA template, RNA in vitro transcription, and RNA purification by denaturing PAGE. *Methods Mol Biol* **941**, 43-58
24. Dunstan, M. S., Guhathakurta, D., Draper, D. E., and Conn, G. L. (2005) Coevolution of protein and RNA structures within a highly conserved ribosomal domain. *Chem Biol* **12**, 201-206
25. Draper, D. E., Bukhman, Y. V., and Gluick, T. C. (2001) Thermal methods for the analysis of RNA folding pathways. *Current protocols in nucleic acid chemistry / edited by Serge L. Beaucage ... [et al.]* **Chapter 11**, Unit 11 13

26. Zearfoss, N. R., and Ryder, S. P. (2012) End-labeling oligonucleotides with chemical tags after synthesis. *Methods Mol Biol* **941**, 181-193
27. Liu, R. J., Zhou, M., Fang, Z. P., Wang, M., Zhou, X. L., and Wang, E. D. (2013) The tRNA recognition mechanism of the minimalist SPOUT methyltransferase, TrmL. *Nucleic Acids Res* **41**, 7828-7842
28. Conn, G. L., Gittis, A. G., Lattman, E. E., Misra, V. K., and Draper, D. E. (2002) A compact RNA tertiary structure contains a buried backbone-K<sup>+</sup> complex. *J Mol Biol* **318**, 963-973
29. Laing, L. G., Gluick, T. C., and Draper, D. E. (1994) Stabilization of RNA structure by Mg ions. Specific and non-specific effects. *J Mol Biol* **237**, 577-587
30. Xing, Y., and Draper, D. E. (1995) Stabilization of a ribosomal RNA tertiary structure by ribosomal protein L11. *J Mol Biol* **249**, 319-331
31. Conn, G. L., Draper, D. E., Lattman, E. E., and Gittis, A. G. (1999) Crystal structure of a conserved ribosomal protein-RNA complex. *Science* **284**, 1171-1174
32. Lu, M., and Draper, D. E. (1994) Bases defining an ammonium and magnesium ion-dependent tertiary structure within the large subunit ribosomal RNA. *J Mol Biol* **244**, 572-585
33. Tkaczuk, K. L., Dunin-Horkawicz, S., Purta, E., and Bujnicki, J. M. (2007) Structural and evolutionary bioinformatics of the SPOUT superfamily of methyltransferases. *BMC Bioinformatics* **8**, 73
34. Nureki, O., Watanabe, K., Fukai, S., Ishii, R., Endo, Y., Hori, H., and Yokoyama, S. (2004) Deep knot structure for construction of active site and cofactor binding site of tRNA modification enzyme. *Structure* **12**, 593-602

35. Zhang, H., Wan, H., Gao, Z. Q., Wei, Y., Wang, W. J., Liu, G. F., Shtykova, E. V., Xu, J. H., and Dong, Y. H. (2012) Insights into the catalytic mechanism of 16S rRNA methyltransferase RsmE (m(3)U1498) from crystal and solution structures. *J Mol Biol* **423**, 576-589
36. Forouhar, F., Shen, J., Xiao, R., Acton, T. B., Montelione, G. T., and Tong, L. (2003) Functional assignment based on structural analysis: crystal structure of the yggJ protein (HI0303) of *Haemophilus influenzae* reveals an RNA methyltransferase with a deep trefoil knot. *Proteins* **53**, 329-332
37. Mosbacher, T. G., Bechthold, A., and Schulz, G. E. (2005) Structure and function of the antibiotic resistance-mediating methyltransferase AviRb from *Streptomyces viridochromogenes*. *J Mol Biol* **345**, 535-545
38. Klein, D. J., Schmeing, T. M., Moore, P. B., and Steitz, T. A. (2001) The kink-turn: a new RNA secondary structure motif. *Embo J* **20**, 4214-4221
39. Lee, T. T., Agarwalla, S., and Stroud, R. M. (2005) A unique RNA Fold in the RumA-RNA-cofactor ternary complex contributes to substrate selectivity and enzymatic function. *Cell* **120**, 599-611
40. Dunkle, J. A., Vinal, K., Desai, P. M., Zelinskaya, N., Savic, M., West, D. M., Conn, G. L., and Dunham, C. M. (2014) Molecular recognition and modification of the 30S ribosome by the aminoglycoside-resistance methyltransferase NpmA. *Proc Natl Acad Sci U S A* **111**, 6275-6280

**CHAPTER 5:****FUNCTIONAL ROLES IN S-ADENOSYL-L-METHIONINE BINDING AND CATALYSIS FOR ACTIVE SITE RESIDUES OF THE THIOSTREPTON-RESISTANCE METHYLTRANSFERASE**

Cullen L. Myers, Emily G. Kuiper, Pei C. Grant, Jennifer Hernandez, Graeme L. Conn and John F. Honek

This work was previously published in FEBS Letters. License number 38749001994 was granted to reprint this article. Myers, C.L., Kuiper, E.G., Grant, P.C., Hernandez, J., Conn, G.L. and Honek, J.F. Functional roles in S-adenosyl-L-methionine binding and catalysis for active site residues of the thiostrepton resistance methyltransferase. *FEBS Lett*, 2015; 589, 3263-3270. © John Wiley and Sons.

EGK directly contributed to figures: 5.1A, 5.1B-SAH binding, 5.4A-B, S5.3 and Table 5.2. JFH and CLM conceived the study and designed the experiments; PCG cloned the Tsr gene and developed methods for recombinant protein expression; EGK and JH performed SAH binding experiments and Tsr filter binding assays; all other experiments were performed by CLM. CLM and EGK analyzed the data; JFH and CLM wrote the manuscript with input from EGK and GLC.

## 5.1 ABSTRACT

Resistance to the antibiotic thiostrepton, in producing *Streptomyces*, is conferred by the *S*-adenosyl-l-methionine (SAM)-dependent SPOUT methyltransferase Tsr. For this and related enzymes, the roles of active site amino acids have been inadequately described. Herein, we have probed SAM interactions in the Tsr active site by investigating the catalytic activity and the thermodynamics of SAM binding by site-directed Tsr mutants. Two arginine residues were demonstrated to be critical for binding, one of which appears to participate in the catalytic reaction. Additionally, evidence consistent with the involvement of an asparagine in the structural organization of the SAM binding site is presented.

## 5.2 INTRODUCTION

The methylation of rRNA is vital to the structure and function of ribosomes across all domains of life [1]. Many of these modifications are carried out by methyltransferases that recruit *S*-adenosyl-l-methionine (SAM) for highly specific methylations of RNA base targets. Such enzymes are in various instances responsible for rRNA methylations that bring about bacterial resistance to certain ribosome-targeting antibiotics, noteworthy examples of which can be found in clinically relevant classes such as aminoglycosides and macrolides [2]. This resistance mechanism also accounts for the majority of natural bacterial immunity to thiostrepton, the prototype of the ribosome-targeting thiopeptide antibiotics that have attracted renewed attention as a potential source for antimicrobial lead compounds [3-6].

Thiostrepton exhibits potent bactericidal effects against Gram-positive bacteria by binding the bacterial ribosome at the GTPase center on 50S subunit through interactions with ribosomal protein L11 and 23S rRNA, imposing conformational restrictions on L11 that perturb elongation factor activities and ultimately cause the arrest of protein synthesis at the translocation step of the elongation cycle [7-9]. Organisms that produce thiostrepton (*S. cyaneus*, *S. laurentii*) [10] express a SAM-dependent methyltransferase, Tsr, that catalyzes a 2'-*O*-ribose methylation of an adenine

nucleotide (A1067; *E. coli* numbering) at the thiostrepton binding site [11], preventing its association and rendering the organisms resistant to its effects. Analogously, protection from the related thiopeptide nosiheptide, in the producing organism *S. actuosus*, is afforded by a methyltransferase (Nhr) that shares 74% sequence similarity with Tsr [12].

Crystal structures for Tsr and Nhr assign these enzymes to the SPOUT family of methyltransferases [11,12] that have thus far been found to exclusively target RNA bases [13], with the exception of a single protein SPOUT methyltransferase [14]. Apart from antibiotic resistance [11,12,15-18], known biological functions for enzymes from this class include tRNA modification [19] and roles in ribosome biogenesis [20,21]. Putative SPOUT methyltransferase genes have also been identified in the biosynthetic gene clusters of other thiopeptide-producing bacteria, which may indicate that SPOUT-enzyme RNA methylation is perhaps a more general form of thiopeptide resistance [22,23]. Structural studies show that SPOUT methyltransferases are functional homodimers, typified by an  $\alpha/\beta$  Rossmann-like fold with a deep trefoil knot at the C-terminal end that binds SAM, and an active site near the dimeric interface that is constructed from residues contributed by both subunits [11,12,20,24-27]. Molecular models of RNA substrates bound to Tsr [11] or to other SPOUT methyltransferases [12,24,27] suggest that methyl transfer is accomplished by a single catalytic site, although these homodimeric enzymes appear capable of binding two SAM molecules.

Methylation of rRNA by Tsr, and by SPOUT enzymes in general, proceeds according to the scheme depicted in Fig. 1A. Implicit from this mechanism is the activation of the methyl group acceptor that precedes and facilitates nucleophilic attack. Detailed descriptions regarding this step of the catalytic mechanism, however, are limited to few examples notwithstanding considerable structural knowledge on this enzyme class. For instance, an Arg residue in the active site of the tRNA methyltransferase TrmH is thought to carry out deprotonation on the targeted guanine base that allows for 2'-*O*-ribose methylation [28], while *N*-methylation of the guanine targeted by Trm5 was shown to follow deprotonation at *N1* by an active site Glu [29]. In a number of

additional cases, Arg or Glu residues have again been suggested for this role [18,19,25,27], but these proposals have broadly lacked substantiation through biochemical investigations.

Tsr is among the SPOUT methyltransferases for which the roles of active site amino acids in the catalytic mechanism and in interactions with SAM are unresolved. Moreover, Tsr catalysis is not well understood within the context of two simultaneously occupied cosubstrate (SAM)-binding sites. In this work, we have examined the interactions of SAM in the Tsr active site by investigating the catalytic and SAM-binding properties of structure-guided active site mutants. These studies have led to the assignment of functional roles in SAM binding to specific residues, and highlighted the likely steps involved in activation of the methyl group acceptor in the Tsr catalytic mechanism.

## 5.3 MATERIAL AND METHODS

### 5.3.1. Protein expression & purification

The pET28a plasmid construct bearing the Tsr gene fused to a sequence encoding an N-terminal hexahistidine tag followed by a thrombin protease cleavage site was previously created [11]. Single amino acid mutations (N129A/D, R135A/K, R165A/K, E220A/Q, K221A, S246A and N248A/D) were introduced into the *S. cyaneus* Tsr gene by using this plasmid as the template in PCR overlap extension reactions with vector-specific T7 primers and Tsr-gene-specific primers (Supplementary material, Table S1). Mutations were confirmed by DNA sequencing (Mobix Lab, McMaster University, Hamilton, Ontario, Canada). *E. coli* BL21 (DE3) pLysS transformed with plasmid bearing the wt or mutated Tsr gene was cultured at 37°C in Luria Bertani media supplemented with kanamycin (30 mg/ mL) and chloramphenicol (34 mg/ mL), and protein expression was induced by addition of IPTG (1 mM) after bacterial growth reached an OD<sub>600</sub> of 0.6 – 0.8. Expression was continued for 4 hours and the cells harvested by centrifugation, then resuspended in buffer comprised of 50 mM Tris (pH 8.0), 500 mM KCl, 20 mM imidazole and 10% glycerol (v/v). Cells were lysed using an EmulsiFlex-C5 homogenizer (Avestin, Ottawa,

Ontario, Canada) and the cellular debris removed by centrifugation. For Ni<sup>2+</sup>-affinity purification of his-tagged proteins, the clarified lysate was applied to a 1 mL HisTrap HP column (GE Healthcare, Mississauga, Ontario, Canada) pre-equilibrated with resuspension buffer. The column was eluted with resuspension buffer to remove non-binding proteins, after which his-tagged proteins were obtained by elution with a buffer comprising 50 mM Tris (pH 8.0), 500 mM KCl, 500 mM imidazole and 10% glycerol (v/v), and then dialyzed overnight at 4°C against a buffer containing 50 mM Tris pH 7.5, 150 mM KCl, 10% glycerol (v/v). The his-tag was removed by subsequent incubation with thrombin protease (GE Healthcare) for 16 hours at 4°C. Cleaved and uncleaved protein were separated with the same chromatographic conditions as for obtaining his-tagged protein. Protein purity was assessed by SDS-PAGE and the expected molecular mass for mutant Tsr proteins was confirmed by positive ion ESI-MS. If necessary, further purification was performed by anion exchange chromatography using a MonoQ column (GE Healthcare); Tsr eluted between 250 and 300 mM of KCl during a linear KCl gradient (50 – 500 mM over 100 minutes) in a buffer containing 50 mM Tris (pH 8) and 10% glycerol (v/v). Purified, his-tag-cleaved protein was dialyzed as described above, then stored at -80°C for future use.

### 5.3.2. Size exclusion chromatography

Analytical size exclusion chromatography was performed in a buffer comprised of 50 mM Tris (pH 8.0), 150 mM KCl and 10% glycerol (v/v), using a Superdex-75 size exclusion column (GE Healthcare). A mixture of protein standards containing blue dextran, bovine serum albumin, carbonic anhydrase and cytochrome c was used for the estimation of relative molecular weight.

### 5.3.3. Methylation assays

Methylation of 16S/23S rRNA isolated from *E. coli* MRE600 (Roche Life Sciences, Laval, Québec, Canada) by purified, recombinant wt Tsr or its mutants was assessed using an enzyme-coupled fluorescent assay (Cayman Chemical Company, Ann Arbor, Michigan, USA) following

established methods [21,30-32]. The principle of the assay is as follows: the adenine moiety is enzymatically cleaved from SAH generated as a by-product of methylation [33,34], and then enzymatically converted to urate with the stoichiometric production of H<sub>2</sub>O<sub>2</sub> that is quantified by conversion of added 10-acetyl-3,7,-dihydroxyphenoxazine (ADHP) into the fluorescent compound 7-hydroxy-3H-phenoxazin-3-one (resorufin). Assays were performed according to the manufacturer's specifications, except that the reaction buffer was supplemented with MgCl<sub>2</sub> (5 mM) and NH<sub>4</sub>Cl (25 mM) and the pH adjusted to 7.5 to satisfy the optimum requirements for Tsr activity. These minor alterations did not affect the performance of the commercial assay, which was robust, displaying linearity with respect to time and enzyme concentration (Supplementary material, Fig. S1). Fluorescence measurements were carried out in black, 96-well microplates (Corning Life Science, Corning, NY, USA) using a SpectraMax M5 microplate reader (Molecular Devices, Sunnyvale, California, USA) that was calibrated to an internal standard. Excitation and emission wavelengths were 530 nm and 584 nm, respectively, with an emission filter at 570 nm. Assays monitoring catalytic activity under non-limiting substrate conditions contained 0.35 mM of 16S/23S rRNA, 1 mM SAM and 0.1 mM of enzyme. For the determination of enzyme kinetic parameters, SAM concentrations were varied from 0.005 mM to 0.5 mM and initial rate data fit by non-linear regression to equation 1 (GraphPad Prism 6.0);  $v$  is the initial rate at a given SAM concentration  $[S]$ ,  $K_M$  and  $k_{cat}$  are the Michaelis constant and enzyme turnover, respectively and  $[E]_t$  is total enzyme concentration.

$$\text{(eqn. } v = \frac{k_{cat}E_t[S]}{K_M + [S]} \text{ 1)}$$

#### 5.3.4. Isothermal titration calorimetry

Assessments of SAM binding for wt and mutant Tsr proteins mutants were performed with an ITC200 calorimeter (GE Healthcare, Mississauga, ON, Canada). Enzyme used for these experiments was dialyzed extensively against a buffer comprised of 50 mM Tris (pH 7.5), 75 mM KCl and 10% glycerol (v/v), and the dialysate was used to prepare fresh working solutions of

protein and SAM. Titrations were performed at 25 °C and consisted of a single initial injection of 0.5  $\mu$ L, followed by 29 injections of 1.25 mL of SAM (1.98 - 2.50 mM) into a sample cell containing wt or mutant Tsr (0.0822 - 0.098 mM). Heats from dilution and mixing were obtained from injections of SAM into ITC buffer lacking protein. Thermodynamic data were analyzed using Origin 7.0 (GE Healthcare), and fit by non-linear regression to models for single or sequential binding sites.

Experiments measuring SAH binding were performed essentially as those described for SAM binding, but using an Auto-iTC200 microcalorimeter (GE Healthcare) and with the following adjustments: after dialysis against ITC buffer, Tsr was concentrated to 0.05 mM and working stocks of SAH (1 mM) were prepared using the final dialysate. Titrations were performed at 25 °C and consisted of a single initial injection of 0.5 mL followed by 15 injections of 2.4 mL.

#### *5.3.5. Circular dichroism spectroscopy*

Spectra were measured with a Jasco J715 spectropolarimeter (Jasco Analytical Instruments, Easton, Maryland, USA) in the low UV region (190 – 250 nm), with a bandwidth of 1 nm and a scanning speed of 100 nm/ min. Spectra from 15 consecutive scans, performed at least twice, were averaged. Samples were prepared at 2.7 mM, in a buffer comprised of 50 mM Tris (pH 7.5), 150 mM KCl and 10% glycerol (v/v).

### 5.4 RESULTS

#### *5.4.1. Characterization of SAM binding and turnover by Tsr*

Cocrystal structures of SPOUT methyltransferases with SAM, SAH or the methyltransferase inhibitor sinefungin show a cosubstrate/ inhibitor molecule bound at the CTD of each subunit in the enzyme dimer [11,12,24,25,27]. We investigated this crystallographically observed stoichiometry by ITC, determining a 2:1 binding stoichiometry for SAM or SAH with the Tsr dimer on analysis of thermodynamic binding data with a model for a single set of identical sites;

i.e. one binding site per enzyme subunit (**Fig. 5.1B**). The affinity of the methylation by-product SAH was noted to be 4 times higher than that of SAM (**Fig. 5.1B**). In the Tsr-SAM crystal structure, SAM adopts different conformations in structurally non-equivalent binding sites (**Fig. 5.1C**), which could manifest as differential binding parameters for the two sites. Binding data were therefore also evaluated with a model for sequential independent sites, as has been used elsewhere for characterizations of SAM binding by other dimeric methyltransferases [21,26]. Interestingly, this fit generated different SAM affinities for the two binding sites ( $K_{D1}$  and  $K_{D2}$  of 56.8 mM and 209.6 mM), while the other SAM binding parameters for the two sites were found to be comparable (DH1,  $-4.07 \pm 0.11$  (kcal/ mol); DH2:  $-3.89 \pm 0.17$  (kcal/ mol); DS1, 5.54 (cal.mol<sup>-1</sup>. deg<sup>-1</sup>); DS2, 3.50 (cal.mol<sup>-1</sup>. deg<sup>-1</sup>)). This fit, however, did not offer a statistically significant improvement over that from the single site model and furthermore, showed no distinction in SAH binding between the two sites. Together, these findings were taken to signify equivalent SAM binding at the two sites on the Tsr dimer despite the previously observed apparent differences in SAM binding conformation.

Equivalent binding of SAM at two binding sites in the Tsr homodimer conceivably allows for two catalytic sites in the enzyme, yet Tsr is thought to use a single catalytic center. To examine this further, initial rate data for SAM turnover by Tsr was analyzed with various kinetic models, using *E. coli* 16S/ 23S rRNA as the methyl acceptor. Indeed, Tsr also efficiently methylates RNA oligonucleotides composed of the minimum target RNA sequence [11,35], but a ribosomal intermediate has been suggested to be the cellular target [36]. Hence, 16S/ 23S rRNA was used here to study Tsr activity in the context of a methyl acceptor that perhaps more closely resembles the biological substrate. In line with catalysis by a single active site, we observed hyperbolic Michaelis-Menten kinetics for SAM (**Fig. 5.1D**), with a  $K_M$  comparable to that previously reported for Tsr-catalyzed methylation of total *E. coli* rRNA [36] or a 93 nt RNA substrate [35]. To investigate the influence of simultaneously occupied SAM binding sites on kinetics, additional analyses using non-Michaelis-Menten models were performed. Initial rate data did not fit models

that describe cooperative, allosteric or effector kinetics [37], but a fit was obtained from a model that accounts for the presence of two independent substrate binding sites, one of which functions catalytically [37,38] (not shown). Still, as with assessments of SAM/ SAH binding, this fit did not offer a statistically significant improvement over the single substrate (Michaelis-Menten) model. These findings therefore support the hypothesis of a single catalytic site and importantly, further suggest that SAM binding at the non-catalytic site does not affect overall enzyme turnover.

#### *5.4.2. Effect of active site mutations on Tsr activity*

The NTD of Tsr and related SPOUT enzymes has been implicated as being principally responsible for RNA binding [11,12,39]. To identify some of the critical interactions of SAM with amino acids in the Tsr active site, we introduced single amino acid mutations at a number of CTD amino acid residues in the vicinity of bound SAM as observed in the crystal structure (**Fig. 5.2A**, Supplementary Material **Fig. S5.2**). The catalytic activity of these Tsr variants was then monitored in the presence of a non-limiting concentration of SAM (~10-fold  $K_M$ ), and an excess of 16S/ 23S rRNA acceptor relative to Tsr. (Fig. 2B). Mutations to N129, R135 and R165 were most deleterious to activity; both N129 variants exhibited approximately 20% relative activity, and the Ala variants at R135 and R165 showed 30% and 35% relative activity, respectively. These effects from the Arg mutations matched those for equivalent mutations on the methylation of 29 and 60 nt RNA substrates by Nhr [12]. For further examinations into the nature of the contribution made by these Arg residues, especially the presence of electrostatic interactions, Lys mutants were also generated. For R135, activity remained similar (35%) to that of the corresponding Ala mutant, but activity for the Lys mutation of R165 was almost 2-fold greater (65%) than the Ala. Mutations to K221 and E220 resulted in an approximate 50% reduction to enzymatic activity, while modest effects were noted from mutations to S246 and N248.

#### 5.4.3. Thermodynamics of SAM binding and kinetics of SAM turnover by select Tsr mutants

The survey of catalytic activity by Tsr variants showed the greatest effects arising from mutations to N129, R135 and R165. Filter-binding enzymatic assays where a 29 nt RNA served as the methyl acceptor also confirmed severely impaired activity by the mutants with Ala substituted at these positions (Supplementary material, **Fig. S5.3**). The relative activity of these mutants was lessened further with the 29nt RNA acceptor as compared to 16S/23S rRNA. This discrepancy was attributed to the significantly shorter sequence length of the former, especially considering that methylation activity by Tsr (and Nhr) is influenced by the RNA acceptor length and consequently, tertiary structure [11,12]. We focused subsequent investigations on more in-depth examinations into the roles of these amino acids, first with evaluations of SAM binding. Consistent with effects on enzyme activity, SAM binding affinity was significantly reduced (approximately 2-6 fold increases in K<sub>d</sub>) for both N129 mutants and by Ala mutation of R135 or R165 (**Table 5.1**). The largest entropic penalties were observed from mutation of R135 and N129 to Ala and Asp, respectively, suggesting the binding sites in these mutants were the least accommodating to SAM. Tsr mutants with Lys substitutions for R135 or R165, however, exhibited SAM affinities similar to wt Tsr, with entropic losses offset by favorable changes to enthalpy (**Table 5.1**). Notably, SAH binding affinity was markedly less affected by individual mutants in this group of amino acids as compared to SAM (**Table 5.2**), possibly due to relaxed binding constraints in the absence of the methyl group and the absence of positive charge on the sulfur atom. Also, for Ala mutations of N129 and R135, the slight increase in SAH affinity accompanied by favorable entropic shifts, may have partly contributed to diminished activity by these mutants since SAH is known to inhibit the methylation reaction. Collectively, these results confirm that N129, R135 and R165 engage in interactions with SAM that are integral to its productive binding. With respect to R135 and R165, electrostatic interactions appear compulsory as impaired SAM binding resulting from Ala mutations at these sites correlated with the loss of enzyme activity, but affinity was restored by Lys substitutions presumably because of the

presence of a side chain that mimics the charge properties of the native Arg. Unlike for R165, the Lys mutant of R135 did not recover catalytic activity, suggesting that the former is primarily involved in SAM binding, while the latter contributes an additional role to catalysis.

It seemed probable that this additional function of R135 was related to activation of the methyl group acceptor. We attempted further verification of this through the determination of enzyme kinetic parameters for Ala mutants of N129 and R135, in which the respective side chain functionalities would be abolished. However, activity by these variants could not be detected under the conditions of the kinetic assay (not shown), emphasizing their indispensable function. On the other hand, reductions to  $k_{\text{cat}}$  and  $k_{\text{cat}}/K_M$  observed for the Ala mutant of R165 offered additional support for a primary role in SAM binding for this residue (**Figure 5.3A**). Considering that R135 appears more suitably positioned for methyl acceptor activation than N129, the observations above are consistent with the catalytic mechanism depicted in **Fig. 5.3B**.

#### *5.4.4. N129 is involved in the structural organization of Tsr*

The orientation of the N129 side chain observed in the Tsr X-ray structure appears prohibitive to interactions with SAM, yet this amino acid was found essential for SAM binding and Tsr activity. As well, both N129 mutants exhibited a similar loss of SAM binding affinity in spite of their differing side chain properties. Such conflicting observations may be explained by changes to protein structure in response to the alteration of N129, as this amino acid is located in a region central to Tsr dimerization and construction of the SAM binding pocket [11] (**Figs. 5.4A & 4B**). We therefore looked for an effect on Tsr dimerization by the mutation of N129 to Ala, a substitution that would remove the polar side-chain interactions at this position. On the basis of size exclusion chromatography, enzyme dimerization appeared unaffected (**Fig. 5.4C**) and so the effect of this mutation on protein secondary structure was examined by CD spectroscopy. This analysis showed a distinct divergence of the spectrum for the mutant from that of wt Tsr (**Fig. 5.4D**), indicative of differences in  $\alpha$ -helical content.

## 5.5 DISCUSSION

Tsr and related enzymes have been presumed to use a single catalytic site for methyl transfer. Here, the Tsr dimer was confirmed to bind two SAM molecules *in vitro*, but shown to exhibit Michaelis-Menten kinetics for SAM turnover, which suggests that a single catalytic SAM binding site operates independently of a non-catalytic binding site when both are occupied with SAM. This coincides with the recent findings by Yin and co-workers that showed catalytic activity for an Nhr heterodimer containing a functionally inactivated subunit [40]. However, it could not be determined whether this functional difference in Tsr is structurally predefined. The *apo*-structure for Tsr has not been reported, but *apo*- and SAM-bound structures of Nhr are largely similar [12], implying that the catalytic site is fixed and inherently defined. As well, although SAM binding by the Nhr heterodimer was not evaluated [40], our present findings predict that SAM would distinguish between two potential binding sites on the Nhr heterodimer and accordingly, catalysis would proceed from a structurally pre-defined catalytic site. Such structure-defined functional asymmetry in a homodimeric enzyme is exemplified by the *E. coli* glyoxylase I, where only one of the enzyme subunits is able to bind metal and function catalytically [41]. Nonetheless, mutually exclusive catalysis at either SAM binding site in Tsr cannot be excluded based on our findings. Indeed, that the cosubstrate binding sites on the Tsr dimer exhibit equivalent binding of SAM or SAH, with greater affinity for the latter, could imply that SAH release is a rate-limiting step in catalysis at either binding site. Moreover, considering that RNA binding to the Tsr dimer ostensibly follows that of SAM, it is possible that the catalytic site becomes designated from the association of RNA with the Tsr-SAM complex, which could allow for switching of the catalytic site when RNA substrates are encountered subsequent to dissociation of a methylated RNA product. Supporting evidence for this is seen by the demonstration of Tsr-induced structural changes within the RNA substrate that facilitate recognition [39]. Additional study is required to delineate the interplay between SAM and RNA binding on the catalytic activity of Tsr, particularly in the context of biologically relevant RNA acceptor substrates.

In agreement with previous studies, R135 and R165 were found essential for enzymatic activity and we have shown here that this could be linked to their importance in SAM binding. It is noteworthy to consider that the observed effects on enzyme activity resulting from mutations of these amino acids could in part be due to perturbed interactions with the RNA substrate. However, this seems in contradiction with structural evidence and molecular modeling that largely excludes these amino acids from such interactions [11,39]. In any event, our findings clearly demonstrate roles in SAM binding by these amino acids. Moreover, from the comparative effects from mutations with opposing side chain properties on SAM binding and enzyme activity, R135 emerged as the most likely candidate responsible for activation of the methyl group acceptor. Structural studies of SPOUT methyltransferases have often pointed towards Arg in this role, resembling its function as the catalytic base in the mechanisms of unrelated enzymes such as inosine 5-monophosphate dehydrogenase [42] and l-aspartate oxidase [43]. A factor common to these examples is the interaction of the catalytic Arg with a proximal carboxylate group that can be supplied by the enzyme substrate, and this is believed to exert steric and conformational effects on the guanidinium ion that result in a net deprotonated state with a lowered pKa that allows for proton abstraction [44]. Although pKa measurements of R135 were not attempted here, SAM binding was found here to be highly dependent upon R135, and it is thus surmised that the interaction between R135 and SAM promotes a proton-accepting guanidinium conformation that can lead to activation of the 2'-OH acceptor and facilitate transmethylation.

Intriguingly, N129 was found essential for SAM binding despite appearing unable to directly engage in meaningful interactions with SAM. The introduction of negative charge from the replacement of this amino acid with Asp might hinder SAM association, yet this explanation would not account for the loss of SAM binding observed for the corresponding mutation to Ala, which presents an uncharged, non-polar and smaller side-chain. N129 is highly conserved among SPOUT methyltransferases, residing on an equally conserved helix (helix 6) that is integral to the formation of the dimer interface and for the construction of the characteristic CTD knot [11]

known to be essential for proper structural conformation and activity of enzymes in which it occurs [45]. Further, R135 is also located on this aforementioned helix. Hence, owing to its central location in a region of Tsr that supplies much of the structural elements required for SAM binding, N129 appears to play a pivotal role in the organization of Tsr active site architecture. It is also plausible that structural features reliant on N129 are required for proper association of the RNA substrate with the enzyme dimer. The alteration of N129 may therefore have ramifications on proper binding and/or positioning of the RNA substrate, further alluding to the likelihood of a functional interrelation between the interactions of Tsr with SAM and RNA.

In summary, this work has provided new details on SAM binding and turnover by Tsr. We propose that an active site Arg performs a key step in the catalytic mechanism, enabled by its interaction with SAM. Further, our findings implicate an active site-adjacent Asn as a structural lynchpin in the formation of the SAM binding site. Given the high degree to which these amino acids residues are conserved among SPOUT enzymes, the insights provided here are likely to be applicable to other enzymes of this class, and relevant to the continued understanding of the biological methylations they accomplish.

## 5.6 ACKNOWLEDGEMENTS

We are grateful to Drs. T. Dieckmann and G. Guillemette (University of Waterloo) for access to ITC and CD instrumentation, respectively. Financial support was provided by the Natural Sciences and Engineering Research Council of Canada (JFH), the Ontario Graduate Scholarship program (CLM), the USDA National Institute of Food and Agriculture (Agriculture and Food Research Initiative Competitive Grant No. 2013-67011-21133) (EGK), the National Institutes of Health (R01-AI088025) (GLC), the Howard Hughes Medical Institute Science Education Program (award #52006923) and the National Science Foundation (MRI program grant 104177)

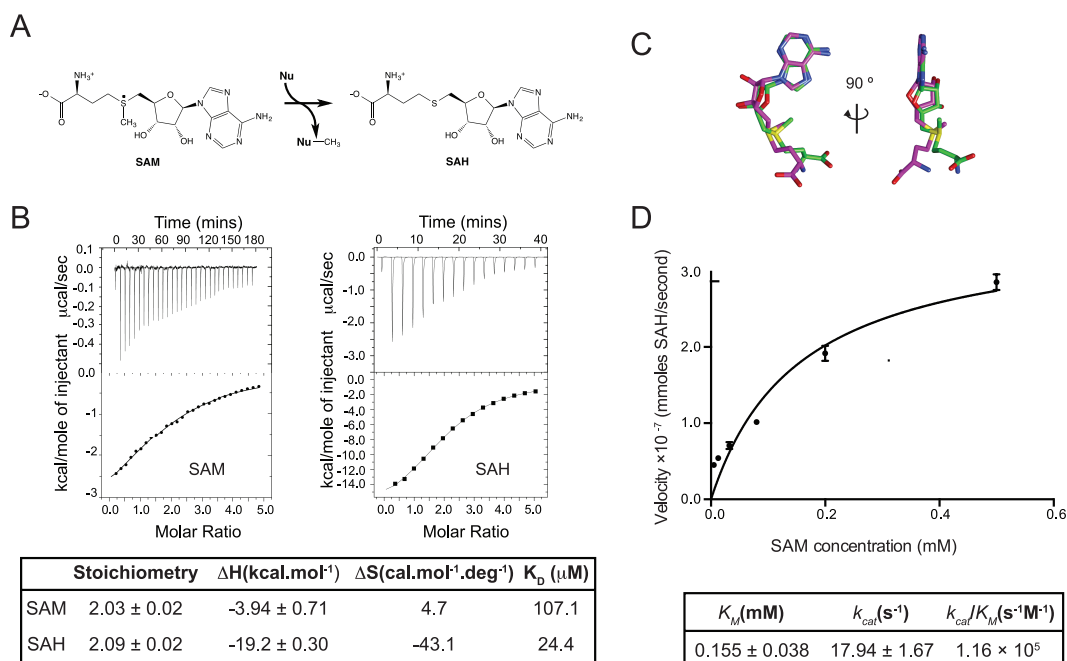


**FIGURE 5.1 SAM binding and turnover by Tsr.** (A) General scheme for SAM-dependent transmethylation. “Nu” represents a generic nucleophilic acceptor on the substrate (e.g. activated hydroxyl, aromatic nitrogen) that is methylated by the electron deficient methyl group from SAM. The reaction proceeds via an energetically favored  $S_N2$ -type mechanism, with an inversion of stereochemistry at the methyl group, resulting in co-production of the methylated substrate and SAH. (B) Representative ITC measurements showing the background-subtracted heats/ injection (top panels) and binding isotherms (bottom panels) for titrations of SAM and SAH with Tsr. Average integrated heats/ injection from two independent experiments were fit by non-linear regression to a model for a single set of sites. Where reported, errors are the S.E. associated with the fit. (C) Overlay of SAM molecules in the conformations found when bound to each Tsr monomer as shown in the Tsr-SAM crystal structure [11]. The skeleton of SAM in each conformation is colored magenta and green, respectively. (D) Michaelis-Menten plot for the methylation of  $0.35 \mu\text{M}$  16S/23S rRNA by  $0.1 \mu\text{M}$  Tsr. The fit was obtained by non-linear regression of the average initial rates from three independent experiments. Error bars are the S.D. and the S.E. associated with the fit is reported for  $K_M$  and  $k_{cat}$ .

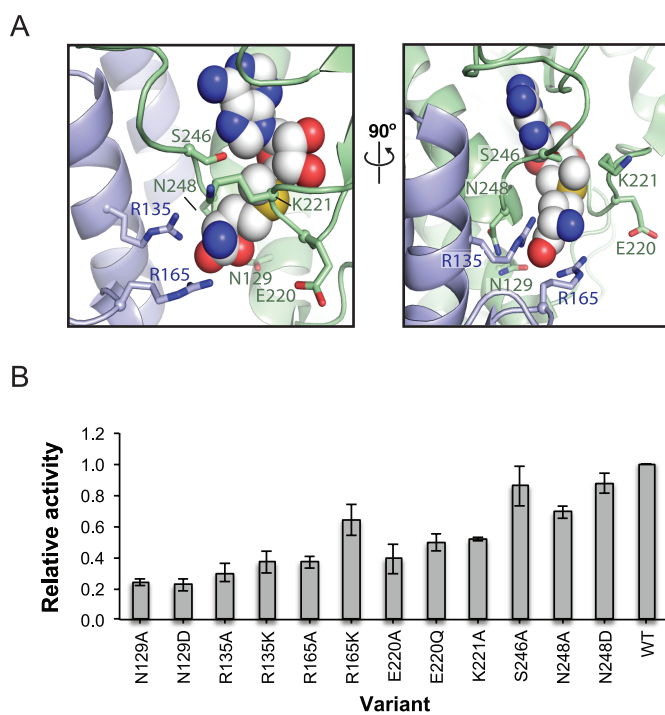


**FIGURE 5.2 Enzymatic activity of Tsr mutants.** (A) Active site residues selected for mutation surround the bound SAM (spheres). (B) Catalytic activity of Tsr active site mutants with 16S/23S rRNA. Activity is expressed as the average initial rate of methylation from three independent experiments, normalized to that of native Tsr. Error bars are the S. E.

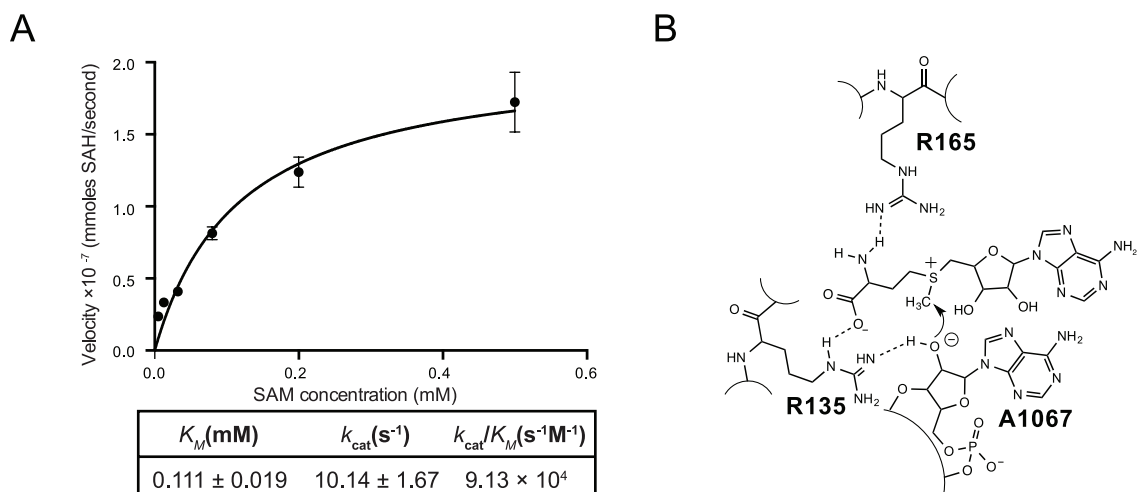


**FIGURE 5.3 R165 functions in SAM binding.** (A) Michaelis-Menten plot for the methylation of 16S/23S rRNA by the R165A mutant. Average initial rates from triplicate experiments were analyzed as with native Tsr. Error bars are the S.D. and S.E. associated with the fit is reported for  $K_M$  and  $k_{cat}$ . (B) Proposed mechanism for SAM-dependent methylation of rRNA by Tsr. SAM is stabilized in the active site/binding pocket through H-bonding with R165. The interaction between R135 and the carboxylate from SAM promotes activation of the ribose 2'-OH, leading to consequent attack by the SAM methyl group.

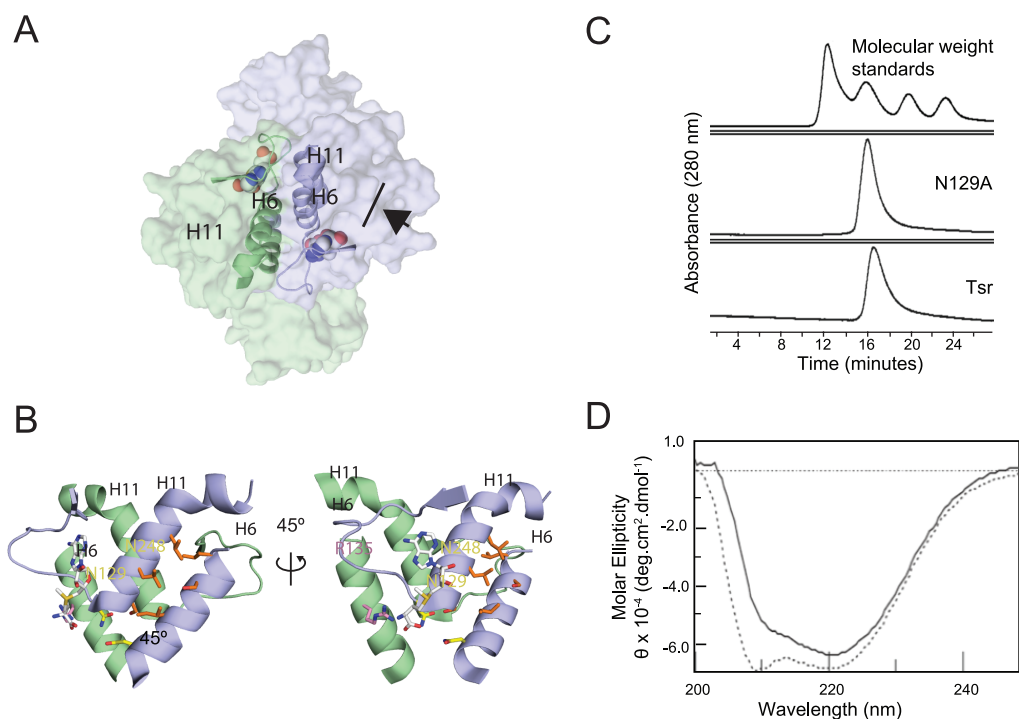


**FIGURE 5.4 Structural significance of N129.** (A) Surface representation of Tsr illustrating the contribution of helices 6 and 11 to the dimerization interface. Helices 6 and 11, and the loop corresponding to amino acids 234-247 are shown as a cartoon and SAM is shown as spheres. The arrowhead denotes the viewpoint shown in close-up in panel B. (B) Zoomed in view of the Tsr active site with the hydrophobic amino acid interface between helix 6 and helix 11 highlighted (orange). (C) Size exclusion chromatography of wt Tsr and the N129A mutant. The peak identities (left to right) for the molecular weight standards are as follows: blue dextran (2000 kDa), bovine serum albumin (66 kDa), carbonic anhydrase (29 kDa) and cytochrome C (12.4 kDa). Chromatograms show an identical elution volume for Tsr and the N129A variant, with an estimated relative molecular weight of 60 kDa (dimeric molecular weight of Tsr: 58364 Da). (D) Representative circular dichroism spectra for Tsr (dashed line) and N129A (solid line). The changes in ellipticity for the Ala variant of N129 indicate the absence of secondary structural features present in native Tsr.

**Table 5.1. Parameters for SAM binding by Tsr and N129, R135 or R165 mutants**

Variant	Stoichiometry	$\Delta H$ (kcal/ mol)	$\Delta S$ (cal.mol <sup>-1</sup> .deg <sup>-1</sup> )	$K_D$ ( $\mu M$ )
<i>wt</i>	$2.03 \pm 0.02$	$-3.94 \pm 0.71$	4.7	107.1
N129A	$2.19 \pm 0.13$	$-8.95 \pm 0.73$	-15.3	493.0
N129D	$1.87 \pm 0.28$	$-21.31 \pm 3.98$	-57.2	411.5
R135A	$2.22 \pm 0.18$	$-43.50 \pm 4.52$	-134.0	613.5
R135K	$1.89 \pm 0.03$	$-9.36 \pm 0.25$	-14.4	142.3
R165A	$1.71 \pm 0.08$	$-8.16 \pm 0.51$	-10.8	188.7
R165K	$2.13 \pm 0.03$	$-6.52 \pm 0.15$	-4.0	97.1

Average integrated heats of injection from two independent titrations of SAM into solution of Tsr mutations, after subtraction of heats from dilution and mixing, were fit by non-linear regression to a model from a single set of binding sites. This dissociation constant  $K_D$  is the reciprocal of the association constant  $K_A$  that is generated by Origin software. E.E. associated with the fit to the single sites model is reported for stoichiometry and  $\Delta H$ . Binding parameters for wt Tsr are included for comparison.

**Table 5.2. Parameters for SAH binding by Tsr and mutants with Ala substituted for N129, R135 or R165**

Variant	Stoichiometry	$\Delta H$ (kcal/ mol)	$\Delta S$ (cal.mol <sup>-1</sup> .deg <sup>-1</sup> )	$K_D$ ( $\mu M$ )
<i>wt</i>	$2.09 \pm 0.02$	$-19.2 \pm 0.30$	$-43.1$	24.4
N129A	$2.45 \pm 0.03$	$-13.0 \pm 0.27$	-21.6	16.4
R135A	$2.70 \pm 0.02$	$-15.2 \pm 0.18$	-28.3	11.0
R165A	$2.03 \pm 0.02$	$-18.5 \pm 0.28$	-40.7	20.5

<sup>b</sup> Titrations and analyses of thermodynamic data were performed as with SAM. S.E. associated with the fit is reported for stoichiometry and DH. Binding parameters for wt Tsr are shown for comparison.

## 5.7 SUPPLEMENTARY MATERIAL

**Table S5.1. Primers used to generate Tsr point mutant variants**

N129A	5'-ATCGGCGCGATAGTACGCACGTCG-3' 5'-GCGTACTATCGCGCCGATCGCCCCGACGATCTTCACCCC-3'
N129D	5'-ATCGGCGCGATAGTACGCACGTCG-3' 5'-GCGTACTATCGCGCCGATGTCCCCGACGATCTTCACCCC-3'
R135A	5'-ACGTCGCTCGCGCTCGGAGCGTCG-3' 5'-TCCGAGCGCGAGCGACGTCGCTACTATCGCGCCGATGTT-3'
R135K	5'-ACGTCGCTCGCGCTCGGAGCGTCG-3' 5'-TCCGAGCGCGAGCGACGCTTTACTATCGCGCCGATGTT-3'
R165A	5'-ACGTCGCTCGCGCTCGGAGCGTCG-3' 5'-TCCGAGCGCGAGCGACGTCGCTACTATCGCGCCGATGTT-3'
R165K	5'-ACGTCGCTCGCGCTCGGAGCGTCG-3' 5'-CGCTCCGAGCGCGAGCGACGCTTTACTATCGCGCCGATGTTCCC-3'
E220A	5'-AAGGGTGGGCCTTCCGACCTGTTC-3' 5'-GTCGGAAGGCCACCCTTCGCGCTGCCAACAGCAAGGC-3'
E220Q	5'-AAGGGTGGGCCTTCCGACCTGTTC-3' 5'-GTCGGAAGGCCACCCTTCTGGCTGCCAACAGCAAGGC-3'
K221A	5'-AAGGGTGGGCCTTCCGACCTGTTC-3' 5'-GTCGGAAGGCCACCCTTCGCGCTGCCAACAGCAAGGC-3'
S246A	5'-CTCAACGTTTCCGTTTCCCTCGGA-3' 5'-GGAAACGGAAACGTTGAGCGCCTCGGTCTGGCTCATCAT-3'
N248A	5'-GTTTCCGTTTCCCTCGGAATCGCG-3' 5'-TCCGAGGGAAACGGAAACCGCGAGAGACTCGGTCTGGCT-3'
N248D	5'-GTTTCCGTTTCCCTCGGAATCGCG-3' 5'-GATCCGAGGGAAACGGAAACGTCGAGAGACTCGGTCTGGCT-3'
T7	5'-TAATACGACTCACTATAGGG-3' 5'-CCGCTGAGCAATAACTAGC-3'

<sup>a</sup>Point mutagenesis of *tsr* was performed with two consecutive PCR reactions. In the first reaction, pET28a harboring the *tsr* gene was used as template to generate two overlapping fragments of the *tsr* gene, by using the T7 forward primer with *tsr*-specific reverse primers and *tsr*-specific forward primers with the T7 reverse primer. *Tsr*-specific primers were designed to introduce the desired mutation into the complimentary sequence of the two gene fragments. The gene fragments were joined by a second the second PCR reaction using only T7 primers.

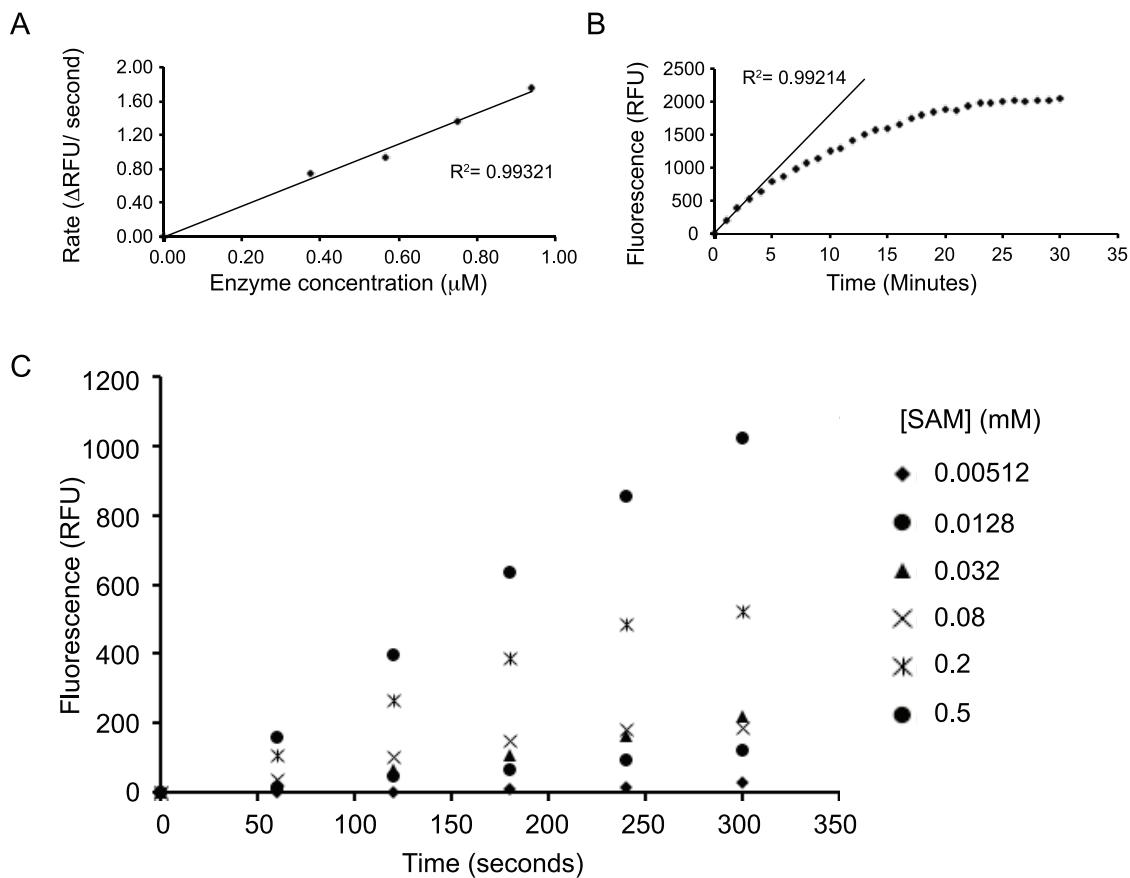


**FIGURE S5.1. Development of the coupled fluorometric assay for monitoring Tsr catalyzed methylation of 16S/ 23S rRNA in kinetic evaluations of SAM turnover.** (A) Linear dependence of Tsr activity on enzyme concentration. (B) Time course for SAM-dependent methylation of 16S/ 23S rRNA (0.35 mM) by Tsr (0.1 mM). Initial rate conditions (product formation  $\leq 10 - 15\%$ ) occur within the first 5 minutes. (C). Effect of SAM concentration on the initial rate of Tsr activity, using 0.1  $\mu$ M of Tsr in the presence of saturating concentrations of 16S/ 23S rRNA (0.35 mM). Background fluorescence has been subtracted from each of the above plots.



*thermophilus* (1IPA); RLMB: RlmB from *Escherichia coli* (1GZ0); TRMH-A: TrmH from *Aquifex aeolius* (IZJR); TRMH-P: TrmH from *Porphyromonas gingivalis* (2I6D). Amino acid residues are colored as follows; red: small, hydrophobic; blue: acidic; magenta: basic; green: hydroxyl, sulfhydryl, amine. Conservation is denoted below the sequence alignment as either identical (\*), strongly similar (:), or weakly similar (.). Regions corresponding to  $\alpha$ -helices observed in the various crystal structures are shaded grey. Amino acids selected for mutagenesis in this work are marked by an arrow.

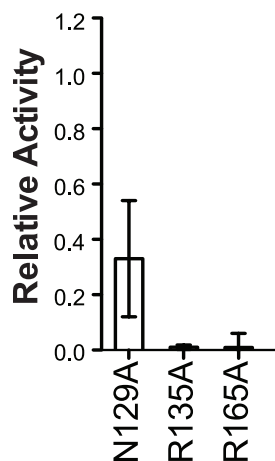


**FIGURE S5.3. Tsr mutants with Ala substitutions at N129, R135 or R165 are impaired in the methylation of a 29 nt RNA substrate.** End-point RNA methylation assays of the 29 nt RNA, transcribed *in vitro* as previously described<sup>1</sup>, were performed in triplicate, with 0.1  $\mu\text{M}$  Tsr, 0.35  $\mu\text{M}$  RNA, 100 mM SAM and 1.1  $\mu\text{Ci}$   $^3\text{H}$ -SAM in a 200  $\mu\text{L}$  reaction in assay buffer (50 mM Tris pH 7.5, 75 mM KCl, 5 mM  $\text{MgCl}_2$ ). After a 30 minute incubation at 37  $^\circ\text{C}$ , samples of 50  $\mu\text{L}$  were applied to Illustra Microspin G-25 column (GE Healthcare, Buckinghamshire, UK). The filtrate (40  $\mu\text{L}$ ) was counted in 2 mL of scintillation fluid. Assays to assess enzyme turnover were performed as described above but contained 0.165  $\mu\text{M}$  enzyme and 1  $\mu\text{M}$  29 nt RNA. Counts per minute (cpm) of control reactions without RNA were subtracted from each sample and normalized to cpm transferred by wild-type Tsr. Relative activity normalized to wild-type Tsr for active site mutants with the 29 nt RNA substrate using a  $^3\text{H}$ -AdoMet end-point assay. Error bars show SEM from three independent experiments. Comparable levels of inactivity were found for the Tsr mutants when activity was assessed using the fluorescence-based assay, with 16S/23S rRNA acceptor and similar SAM concentrations as above.

## 5.8 REFERENCES

1. Motorin Y & Helm M (2011) RNA nucleotide methylation. *WIREs RNA* **2**, 611–631.
2. Wilson DN (2014) Ribosome-targeting antibiotics and mechanisms of bacterial resistance. *Nat Rev Micro* **12**, 35–48.
3. Myers CL, Hang PC, Ng G, Yuen J & Honek JF (2010) Semi-synthetic analogues of thiostrepton delimit the critical nature of tail region modifications in the control of protein biosynthesis and antibacterial activity. *Bioorg. Med. Chem.* **18**, 4231–4237.
4. Aminake MN, Schoof S, Sologub L, Leubner M, Kirschner M, Arndt HD & Pradel G (2011) Thiostrepton and Derivatives Exhibit Antimalarial and Gametocytocidal Activity by Dually Targeting Parasite Proteasome and Apicoplast. *Antimicrob. Agents Chemother.* **55**, 1338–1348.
5. Myers CL, Harris J, Yeung JCK & Honek JF (2014) Molecular Interactions between Thiostrepton and the TipAS Protein from *Streptomyces lividans*. *ChemBioChem* **15**, 681–687.
6. Just-Baringo X, Albericio F & Álvarez M (2014) Thiopeptide engineering: a multidisciplinary effort towards future drugs. *Angew. Chem. Int. Ed.* **53**, 6602–6616.
7. Harms JM, Wilson DN, Schluenzen F, Connell SR, Stachelhaus T, Zaborowska Z, Spahn CMT & Fucini P (2008) Translational Regulation via L11: Molecular Switches on the Ribosome Turned On and Off by Thiostrepton and Micrococcin. *Mol. Cell* **30**, 26–38.
8. Bowen WS, Van Dyke N, Murgola EJ, Lodmell JS & Hill WE (2005) Interaction of thiostrepton and elongation factor-G with the ribosomal protein L11-binding domain. *J. Biol. Chem.* **280**, 2934–2943.
9. Walter JD, Hunter M, Cobb M, Traeger G & Spiegel PC (2012) Thiostrepton inhibits stable 70S ribosome binding and ribosome-dependent GTPase activation of elongation factor G and elongation factor 4. *Nucleic Acids Res.* **40**, 360–370.
10. Mocek U, Zeng Z, O'Hagan D, Zhou P, Fan LDG, Beale JM & Floss HG (1993) Biosynthesis of the modified peptide antibiotic thiostrepton in *Streptomyces azureus* and *Streptomyces laurentii*. *J. Am. Chem. Soc.* **115**, 7992–8001.

11. Dunstan MS, Hang PC, Zelinskaya NV, Honek JF & Conn GL (2009) Structure of the Thiostrepton Resistance Methyltransferase· S-adenosyl-l-methionine Complex and Its Interaction with Ribosomal RNA. *J. Biol. Chem.* **284**, 17013–17020.
12. Yang H, Wang Z, Shen Y, Wang P, Jia X, Zhao L, Zhou P, Gong R, Li Z, Yang Y, Chen D, Murchie AIH & Xu Y (2010) Crystal structure of the nosiheptide-resistance methyltransferase of *Streptomyces actuosus*. *Biochemistry* **49**, 6440–6450.
13. Tkaczuk KL, Dunin-Horkawicz S, Purta E & Bujnicki JM (2007) Structural and evolutionary bioinformatics of the SPOUT superfamily of methyltransferases. *BMC Bioinformatics* **8**, 73.
14. Young BD, Weiss DI, Zurita-Lopez CI, Webb KJ, Clarke SG & McBride AE (2012) Identification of Methylated Proteins in the Yeast Small Ribosomal Subunit: A Role for SPOUT Methyltransferases in Protein Arginine Methylation. *Biochemistry* **51**, 5091–5104.
15. Mann PA, Xiong L, Mankin AS, Chau AS, Mendrick CA, Najarian DJ, Cramer CA, Loebenberg D, Coates E, Murgolo NJ, Aarestrup FM, Goering RV, Black TA, Hare RS & McNicholas PM (2001) EmtA, a rRNA methyltransferase conferring high-level evernimicin resistance. *Mol. Microbiol.* **41**, 1349–1356.
16. Gaynor M & Mankin AS (2003) Macrolide antibiotics: Binding site, mechanism of action, resistance. *Cur. Top. Med. Chem.* **3**, 949–960.
17. Mosbacher TG, Bechthold A & Schulz GE (2005) Structure and Function of the Antibiotic Resistance-mediating Methyltransferase AviRb from *Streptomyces viridochromogenes*. *J. Mol. Biol.* **345**, 535–545.
18. Kumar A, Kumar S & Taneja B (2014) The structure of Rv2372c identifies an RsmE-like methyltransferase from *Mycobacterium tuberculosis*. *Acta Crystallogr. D Biol. Crystallogr.* **70**, 821–832.
19. Shao Z, Yan W, Peng J, Zuo X, Zou Y, Li F, Gong D, Ma R, Wu J, Shi Y, Zhang Z, Teng M, Li X & Gong Q (2014) Crystal structure of tRNA m1G9 methyltransferase Trm10: insight into the catalytic mechanism and recognition of tRNA substrate. *Nucleic Acids Res.* **42**, 509–525.

20. Meyer B, Wurm JP, Kötter P, Leisegang MS, Schilling V, Buchhaupt M, Held M, Bahr U, Karas M, Heckel A, Bohnsack MT, Wöhnert J & Entian K-D (2011) The Bowen-Conradi syndrome protein Nep1 (Emg1) has a dual role in eukaryotic ribosome biogenesis, as an essential assembly factor and in the methylation of  $\Psi$ 1191 in yeast 18S rRNA. *Nucleic Acids Res.* **39**, 1526–1537.
21. Zhang H, Wan H, Gao Z-Q, Wei Y, Wang W-J, Liu G-F, Shtykova EV, Xu J-H & Dong Y-H (2012) Insights into the catalytic mechanism of 16S rRNA methyltransferase RsmE (m<sup>3</sup>U1498) from crystal and solution structures. *J. Mol. Biol.* **423**, 576–589.
22. Engelhardt K, Degnes KF & Zotchev SB (2010) Isolation and Characterization of the Gene Cluster for Biosynthesis of the Thiopeptide Antibiotic TP-1161. *App. Environ. Microb.* **76**, 7093–7101.
23. Malcolmson SJ, Young TS, Ruby JG, Skewes-Cox P & Walsh CT (2013) The posttranslational modification cascade to the thiopeptide berninamycin generates linear forms and altered macrocyclic scaffolds. *Proc. Natl. Acad. Sci. U.S.A.* **110**, 8483–8488.
24. Leulliot N, Chaillet M, Durand D, Ulryck N, Blondeau K & van Tilbeurgh H (2008) Structure of the Yeast tRNA m7G Methylation Complex. *Structure* **16**, 52–61.
25. Taylor AB, Meyer B, Leal BZ, Kötter P, Schirf V, Demeler B, Hart PJ, Entian KD & Wöhnert J (2008) The crystal structure of Nep1 reveals an extended SPOUT-class methyltransferase fold and a pre-organized SAM-binding site. *Nucleic Acids Res.* **36**, 1542–1554.
26. Boundy S, Safo MK, Wang L, Musayev FN, O'Farrell HC, Rife JP & Archer GL (2013) Characterization of the *Staphylococcus aureus* rRNA Methyltransferase Encoded by orfX, the Gene Containing the Staphylococcal Chromosome Cassette mec (SCCmec) Insertion Site. *J. Biol. Chem.* **288**, 132–140.
27. Thomas SR, Keller CA, Szyk A, Cannon JR & LaRonde-LeBlanc NA (2011) Structural insight into the functional mechanism of Nep1/Emg1 N1-specific pseudouridine methyltransferase in ribosome biogenesis. *Nucleic Acids Res.* **39**, 2445–2457.

28. Ochi A, Makabe K, Kuwajima K & Hori H (2010) Flexible recognition of the tRNA G18 methylation target site by TrmH methyltransferase through first binding and induced fit processes. *J. Biol. Chem.* **285**, 9018–9029.
29. Christian T, Lahoud G, Liu C, Hoffmann K, Perona JJ & Hou YM (2010) Mechanism of N-methylation by the tRNA m1G37 methyltransferase Trm5. *RNA* **16**, 2484–2492.
30. Couture J-F, Dirk LMA, Brunzelle JS, Houtz RL & Trievel RC (2008) Structural origins for the product specificity of SET domain protein methyltransferases. *Proc. Natl. Acad. Sci. U.S.A.* **105**, 20659–20664.
31. Del Rizzo PA, Couture J-F, Dirk LMA, Strunk BS, Roiko MS, Brunzelle JS, Houtz RL & Trievel RC (2010) SET7/9 catalytic mutants reveal the role of active site water molecules in lysine multiple methylation. *J. Biol. Chem.* **285**, 31849–31858.
32. Wu H, Mathioudakis N, Diagouraga B, Dong A, Dombrowski L, Baudat F, Cusack S, de Massy B & Kadlec J (2013) Molecular basis for the regulation of the H3K4 methyltransferase activity of PRDM9. *Cell Rep* **5**, 13–20.
33. Collazo E, Couture JF, Bulfer S & Trievel RC (2005) A coupled fluorescent assay for histone methyltransferases. *Anal. Biochem.* **342**, 86–92.
34. Dorgan KM, Wooderchak WL, Wynn DP, Karschner EL, Alfaro JF, Cui Y, Zhou ZS & Hevel JM (2006) An enzyme-coupled continuous spectrophotometric assay for S-adenosylmethionine-dependent methyltransferases. *Anal. Biochem.* **350**, 249–255.
35. Bechthold A & Floss HG (1994) Overexpression of the Thiostrepton-resistance Gene from *Streptomyces azureus* in *Escherichia coli* and Characterization of Recognition sites of the 23S rRNA A1067 2' -methyltransferase in the Guanosine Triphosphatase Center of 23S Ribosomal RNA. *Eur. J. Biochem.* **224**, 431–437.
36. Thompson J & Cundliffe E (1981) Purification and Properties of an RNA Methylase Produced by *Streptomyces azureus* and Involved in Resistance to Thiostrepton. *Microbiol.* **124**, 291–297.

37. Copeland RA (2000) *Enzymes: A Practical Introduction to Structure, Mechanism, and Data Analysis* (John Wiley & Sons, New York) 2<sup>nd</sup> Edition, pp 109-144.
38. Korzekwa KR, Krishnamachary N, Shou M, Ogai A, Parise RA, Rettie AE, Gonzalez FJ & Tracy TS (1998) Evaluation of atypical cytochrome P450 kinetics with two-substrate models: evidence that multiple substrates can simultaneously bind to cytochrome P450 active sites. *Biochemistry* **37**, 4137–4147.
39. Kuiper EG & Conn GL (2014) Binding induced RNA conformational changes control substrate recognition and catalysis by the thiostrepton resistance methyltransferase (Tsr). *Journal of Biological Chemistry* **289**, 26189–26200.
40. Yin S, Jiang H, Chen D & Murchie AIH (2015) Substrate recognition and modification by the nosiheptide resistance methyltransferase. *PLoS ONE* **10**, e0122972.
41. Su Z, Sukdeo N & Honek JF (2008) <sup>15</sup>N-<sup>1</sup>H HSQC NMR evidence for distinct specificity of two active sites in *Escherichia coli* glyoxalase I. *Biochemistry* **47**, 13232–13241.
42. Guillén Schlippe YV & Hedstrom L (2005) Guanidine Derivatives Rescue the Arg418Ala Mutation of *Tritrichomonas foetus* IMP Dehydrogenase. *Biochemistry* **44**, 16695–16700.
43. Tedeschi G, Ronchi S, Simonic T, Treu C, Mattevi A & Negri A (2001) Probing the Active Site of L-Aspartate Oxidase by Site-Directed Mutagenesis: Role of Basic Residues in Fumarate Reduction. *Biochemistry* **40**, 4738–4744.
44. Guillén Schlippe YV & Hedstrom L (2005) A twisted base? The role of arginine in enzyme-catalyzed proton abstractions. *Arch. Biochem. Biophys.* **433**, 266–278.
45. Mallam AL & Jackson SE (2007) The Dimerization of an  $\alpha/\beta$ -Knotted Protein Is Essential for Structure and Function. *Structure* **15**, 111–122.

## CHAPTER 6: DISCUSSION

In the present studies I have elucidated novel structural and molecular mechanisms by which methyltransferases recognize and methylate their cellular targets, which allow the bacterium to adapt to their environments. In the preceding chapters, I have tested structural features of three different methyltransferases, EftM, TlyA and Tsr determined what amino acids govern cosubstrate binding and developed new models for substrate recognition (**Figure 6.1**). These novel molecular studies complement cellular studies to develop a thorough understanding of how posttranscriptional and posttranslational modifications of the ribosome and translation factors aid or control translation and thus microbial survival.

### 6.1 STRUCTURAL INSIGHTS

Insights into the structure of the three methyltransferases in this work identified important and previously unknown functional qualities of these enzymes. Either by modeling or solving the structure of these enzymes we have discovered novel mechanisms of enzyme control, including instability at elevated temperature controlling activity, novel structural elements that aid in SAM-binding and potentially interdomain interactions, and a role for quaternary structure in methyltransferase catalysis.

#### *6.1.1 Structural Instability Regulates EftM Activity*

EftM was a hypothetical protein in *P. aeruginosa* until Barbier *et al.* (2013) discovered that it was responsible for the temperature-sensitive modification of EF-Tu (ON at 25°C, OFF at 37°C)

which aided in *P. aeruginosa* infection (1). Using homology modeling, we showed that EftM possesses a Class I methyltransferase fold and an axillary domain composed mainly of  $\beta$ -strands. We also identified and functionally tested the SAM-binding motif (discussed below). Further, we showed that the instability of the protein structure is responsible for the temperature-regulation of the modification as EftM unfolds at 37°C, the temperature at which the modification is OFF. EftM unfolding likely correlates with a decreased half-life in the cell, which results in the observed repression of EF-Tu modification. A similar temperature instability regulation mechanism was described in *Yersinia pestis* (the etiological agent of the bubonic plague) where the temperature instability and degradation of the repressor YmoA was necessary for Type III secretion system expression for virulence (2). However, the direct control of a posttranscriptional modification by temperature instability of the enzyme is a novel regulatory mechanism.

#### 6.1.2. *TlyA Linker May Coordinate Interdomain Interactions*

I solved the structure of the TlyA methyltransferase domain confirming previous homology models that classified TlyA as a Class I methyltransferase. Additionally, we demonstrated the importance of a tetrapeptide sequence (RAWV) N-terminal to the catalytic domain in 1) cosubstrate binding (discussed below) and 2) interaction with the substrate recognition domain. Structures of the TlyA<sup>RAWV</sup>CTD protein place the linker peptide in two different conformations, either loop or  $\alpha$ -helical. As a loop, this linker could give TlyA the flexibility it needs to recognize each of its targets, which reside in different structural contexts. Once TlyA recognizes its target, a conformational change into an  $\alpha$ -helical structure could allow TlyA to orient the nucleotide into the active site. A similar conformational change in a linker between a substrate recognition domain and catalytic domain was observed in the structure of TrmD methyltransferase bound to tRNA, where the linker could not be modeled in structures of the enzyme alone, but formed a

helix upon binding its substrate (3). Structures of TlyA bound to its substrate will be necessary to determine the conformation of the linker in the catalytically active complex.

### *6.1.3 Tsr Protomers Act Independently of Each Other in Catalysis*

The structure and molecular characterization of Tsr by Dunstan *et al.* (2009) definitively classified Tsr as a Class IV ‘SPOUT’ methyltransferase (4). Tsr is a homodimer, with each protomer containing an N-terminal substrate recognition domain and C-terminal SPOUT domain (4). Most SPOUT methyltransferases are obligate homodimers with one only known exception: the yeast tRNA methyltransferase Trm10 (5). However, little is known about why most SPOUT methyltransferases are dimers. In the study by Dunstan *et al.* (2009), the Tsr structure was solved with one SAM molecule bound in each protomer. In Chapter 5 we showed that Tsr binds two SAM molecules per dimer via ITC and that catalysis conforms to Michaelis-Menten kinetics. This suggests that each protomer acts independently of the other. The significance of this work is expanded by studies of the nosiheptide resistance methyltransferase (Nhr), which methylates the same nucleotide as Tsr and shares 74% amino acid identity (6). Methylation reactions of heterodimers of Nhr, containing a WT and a catalytically inactive protomer, showed that only one active protomer was necessary for catalysis although the amount of methylation was reduced compared to wild-type (7). When the dimerization interface of another SPOUT methyltransferase TrmL was disrupted, the TrmL monomer could still bind SAM, but substrate recognition was impaired (8). These data show that for SPOUT methyltransferases dimerization is important for structural support or substrate recognition but not specifically required for catalysis as the protomers can act independently of each other.

## 6.2 COSUBSTRATE BINDING

Binding of the obligate cosubstrate *S*-adenosyl-L-methionine is a prerequisite for catalysis by the vast majority of methyltransferase enzymes. Therefore, characterizing the cosubstrate binding pocket defines critical residues involved in each enzyme's catalytic mechanism.

### *6.2.1 Identification and Characterization of the SAM Binding Motif in EftM*

EftM is a member of the Class I methyltransferases which have a number of conserved motifs including a SAM binding motif with a canonical sequence **GxGxG** (or **GxG**) (9). We found that EftM binds cosubstrate and product with similar affinity and showed that SAM binding is abrogated by a G50R mutation of the putative SAM binding motif **ACG<sup>50</sup>TG<sup>52</sup>**. Our homology model suggests that inhibition is caused by the arginine side chain (G50R) sterically occluding SAM binding. Mutation of G135A in the minimal SAM binding motif, **ACG<sup>135</sup>**, in the aminoglycoside-resistance methyltransferase Sgm disrupted cosubstrate binding and made Sgm-expressing *E. coli* more susceptible to gentamicin and kanamycin as evident by decreased antibiotic minimal inhibitory concentration (MIC) (10,11). Additionally, G37E mutation in the SAM binding motif, **G<sup>37</sup>TGKG**, of the macrolide resistance-conferring enzyme ErmB also decreased the erythromycin MIC (12). Thus, assessment of G50R confirmed the presence and functionality of the Class I SAM binding motif in EftM.

### *6.2.2 A Novel Auxiliary SAM Binding Motif in TlyA*

The studies of TlyA described in Chapter 3 began with the surprising finding that when expressed alone the methyltransferase domain of TlyA was unable to bind SAM cosubstrate, even though the domain was properly folded and contained the SAM binding motif **G<sup>96</sup>ASTG<sup>92</sup>**. Further, we

showed that two amino acids, Trp62 and Val63, of the interdomain tetrapeptide linker were necessary for SAM binding. Structural studies of the <sup>RAWV</sup>CTD, show that although this sequence does not directly interact with the cosubstrate, Val63 likely properly orients Thr93 to bind the methionine end of SAM. This is the first auxiliary SAM-binding motif described for a Class I methyltransferase. In functionally characterized TlyA homologs, Trp62 and Val63 are conserved suggesting that the function of this motif is not limited to TlyA from *M. tuberculosis* but also important in homologs with amino acid identity as low as 38%.

### 6.2.3 Tsr Cosubstrate Recognition and Catalysis

In Chapter 5 we determined SAM and SAH binding affinities of Tsr and identified amino acids important for SAM binding and catalysis. Tsr binds SAM more weakly than SAH (~100  $\mu$ M and 20  $\mu$ M, respectively), which has been described for other methyltransferases (13,14). Furthermore, mutation of residues within the SAM binding site had a greater effect on SAM binding than SAH, likely due to relaxed binding constraints in the absence of the methyl group. In both Tsr and Nhr, Arg135 is proposed to abstract a proton from the ribose 2'-hydroxyl creating a nucleophile that will attack the methyl-sulfonium group of SAM (6,15). This results in the transfer of the methyl to the 2' oxygen creating a 2'-methoxy group. Together, the structure and functional data have elucidated the catalytic mechanism for Tsr and its homologs.

## 6.3 SUBSTRATE RECOGNITION

While the structures of many ribosomal RNA-modifying methyltransferases have been solved and their cofactor binding properties elucidated, less is known about the molecular specificity of methyltransferase-substrate interactions. Biochemical studies like those presented in Chapter 4 and structures of the complexes are necessary to fully understand methyltransferase-substrate

recognition mechanisms. As many methyltransferases recognize ribosomal subunits, the technology to probe these interactions is now available as high-resolution structures of the subunits were solved in 2000 and the assembled ribosome in 2006 (16-18). Cryo-EM was used to determine the ribosome-binding site of the methyltransferase KsgA at  $\sim 13\text{\AA}$  in 2012 (19). As the resolution of ribosome structures determined by cryo-EM is now rivaling that of X-ray crystallography, and advances in X-ray crystallography make it easier to solve structures of ribosomes (i.e. intense beamlines, more sensitive detectors, as well as mechanisms to trap complexes) we can expect more enzyme-substrate complexes to be solved and thus an acceleration in our understanding of substrate recognition mechanisms for ribosome modifying enzymes.

### *6.3.1 A new Model of Tsr Substrate Recognition*

Tsr recognizes and methylates a contiguous domain of 23S rRNA prior to binding of the ribosomal protein L11. In Chapter 4, we proposed a new mechanism of substrate recognition for Tsr, which included previously unidentified conformational changes in the RNA promoted by the Tsr-NTDs that were necessary for catalysis. These conformational changes are likely necessitated by the compact structure of this RNA, which need to be rearranged to for enzyme access to the target nucleotide.

Changes in RNA conformation is a common theme in enzyme-RNA substrate structures. In the co-crystal structure of the SPOUT methyltransferase TrmD-tRNA<sup>Leu</sup> complex, the TrmD-CTD of the non-catalytic protomer probes the anticodon stem of the tRNA causing a structural change in the enzyme's intersubunit linker. This is followed by orientation of the anticodon loop near the catalytic domain, and flipping the target nucleotide (G37) out of the anticodon loop and into the catalytic site. The most significant changes in the tRNA structure are involved in base flipping

G37 (3). This is unlike our model of Tsr recognition where Tsr-mediated changes in RNA structure are distant from the target nucleotide. These changes by Tsr are likely necessitated by the compact packing of the two RNA helices of the RNA substrate. Like the TrmD structure, we additionally propose that structural changes in the target loop are also necessary to orient the target nucleotide for catalysis, however additional studies or an enzyme-substrate structure will be necessary to define changes in the target loop.

Structural changes were also identified in the RNA target loop for two m<sup>5</sup>U methyltransferases: RlmD (formerly RumA, U1939 23S rRNA) and TrmA (U54, tRNA) bound to model rRNA substrates (37 nts 1932-1961 and 19 nts tRNA T-arm analog, respectively) (20,21). Furthermore, in the RlmD-rRNA structure, a stem loop 3' to the target nucleotide is recognized by an NTD of RlmD illustrating a mechanism of substrate recognition of disparate RNA structures similar to what we proposed for Tsr.

### 6.3.2 *TlyA Recognizes Two Different Substrates*

TlyA methylates two different nucleotides of the ribosome, C1409 of 16S rRNA and C1920 of 23S rRNA, but the precise mechanism of substrate recognition remains to be elucidated. While these nucleotides are in close proximity in the assembled ribosome, TlyA recognizes and methylates these nucleotides on individual subunits (22). C1409 in the *E. coli* ribosome is part of h44 within the following base paired region: <sup>1408</sup>A·A<sup>1494</sup> / C-G / <sup>1410</sup>A-U<sup>1490</sup>, while C1920 is part of a stem loop with the sequence <sup>1919</sup>A-Ψ<sup>1912</sup> / C-G / <sup>1921</sup>G-C<sup>1911</sup>. While both cytidine residues are contained within a similar sequence, their structure a part of the subunit is very different. C1409 is packed near 4 other rRNA helices whereas C1420 is extended from the 50S surface. Monshupanee *et al.* (2012) grouped TlyA orthologs in one of two groups, TlyA<sup>I</sup> or TlyA<sup>II</sup>, based on their ability to methylate just C1920 or both C1409 and C1920, respectively (22). This

suggests that some TlyA orthologs do not contain a single unified mechanism of substrate recognition for two different nucleotides and the rRNA structure on the 30S may decrease the ability of some orthologs to recognize and methylate C1409.

The structure of the NpmA methyltransferase (16S rRNA m<sup>1</sup>A1408) bound to the 30S subunit structure may highlight a potential TlyA-30S binding site as these enzymes methylate nucleotides immediately adjacent to each other. The NpmA binding surface is made up of nucleotides from four different rRNA helices (h24, h27, h44, and h45) and conformational changes in nucleotides C1407-C1409 were necessary to position the A1408 in the enzyme active site (23). If the TlyA methyltransferase domain bound in a similar position as NpmA, it would suggest that TlyA would also interact with rRNA from multiple rRNA helices of the 30S subunit. Furthermore, unlike NpmA, TlyA contains a NTD that aids in substrate recognition. As modeling the NTD onto the CTD-helix structure predicts that the NTD sets on top of the methyltransferase domain, the NTD could interact more extensively with the rRNA backbone nucleotides on either side of the RNA helix. Solving a TlyA-30S structure is an active area of research that will be essential to elucidate the TlyA substrate recognition mechanism.

### 6.3.3 *EF-Tu Lysine Recognition by EftM*

In Chapter 3, EftM was characterized as an EF-Tu lysine 5 trimethyltransferase. However, currently nothing is known about EftM's substrate recognition mechanism. In the structure of Des IV, the enzyme used as the template for EftM homology modeling, a substrate analog was bound between the auxiliary and methyltransferase domain, suggesting a potential substrate-binding site (24). Multiple unpublished observations suggest a substrate recognition mechanism where the EF-Tu N-terminus, which lacks defined secondary structure (i.e.  $\alpha$ -helical or  $\beta$ -strand), could potentially snake through a channel between the methyltransferase and auxiliary domains,

positioning Lys5 near the SAM molecule. Amino acids that line the domain interface are highly conserved and likely functionally important. Further, mutation of Trp170 in the auxiliary domain rendered the enzyme inactive, although the mutant could still bind SAM, suggesting that this amino acid is important for substrate recognition. Identifying the substrate requirements for the modification is an active area of research and will lead to a better characterization of both EftM and EF-Tu, which will underpin studies into their role in bacterial physiology and virulence.

#### 6.4 MODIFICATION ENZYMES AID IN BACTERIAL ADAPTATION

The canonical role for rRNA modification is to aid in ribosome function or assembly under normal cellular growth conditions (although some modifications do not seem to be essential for function or assembly). However, additional cellular roles for modification enzymes and their modifications outside of their classical role in ribosome biology have been described. Commonly, these ‘moonlighting roles’ aid in the bacteria’s adaptation to stress or their changing environments (like infecting a host). For example, in the *E. coli* heat shock response, the 23S rRNA Um2552 methyltransferase RrmJ is overexpressed with other rRNA processing and ribosome recycling proteins (YbeY and Hsp15) to generate new ribosomes and recycle stalled ribosomes to adapt to the higher growth temperature (25,26). Additionally, the S5 acetyltransferase RimJ, but not its catalytic activity, was shown to suppress ribosomal assembly defects caused by mutation in S5, suggesting a role for RimJ in ribosome assembly other than acetylation (27). Furthermore, deletion of *rimJ* disrupted the temperature-regulated transcription of P pili genes in *E. coli* allowing pili formation at restrictive temperatures of 23°C. This suggests that RimJ acts as a transcription regulator for genes that aid in bacterial virulence as pili are needed to colonize the urinary tract (28). These examples illustrate a fascinating area of research that continues to expand our understanding of the roles of modification enzymes in biology.

#### 6.4.1 TlyA is a Methyltransferase and Hemolysin

Both the primary sequence and tertiary structure suggest a dual function for TlyA as a methyltransferase and an alpha-hemolysin. TlyA was first identified as a hemolysin due to its homology with *Serpulina hydrosenteria* alpha-hemolysin (29). In Chapter 3 we solved the structure of the TlyA methyltransferase domain, confirming its homology to Class I methyltransferases. These two functionalities seem counter-intuitive. As a methyltransferase TlyA is a monomer and cytosolic, whereas hemolytic proteins are multimeric and either membrane-bound or extracellular where they form pores in red blood cell membranes. Rahman *et al.* (2010) showed that TlyA oligomers were formed in the presence of red blood cells during hemolysis by SDS-PAGE with reduced levels of reducing agents (30). Mutations in the RNA binding domain or the catalytic tetrad, failed to decrease the hemolytic ability of TlyA, suggesting that methyltransferase catalytic activity is not needed for hemolysis (30,31). TlyA has also been implicated in *Helicobacter pylori* virulence using similar hemolytic functions and new studies have defined TlyA as a virulence factor for *M. tuberculosis* (32,33). The exogenous expression of TlyA in *E. coli* or *M. smegmatis* increases host cell adherence and phagocytosis of these bacteria by macrophages (34). Further, bacteria expressing TlyA modulate cellular trafficking mechanisms to avoid the phagolysosome (34). TlyA is a strong example of a ribosome-modifying enzyme that has moonlighting roles to aid in bacterial adaptation to a new environment. However, it is unknown why *M. tuberculosis* ribosomes contain the TlyA-mediated rRNA modifications. Perhaps methylation at C1409 and C1920 aids in stabilizing the ribosome structure for growth at 37°C or allows translation control factors to bind, allowing *M. tuberculosis* to adapt to the macrophage environment.

#### 6.4.2 *EftM Mediated Trimethylation Aids in P. aeruginosa Infection*

Moonlighting roles for a number of classical cytoplasmic proteins, e.g. EF-Tu, GroEL, GAPDH and endolase, in promoting bacterial adherence to host cells have been identified (reviewed in (35)). EftM was a protein of unknown function until studies in the Goldberg lab, which aimed to characterize adhesions in *P. aeruginosa*, identified EftM as an EF-Tu trimethyltransferase. The trimethylation of EF-Tu was sensitive to temperature, a typical attribute of adhesions (1,36), and in Chapter 3 we showed that the novel temperature regulation of the EF-Tu modification is due to the structural instability of EftM, which unfolds at 37°C, the host temperature. However, we do not yet know why methylation needs to be repressed at 37°C. One possibility is that the modification of EF-Tu is immunogenic and that *P. aeruginosa* represses EftM as an adaptive response to evade the host immune system.

#### 6.4.3 *Thiopeptides and the Antibiotic Resistome*

The global epidemic of antibiotic resistant bacterial infections is a problem, at its core, of bacteria adapting to a stress in their environment. Pathogenic bacteria acquire genes that help them adapt to living in an environment with antibiotics. These genes have been acquired either from antibiotic producing bacteria, which contain mechanisms to protect themselves from their own toxic products, or have evolved as a new antibiotic inhibitory function (reviewed in (37)). Collectively, all resistance genes form the ‘antibiotic resistome’ as they represent potential resistance mechanisms that could spread to pathogens given the right selective pressures. Fighting antibiotic resistance is a molecular arms race with bacteria acquiring genes to inactivate antibiotics as we attempt to develop new antibiotics or novel strategies to circumvent resistance. Thiopeptides offer an untapped source for future antibiotic development. Thiopeptides are ribosomally translated peptides that are extensively posttranslationally modified. Over a hundred

thiopeptides have been discovered, typically from soil or marine environments. Differences in the macrocyclic ring of the thiopeptide dictate which of two cellular targets they inhibit (reviewed in (38)). Thiopeptides with 26-member rings, like thiostrepton, bind to the GTPase activating center of the ribosome and inhibit translocation by EF-G. In contrast, 29-member ring thiopeptides bind EF-Tu to inhibit tRNA binding and thus the interaction of the ternary complex with the ribosome. The clinical use of thiopeptides has been limited due to their poor solubility. However, new studies have improved the solubility of some compounds, potentially reinvigorating studies that aim to develop thiopeptides as clinically useful antibiotics (39). With little use of thiopeptides to date in the clinic, resistance mechanisms to these antibiotics are those that are found in antibiotic-producing bacteria. Characterizing antibiotic resistance enzymes now, arms us for the future when we may need to inhibit these enzymes if they spread to pathogens.

## 6.5 FUTURE DIRECTIONS

In the previous chapters we have expanded the molecular characterization of three unique methyltransferases. However, many questions remain regarding each enzyme's molecular mechanism of action and role in bacterial physiology.

### 6.5.1 *EftM*

*EftM* is a newly identified enzyme that aids in *P. aeruginosa* virulence. A complete molecular characterization of *EftM* will describe the substrate recognition and catalytic mechanism of the enzyme as well as revealing the structure of *EftM* and *EftM*:EF-Tu complex. Additionally, studies are needed to explore the potential role for this modification in EF-Tu's canonical function as a translation factor, for example, to determine if trimethylation affects EF-Tu kinetics (e.g. GTP hydrolysis, tRNA binding). Furthermore, as a temperature-regulated modification it

will be critical to evaluate if modified EF-Tu aids in the translation of subsets of proteins necessary for growth at environmental temperatures.

Deletion of EftM decreased *P. aeruginosa* attachment to and invasion of epithelial cells and increased survival of infected mice (1). As trimethylation mimics phosphocholine, which looks like platelet-activating factor (PAF), it is likely that methylated EF-Tu interacts with the PAF-receptor on host cells. However, we do not currently know how EF-Tu accesses the bacterial outer membrane as it does not have a recognized export sequence. Experiments correlating the amount secreted or membrane bound EF-Tu with gene deletion libraries could be the first steps in identifying the proteins involved in the membrane trafficking of EF-Tu. As a modulator of ribosome function and cellular adherence, EftM's inhibition could be a novel target for antimicrobial therapy.

### 6.5.2 *TlyA*

While loss of TlyA in *M. tuberculosis* confers resistance to capreomycin, the canonical role for TlyA methylation remains elusive in this and other bacteria that possess the enzyme. Do TlyA methylations aid the ribosome in resisting stress either in the environment or as an intracellular pathogen? Furthermore, how does TlyA recognize two different rRNA substrates and does recognition cause our identified structural changes in the flexible linker? Structural studies of TlyA bound to a substrate will be needed to answer this question.

### 6.5.3 *Tsr*

Studies in the last eight years have aided in the characterization of Tsr and its homolog Nhr (4,6,7,40). However, an enzyme-substrate structure for either remains elusive and not until 2015

was another bacterial SPOUT methyltransferase-substrate complex solved (3). As these methyltransferases are dimers and contain additional substrate recognition domains, their recognition of rRNA structures with complex tertiary structures is not completely understood. Structures of either enzyme bound to a substrate RNA will be essential to understand this coordination.

Thiostrepton is a member of the thiopeptide class of antibiotics of which over 100 have been identified. Thiostrepton's antibiotic properties are understood, but little is known about what role thiostrepton plays in the bacterial community. Are thiopeptides a mechanism of interspecies communication or chemical warfare? Assessment of mRNA transcript or proteomic changes induced by growth in the presence of thiopeptides could begin to answer these questions. Furthermore, what other resistance determinants lay in the antibiotic resistome for thiopeptides? As resistance genes commonly are encoded near biosynthetic gene clusters, sequencing the genome of antibiotic producers and identifying the biosynthetic genes will aid in identifying resistance genes that are homologous to known proteins.

## 6.6 CONCLUDING REMARKS

With the emergence of antibiotic-resistant bacteria and a lag in the antibiotic development pipeline, the future of infection control is uncertain and unsettling. It will take the work of microbiologists and molecular and structural biologists to identify and characterize new molecular pathways and enzymes in bacteria that could serve as antibiotic targets for the development of new antibiotics. Our work, combined with antibiotic stewardship programs in hospitals and agriculture are vital to control the emerging antibiotic crisis.

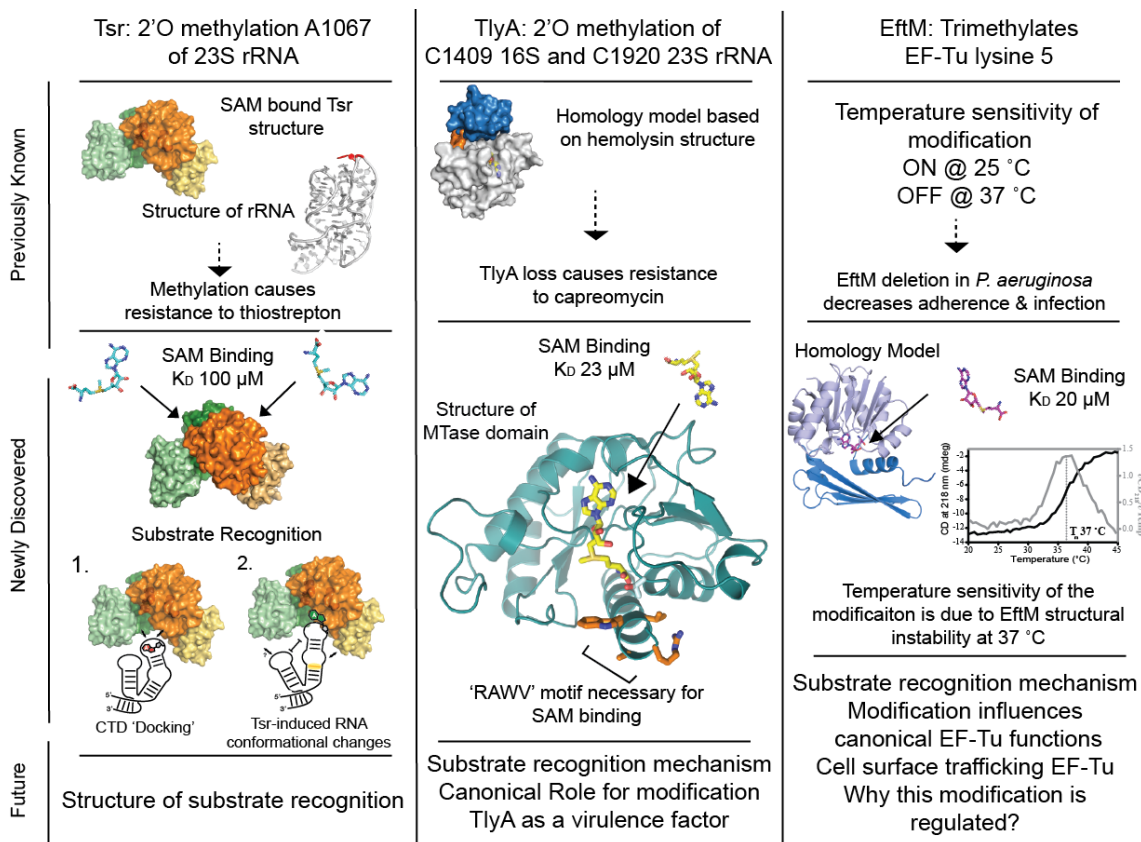


**FIGURE 6.1 Current knowledge of methyltransferase structure, cosubstrate binding, substrate recognition and enzyme control.** Summaries of our novel molecular mechanisms for these enzymes are depicted in the middle and future directions summarized at the bottom.

## 6.7 REFERENCES:

1. Barbier, M., Owings, J. P., Martinez-Ramos, I., Damron, F. H., Gomila, R., Blazquez, J., Goldberg, J. B., and Alberti, S. (2013) Lysine trimethylation of EF-Tu mimics platelet-activating factor to initiate *Pseudomonas aeruginosa* pneumonia. *mBio* **4**, e00207-00213
2. Jackson, M. W., Silva-Herzog, E., and Plano, G. V. (2004) The ATP-dependent ClpXP and Lon proteases regulate expression of the *Yersinia pestis* type III secretion system via regulated proteolysis of YmoA, a small histone-like protein. *Molecular microbiology* **54**, 1364-1378
3. Ito, T., Masuda, I., Yoshida, K., Goto-Ito, S., Sekine, S., Suh, S. W., Hou, Y. M., and Yokoyama, S. (2015) Structural basis for methyl-donor-dependent and sequence-specific binding to tRNA substrates by knotted methyltransferase TrmD. *Proc Natl Acad Sci U S A* **112**, E4197-4205
4. Dunstan, M. S., Hang, P. C., Zelinskaya, N. V., Honek, J. F., and Conn, G. L. (2009) Structure of the thiostrepton resistance methyltransferase.S-adenosyl-L-methionine complex and its interaction with ribosomal RNA. *J Biol Chem* **284**, 17013-17020
5. Shao, Z., Yan, W., Peng, J., Zuo, X., Zou, Y., Li, F., Gong, D., Ma, R., Wu, J., Shi, Y., Zhang, Z., Teng, M., Li, X., and Gong, Q. (2014) Crystal structure of tRNA m1G9 methyltransferase Trm10: insight into the catalytic mechanism and recognition of tRNA substrate. *Nucleic Acids Res* **42**, 509-525
6. Yang, H., Wang, Z., Shen, Y., Wang, P., Jia, X., Zhao, L., Zhou, P., Gong, R., Li, Z., Yang, Y., Chen, D., Murchie, A. I., and Xu, Y. (2010) Crystal structure of the nosiheptide-resistance methyltransferase of *Streptomyces actuosus*. *Biochemistry* **49**, 6440-6450
7. Yin, S., Jiang, H., Chen, D., and Murchie, A. I. (2015) Substrate recognition and modification by the nosiheptide resistance methyltransferase. *PLoS One* **10**, e0122972

8. Liu, R. J., Zhou, M., Fang, Z. P., Wang, M., Zhou, X. L., and Wang, E. D. (2013) The tRNA recognition mechanism of the minimalist SPOUT methyltransferase, TrmL. *Nucleic Acids Res* **41**, 7828-7842
9. Kagan, R. M., and Clarke, S. (1994) Widespread occurrence of three sequence motifs in diverse S-adenosylmethionine-dependent methyltransferases suggests a common structure for these enzymes. *Archives of biochemistry and biophysics* **310**, 417-427
10. Maravic Vlahovicek, G., Cubrilo, S., Tkaczuk, K. L., and Bujnicki, J. M. (2008) Modeling and experimental analyses reveal a two-domain structure and amino acids important for the activity of aminoglycoside resistance methyltransferase Sgm. *Biochim Biophys Acta* **1784**, 582-590
11. Savic, M., Ilic-Tomic, T., Macmaster, R., Vasiljevic, B., and Conn, G. L. (2008) Critical residues for cofactor binding and catalytic activity in the aminoglycoside resistance methyltransferase Sgm. *J Bacteriol* **190**, 5855-5861
12. Farrow, K. A., Lyras, D., Polekhina, G., Koutsis, K., Parker, M. W., and Rood, J. I. (2002) Identification of essential residues in the Erm(B) rRNA methyltransferase of *Clostridium perfringens*. *Antimicrob Agents Chemother* **46**, 1253-1261
13. Savic, M., Sunita, S., Zelinskaya, N., Desai, P. M., Macmaster, R., Vinal, K., and Conn, G. L. (2015) 30S Subunit-dependent activation of the *Sorangium cellulosum* So ce56 aminoglycoside resistance-conferring 16S rRNA methyltransferase Kmr. *Antimicrob Agents Chemother* **59**, 2807-2816
14. Witek, M. A., and Conn, G. L. (2014) Expansion of the aminoglycoside-resistance 16S rRNA (m(1)A1408) methyltransferase family: expression and functional characterization of four hypothetical enzymes of diverse bacterial origin. *Biochim Biophys Acta* **1844**, 1648-1655

15. Myers, C. L., Kuiper, E. G., Grant, P. C., Hernandez, J., Conn, G. L., and Honek, J. F. (2015) Functional roles in S-adenosyl-L-methionine binding and catalysis for active site residues of the thiostrepton resistance methyltransferase. *FEBS Lett* **589**, 3263-3270
16. Wimberly, B. T., Brodersen, D. E., Clemons, W. M., Jr., Morgan-Warren, R. J., Carter, A. P., Vornrhein, C., Hartsch, T., and Ramakrishnan, V. (2000) Structure of the 30S ribosomal subunit. *Nature* **407**, 327-339
17. Ban, N., Nissen, P., Hansen, J., Moore, P. B., and Steitz, T. A. (2000) The complete atomic structure of the large ribosomal subunit at 2.4 Å resolution. *Science* **289**, 905-920
18. Selmer, M., Dunham, C. M., Murphy, F. V. t., Weixlbaumer, A., Petry, S., Kelley, A. C., Weir, J. R., and Ramakrishnan, V. (2006) Structure of the 70S ribosome complexed with mRNA and tRNA. *Science* **313**, 1935-1942
19. Boehringer, D., O'Farrell, H. C., Rife, J. P., and Ban, N. (2012) Structural insights into methyltransferase KsgA function in 30S ribosomal subunit biogenesis. *J Biol Chem* **287**, 10453-10459
20. Lee, T. T., Agarwalla, S., and Stroud, R. M. (2005) A unique RNA Fold in the RumA-RNA-cofactor ternary complex contributes to substrate selectivity and enzymatic function. *Cell* **120**, 599-611
21. Alian, A., Lee, T. T., Griner, S. L., Stroud, R. M., and Finer-Moore, J. (2008) Structure of a TrmA-RNA complex: A consensus RNA fold contributes to substrate selectivity and catalysis in m5U methyltransferases. *Proc Natl Acad Sci U S A* **105**, 6876-6881
22. Monshupanee, T., Johansen, S. K., Dahlberg, A. E., and Douthwaite, S. (2012) Capreomycin susceptibility is increased by TlyA-directed 2'-O-methylation on both ribosomal subunits. *Molecular microbiology* **85**, 1194-1203

23. Dunkle, J. A., Vinal, K., Desai, P. M., Zelinskaya, N., Savic, M., West, D. M., Conn, G. L., and Dunham, C. M. (2014) Molecular recognition and modification of the 30S ribosome by the aminoglycoside-resistance methyltransferase NpmA. *Proc Natl Acad Sci U S A* **111**, 6275-6280
24. Burgie, E. S., and Holden, H. M. (2008) Three-dimensional structure of DesVI from *Streptomyces venezuelae*: a sugar N,N-dimethyltransferase required for dTDP-desosamine biosynthesis. *Biochemistry* **47**, 3982-3988
25. Jacob, A. I., Kohrer, C., Davies, B. W., RajBhandary, U. L., and Walker, G. C. (2013) Conserved bacterial RNase YbeY plays key roles in 70S ribosome quality control and 16S rRNA maturation. *Mol Cell* **49**, 427-438
26. Korber, P., Stahl, J. M., Nierhaus, K. H., and Bardwell, J. C. (2000) Hsp15: a ribosome-associated heat shock protein. *Embo J* **19**, 741-748
27. Roy-Chaudhuri, B., Kirthi, N., Kelley, T., and Culver, G. M. (2008) Suppression of a cold-sensitive mutation in ribosomal protein S5 reveals a role for RimJ in ribosome biogenesis. *Molecular microbiology* **68**, 1547-1559
28. White-Ziegler, C. A., Black, A. M., Eliades, S. H., Young, S., and Porter, K. (2002) The N-acetyltransferase RimJ responds to environmental stimuli to repress pap fimbrial transcription in *Escherichia coli*. *J Bacteriol* **184**, 4334-4342
29. Wren, B. W., Stabler, R. A., Das, S. S., Butcher, P. D., Mangan, J. A., Clarke, J. D., Casali, N., Parish, T., and Stoker, N. G. (1998) Characterization of a haemolysin from *Mycobacterium tuberculosis* with homology to a virulence factor of *Serpulina hyodysenteriae*. *Microbiology* **144** (Pt 5), 1205-1211

30. Rahman, A., Srivastava, S. S., Sneh, A., Ahmed, N., and Krishnasastry, M. V. (2010) Molecular characterization of tlyA gene product, Rv1694 of Mycobacterium tuberculosis: a non-conventional hemolysin and a ribosomal RNA methyl transferase. *BMC biochemistry* **11**, 35
31. Rahman, M. A., and Krishnasastry, M. V. (2014) Hemolytic activity of mycobacterial TlyA (Rv1694) is independent of its rRNA methylation activity. *Curr Sci India* **106**, 725-729
32. Lata, K., and Chattopadhyay, K. (2014) Helicobacter pylori TlyA agglutinates liposomes and induces fusion and permeabilization of the liposome membranes. *Biochemistry* **53**, 3553-3563
33. Rahman, M. A., Sobia, P., Dwivedi, V. P., Bhawsar, A., Singh, D. K., Sharma, P., Moodley, P., Van Kaer, L., Bishai, W. R., and Das, G. (2015) Mycobacterium tuberculosis TlyA Protein Negatively Regulates T Helper (Th) 1 and Th17 Differentiation and Promotes Tuberculosis Pathogenesis. *J Biol Chem* **290**, 14407-14417
34. Mittal, E., Kumar, S., Rahman, A., and Krishnasastry, M. V. (2014) Modulation of phagolysosome maturation by bacterial tlyA gene product. *Journal of biosciences* **39**, 821-834
35. Wang, G., Xia, Y., Cui, J., Gu, Z., Song, Y., Chen, Y. Q., Chen, H., Zhang, H., and Chen, W. (2014) The Roles of Moonlighting Proteins in Bacteria. *Current issues in molecular biology* **16**, 15-22
36. Barbier, M., Oliver, A., Rao, J., Hanna, S. L., Goldberg, J. B., and Alberti, S. (2008) Novel phosphorylcholine-containing protein of Pseudomonas aeruginosa chronic infection isolates interacts with airway epithelial cells. *J Infect Dis* **197**, 465-473
37. Woodford, N., and Ellington, M. J. (2007) The emergence of antibiotic resistance by mutation. *Clinical microbiology and infection : the official publication of the European Society of Clinical Microbiology and Infectious Diseases* **13**, 5-18

38. Just-Baringo, X., Albericio, F., and Alvarez, M. (2014) Thiopeptide antibiotics: retrospective and recent advances. *Marine drugs* **12**, 317-351
39. Leeds, J. A., LaMarche, M. J., Brewer, J. T., Bushell, S. M., Deng, G., Dewhurst, J. M., Dzink-Fox, J., Gangl, E., Jain, A., Lee, L., Lilly, M., Manni, K., Mullin, S., Neckermann, G., Osborne, C., Palestrant, D., Patane, M. A., Raimondi, A., Ranjitkar, S., Rann, E. M., Sachdeva, M., Shao, J., Tiamfook, S., Whitehead, L., and Yu, D. (2011) In vitro and in vivo activities of novel, semisynthetic thiopeptide inhibitors of bacterial elongation factor Tu. *Antimicrob Agents Chemother* **55**, 5277-5283
40. Kuiper, E. G., and Conn, G. L. (2014) Binding induced RNA conformational changes control substrate recognition and catalysis by the thiostrepton resistance methyltransferase (tsr). *J Biol Chem* **289**, 26189-26200